

Sedimentology, stratigraphy and  
geological history of part of the northern  
KwaZulu-Natal coastal dune cordon,  
South Africa

by

Pascal Sudan

November 1999

Submitted in fulfilment of the academic requirements

for the degree of Master of Science

School of Geological and Computer Sciences

University of Natal

Durban

## ABSTRACT

The northern KwaZulu-Natal coast is backed by a continuous aeolian dune cordon that rises in places, to a height of more than 100 metres and a width of 2 kilometres. This MSc thesis documents the geomorphology of the area, as well as the mineralogical, geochemical and textural variation of nine boreholes within a small part of the coastal dune cordon between Lake Nhlabane and Cape St.-Lucia. The results provide useful constraints on the identification of individual beach and aeolian dune systems, their age relationships and spatial distribution.

Aeolian dunes within the coastal dune cordon were studied using aerial photographs and grouped into five dune classes that reflect their relative age. These comprise 1) a system of highly weathered dunes inland of the present coastal dune cordon, that are thought to represent older dune cordons; 2) a system of weathered and reworked dunes located on the most inland portion of the coastal dune cordon; 3) a less altered, large field of linear parallel dunes located in the northern part of the study area; 4) a system of large scale parabolic dunes; and 5) a system of coastal, relatively unweathered small parabolic dunes.

Mineralogy, geochemistry, texture and SEM analysis of borehole samples revealed a complex internal structure within the present coastal dune cordon. In the most inland part of the dune cordon, a basal light grey unit (Unit K) presents similar characteristics to the Kosi Bay Formation. This is overlain by Unit A, comprising beach and dune systems, characterised by a very high heavy mineral content. Unit A also forms the basal unit of the central and coastal portions of the dune cordon. Unit B contains a mixture of reworked sediments from Unit A and younger sediments. Aeolian Units D and E form the upper part of the dune cordon. Units D and E were derived from beach – foredune systems and contain a high carbonate bioclast content. All units are interpreted to be derived from immature sediment from the Tugela River and mature sediment from the continental shelf. In the southern part of the study area, an additional unit (Unit C) with unique characteristics has been interpreted as an aeolian deposit reworked from local fluvial sediments. The units identified from their sedimentological characteristics can be directly correlated to the regional dune classes identified from the geomorphology.

Luminescence dating of two calcareous dunes was undertaken, revealing that only the sediment of the small coastal parabolic dunes (Dune Class 5, Unit E2) is of Holocene age. The deposition of the large field of linear dunes (Dune Class 3, Unit D2) took place between 15 000 and 11 000 BP, during the marine transgression following the last glaciation. Luminescence dating also indicated that both dunes were subject to at least one major reworking event.

A study on the weathering characteristics of the dunes can be used to attribute a relative age to the nine sedimentological units. With the help of sea level curves and the two luminescence dates, the nine units were attributed an approximate absolute age and regrouped into four sediment packages thought to broadly represent four interglacial periods. The three younger packages are attributed to the penultimate interglacial (lower part of Unit A), last interglacial (upper part of Unit A, Units B and C) and “Holocene” interglacial (Units D and E). Hence the northern KwaZulu-Natal coastal dune cordon under study represents a complex stacking of three generations of coastal dune cordons, and appears to be constituted of sediments with age ranging from at least two hundred thousand years ago to present.

The oldest sediment package (Unit K), interpreted as the Kosi Bay Formation, and the older dune cordons (Dune Class 1) must be older than 200 000 years, which is older than considered by previous studies. The “Holocene” dune cordon (Units D and E) is interpreted as the Sibayi Formation.

## **PREFACE**

The experimental work described in this dissertation was carried out in the School of Geological and Computer Sciences, University of Natal, Durban, from February 1998 to November 1999, under the supervision of Dr. Gregory P. Whitmore and Dr. Ron Uken.

These studies represent original work by the author and have not otherwise been submitted in any form for any degree or diploma to any tertiary institution. Where use has been made of the work of others it is duly acknowledged in the text.

## LIST OF CONTENTS

### I. INTRODUCTION

I.1. Richards Bay Minerals .....	1
I.2. Aim of study .....	2
I.3. Methodology .....	2

### II. REGIONAL PHYSIOGRAPHY

II.1. Introduction .....	4
II.2. Climate .....	4
II.2.1. Pressure systems and winds .....	5
II.2.2. Precipitation and temperature .....	7
II.3. Oceanography .....	8
II.3.1. Swell and wave regimes .....	8
II.3.2. Tides .....	9
II.3.3. Ocean currents and sediment drift .....	9
II.4. Quaternary palaeoclimatology and sea level changes .....	9

### III. REGIONAL GEOLOGY

III.1. Archaean .....	14
III.1.1. Kaapvaal Craton .....	14
III.1.2. Pongola Supergroup .....	14
III.2. Proterozoic .....	16
III.2.1. Natal Metamorphic Province .....	16
III.3. Palaeozoic – Mesozoic .....	16
III.3.1. Natal Group .....	16
III.3.2. Karoo Supergroup .....	17
III.3.3. Zululand Group .....	17
III.4. Cenozoic .....	18
III.4.1. Maputaland Group .....	18
III.4.1.1. Uloa Formation .....	19
III.4.1.2. Umkwelane Formation .....	20
III.4.1.3. Port Durnford Formation .....	20
III.4.1.4. Kosi Bay Formation .....	21
III.4.1.5. Suggested ages of the Port Durnford and Kosi Bay Formations .....	23
III.4.1.6. Kwa-Mbonambi Formation .....	23
III.4.1.7. Sibayi Formation .....	24
III.5. Provenance of coastal heavy minerals .....	24

## IV. GEOMORPHOLOGY AND DUNE CLASSIFICATION

IV.1. Introduction .....	26
IV.1.1. Regional geomorphology .....	26
IV.1.2. Terminology and dune types .....	26
IV.1.2.1. Bare dunes (wind formed) .....	28
IV.1.2.2. Vegetated dunes (wind and plant formed) .....	28
IV.2. Dune classification .....	29
IV.2.1. Dune Class 1: older dune cordons .....	31
IV.2.2. Dune Class 2: Inland dunes .....	31
IV.2.3. Dune Class 3: Linear parallel dunes .....	32
IV.2.4. Dune Class 4: Large scale parabolic dunes .....	34
IV.2.5. Dune Class 5: Small scale parabolic dunes .....	35
IV.3. Luminescence dating .....	36
IV.3.1. Results .....	38

## V. SOUTHERN ZULTI NORTH ORE BODY (NORTHING LINE 380)

V.1. Introduction .....	39
V.1.1. RBM reference and denomination systems .....	39
V.1.2. Sample location and description .....	40
V.2. Mineralogy .....	42
V.2.1. Mineral point counting .....	43
V.2.1.1. Heavy mineral variation .....	48
V.2.1.2. Rock fragments and carbonate grains .....	48
V.2.1.3. Pyroxene and amphibole .....	49
V.2.2. Heavy mineral abundance .....	53
V.2.2.1. Absolute heavy mineral content .....	53
V.2.2.2. IRZ / OHM ratio .....	56
V.2.2.3. Magnetite / THM ratio .....	61
V.2.2.4. Magnetite / Ilmenite ratio .....	63
V.3. Geochemistry .....	66
V.3.1. General description .....	66
V.3.1.1. Foredunes .....	66
V.3.1.2. Borehole S3 (coastal) .....	66
V.3.1.3. Borehole S2 (central) .....	67
V.3.1.4. Borehole S1 (inland) .....	68
V.3.2. Chemical element ratios .....	73
V.3.2.1. TiO <sub>2</sub> / MgO ratio .....	73
V.3.2.2. Chemical Index of Alteration .....	73
V.3.2.3. Trace element ratios and Unit C characteristics .....	76
V.4. Grain size .....	78
V.4.1. Introduction .....	78
V.4.2. Mean grain size .....	78
V.4.3. Distribution curves .....	81

V.5. SEM studies on quartz grains .....	87
V.5.1. Foredunes .....	87
V.5.2. Aeolian Units B, D and E .....	88
V.5.3. Units A and C .....	88
V.5.4. Other features .....	89
V.6. Summary: geological section of Northing Line 380 .....	95
<b>VI. NORTHERN ZULTI NORTH ORE BODY (NORTHING LINE 1200)</b>	
VI.1. Introduction .....	100
VI.1.1. Sample location and description .....	102
VI.2. Mineralogy .....	103
VI.2.1. Mineral point counting .....	103
VI.2.1.1. Rock fragments and carbonate grains .....	103
VI.2.1.2. Pyroxene and amphibole .....	103
VI.2.2. Heavy mineral abundance .....	106
VI.2.2.1. Absolute heavy mineral content .....	106
VI.2.2.2. IRZ / OHM ratio .....	106
VI.2.2.3. Magnetite / THM .....	109
VI.2.2.4. Magnetite / Ilmenite .....	111
VI.3. Geochemistry .....	113
VI.3.1. General description .....	113
VI.3.1.1. Borehole N5b .....	113
VI.3.1.2. Borehole N4 .....	113
VI.3.1.3. Borehole N3 .....	113
VI.3.1.4. Borehole N2 .....	114
VI.3.1.5. Borehole N1 .....	114
VI.3.2. Chemical element ratios .....	121
VI.3.2.1. TiO <sub>2</sub> / MgO ratio .....	121
VI.3.2.2. Chemical Index of Alteration .....	121
VI.4. Grain size .....	124
VI.4.1. Mean grain size .....	124
VI.4.2. Distribution curves .....	124
VI.5. SEM studies on quartz grains .....	132
VI.6. Summary: geological section of Northing Line 1200 .....	133
<b>VII. STRUCTURE AND GEOLOGICAL HISTORY OF THE ZULTI NORTH ORE BODY</b>	
VII.1. Unit characteristics .....	138
VII.1.1. Sediment provenance based on Nb, Zr and Ti elements .....	142
VII.2. Structure and geological history of the Zulti North ore body .....	145
VII.2.1. Surface geology of the Zulti North ore body .....	145
VII.2.2. Internal structure of the Zulti North ore body .....	145
VII.4 Conclusion .....	151

<b>REFERENCES</b>	<b>152</b>
<b>APPENDIX A: LUMINESCENCE DATING</b>	<b>159</b>
<b>APPENDIX B: GEOCHEMICAL DATA</b>	<b>168</b>
<b>APPENDIX C: GRAIN SIZE DATA</b>	<b>173</b>
<b>APPENDIX D: POINT COUNT DATA (LINE 1200)</b>	<b>180</b>

## LIST OF FIGURES

<b>Figure I.1.</b> Dune mining technique used by RBM (Hugo, 1993).	<b>1</b>
<b>Figure II.1.</b> Location of the study area in the northern KwaZulu-Natal coastal plain (modified from Hobday & Orme, 1974).	<b>5</b>
<b>Figure II.2.</b> Annual wind rose for the St.-Lucia area (Van Heerden & Swart, 1986).	<b>6</b>
<b>Figure II.3.</b> Winter and summer wind rose for the St.-Lucia area (Hunter, 1988).	<b>6</b>
<b>Figure II.4.</b> Climograph of the Cape St.-Lucia (modified from Tinley, 1985).	<b>7</b>
<b>Figure II.5.</b> Wave direction distribution for Richards Bay (Rossouw, 1984).	<b>8</b>
<b>Figure II.6.</b> Swell observations (direction and height) at Cape St.-Lucia (Begg, 1978).	<b>8</b>
<b>Figure II.7.</b> Oxygen isotopic record and definition of isotope stages and sub-stages from Pacific core V19-29 and Atlantic core M12392-1 (Climap Project Members, 1984).	<b>10</b>
<b>Figure II.8.</b> Correlation between oxygen isotope and global sea level changes (GCS, 1990).	<b>11</b>
<b>Figure II.9.</b> Late Quaternary sea level curve for southern Africa (Ramsay, 1997).	<b>12</b>
<b>Figure II.10.</b> Holocene sea level curve for southern Africa (Ramsay, 1995).	<b>13</b>
<b>Figure II.11.</b> Oxygen isotopes and calculated changes of local sea surface temperature (SST). Data from the deep sea core RC17-69, offshore Durban (Howard, 1985).	<b>13</b>
<b>Figure III.1.</b> Regional geology within the catchment area of KwaZulu-Natal rivers (from Whitmore et al., 1999).	<b>15</b>
<b>Figure III.2.</b> Catchment areas and characteristics of major KwaZulu-Natal rivers (from Ware, in prep.).	<b>15</b>
<b>Figure III.3.</b> Lithostratigraphy of the Maputaland Group (from Botha, 1997a).	<b>19</b>
<b>Figure III.4.</b> Geological section across the northern KwaZulu-Natal coastal plain, near Richards Bay (from Maud & Orr, 1975).	<b>20</b>
<b>Figure III.5.</b> Geological sections near Lake Nhlabane (from Fockema, 1986).	<b>22</b>
<b>Figure IV.1.</b> Aerial photograph (1985) of the northern KwaZulu-Natal coastal dune cordon between Lake Nhlabane and St.-Lucia.	<b>27</b>
<b>Figure IV.2.</b> Geomorphological map for the Zulti North ore body, showing studied field samples, and all recognised dunes regrouped in 5 dune classes.	<b>30</b>
<b>Figure IV.3.</b> Orange brown inland dune (Dune Class 2) as exposed in MPC (N330).	<b>33</b>
<b>Figure IV.4.</b> Landward side of the most inland dune of the linear parallel dunes (Dune Class 3).	<b>33</b>
<b>Figure IV.5.</b> Morphological variants of parabolic dunes (Pye, 1993).	<b>34</b>
<b>Figure IV.6.</b> View from MPC: recent transgressive dune field overlying a palaeosol of a parabolic dune (Dune Class 4); small scale parabolic dunes (Dune Class 5).	<b>35</b>
<b>Figure IV.7.</b> Retreating shoreline north of Dawson's Rock. The cliffs are constituted of older orange sands overlain by younger sand from the small scale parabolic dunes (Dune Class 5).	<b>37</b>

<b>Figure IV.8.</b> Small parabolic dune (Dune Class 5, Unit E2) separated from the underlying sand (Unit E2) by a palaeosol. Also shown is the location of samples RBM2 and D'Rock 1. ....	37
<b>Figure V.1.</b> Geomorphological map of the southern Zulti North ore body, showing the location of the three boreholes studied that intercept Dune Classes 2, 4 and 5. ....	41
<b>Figure V.2.</b> Topographic section along Line 380, showing the morphology and the location of field samples, palaeosols and the three boreholes studied. ....	42
<b>Figure V.3.</b> Mineral abundance for samples from borehole S1 (Line 380). ....	44
<b>Figure V.4.</b> Mineral abundance for samples from borehole S2. ....	45
<b>Figure V.5.</b> Mineral abundance for samples from borehole S3. ....	46
<b>Figure V.6.</b> Mineral abundance of D'Rock 1 and F-dune 4 field samples. ....	47
<b>Figure V.7.</b> Heavy mineral content for samples from Line 380 boreholes, F-dune 4 and D'Rock 1 field samples, plotted to the elevation above msl for each sample. ....	50
<b>Figure V.8.</b> Rock fragment and carbonate abundance for samples from Line 380 boreholes and F-dune 4 and D'Rock 1 field samples. ....	51
<b>Figure V.9.</b> Ratio of pyroxene divided by total heavy mineral for samples from Line 380 boreholes and F-dune 4 and D'Rock 1 field samples. ....	52
<b>Figure V.10.</b> Heavy mineral content for samples from Line 380 boreholes (recalculated from RBM data). ....	55
<b>Figure V.11.</b> Average heavy mineral proportions in Zululand beaches and coastal dunes (Hugo, 1993). ....	56
<b>Figure V.12.</b> Average grain size distribution of selected heavy minerals from coastal dunes near Richards Bay (data from Fockema, 1986 and Hugo, 1993). ....	57
<b>Figure V.13.</b> Ratio of ilmenite, rutile and zircon divided by other heavy minerals (IRZ/OHM) for samples from Line 380 boreholes and field samples from Hugo (1993) and Jordaan (1996). ....	60
<b>Figure V.14.</b> Ratio of Magnetite divided by total heavy mineral content (Magnetite / THM) for samples from Line 380 boreholes and field samples from Hugo (1993) and Jordaan (1996). ....	62
<b>Figure V.15.</b> Average iron-titanium oxide proportions in Zululand beaches and coastal dunes (Hugo, 1993). ....	63
<b>Figure V.16.</b> Ratio of Magnetite divided by ilmenite (Magnetite / Ilmenite) for samples from Line 380 boreholes and field samples from Hugo (1993) and Jordaan (1996). ....	65
<b>Figure V.17.</b> Major elements (without SiO <sub>2</sub> ) of the foredune samples F-dune 2 and F-dune 4. ....	69
<b>Figure V.18.</b> Major elements (excluding SiO <sub>2</sub> ) for samples from borehole S3. ....	70
<b>Figure V.19.</b> Major elements (excluding SiO <sub>2</sub> ) for samples from borehole S2. ....	71
<b>Figure V.20.</b> Major elements (excluding SiO <sub>2</sub> ) for samples from borehole S1. ....	72
<b>Figure V.21.</b> TiO <sub>2</sub> / MgO ratio values for samples from the three Line 380 boreholes and the two foredune samples (F-dune 2 and 4). ....	74
<b>Figure V.22.</b> Chemical Index of Alteration for samples from the three Line 380 boreholes and the two foredune samples (F-dune 2 and 4). ....	75
<b>Figure V.23.</b> P <sub>2</sub> O <sub>5</sub> / Zr ratio values for samples from the three Line 380 boreholes and the two foredune samples (F-dune 2 and 4). ....	77
<b>Figure V.24.</b> Mean grain size for samples from the three Line 380 boreholes and field samples (F-dune 1, 2, 4 and D'Rock 1, 3, 4). ....	80
<b>Figure V.25.</b> Grain size frequency distribution curve for samples from borehole S1. ....	83
<b>Figure V.26.</b> Grain size frequency distribution curve for samples from borehole S2. ....	84
<b>Figure V.27.</b> Grain size frequency distribution curve for samples from borehole S3. ....	85
<b>Figure V.28.</b> Grain size frequency distribution curve for the field samples. ....	86
<b>Figure V.29 (a-p).</b> Physical and chemical features on quartz grain surfaces from aeolian, non-aeolian and diagenetic environments, as observed by SEM (scanning electron microscopy). ..	90 to 94
<b>Figure V.30.</b> Geological section of Northing Line 380, showing the lateral extension of the height units defined in Chapter V and the location of the sample RBM 2 dated by luminescence. ....	96
<b>Figure V.32 (a-i).</b> Evolutionary model for the southern cross-section (Line 380), showing the depositional and reworking events correlated with time and sea level fluctuations. ....	98 to 99
<b>Figure VI.1.</b> Geomorphological map of the northern Zulti North ore body, showing the location of the five boreholes studied that intercept Dune Classes 2, 3 and 4. ....	101
<b>Figure VI.2.</b> Topographic section along Line 1200, showing the morphology and the location of sample RBM1 (dated by luminescence) and the five boreholes studied. ....	102

<b>Figure VI.3.</b> Rock fragment and carbonate abundance for samples from Line 1200 boreholes and F-dune 4 and D'Rock 1 field samples. ....	104
<b>Figure VI.4.</b> Ratio of pyroxene divided by total heavy mineral for samples from Line 1200 boreholes and F-dune 4 and D'Rock 1 field samples. ....	105
<b>Figure VI.5.</b> Heavy mineral content for samples from Line 1200 boreholes (recalculated from heavy mineral ratios and ilmenite content determined by RBM). ....	107
<b>Figure VI.6.</b> Ratio of ilmenite, rutile and zircon divided by other heavy minerals (IRZ/OHM) for samples from Line 1200 boreholes and field samples from Hugo (1993) and Jordaan (1996). ...	108
<b>Figure VI.7.</b> Ratio of Magnetite divided by total heavy mineral content (Magnetite / THM) for samples from Line 1200 boreholes and field samples from Hugo (1993) and Jordaan (1996). ...	110
<b>Figure VI.8.</b> Ratio of Magnetite divided by ilmenite (Magnetite / Ilmenite) for samples from Line 1200 boreholes and field samples from Hugo (1993) and Jordaan (1996). ....	112
<b>Figure VI.9.</b> Major elements (excluding SiO <sub>2</sub> ) of borehole N5b. ....	116
<b>Figure VI.10.</b> Major elements (excluding SiO <sub>2</sub> ) for samples from borehole N4. ....	117
<b>Figure VI.11.</b> Major elements (excluding SiO <sub>2</sub> ) for samples from borehole N3. ....	118
<b>Figure VI.12.</b> Major elements (excluding SiO <sub>2</sub> ) for samples from borehole N2. ....	119
<b>Figure VI.13.</b> Major elements (excluding SiO <sub>2</sub> ) for samples from borehole N1. ....	120
<b>Figure VI.14.</b> TiO <sub>2</sub> / MgO ratio values for samples from the five Line 1200 boreholes and the two foredune samples (F-dune 2 and 4). ....	122
<b>Figure VI.15.</b> Chemical Index of Alteration for samples from the five Line 1200 boreholes and the two foredune samples (F-dune 2 and 4). ....	123
<b>Figure VI.16.</b> Mean grain size for samples from the five Line 1200 boreholes and foredune samples (F-dune 1, 2, 4). ....	125
<b>Figure VI.17.</b> Grain size frequency distribution curves for samples from borehole N1. ....	127
<b>Figure VI.18.</b> Grain size frequency distribution curves for samples from borehole N2. ....	128
<b>Figure VI.19.</b> Grain size frequency distribution curves for samples from borehole N3. ....	129
<b>Figure VI.20.</b> Grain size frequency distribution curves for samples from borehole N4. ....	130
<b>Figure VI.21.</b> Grain size frequency distribution curves for samples from borehole N5b. ....	131
<b>Figure VI.22.</b> Aeolian quartz grain of Unit K, showing two generations of silica layers. ....	132
<b>Figure VI.23.</b> Geological section of Northing Line 1200, showing the lateral extension of the seven units defined in Chapter VI and the location of sample RBM 1 dated by luminescence. ...	134
<b>Figure VI.24(a-i).</b> Evolutionary model for the northern cross-section (Line 1200), showing the depositional and reworking events correlated with time and sea level fluctuations. ....	136 to 137
<b>Figure VII.1.</b> Schematic evolutionary model for part of the northern KwaZulu-Natal dune cordon, showing the depositional and reworking events correlated with time and sea level fluctuations. ...	141
<b>Figure VII.2.</b> TiO <sub>2</sub> / Nb and TiO <sub>2</sub> / Zr ratio values for all samples of the present study and for various fluvial and marine samples near the Tugela river mouth (data from Felhaber, 1984). ....	143
<b>Figure VII.3.</b> Geological map of the Zulti North ore body, showing the lateral extension of the nine sedimentological units and the relationship with the surface morphology. ....	146
<b>Figure VII.4.</b> Geological map of the base of the Zulti North ore body along a horizontal plane at ca. 5 - 10 m above msl. Underlying beach placers have been projected onto this plane. ....	149
<b>Figure VII.5.</b> Geological map of the Zulti North ore body along a horizontal plane at ca. 30 - 35 m above msl. ....	150

## LIST OF TABLES

<b>Table II.1.</b> Border Cave palaeoclimatic inferences based on micromammalian analyses (Avery, 1982). ....	12
<b>Table V.1.</b> Nomenclature, location and characteristics of boreholes S1, S2 and S3 from Line 380. ....	40

---

<b>Table V.2.</b> Semi-quantitative chemical analysis of a globular silica layer on a quartz grain of Unit E2. ....	88
<b>Table V.3.</b> Semi-quantitative chemical analysis of a globular silica layer on a quartz grain of Unit A1, reflecting the average chemical composition of silica layers for Units A1 and A2. ....	89
<b>Table VI.1.</b> Nomenclature, location and characteristics of the six boreholes N1 to N5b of Line 1200. ....	102
<b>Table VII.1.</b> Discriminative characteristics for the nine sedimentological units defined in the Zulti North ore body. ....	139
<b>Table VII.2.</b> Summary table of discriminative characteristics and interpretation of the nine sedimentological units defined in the Zulti North ore body. ....	140

## ACKNOWLEDGEMENTS

This study was made possible by funding from Richards Bay Minerals (RBM). I would like to direct a special acknowledgement to Mr. John Selby who gave me the opportunity to discover the South African world of mining geology. I thank also Mr. John Selby for the use of analytical equipment and accommodation in Richards Bay.

Many have contributed to the accomplishment of this thesis. I would like here to thank:

- Dr. Gregory Whitmore and Dr. Ron Uken, my supervisors, for having introduced me to the world of siliciclastic sedimentology, and for their scientific advice and their patience during the spelling and grammatical corrections of my written reports, papers and thesis.
- Mr. Kevin Pietersen for having taken care of me during my stays in Richards Bay and for his unconditional help throughout the project.
- Mrs Audrey Pietersen, Mr. Kevin Pietersen, Mr. John Barnes and many other people from RBM who helped me in various occasions and spent some of their time to organise my field work in the coastal dunes.
- Stephan Woodborne from the CSIR for the luminescence dating and the interesting discussions about the results.
- Mrs Fiona Graham from the Electron Microscope Unit at the University of Natal for her help in SEM analyses.
- Professor Allan Wilson, Head of School, and all staff members and technicians of the School of Geological and Computer Sciences for their welcome and support during my stay in South Africa. I also thank Dr. Peter Ramsay from the Marine Geoscience Unit for his critical and fruitful comments on part of my thesis.
- my family and my South African and Swiss friends.
- The Ernst Bürri Foundation in Switzerland and RBM for having generously given me scholarships that allowed me to enjoy a basic and social life.

# I. INTRODUCTION

Scientific understanding of coastal aeolian dune cordons, their internal structure and geological history are generally lacking. This is largely due to difficulties involved with sampling, imaging and dating of modern dune cordons and relatively poor preservation in the geological record. Companies actively exploiting modern coastal dune sands for economic minerals have large diverse data sets collected over wide areas. Access to these data sets is beginning to come into the public domain. This, combined with recent advances in luminescence dating of relatively young sand allows to define and document internal sedimentological units within coastal dune cordons, and to unravel spatial and temporal interactions with their surrounding environments.

## I.1. Richards Bay Minerals

This research project is supported by Richards Bay Minerals (RBM) in order to improve the scientific understanding of one of their heavy mineral ore bodies.

RBM is currently mining unconsolidated aeolian deposits of the coastal dune cordon near Richards Bay. The dune cordon presently mined has been subdivided by RBM into three ore bodies: Zulti South, Tisand and Zulti North. These deposits contain five economic heavy minerals: ilmenite, rutile, leucoxene, zircon and monazite. The aeolian dunes are mined by suction dredges, which feed the sand to floating concentrators in a shallow mining pond (Figure I.1). Gravity circuits are used to separate the heavy minerals from the lighter gangue, which is redeposited in the dunes by tailing stackers. Magnetite is removed by low intensity wet magnets and combined with tailings. The heavy mineral concentrate is then transported to the mineral separation plant.

Due to the presence of non-exploitable "clay floor", the base level of the mining ponds vary between sea level and 5 to 10 m above msl (Pietersen, 1999, pers. comm.). The Zulti North ore body is currently being mined by three mining ponds: Mining Pond A (MPA), Mining Pond C (MPC) and Mining Pond D (MPD). In October 1999 a third mining pond, MPE, was under construction.

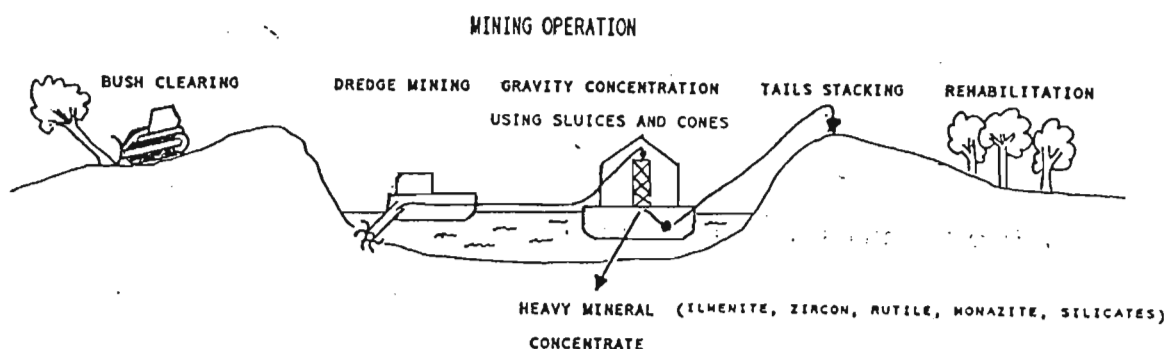


Figure I.1. Dune mining technique used by RBM (Hugo, 1993).

## I.2. Aim of study

Mining activities and the efficiency of heavy mineral recovery is greatly influenced by the nature and weathering state of the host sediment. Important sediment characteristics include clay content, grain coatings, mineralogy and mineral chemistry. These characteristics have been noted to change during dune mining, as dune cordons are rarely homogeneous. The aim of this study is to establish the stratigraphy and structure of the Zulti North ore body. The surface of the ore body is analysed geomorphologically, characterising the aeolian dunes and their spatial relationships. The internal structure of the ore body is investigated by defining sedimentological units. These are characterised by weathering state, mineralogy, geochemistry and grain size analyses obtained from borehole samples. Luminescence dating of selected aeolian dunes and their correlation to sea level fluctuations are used to propose a geological history of the coastal dune cordon formation. It is hoped that this study will provide a spatial understanding of the ore body characteristics, as well as providing a basis for future detailed studies. This broad project has been subdivided into two sections – this study focuses on sand size sediment from the coastal dune cordon, and a concurrent study is underway to examine the silt and clay sized fraction (Ware, in prep.).

## I.3. Methodology

A geomorphological map of the region under study was compiled from a set of colour 1:10 000 scale aerial photographs flown in 1995 and an additional set of monochromatic 1:150 000 scale aerial photographs flown in 1985 (The Air Survey). The geomorphological map was refined by field observations in August 1998.

Luminescence dating of two aeolian dunes was carried out, using a combination of two techniques: “thermoluminescence” (TL) on quartz grains and “infrared stimulated luminescence” (IRSL) on feldspar grains. Both techniques, including dating results, are detailed in the report compiled by Woodborne & Collett (1999) from the CSIR (Appendix A). Dating results are interpreted in Section IV.3.

RBM has drilled approximately 6500 boreholes on a 50 m grid spacing in order to assess ore reserves within the Zulti North ore body. The internal structure of the dune cordon under study was defined using 6 field samples and 119 samples from eight boreholes selected from two cross-sections through the ore body. Each borehole sample represents the average composition of a six-metre interval of dune sand. Each bulk sample was split to 200 g aliquots for laboratory analyses.

The mineral abundance in samples studied is derived from two different data sets. The first data set has been obtained by point counting of all samples. After removal of the <63µm fraction by dry sieve, polished thin sections were prepared for each sample for petrographic studies. Mineralogical composition was determined by point counting 500 grains for each thin section. Analysis of the point counting results indicate that mineral segregation occurred during

thin section preparation, resulting in an increased heavy mineral content (by a factor of 3 to 5) and an antipathetic decrease of light minerals.

The second mineralogy data set was supplied by RBM. This contains a wide variety of heavy mineral abundance ratios and selected ilmenite grades obtained by in house heavy mineral separation techniques. Each borehole sample, intercepting 6 m of sand, was split using a rotary splitter. Slime content ( $< 63 \mu\text{m}$ ) was removed by wet sieve. Heavy mineral concentrate was then separated by heavy liquid separation (Tetrabromoethane). The sample was further subdivided into magnetic fractions using a Carpco HIDMS magnetic separator.

Magnetite, which has a high magnetic susceptibility property, was separated from the sample by applying a current of up to 0.05 amperes. This magnetic fraction is called "Magnetite" by RBM, even though it contains trace amounts of other minerals. Between 0.05 and 0.8 amperes "Magnetics" were recovered, from which ilmenite is calculated by multiplying the  $\text{TiO}_2$  content, identified using X-ray fluorescence (XRF), by two (Pietersen, 1999, pers. comm.). "Magnetic others" is the magnetic fraction including minerals recovered from 0.8 to 2.4 amperes. Any minerals separated at greater than 2.4 amperes have a low magnetic susceptibility. Rutile and zircon were identified using XRF and the remaining minerals were termed "Non magnetic others". The efficiency of these separation techniques and the resulting mineralogy of the magnetic-electrostatic fractions are discussed in detail in Section V.2.2.

Geochemical analysis of bulk sediment samples (milled in a carbon steel vessel) was carried out by XRF using Philips 1404 and Philips X'Unique II machines in the School of Geological and Computer Sciences. Major elements were analysed from fused disks (0.35 g of sediment mixed with 2 g of Spectroflux, in a Pt/Au crucible for 2 hours at  $1000^\circ\text{C}$ ) and trace elements from pressed powder pellets (8 g of sediment mixed with 0.6 ml of Mowiol glue and compressed by a 8 ton press). Analytical accuracy falls within 0.2 to 0.5 % of the abundance for major elements, and within 5 to 10 % of the abundance for trace elements.

The sediment samples analysed were thought to represent bulk samples obtained from the boreholes. However, as discussed in Section V.4.1, a significant loss of fine fractions ( $< 90 \mu\text{m}$ ) occurred during sample manipulation by RBM. Therefore the geochemical results, presented in Sections V.3 and VI.3, characterise mainly the sand size fraction of the bulk sample.

Grain size analysis was carried out using a Malvern 2600 laser particle sizer (dry powder feeder) in the RBM laboratory. Grain size results are also affected by loss of the fine fraction. In order to characterise and quantify the grain size distribution of studied samples, textural parameters defined by Friedman (1961; 1979) have been utilised and are presented below:

$$\text{Mean } (\bar{x}) = 1/100 \sum f m_{\phi}$$

$$\text{Standard deviation } (\sigma) = (\sum f (m_{\phi} - \bar{x}_{\phi})^2 / 100)^{1/2}$$

$$\text{Cubed deviation } (\sigma^3) = (\sum f (m_{\phi} - \bar{x}_{\phi})^3 / 100)^{3/2}$$

$$\text{Skewness or Third moment } (\alpha_3) = 1/100 \sigma^{-3} \sum f (m_{\phi} - \bar{x}_{\phi})^3$$

$$\text{Mean-cubed deviation } (\alpha_3 \sigma^3) = 1/100 \sum f (m_{\phi} - \bar{x}_{\phi})^3$$

$$\text{Kurtosis } (\alpha_4) = 1/100 \sigma^{-4} \sum f (m_{\phi} - \bar{x}_{\phi})^4$$

$$\text{Simple sorting measure } (So_s) = 1/2 (\phi_{95} - \phi_5)$$

$$\text{Simple skewness measure } (\alpha_s) = (\phi_{95} + \phi_5) - 2 (\phi_{50})$$

Where "f" is the frequency or abundance of the different grain-size grades present in the sediment and " $m_{\phi}$ " is the mid point of each grain-size grade in phi values.

Quartz grain surfaces were studied using a Hitachi S-520 scanning electron microscope (SEM) of the Electron Microscope Unit, University of Natal, Durban. Semi-quantitative chemical composition of grain surfaces was obtained by energy dispersive (ED) X-ray analysis, giving element abundance in weight percentage (% element) and in mole (% atomic) (Tables V.2 and V.3).

## II. REGIONAL PHYSIOGRAPHY

### II.1. Introduction

The KwaZulu-Natal coastal plain, formed during the break up of Gondwana and has been evolving ever since. It stretches from Mtunzini in the south to Mozambique in the north, and is delimited to the east by the Indian Ocean and to the west by the elevated topography of the Lebombo Mountains (Figure II.1). The coastal plain can be subdivided into two sectors north and south of St.-Lucia (Figure II.1). The shoreline changes from a northeasterly trend to a north-northeasterly direction at this point. This change is believed to be closely correlated to faulting during Gondwana break up (Section III.3.3).

The elevation of the southern part of the KwaZulu-Natal coastal plain ranges from 20 m to 70 m above msl. Localised depressions in the coastal plain are related to the river systems and their associated coastal lagoons/lakes. Five rivers (Mlalazi, Mhlatuze, Nseleni, Msunduzi and Mfolozi) form insized valleys into the coastal plain (Figure II.1). During high sea level periods (such as much of the Holocene), alluvial plains, lagoons, lakes and swamps formed in the river valleys. The low lying coastal plain is separated from the ocean by a 1 to 2 km wide, and 45 m to 180 m high aeolian dune cordon, which extends northwards into Mozambique.

The study area is located 30 km northeast of Richards Bay (32°33' E, 28°58' S) and represents a small portion of the northern KwaZulu-Natal coastal dune cordon (Figure II.1). It is delineated by Lake Nhlabane and its estuary in the south, and by Cape St.-Lucia to the north. Lake Nhlabane was until recently a natural lagoon connected to the Indian Ocean. To supply the mining operation with water, a dam was built to elevate the water level, reducing water circulation between the lake and the ocean. Consequently, the estuary mouth has now been infilled by washover and aeolian sediments (Section IV.1.1).

### II.2. Climate

The processes of present day dune cordon formation under the influence of known weather parameters needs to be clearly understood if any attempt is to be made at reconstructing palaeoenvironments and assessing older dune systems.

The present climate of the east coast of South Africa is classified as “mild humid climate with no dry season, and mean temperature greater than 22°C for the warmest month” (Cfa type) using the Köppen-Geiger system of climate classification (Strahler & Strahler, 1992). Strahler’s classification defines the climates in reference to their position within global pressure and wind systems; the South African east coast climate experiences a “moist subtropical climate”, a sub-type of the “monsoon and trade wind littoral climate” (Strahler & Strahler, 1992).

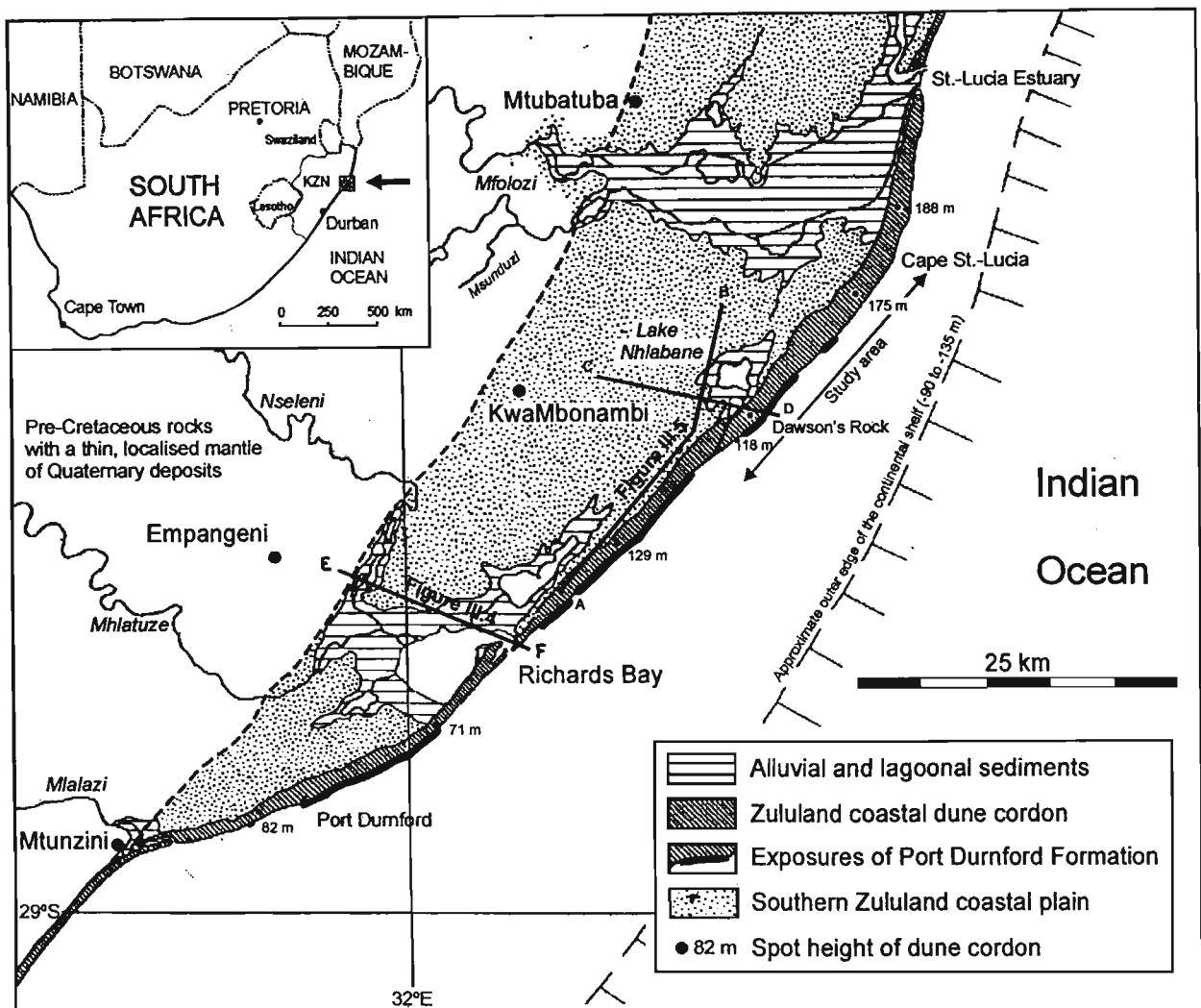


**Figure II.1.** Location of the study area in the northern KwaZulu-Natal coastal plain (modified from Hobday & Orme, 1974). Also shown is the position of coastal outcrops and the onshore sections A-B, C-D and E-F described in Chapter III (Figures III.4 and III.5).

### II.2.1. Pressure systems and winds

Due to its subtropical geographical position, weather processes in southeastern Africa are dominated by three major pressure systems (Tyson, 1986). The first of these is a semi-permanent high pressure anticyclone centred over the Indian Ocean (30° S). The second major system is a seasonal high pressure zone that extends above northeastern South Africa during the winter (the “Limpopo High”). The third system is represented by circumpolar westerlies generated in the “Roaring Forties” or the “Subtropical Convergence Zone”. In this zone low pressure cyclones interact with anticyclones to building east-moving cold fronts (Tinley, 1985).

A latitudinal shift of 5° - 10° is noted for the Indian Ocean high pressure and the Subtropical Convergence Zone between summer and winter (Jackson & Tyson, 1971).

The predominant winds along the northern KwaZulu-Natal coast are thus bidirectional, and oblique or quasi parallel to the coastline trend (Figure II.2). Coastal perpendicular winds, such as land - sea breezes and "Berg winds", are minor in terms of duration and velocity, yet have to be taken into account for a complete understanding of the regional wind patterns (Tyson, 1986) (Figure II.2).

In summer (December of Figure II.3), anticyclonic north to northeasterly winds dominate. In winter (June of Figure II.3), the Indian Ocean high pressure and the circumpolar westerlies alternate with minor winds such as the west to northwesterly "Berg winds".

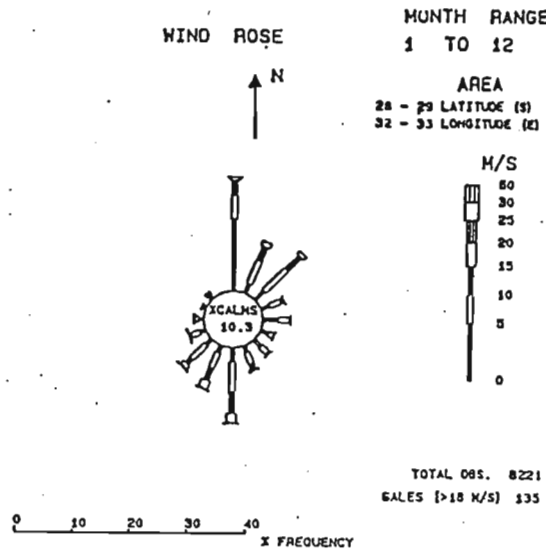


Figure II.2. Annual wind rose for the St.-Lucia area (Van Heerden & Swart, 1986) showing a predominance of northerly, northeasterly and southeasterly winds.

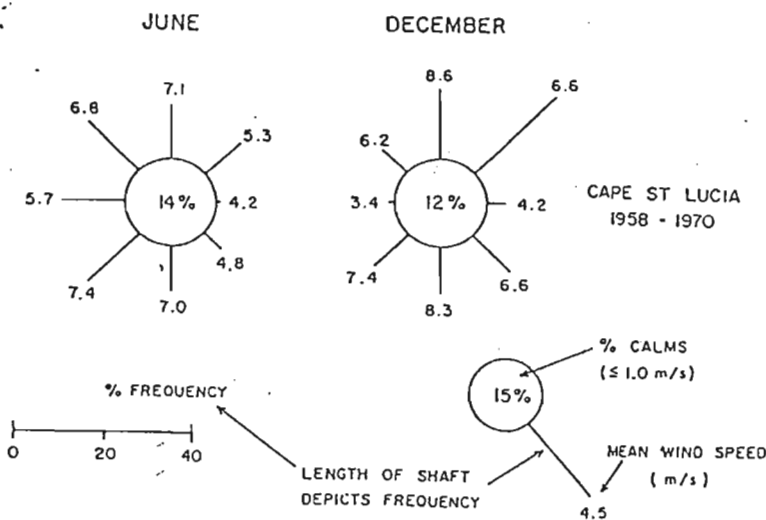
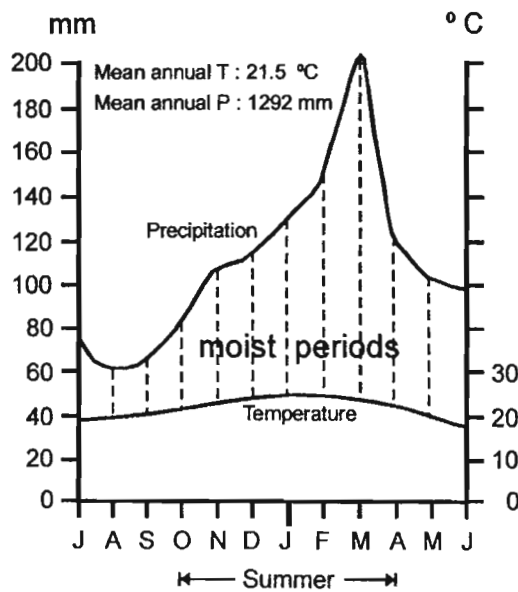


Figure II.3. Winter and summer wind rose for the St.-Lucia area (average over the period 1958-1970) (Hunter, 1988).

## II.2.2. Precipitation and temperature

The precipitation regime in northern KwaZulu-Natal is characterised by a wet summer and a dry winter (Figure II.4). Dry winters are due to the well established continental Limpopo High at this time. Cyclonic frontal rain affects the northern KwaZulu-Natal coast only at the end of the winter (Schulze, 1965). At this time, a low pressure system develops over the warming interior (replacing the Limpopo High). This produces tropical anticyclonic rainfall due to the advection of moist marine air off the Indian Ocean. This situation lasts until April, when cold and dry subsiding air reinstates the Limpopo High for the winter.



**Figure II.4.** Climograph for Cape St.-Lucia (modified from Tinley, 1985), showing the monthly average temperature and precipitation. Note that Cape St.-Lucia does not experience any dry period.

The rainfall pattern for the KwaZulu-Natal coastal plain shows a decreasing trend from above 1000 mm at the coast to less than 700 mm in the eastern margin of the coastal plain (Maud, 1980). The high rain zone along the immediate coast is enhanced considerably by the abrupt relief of the coastal dune cordon, with a concomitantly markedly drier leeward "shadow" zone (Tinley & Van Riet, 1981).

The annual temperature range for coastal KwaZulu-Natal is moderated by marine air influences, increased cloud cover, high atmospheric humidity (70 to 84 % relative humidity at Cape St.-Lucia) and the cooling effect of sea breezes (Tinley, 1985) (Figure II.4). An approximate evaporation rate of 1600 mm per year for Richards Bay can be extrapolated from the data recorded in Durban (1755 mm per year) and Kosi Bay (1500 mm per year) (Tinley, 1985; Wright, 1999). Martonne's Index of Aridity ( $P/(T+10)$ ) attributes a score of 41 for Cape St.-Lucia, which makes this region the wettest area of the coast of southern Africa (Tinley, 1985).

## II.3. Oceanography

### II.3.1. Swell and wave regimes

The swell and wave regimes affecting the northern KwaZulu-Natal coast show negligible seasonal differences in height and direction (Rossouw, 1984). Large amplitude swells from the southeast dominate the northern KwaZulu-Natal coast approximately 40 % of the year (Figures II.5 and II.6). They originate by continental refraction of the southwest swell generated in the "Roaring Forties" (Van Heerden & Swart, 1986). Northeasterly to easterly low amplitude and short period swells prevail for a further 40 % of the year. These are generated by anticyclonic easterly winds (Davies, 1964).

The northern KwaZulu-Natal coastline represents a moderate to high wave energy environment. At Richards Bay, 72 % of the year is characterised by waves with heights of 1 to 2 m. Waves higher than 2 m (max. 5 m) are experienced for ca. 14 % of the year (Rossouw, 1984). Slightly higher waves are observed at Cape St.-Lucia and northwards (Figure II.6).

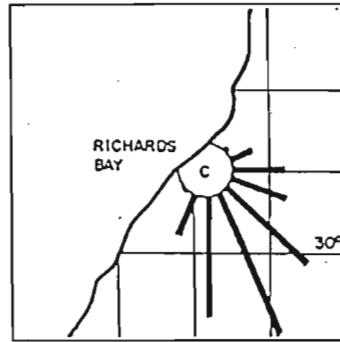


Figure II.5. Wave direction distribution recorded from deep sea clinometer data for Richards Bay (Rossouw, 1984).

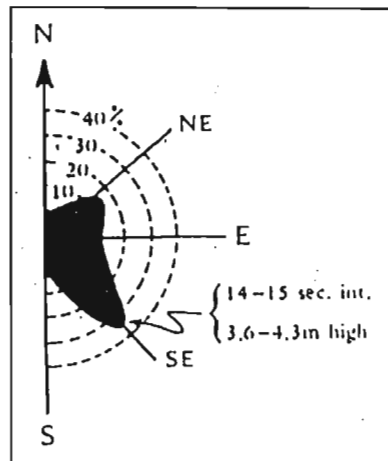


Figure II.6. Swell observations (direction and height) at Cape St.-Lucia (Begg, 1978).

### II.3.2. Tides

At Richards Bay, the mean spring tidal range is 1.80 m and the neap tidal range is 0.52 m. The difference between the highest and lowest astronomical tides is 2.48 m (Hayes, 1979). The northern KwaZulu-Natal coastline can therefore be classified as an upper microtidal type (Davies, 1964) or a lower mesotidal type (Hayes, 1979). The tide and wave regimes imply a wave-dominated coastal sedimentary environment, characterised by a single beach berm (Tinley, 1985).

### II.3.3. Ocean currents and sediment drift

The Agulhas Current is a major geostrophic current generated by large scale counter-clockwise circulation in the Indian Ocean. Passing through the Mozambique Channel, it brings warm equatorial waters immediately offshore of the shelf break to the eastern and southeastern coasts of southern Africa (Figure III.2) (Schumann, 1988). Surface velocities can exceed 2 m/s (Schumann, 1988), inducing net southward bed load transport along the middle and outer shelf (Flemming & Hay, 1988; Ramsay, 1994). Changes in the coastline orientation produce multiple cyclonic eddies in the bight between Durban and Cape St.-Lucia (Malan & Schumann, 1979), inducing some northward flowing nearshore currents (Flemming, 1981). Offshore of the study area, located at the northern edge of this bight, the Agulhas Current is present (Flemming & Hay, 1988), however no studies have established if the nearshore eddie currents reach the St.-Lucia area (Figure III.2).

As a result of the predominant southeasterly wave approach, the dominant littoral sediment drift along the southern part of the KwaZulu-Natal coastal plain is towards the north with a calculated mean flux at Richards Bay of  $0.8 \times 10^6 \text{ m}^3$  per year (Swart, 1980). Van Heerden & Swart (1986) gave a value of  $10^6 \text{ m}^3$  per year just south of St.-Lucia. Cooper (1991a) noted that these calculations take no account of sediment availability and grain size, and that these values must only be regarded as potential rates. Only when a northeasterly wind blows for a considerable period does it generate a corresponding swell regime (Ramsay *et al.*, 1989), which results in a reversal of longshore sediment transport (Davies, 1964).

## II.4. Quaternary palaeoclimatology and sea level changes

The Cenozoic Era is characterised by a progressive decrease in seafloor spreading activity, global sea level fall (from 150 - 180 m above msl in Cretaceous) and by a decrease in global temperature (GSC, 1990). Overall, the Cenozoic was a time of global cooling with significant ice volume increase in Antarctica during the Oligocene (Brown *et al.*, 1992). By the beginning of the Quaternary, continental ice sheets had expanded to reach the present situation.

During the Quaternary, long term cyclic changes in ocean circulation, atmospheric composition and amount of solar radiation received by the Earth initiated a series of long glacial and shorter interglacial periods. Their periodicity has progressively decreased since the beginning of the Quaternary to reach a little more than 100 000 years for the last cycle

(Milankovitch, 1938; Fairbridge, 1983). The Holocene is characterised by an interglacial climate, while glacial periods are defined by a colder climate, an expansion of continental ice cover and a resulting lower sea level (Foucault & Raoult, 1995). This section will focus mainly on the last two glacial – interglacial cycles.

Global temperature changes can be extrapolated from oxygen isotopes measured on foraminifera tests (GSC, 1990). A relative chronostratigraphic scale has been built using the changes of the oxygen isotope ratios (Climap Project Members, 1984). The last interglacial - glacial cycle has been subdivided into five isotopic stages using two deep sea cores from the equatorial Atlantic and Pacific Oceans that present the same overall global trend (Figure II.7). Isotope stages with even numbers reflect cooler periods, while stages with odd numbers characterise warmer interglacial or interstadial periods. The Holocene represents the oxygen isotope Stage 1 (Figure II.7).

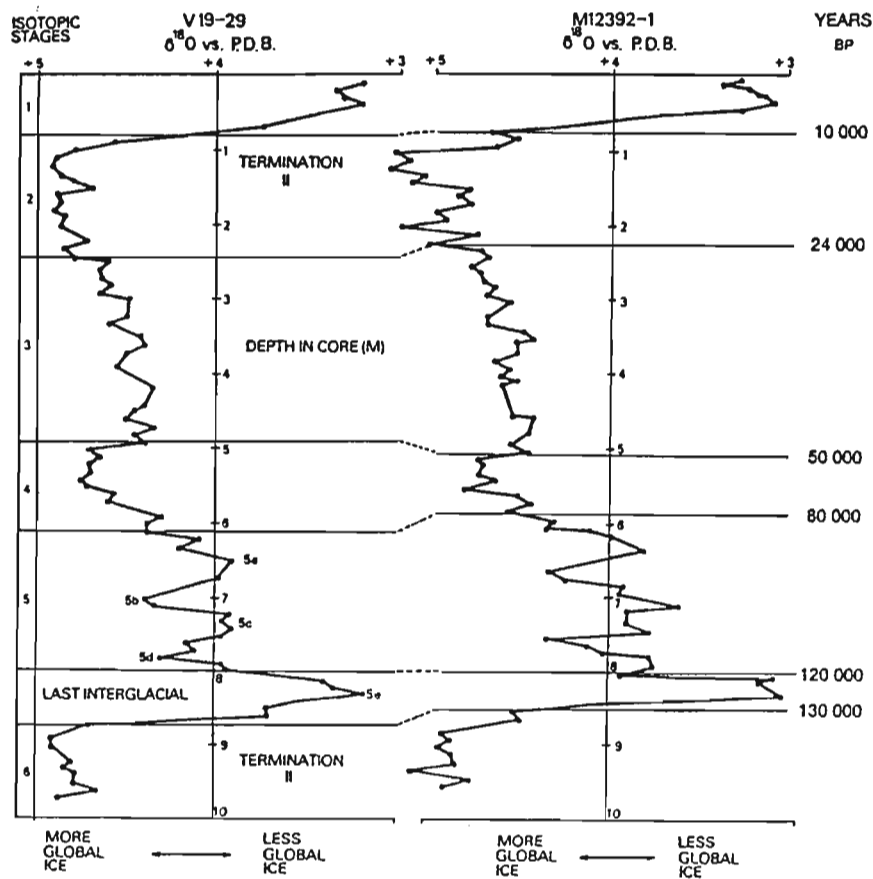


**Figure II.7.** Oxygen isotopic record from Pacific core V19-29 and Atlantic core M12392-1. Marked changes in isotopic ratios define the limits between isotope stages and substages (Climap Project Members, 1984). Isotope stages referred to in the text are defined in the left-hand column.

Global sea level changes can also be extrapolated from oxygen isotopes measured on foraminifera tests (GSC, 1990). Sea level variations over the last 240 000 years, place the last interglacial peak (oxygen isotope Stage 5) at about 125 000 years before present (B.P.) (marking the Middle – Late Pleistocene limit (Haq & Van Eysinga, 1987)) and the last peak of the penultimate interglacial (oxygen isotope Stage 7) at ca. 200 000 BP. (Figure II.8). During the two last glacial periods, progressively decreasing temperatures and regressive sea levels

preceded rapid warming and associated marine transgressions (Figure II.8). In the following chapters the penultimate interglacial and glacial periods will be referred as oxygen isotope Stages 7 and 6 respectively (Figures II.11 and II.8). During the Middle Pleistocene, three possible interglacial periods are identified at ca. 330 000 B.P. (oxygen isotope Stage 9), 420 000 B.P. (oxygen isotope Stage 11) and 520 000 B.P. (oxygen isotope Stage 13) (Figure II.11).

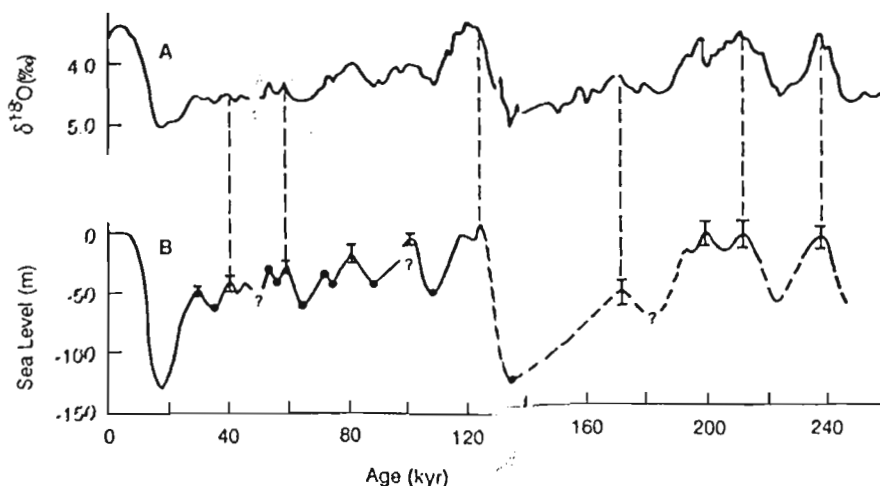


**Figure II.8.** Correlation between oxygen isotope and global sea level changes (GCS, 1990). (A) Isotopic data from the equatorial Pacific core V19-30. (B) Sea level curve from marine terraces of the uplifting Huon Peninsula (Chappell & Shackleton, 1986).

A Late Quaternary sea level curve for southern Africa has been compiled by Ramsay (1997) using dating of preserved beachrocks and marine planation episodes (Figure II.9). Two palaeocoastlines at -55 and -17 m below msl on the KwaZulu-Natal shelf have been radiometrically dated at 41 000 and 84 000 years B.P. respectively (Felhaber, 1984; Ramsay, 1994). The ages of these two sea levels correlate with global and local trends (Figures II.8 and II.9). The last interglacial high stands characterise the early – middle stage of the oxygen isotope Stage 5, representing a period between ca. 125 000 and 95 000 B.P. (compare Figures II.8 and II.9).

Ramsay (1995) further refined the relative sea level curve for southern Africa in the Holocene (Figure II.10). From the last glacial maximum at ca. 18 000 B.P. (Figure II.9), sea level rose rapidly from -130 m below msl to reached the present level at ca. 7000 B.P., and culminated at 3.5 m above msl at 4480 B.P. (Figure II.10). This Middle Holocene high stand is associated with the Climatic Optimum described by Tyson (1986). Sea level then lowered to -2 m below msl approximately 3000 B.P. before rising to 1.5 m above msl at 1610 B.P, reaching its present level ca. 900 B.P. (Figure II.10).

The southeast African sea surface temperature (SST) pattern does not present a regular decreasing trend for the last glacial cycle (Figure II.11). A weaker Agulhas Current replaced seasonally by an upwelling cooler current explains the sharp decrease in SST (Figure II.11) (Heydon and Tyson, 1980; Howard, 1985). During the last glacial maximum (18 000 B.P.), the SST was 5° C lower than today, implying dry summer conditions as cold inshore surface waters inhibit rain (Heydon and Tyson, 1980). Moreover, Howard (1985) estimated that the pressure systems shifted northward (towards the equator) about 3° to 8° during the last glacial maximum. Increased temperature gradients associated with this latitudinal shift are implied to have intensified wind activity.

Palaeoclimatic reconstruction on land is based on evidence from different sources. In northern KwaZulu-Natal, the Middle – Late Pleistocene climatic evolution has been best recorded in Border Cave, eastern border of Swaziland (Deacon & Lancaster, 1988). Table II.1 summarises the palaeoenvironments inferred from micromammalian analysis, and shows that the last glacial maximum (ca. 29 000 to 13 000 B.P.) was characterised by the least vegetation cover. This period was thus most favourable for aeolian reworking as the sea level was low, wind velocity was high and vegetation cover minimal.

**Table II.1.** Border Cave palaeoclimatic inferences based on micromammalian analyses (Avery, 1982).

Level	Approximate age (years BP)	Interpretation
Level 1a	700 BP to present	Limited grit production. Modern conditions of sedimentation and climate. Iron age occupation.
Hiatus	c. 13 000-700	
Level 1b	c. 29 000-13 000	Moderate éboulis and grit production. Moderate frost weathering. Climate cool to cold, possibly dry.
Hiatus	c. 33 000-29 000	
Level 2-3	c. 38 000-33 000	Important éboulis horizon. Effective frost weathering. Climate cold, possibly wet. Early Later Stone Age occupation.
Hiatus	c. <49 000-39 000	
Level 4		Limited grit production. Climate similar to present, possibly wetter. Late Middle Stone Age occupation.
Hiatus	c. 57 000	
Level 5a		Moderate grit production. Climate cooler and very dry.
Level 5b		Major éboulis horizon. Effective frost weathering. Climate cold, possibly wetter. Late Middle Stone Age occupation.
Hiatus	c. 69 000	
Level 6-7a		Minimal grit production. Climate warmer or drier. Unoccupied at first, then Middle Stone Age.
Level 7b-8		Major éboulis horizon. Maximum effectiveness of frost action, becoming less with time. Climate cold, initially wetter. Howiesons Poort occupation.

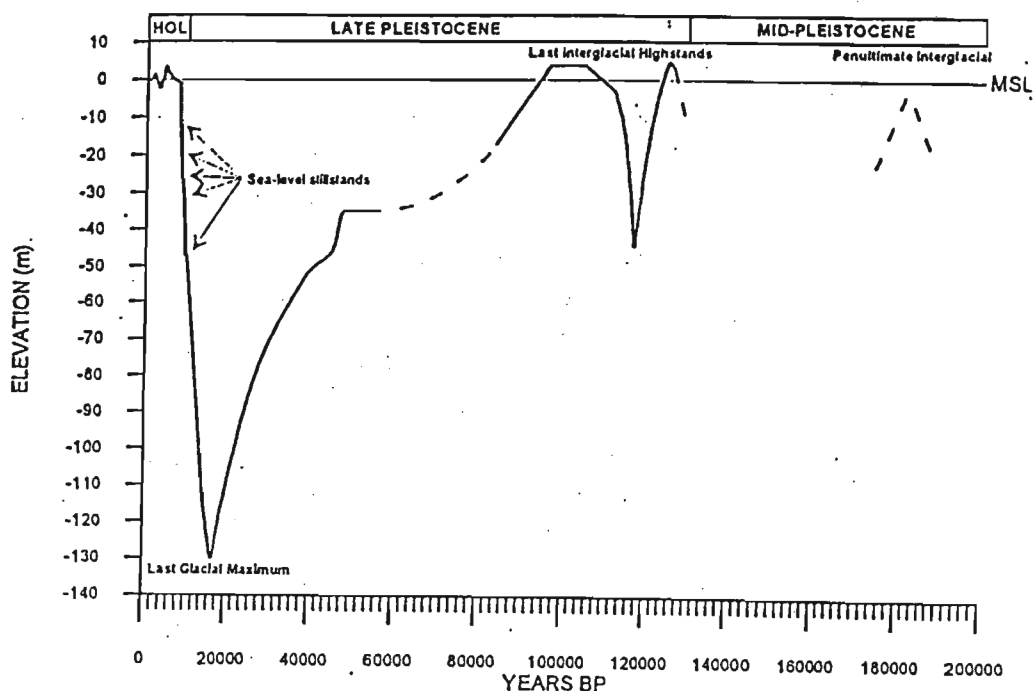


**Figure II.9.** Late Quaternary sea level curve for southern Africa (Ramsay, 1997).

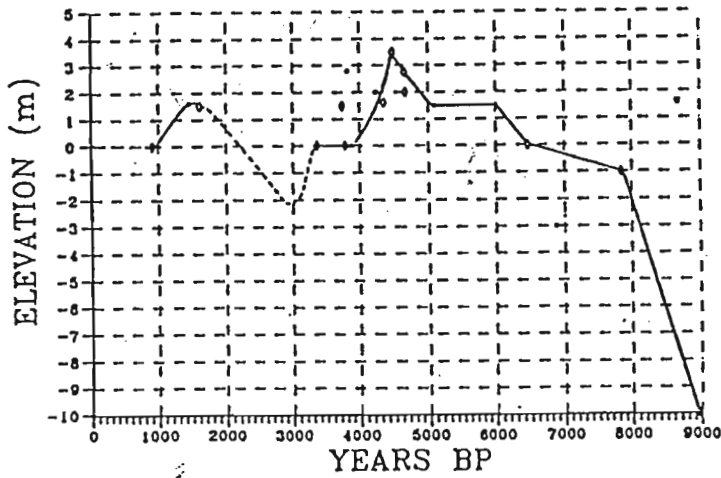


Figure II.10. Holocene sea level curve for southern Africa (Ramsay, 1995).

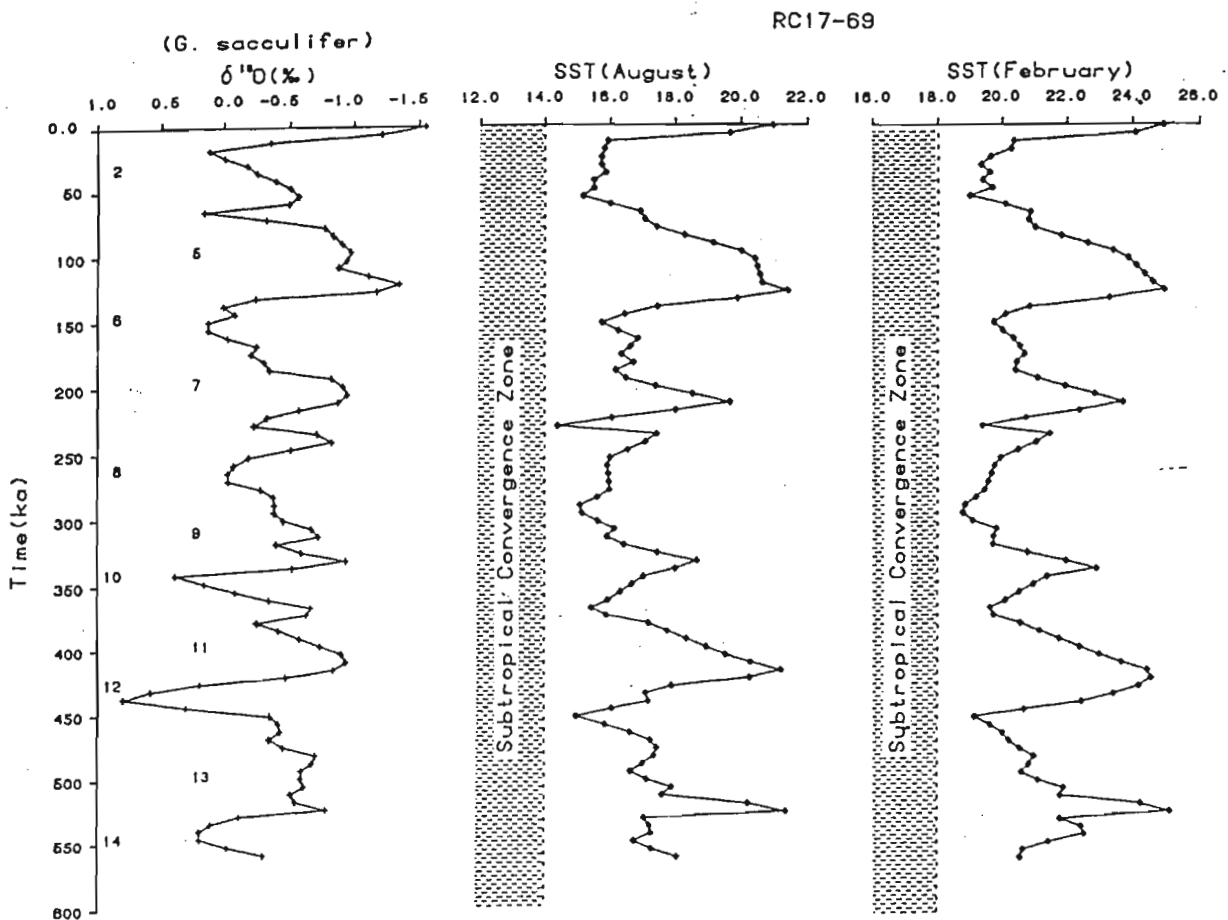


Figure II.11. Oxygen isotopes and calculated changes in local sea surface temperature (SST). Data from the deep sea core RC17-69, offshore Durban (Howard, 1985). Numbers on the oxygen isotope curve refer to isotope stages.

## III. REGIONAL GEOLOGY

The northern KwaZulu-Natal coastal dune cordon contains abundant economic minerals, derived from diverse sources. The nature and volume of sediments delivered to the coastline is controlled by climatic and anthropogenic factors, the geology of the river catchments and by the nature of the nearshore environments. River catchments in southeast Africa comprise rocks and unconsolidated sediments ranging from Archaean to Quaternary in age.

This section presents a regional geological history, combined with a description of the rocks and sediments underlying and/or surrounding the study area (Figure III.1). The region considered is defined by the catchment areas of the rivers that are thought to influence the mineralogy and geochemistry of sediments in the study area (Figure III.2). Marine cyclonic eddies cause partition zones for the coastal sediment (Flemming, 1981; Section II.3.3). The most important fluvial sediment supply to the study area is from the Tugela River and the Mfolozi – Mkuze Rivers (Figure III.2). The Tugela River has the largest catchment area and is the main sediment supplier to the coast in KwaZulu-Natal (Figure III.2). Note that the characteristics of the Mhlatuze River and Nhlabane River are not described in Figure III.2 as the fluvial input to the shelf from these two rivers is insignificant.

### III.1. Archaean

#### III.1.1. Kaapvaal Craton

The Kaapvaal Craton represents one of the earliest Archaean crystalline massifs on Earth. It is located in the central and northeastern part of South Africa, and is amalgamated in the north with two other Archaean provinces, the Limpopo Belt and the Zimbabwe Craton.

Outcrops comprise granitoids and gneisses with deformed greenstone relicts of basic and ultrabasic volcanic (amphibolites) and sedimentary sequences, belonging to the Swaziland Supergroup and the approximately 3.55 Ga Ancient Gneiss Complex (Tankard *et al.*, 1982). This massif was intruded by tonalite/trondhjemite (3.2 Ga) and granitoid (3.0 Ga) plutons.

#### III.1.2. Pongola Supergroup

The earliest evidence of cratonization of the Kaapvaal Craton is seen in the accumulation of the epicontinental Pongola Supergroup, subdivided into two groups. The Nsuze Group is characterised by volcanics (basaltic lavas, 3.09 Ga) and minor sediments (sandstones and carbonates). Shelf and fluvial sedimentation form the overlying Mozaan Group (2.9 Ga), which is comprised of conglomerates, sandstones, shales and minor banded ironstones. Late intrusions of layered gabbros (Usushwana Intrusive Suite) and granitoids indicate the end of the basin infill (Beukes & Cairncross, 1991).

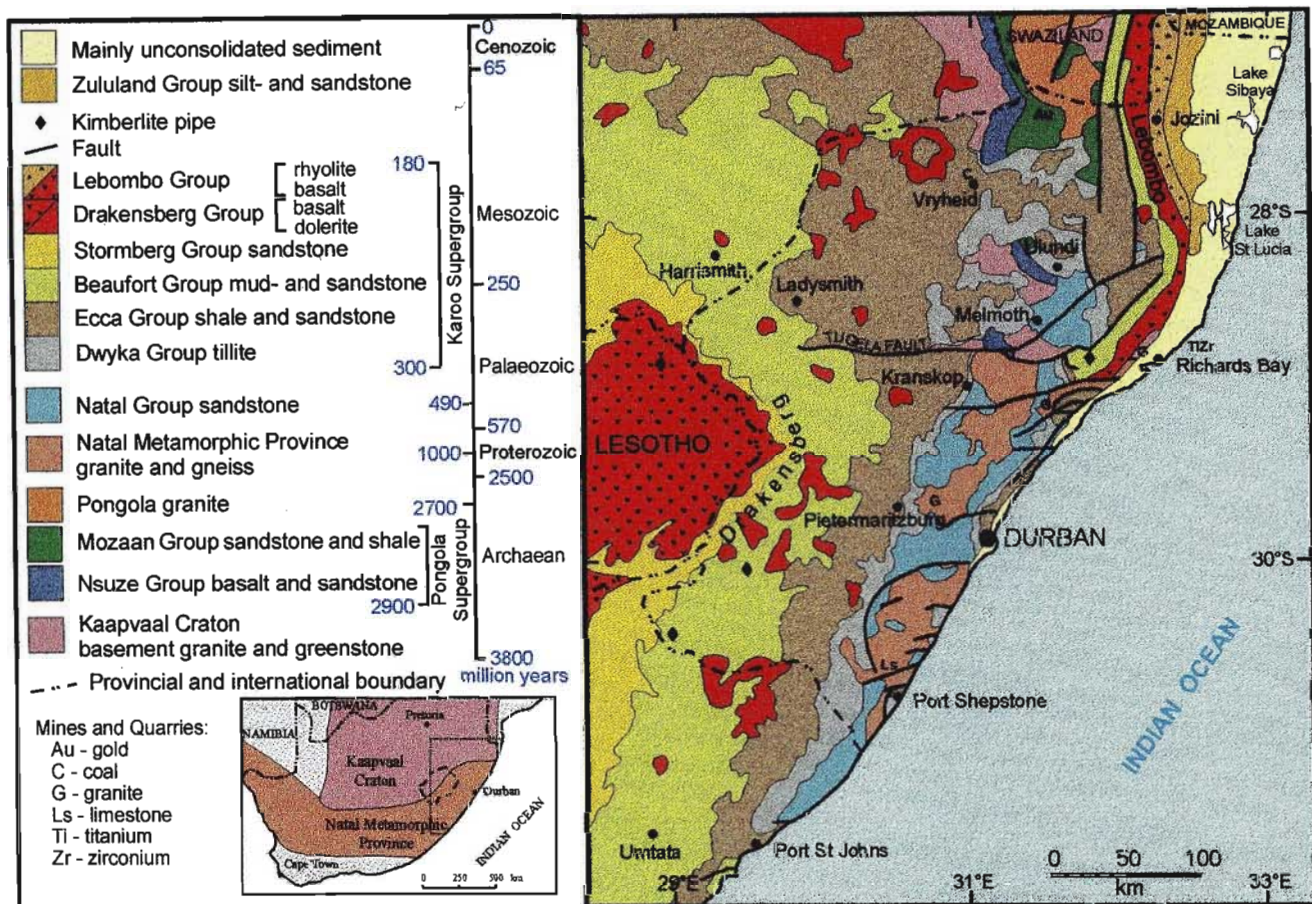
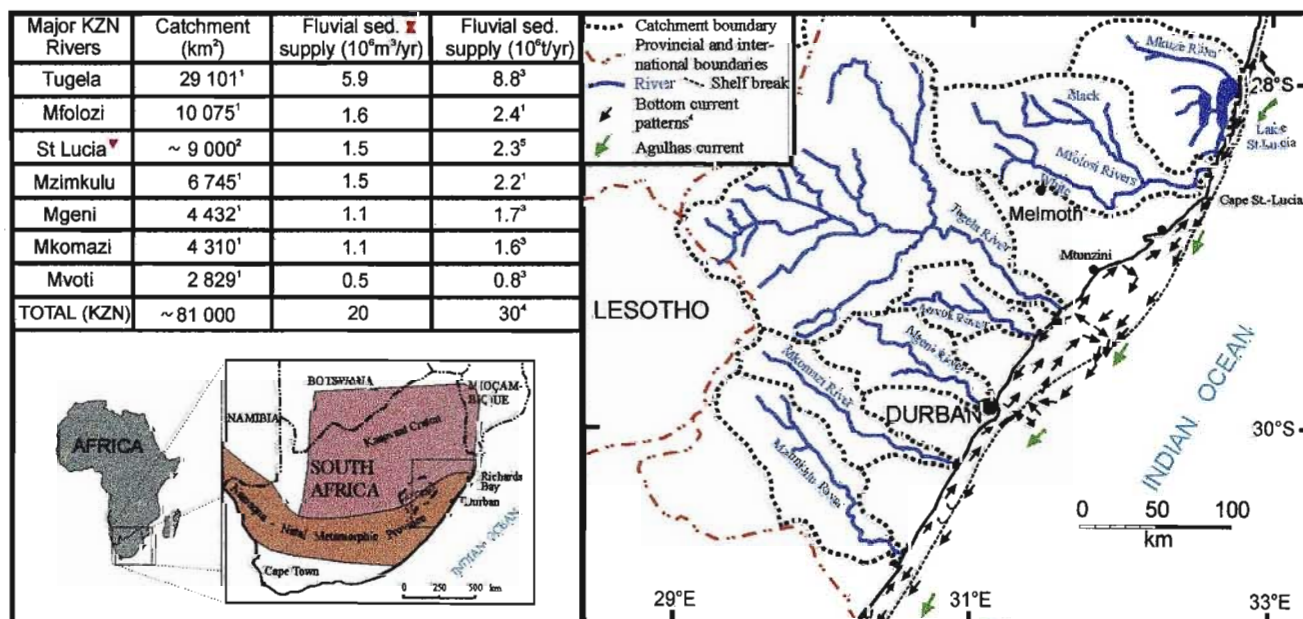


**Figure III.1.** Regional geology within the catchment area of KwaZulu-Natal rivers (see Figure III.2) (from Whitmore et al, 1999).



▼ Main river is the Mkuzi River but smaller fluvial inputs from the Mzinene, Hluhluwe, Nyalazi & Mpate Rivers. ✕ <sup>1</sup>Conversion from t to m<sup>3</sup> = 1.5 t/m<sup>3</sup>

**Figure III.2.** Catchment areas and characteristics of major KwaZulu-Natal rivers (from Ware, in prep.).

## III.2. Proterozoic

### III.2.1. Natal Metamorphic Province

Mesoproterozoic (1.2 to 1.05 Ga) tectonism along the southern margin of the Kaapvaal Craton gave rise to the Natal Metamorphic Province (Tankard *et al.*, 1982; Basson, 1997). Collision between the southern margin of the Kaapvaal Craton and a plate or sub-plate to the south produced a series of allochthonous nappe sheets that were obducted onto the Kaapvaal Craton (Matthews, 1981). These comprise ophiolites and ocean floor material, geosynclinal sequences, accreted island arcs and para-autochthonous granite-gneiss basement (Thomas, 1989).

Thomas (1988, 1989) subdivides the Natal Metamorphic Province into three stratigraphic units: the northern Tugela Terrane (amphibolite, biotite-, hornblende-, plagioclase- and quartz-feldspar gneiss, and magnetite quartzite), the central Mzumbe Terrane (amphibolite-grade gneisses and schists, together with pre- to syn-tectonic granitoid-gneisses) and the southern Margate Terrane (granulite-grade supracrustal gneisses, intruded by granitoid plutons).

Suturing of the Natal Province to the Kaapvaal Craton, along with other crustal components, formed a super craton known as the Kalahari Province, whose outline correlates closely with the present southern Africa (Tankard *et al.*, 1982).

At the end of the Proterozoic, a third period of continental amalgamation formed the Gondwana supercontinent.

## III.3. Palaeozoic - Mesozoic

### III.3.1. Natal Group

During the Early Palaeozoic southern Africa lay at the heart of Gondwana, bounded to the east by Antarctica. Failed rifting resulted in accumulation of continental and marine clastic successions in elongate troughs, to form the Cape Supergroup (Tankard *et al.*, 1982), and in KwaZulu-Natal, the Natal Group (Partridge & Maud, 1987). This Cambrian to Ordovician Natal Group consists predominantly of quartz sandstone, with a basal conglomerate and minor arkosic sandstone, siltstone and shale. Its thickness varies greatly (from a few metres to over 600 m). Although the Natal Group is generally resistant to erosion and forms steep cliffs, it is deeply weathered in places due to prolonged tropical and sub-tropical weathering since the Miocene (Partridge & Maud, 1987).

### III.3.2. Karoo Supergroup

By the Late Carboniferous – Early Permian Period, Gondwana migration towards the northwest placed the KwaZulu-Natal region close to the south pole (Linström, 1987). At this time an extensive ice sheet deposited a massive tillite containing large quartzite, gneiss and schist erratics. Along with intercalated shaley beds, these sediments form the Dwyka Formation (SACS, 1980). This has recently been changed to the Dwyka Group (Figure III.1).

As Gondwana migrated northwards the ice sheet receded and the Ecca Sea invaded a giant intracratonic basin (Tankard *et al.*, 1982). Along the eastern seaboard of southern Africa, progressive infill of this basin is illustrated by the Ecca, Beaufort and Stormberg Groups (Dingle *et al.*, 1983). They consist of shale, siltstone and sandstone from lacustrine, lagoonal or marginal marine, to deltaic, fluvial and aeolian environments, showing increasingly arid conditions (Ryan & Whitfield, 1979; Hobday, 1979; Tavener-Smith *et al.*, 1988).

Prior to the fragmentation of Gondwana, magmatic activity affected the region (Tankard *et al.*, 1982). Thick successions of Late Triassic to Jurassic tholeiitic basalt (Drakensberg Group) covered large areas of the continent. Only small erosional remnants of this once extensive group are present today (Eales *et al.*, 1984).

Precursor rifting during the Early Jurassic to Early Cretaceous produced north-south rifts into which basalt and rhyolite (Lebombo Group) built a thick succession (Dingle *et al.*, 1983; Wolmarans & Du Preez, 1986). Associated with these volcanic rocks are abundant dykes and sills of dolerite and gabbro, which commonly intrude the sedimentary rocks of the Karoo Supergroup (Eales *et al.*, 1984).

### III.3.3. Zululand Group

The initial outline of the southern African coastline was generated by the rifting processes involved in the fragmentation of Gondwana (Dingle *et al.*, 1983; Martin & Flemming, 1988). Rifting and breakup of Gondwana along the proto-coastline of Mozambique and northern KwaZulu-Natal (177-175 Ma) gave rise to extensional faulting of north-south and northeast-southwest directions. This created a series of tilted fault blocks which constitute the basement of the present coastal plain (Partridge & Maud, 1987; Watkeys *et al.*, 1993).

This horst and graben development favoured rapid taphrogenic sedimentation, of terrestrial conglomerates and sandstones, overlain by fossiliferous marine siltstones (Wolmarans & Du Preez, 1986). These Early Cretaceous sediments form the Makatini Formation.

The overlying Early-Late Cretaceous Mzinene Formation consists of shallow marine glauconitic siltstones, sandstones with calcareous concretions, and limestones beds (Wolmarans & Du Preez, 1986).

The fossiliferous Late Cretaceous St.-Lucia Formation consists of a basal conglomerate that is overlain by a succession of cross bedded fine sandstones and siltstones, with abundant glauconitic beds and hardgrounds (Kennedy & Klinger, 1975; Dingle, 1981; Watkeys *et al.*, 1993). Palaeocene sediments of the St.-Lucia Formation are only present close to the coast, around Richards Bay (Maud & Orr, 1975) (Figure III.4).

The Makatini, Mzinene and St.-Lucia Formations form the Zululand Group, which underlies the present coastal plain. Its thickness increases eastward (seaward) and towards the northeast

(Wolmarans & Du Preez, 1986), suggesting an asymmetrical opening of the Indian Ocean. This is confirmed by the contemporary presence of a positive relief region in the southwest, the "Transkei swell" (in Eastern Cape) (Simpson & Dingle, 1973). This feature effectively separated faunas of the Zululand and Algoa-Agulhas basins until the Late Cretaceous (Simpson & Dingle, 1973). Except for few isolated outcrops, the Zululand Group is overlain by Quaternary deposits and has been primarily documented from coastal plain boreholes (Figures III.4 and III.5).

### III.4. Cenozoic

Tertiary sedimentary rocks are strikingly absent in the southern KwaZulu-Natal coastal plain. Two Tertiary sequences (Eocene and Early Miocene), resting unconformably on the Zululand Group, were discovered east of Lake Sibayi by drilling (Meyer, 1997). These deposits are mentioned below as "Tertiary Sequences".

The Late Tertiary eustatic regression exposed the coastal platform, inducing the erosion of the Zululand Group and "Tertiary Sequences". The elevation of the top of the "Tertiary Sequences" has been determined at -30 m below msl at the Lake Sibaya coastline (Pitman & Hutchinson, 1975; Meyer, 1997). In the Richards Bay area Maud and Orr (1975) located the elevation of the top of the Zululand Group at various levels. They nevertheless observed a decreasing trend in elevation: from 2 m above msl inland, to -10 m below msl at the coastline (Figure III.4).

These considerations lead to the conclusion that the Tertiary crustal evolution is different for the northern and southern parts of the KwaZulu-Natal coastal plain.

The nature and location of the boundary between these two regions is not precisely documented. However, from geophysical and borehole data Meyer (1997) highlighted the presence of a north-south striking, normal fault of post Uloa Formation age within the northern KwaZulu-Natal coastal plain. The downthrow side is to the east with a displacement of 15 to 50 m. This fault has not been observed in the southern part of the KwaZulu-Natal coastal plain.

#### III.4.1. Maputaland Group

The stratigraphic nomenclature of the Miocene to Recent Maputaland Group is in a state of flux as attempts are made to resolve the complexities of repeated marine transgressions and marked lateral variations. Moreover the dating of events and depositions is not clear, as many authors attribute different ages to the same lithology. Nevertheless, in order to structure and to allow future comparisons, these lithologies will be grouped into formations, whose nomenclature and age are proposed by the latest (but informal) stratigraphic subdivision (Botha, 1997a) (Figure III.3).

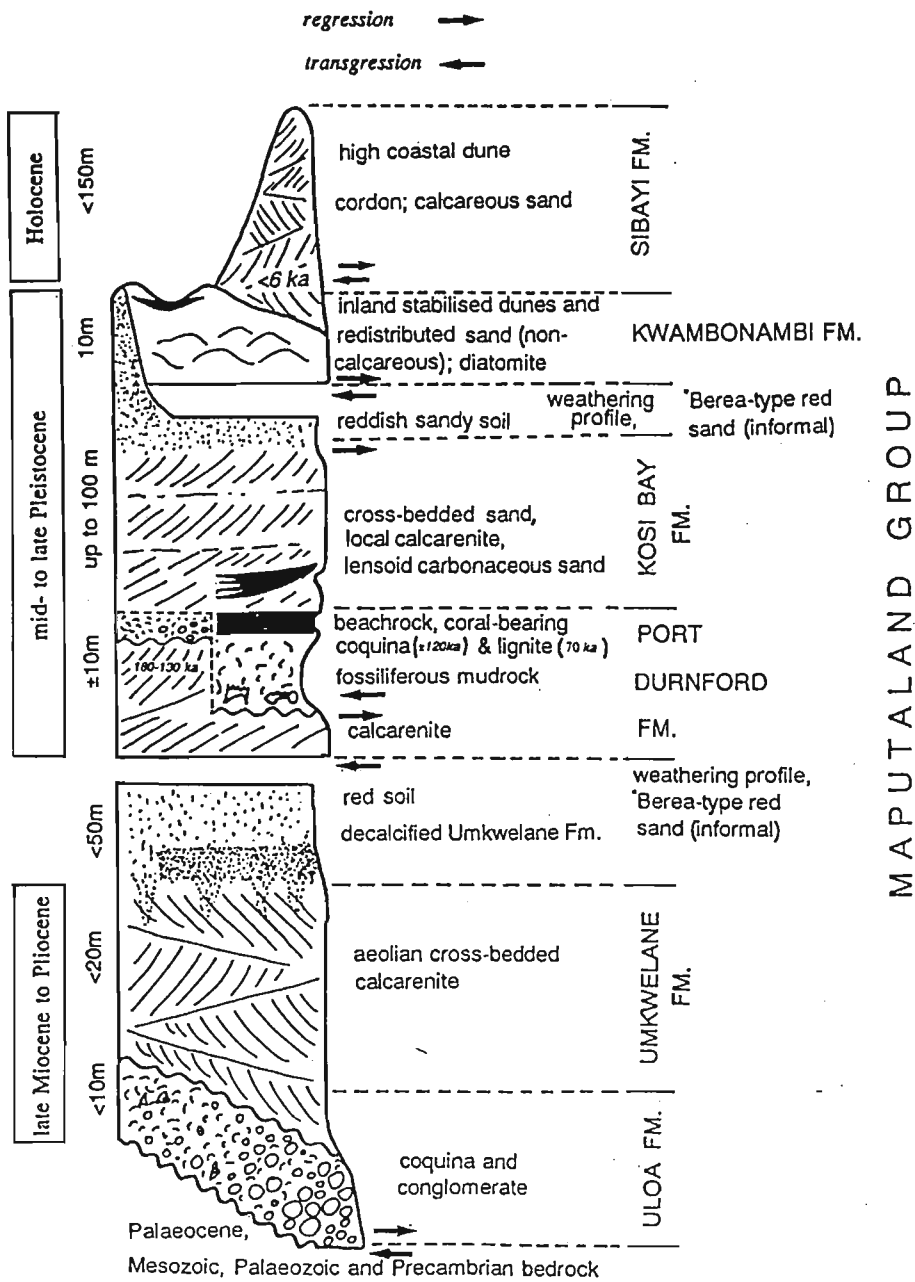


Figure III.3. Lithostratigraphy of the Maputaland Group (from Botha, 1997a). Ages and lateral correlations have to be considered with caution (see Section III.4.1 for discussion).

### III.4.1.1. Uloa Formation

Following a long period of erosion a short marine transgression restarted sedimentation on the southern part of the KwaZulu-Natal coastal plain. This event is believed to be of Late Miocene age by many authors (Watkeys *et al.*, 1993; Liu, 1995; Stewart, 1998). A basal Nodule Bed (conglomerate), Pecten Bed (glauconite-rich and fossiliferous calcrudites), also called the Coquina, as well as overlying calcarenites and algal limestones, constitute the thin Uloa Formation (Dingle *et al.*, 1983; Stewart, 1998) (Figure III.3). The Uloa Formation is highly leached and iron stained on top (Maud & Orr, 1975).

III.4.1.2. Umkwelane Formation

The Umkwelane Formation is up to 4 m in thickness and consists of hard light grey calcarenite (Figure III.3). With the exception of the coarser base (representing a beach or marine facies), the depositional environment of this formation is aeolian. When present, these calcarenites are always separated from the Uloa Formation by a marked lithological break (Maud & Orr, 1975). The age of the Umkwelane Formation is under debate, but is generally attributed to the Early Pliocene (Dingle *et al.*, 1983, Botha, 1997a). The top of the formation is karstified.

The Tertiary unconformity beneath the Uloa and Umkwelane Formations is the most significant in relation with the morphology development of the KwaZulu-Natal coastal plain as it presently exists (Maud & Orr, 1975).

The sporadic distribution of these two formations on the platform led Maud and Orr (1975) to propose another major period of erosion, solution weathering and karst development of post-Early Pliocene age (Figure III.4). This type of weathering is correlated with the inland and coastal outcrops of several "Berea-type red sands" (Maud, 1968; Botha, 1997a).

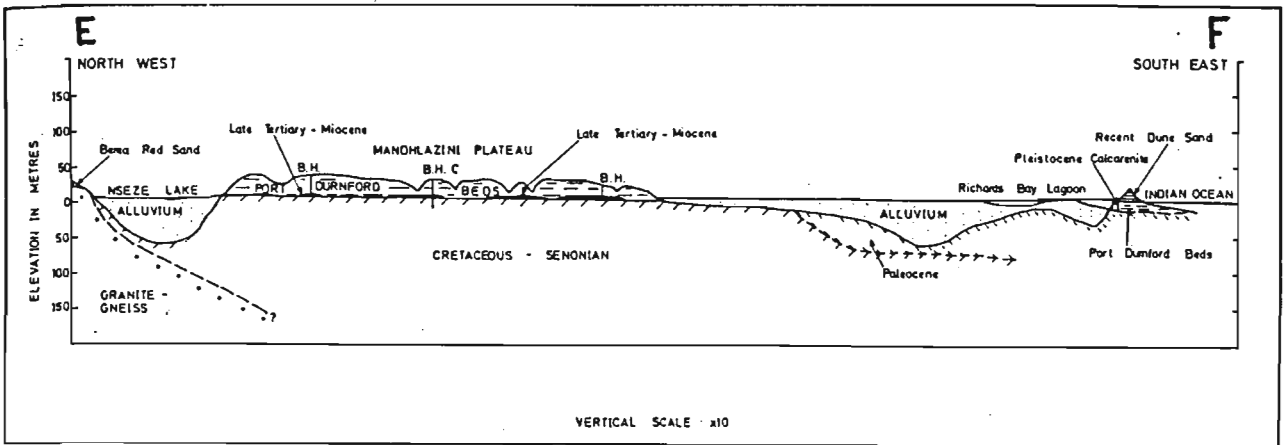


**Figure III.4.** Geological section across the southern part of the KwaZulu-Natal coastal plain, near Richards Bay (from Maud & Orr, 1975). "Late Tertiary – Miocene" sediments refer to the Uloa and Umkwelane Formations. "Port Durnford beds" of Maud and Orr (1975) refers to the Port Durnford and the Kosi Bay Formations (see text). See Figure II.1 for the location of the section.

III.4.1.3. Port Durnford Formation

The latest informal stratigraphic subdivision (Botha, 1997a) of the coastal dune cordon along the southern part of the KwaZulu-Natal coastal plain identifies four formations: the Port Durnford Formation, the Kosi Bay Formation, the KwaMbonambi Formation and the youngest Sibayi Formation. The following description of these four formations, unless noted otherwise, is restricted to lithologies outcropping in coastal cliffs north and south of Richards Bay (Figure II.1).

The lower part of the Port Durnford Formation in the Richards Bay area consists of coarse beach rocks (Pleistocene Calcarenes of Maud and Orr, 1975; "calcarene" in Figure III.3) at a depth varying between 0 m and -4 m below msl (Botha, 1997a). According to Maud and Orr (1975), these rocks are of Pleistocene age and rest on Palaeocene sediments (Tertiary Sequences described in Section III.4) (Figure III.4). Locally however, these authors noted that the Pleistocene Calcarenes overlie the Lower Argillaceous Member of Hobday and Orme (1974) ("fossiliferous mudrock" in Figure III.3; see below). The thin but strongly bedded Pleistocene Calcarenes are unconformably overlain by a reddish sandstone containing fossil mammalian fauna that suggests a Tertiary age (Anderson, 1907) (base of the "fossiliferous mudrock" in Figure III.3). Nevertheless, by comparison with species from the "younger" Vaal gravels, Du Toit (1954), reassigned the fauna described by Anderson to the late Middle Pleistocene age. According to Maud and Orr (1975), this reddish sandstone has disappeared under wave attack erosion during the last century. It has not been observed elsewhere, either on coastal outcrops or in boreholes.

The upper part of the Port Durnford Formation consists of a 10 m thick marine and terrestrial fossiliferous, grey and black mud with sandy laminae defined as the Lower Argillaceous Member by Hobday and Orme (1974) ("fossiliferous mudrock" in Figure III.3). This is overlain by a consistent 0.2 to 2.5 m thick lignite horizon, the Lignite Bed of Hobday and Orme (1974) (Figure III.3).

At Port Durnford (Figure II.1) the Lower Argillaceous Member is described by Maud (1968) as a "basal blue grey sandy mudstone unconformably overlain by a mottled yellow brown and ferruginised sandstone". This contrasts with the description of the same unit by Hobday and Orme (1974).

Boreholes in the Richards Bay area showed that the Lower Argillaceous Member and the Lignite Bed are present only in the immediate vicinity (less than 3 km) of the present coastline (Fockema, 1986). Their basal contact is estimated at less than -8 m below msl (Maud & Orr, 1975). Inlandward, the Lower Argillaceous Member disappears before the Lignite Bed, which is still present 6 km away from the coastline at Lake Nhlaba (Figure III.5, section C-D). In other places, the reverse sequence is observed (Figure III.5, section A-B).

The previous discussion suggests that the Port Durnford Formation is actually composed of laterally discontinuous units of mixed facies and various ages. Lithostratigraphy within this formation is at least approximate.

#### III.4.1.4. Kosi Bay Formation

Aeolian sands (with local washover sediment at the base) up to 15 m in thickness overlie the Port Durnford Formation. These sediments are intercalated locally with clayey, carbonaceous lenses and lignite beds, and were defined as the Upper Arenaceous Member by Hobday & Orme (1974).

Botha (1997a) recommended that the Port Durnford Formation should be restricted to the beds of the Lower Argillaceous Member and the Lignite Bed, and the overlying Upper Arenaceous Member be renamed the Kosi Bay Formation (Section III.4.1.5 and Figure III.3).

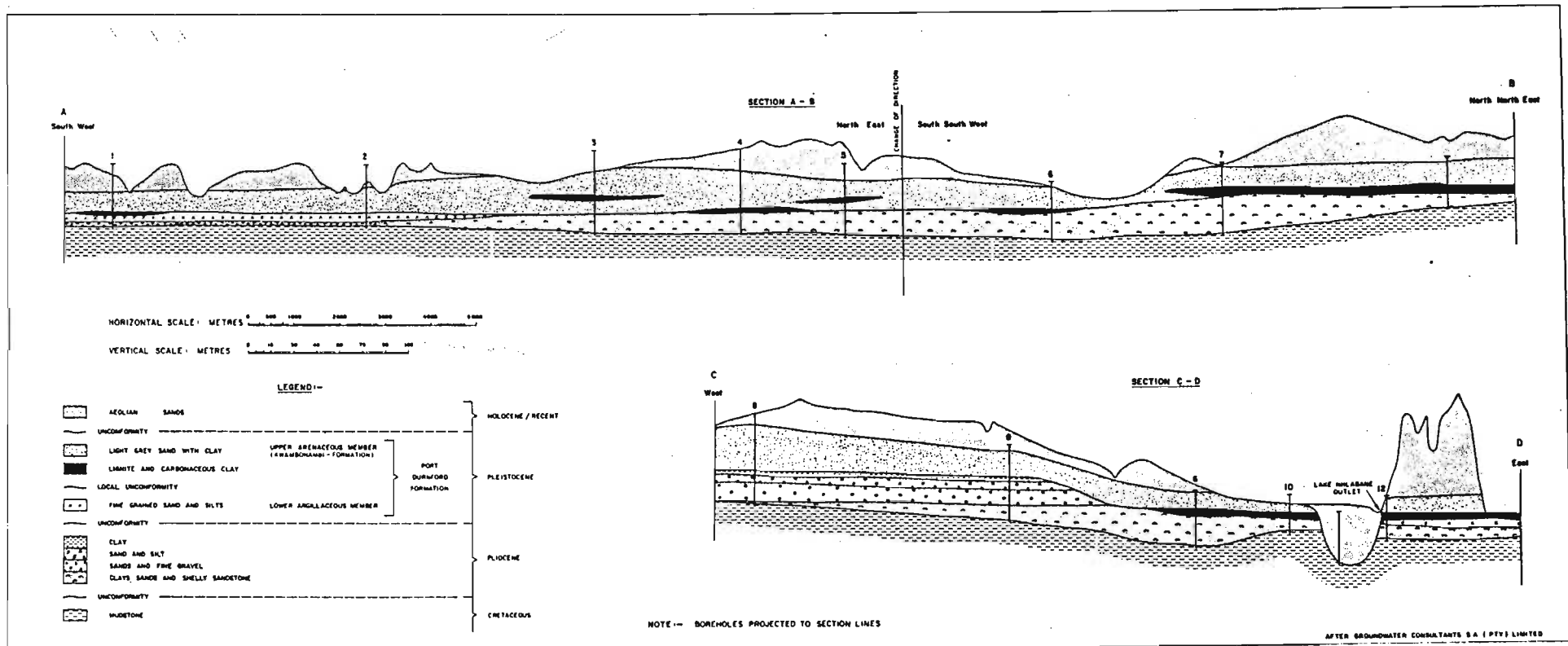


**Figure III.5.** Geological sections near Lake Nhlabane (from Fockema, 1986). Pliocene sediments might refer to the Uloa and Umkwelane Formations. Note that Fockema (1986), named the Port Durnford Formation as historically defined by Hobday and Orme (1974). See Figure II.1 for the location of the sections A-B and C-D.

As observed along the shoreline around Richards Bay, the colour of the semi-consolidated Kosi Bay Formation is typically white to light grey because of its high kaolinite content (10 %) and low heavy mineral abundance (less than 3 - 4 %). This colour grades upwards into a yellow to red brown colour with abundant mottles and concretions (Singh & Dunlevey, 1997). The top of the Formation is locally characterized by the presence of a ferricrete (Maud, 1968; Johnson, 1986; Singh and Dunlevey, 1997). This weathering profile, present on various rocks and sediments in eastern South Africa, is referred to as "Berea-type red sands" (Maud, 1968).

The Kosi Bay Formation is considered to occur over most of the KwaZulu-Natal coastal plain. It comprises orange or grey, weathered dune sands with intercalated carbonaceous lenses and lignites (Maud, 1968; Hobday & Orme, 1974; Maud & Orr, 1975; Fockema, 1986; Botha, 1997a). This correlation over the entire KwaZulu-Natal coastal plain with shoreline outcrops around Richards Bay has been chiefly made on sand colour, the presence of carbonaceous sands and lignites (Figures III.4 and III.5).

#### III.4.1.5. Suggested ages of the Port Durnford and Kosi Bay Formations

Hobday & Orme (1974) interpreted the sediments of the Lower Argillaceous Member, the Lignite Bed and the Arenaceous Member (their Port Durnford Formation) as a major barrier-lagoon complex showing transgressive sedimentation related to the Last Interglacial age (ca. 130 000 B.P.).

However, recent palynological studies have revealed that the Lignite Bed accumulated in a fresh water lake environment and was radiometrically dated at 70 000  $\pm$  5 000 years B.P. (Oschadleus *et al.*, 1996). The overlying sands would therefore have been deposited during the Last Glacial regression. These studies were carried out from borehole sediments near Port Durnford that were correlated to the coastal Lignite Bed. As the Kosi Bay Formation also contains lignite beds, this correlation and thus the proposed Lignite Bed age must therefore be considered cautiously.

Hendey and Volman (1986) identified an Early Pleistocene fossil pig, *Kolpochoerus*, amongst the "Port Durnford fauna". The exact location where this pig remains were found needs to be established, however, this age tends to correlate to the Tertiary age given by Anderson (1907) to the reddish fossiliferous sandstone of the base of the Port Durnford Formation (cf. III.4.1.3).

#### III.4.1.6. KwaMbonambi Formation

The KwaMbonambi Formation comprises many lithologies all believed to have been deposited during the last glaciation cycle (Botha, 1997a). On coastal outcrops around Richards Bay (Figure II.1), this formation unconformably overlies the Port Durnford and the Kosi Bay Formations, is dark brown and comprises decalcified unconsolidated sands (Figure III.3). These contain a less abundant fine fraction and more abundant heavy minerals than the underlying Kosi Bay Formation (Fockema, 1986; Singh, 1995), and are thought to be derived from aeolian reworking of older dune sands (Johnson, 1986; Botha, 1997a).

In the northern part of the KwaZulu-Natal coastal plain, stabilised inland dunes, inter-dune wetland deposits and freshwater diatomites dated at 25 000 to 40 000 B.P. (Maud, pers. comm. in Botha, 1997c) have been correlated mainly on sand colour criteria to the brown sands described above (Figure III.3).

#### III.4.1.7. Sibayi Formation

The Sibayi Formation is the youngest unit in the Maputaland Group (Figure III.3). The calcareous aeolian dunes of the Sibayi Formation are responsible for the present morphology of the entire northern KwaZulu-Natal coastal dune cordon (Botha, 1997a). However, the present study will reveal that the present morphology of the northern KwaZulu-Natal dune cordon is also due to aeolian reworking of older decalcified sediments, which can generate aeolian dunes with elevations higher than 100 m above msl. The aeolian dunes of the Sibayi Formation contain buried palaeosols, indicating different dune formation phases. They are often referred to as “Late Pleistocene to Holocene dunes” or “Holocene dunes”.

### III.5. Provenance of coastal heavy minerals

The mineralogy of the coastal heavy minerals indicates that the provenance is mainly from the rocks of the Karoo Igneous Province and the KwaZulu-Natal basement. The basement comprises the Natal Metamorphic Province and the Kaapvaal Craton (Hammerbeck, 1976; Fockema, 1986; Hugo, 1990) (Figure III.1). Heavy minerals are also reworked from Phanerozoic sedimentary rocks. The sandstones of the Vryheid Formation, Ecca Group and quartzites of the Natal Group are known to contain concentrations of heavy minerals (Hammerbeck, 1976).

The primary source of rutile, zircon and garnet is restricted to the KwaZulu-Natal basement (Hammerbeck, 1976; Fockema, 1986).

The primary sources of ilmenite and magnetite are the extrusive and intrusive rocks of the Karoo Igneous Province and various metamorphic rocks of the KwaZulu-Natal basement (Hammerbeck, 1976; Fockema, 1986). Over 50 % of the magnetite in KwaZulu-Natal coastal sediments are derived from the KwaZulu-Natal basement (Hugo, 1993). The rhyolites of the Lebombo Group have titaniferous magnetite as a common mineral, but ilmenite is rare (Hammerbeck, 1976).

Over 65 % of the ilmenite in KwaZulu-Natal coastal sediments are derived from ultramafic rocks of the KwaZulu-Natal basement and Karoo Igneous Province (Hugo, 1993). Hugo (1993) suggested that the proportion of ilmenite derived from the Karoo Igneous Province is far greater than from the KwaZulu-Natal basement, as the Karoo igneous rocks contain more iron-titanium oxides and have a larger area of outcrop. Moreover the present outcrop area of the Karoo igneous rocks is only a small remnant of the original volume of the basalts and dolerites (Figure III.1) (Eales *et al.*, 1984). Hugo (1993) noted that the KwaZulu-Natal coastal sediments contain more ilmenite derived from granitoids and felsics from the KwaZulu-Natal basement compared to coastal sediments in the Eastern Cape. This suggests that the influence of the granitoids and

felsics are greater in KwaZulu-Natal due to wider outcrops of the KwaZulu-Natal basement (Hugo, 1993) (Figure III.1).

From the above discussion, it can be concluded that the type and outcrop area of source rocks directly determine the type and proportion of coastal heavy minerals. The coastal portion of KwaZulu-Natal can be divided into two parts north and south of the Tugela Fault (Figure III.1). Little information about the abundance and chemistry of iron-titanium oxides is available for the Kaapvaal Craton (Hugo, 1993). It is possible that the Kaapvaal Craton and the Lebombo Group present a distinct mineralogical signature. Thus the mineralogy of the northern KwaZulu-Natal coastal sediments may differ from southern and central KwaZulu-Natal. Sediment studies of the Tugela River and the Mfolozi/Mkuzi Rivers, which drain different types and areas of lithologies (Figure III.1), would provide further information.

## IV. GEOMORPHOLOGY AND DUNE CLASSIFICATION

### IV.1. Introduction

#### IV.1.1. Regional geomorphology

The northern KwaZulu-Natal coast is backed by an almost continuous dune cordon designated as Cordon A by Davies (1975) and Cordon 1 by Wright (1999). In the following chapters, Cordon A (Cordon 1) will be referred as the coastal dune cordon. The dune cordon under study is situated adjacent to Lake Nhlabane (Figures IV.1 and IV.2), which is linked to the Indian Ocean by a narrow estuary. During the Late Quaternary Lake Nhlabane was a lagoon connected to the ocean by a tidal estuary. For mining purposes, a dam was built to elevate the water level, interrupting the water circulation between the lake and the ocean. Consequently, the estuary mouth has been infilled by washover and aeolian sediments. To the north of the study area the Mfolozi River flood plain is separated from the ocean by a dune cordon constituting the northern continuation of the study area.

The prevailing northeast longshore current along the southeast African coast produces erosion at headlands and immediately northward, whereas deposition takes place further to the north. This process forms asymmetric bays that can be observed along the coastline (e.g. Dawson's Rock, Figures IV.1 and IV.2). The coastline thus represents a characteristic "zetaform" shape ("zeta bays"), described from many portions of the South African east coast (Davies, 1980).

The coastal dune cordon under study forms part of a complex coastal barrier system represented by marine, fluvial, estuarine and aeolian environments. Aeolian processes have generated the upper portion of the dune cordon and produced the surface morphology. This study aims to characterise the aeolian dune types present and to determine their spatial extension and relative age. This work is useful for a general understanding of dune formation and assisted subsequent sample selection and correlation of sedimentological units recognised from the study of the southern and northern cross-sections.

#### IV.1.2. Terminology and dune types

This section gives a definition of the terminology used and descriptions of the dunes identified in the study area. The work is based on studies by Bagnold (1941), McKee (1966), Folk (1971), Mabutt (1977) Davies (1980), Thompson (1983), Tinley (1985), Hesp (1988), Short (1988) and Pye (1982, 1993).

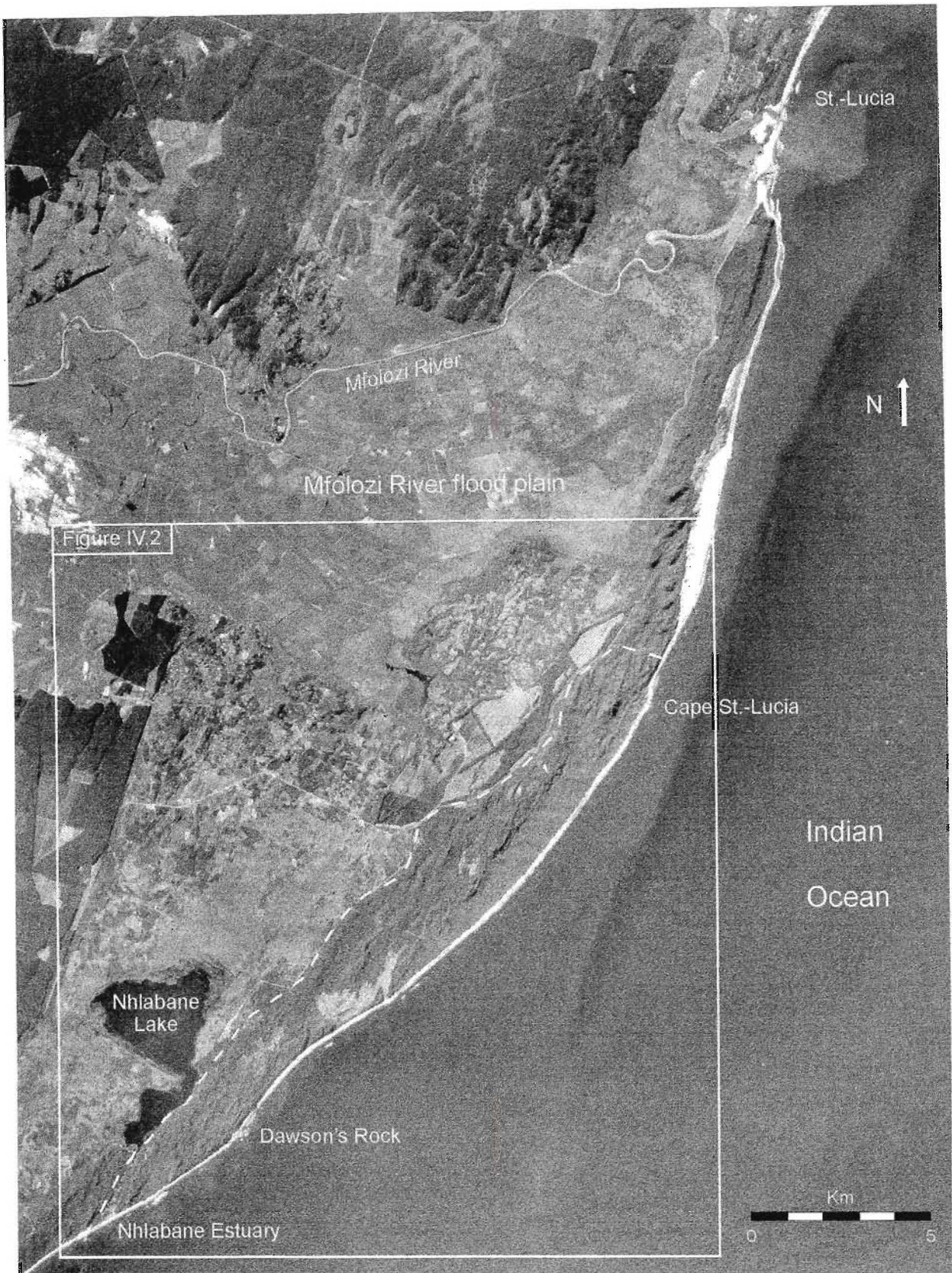


**Figure IV.1.** Aerial photograph (1985) of the northern KwaZulu-Natal coastal dune cordon between Lake Nhlabane and St.-Lucia. Scale at 1:150 000 (The Air Survey, 1985). The area shown in Figure IV.2 is outlined by a white box and the area of the Zulti North deposit by a dashed white line.

Outlined below is the terminology used in the following sections.

- *Interdune area*: a relative flat sand surface between two mounds or hills of sand known as dunes.
- *Effective wind direction*: the travel direction of wind having sufficient force to move appreciable amounts of sand.
- *Crest*: line of highest points on a dune.
- *Slipface*: surface dipping steeply to leeward (at or near angle of repose), down which sand slides or on which it settles from suspension in atmosphere.
- *Arm*: the trailing outer extension of a parabolic dune.
- *Nose*: the central forward part of a parabolic dune.
- *Cliff-top dune*: mobile form occurring on top of a sea cliff.
- *Whaleback dune*: altered dune reduced to a low convex sand hill by erosion.

#### IV.1.2.1. Bare dunes (wind formed)

- *Sand sheet*: bare sheet-like dune with broad, flat surface.
- *Barchan dune*: a dune of crescentic shape, with horns of the crescent extending downwind, formed by an unidirectional wind. They characterise limited sand supply, and thus are widely scattered on flat surfaces.
- *Transverse dune*: straight sand ridge oriented at approximately right angles to the effective wind direction. It is qualified as *barchanoid* when it evolved from coalesced barchans, or as *reversing* when it develops reversal slipfaces due to seasonal shifts in direction of the effective wind. The transverse dune needs an abundant sand supply to form.
- *Seif or longitudinal dune*: a long, nearly straight sand ridge commonly parallel to other similar ridges and separated from them by wide, flat interdune surfaces. It is oriented either along a line that is the vector of two converging wind directions (Bagnold, 1941), or parallel to a helicoidal wind flow of an unidirectional predominant wind (Folk, 1971). The seif dune is a non-migratory reworking of adjacent sand, and is common in deserts.
- *Buttress dune*: transverse dune inclined upwards at right angles from the beach onto the bared or vegetated seaward slope of a high dune cordon. The seaward ends of buttress dunes are frequently truncated and the interdune troughs inundated by storm seas that are coincident with high spring tides.

#### IV.1.2.2. Vegetated dunes (wind and plant formed)

- *Foredune*: shore-parallel aeolian deposit, occupying a foremost beach position at the time of formation. It is largely non-migratory and is colonised by pioneer grasses (rarely shrubs and small trees). It evolves in response to aerodynamic/sand transport interaction within vegetation, and to local coastal process. The foredunes have a maximum height of 10 meters along the northern KwaZulu-Natal coast (Tinley, 1985), but up to 20 metres in southern Australia (Hesp, 1988).
- *Blowout*: crater-like deflation and wind scour hollow initiated in openings or weak spots of dunes partially stabilised by vegetation, moisture, or both. Though variable in shape, it is commonly oval or narrowly elliptic (parabolic). The long axis of the blowout is parallel to a predominant wind. It can evolve into an elongate parabolic dune (Pye, 1982).
- *Parabolic dune*: U- or V-shaped tongue or trough shaped advancing sand with its stationary arms partially stabilised by vegetation. Its leading edge, bare or partially vegetated, is a

concave mound of sand forming a steep rounded nose that migrates slowly downwind. The central trough part is usually a deflation hollow, but the latter can be replaced by a bare sand sheet with transverse ridges (see below). The parabolic dune type can be subdivided into three main sub-types that are presented in Figure IV.5. The “long-walled transgressive” type of a complex parabolic dune is defined by Short (1988) as a *dune field*. When there is a voluminous sand supply (i.e. absence of a central deflation hollow) derived from the foredunes, the inland migrating parabolic dune is qualified as *transgressive* (Davies, 1980; Pye 1993). If, in addition, it grows upwards burying everything in its paths, it is called an *accretion ascending parabolic dune* (Tinley, 1985). Decreasing sand supply allows a deflation hollow to form, and the parabolic dune self-stabilises when the deflation base-level reaches a moist sand zone where plants start colonising. The last site to be covered by plant growth is the dune nose.

- *Deflation hairpin parabolic dune*: parabolic dune on a flat to undulating, sparsely vegetated terrain (e.g. grassland, semi-desert dwarf shrubland), blown across gravels, older clay rich sands or high water table area (Tinley, 1985). Because of a substantial downwind migration, it left paired parallel ridges (arms) behind it.
- *Wind-rift dunes*. They form when a parabolic dune has a wind breached nose. The inner through is thus open at both ends, and the two lateral ridges (arms) parallel to the effective wind are referred to as wind-rift dunes (Mabutt, 1977). A diagnostic feature (to distinguish them from seif dunes) is the strong slope asymmetry of one individual ridge. The steeper slope occurs either on the over-steepened wind-scoured inner slope of a trough (if a deflation hollow was present), or on the outer lateral slipface slope (if an inner sand sheet was present). However, two associated wind-rift dunes must present a mirror symmetry on a section perpendicular to the long axe of the former parabolic dune (Tinley, 1985).

## IV.2. Dune classification

The primary aim of this geomorphology study is not only to identify the dune types present, but also to establish a relative stratigraphy. Therefore special attention has been focussed on the spatial distribution, dimension, inferred original morphology and alteration state of these dunes, in order to classify all recognised dunes into classes representing different relative ages and development phases. Dunes from the same type may be grouped below into different classes to reflect their relative age.

A geomorphological map of the region (Figure IV.2) was compiled from a set of colour 1:10 000 scale aerial photographs flown in 1995, and an additional set of monochromatic 1:150 000 scale aerial photographs flown in 1985 (from The Air Survey). Enlargements of aerial photographs taken in 1937 were used to identify the location and extension of bare dunes, all of which were subsequently stabilised and vegetated by the South African Forestry Department (Weisser & Marques, 1979). Field observations helped to refine the geomorphology map.

All recognised aeolian dunes in the study area were regrouped into five major dune classes. The coastal dune cordon (Cordon A or 1) is characterised by four of these five dune classes, representing at least four dune development phases. The fifth dune class occurs further inland along the coastal plain. The following sections define and describe the five dune classes from the oldest to the youngest.

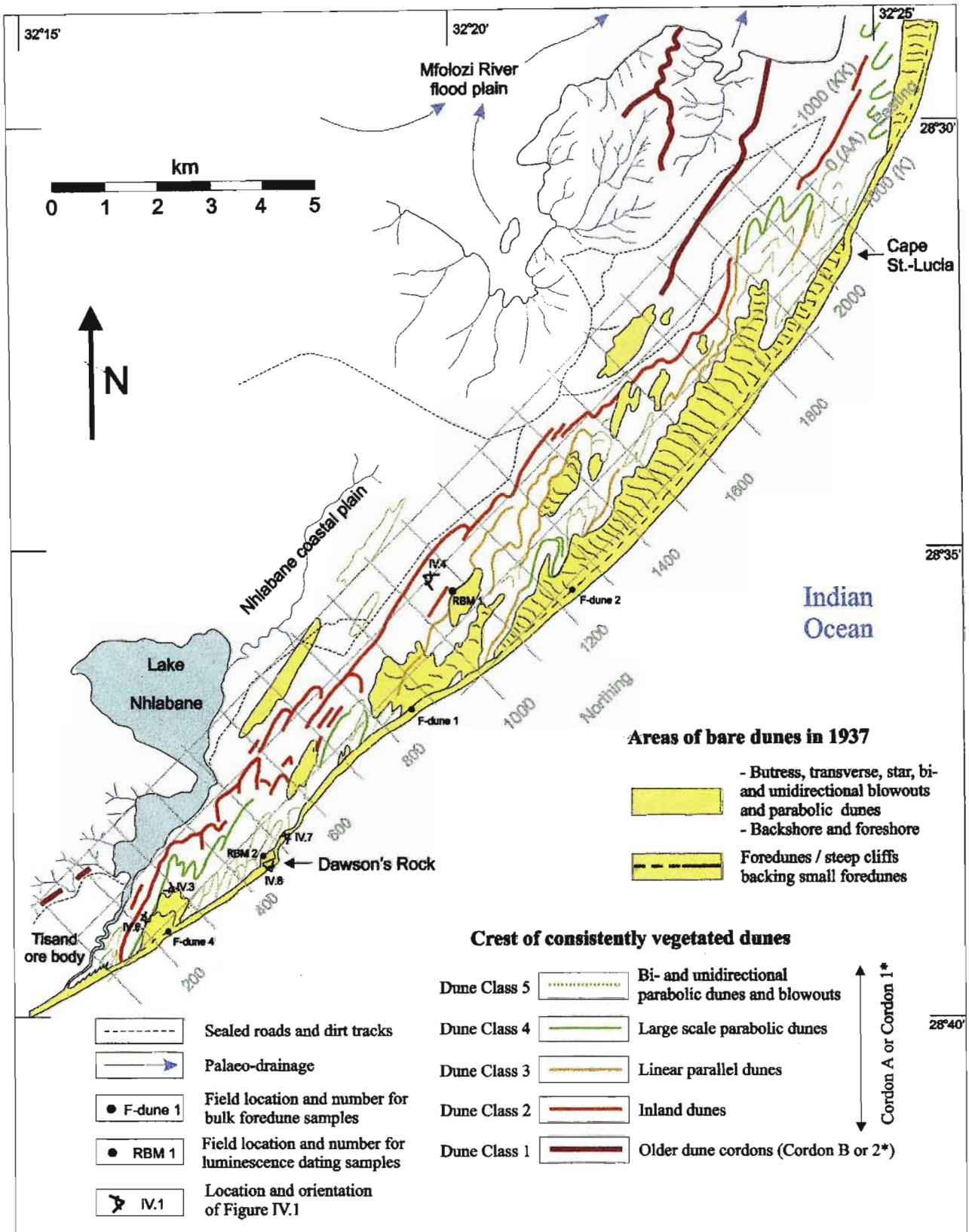


**Figure IV.2.** Geomorphological map for the Zulti North ore body, showing studied field samples, and all recognised dunes regrouped in 5 dune classes. This map also shows the reference system used by RBM (Section V.1.1), along with the location of the two cross-sections studied in detail (Northing Lines 380 and 1200). \*Cordon A and B of Davies (1975), Cordon 1 and 2 of Wright (1999).

Where mining operations or coastal erosion has cut sections into the dunes, information such as sand colour or lamination orientation was recorded. Geographical positions mentioned below refer to the RBM N – E reference system (Figure IV.2).

#### IV.2.1. Dune Class 1: older dune cordons

Davies (1975) and Wright (1999) describe an old dune cordon extending along the western shore of Lake St.-Lucia and designated the feature Cordon B and Cordon 2 respectively. South of the Mfolozi River flood plain, two low-lying red dune cordons (Figure IV.2) were considered by Davies (1975) to represent the southern extension of Cordon B. An extension of this feature is present south of Lake Nhlabane (Figure IV.2). It has a whaleback morphology, surface water erosion gullies, red colour and high clay content (“Berea-type red sand”, Maud, 1968), characteristics of an old dune cordon and is defined here as Dune Class 1. It is suggested that it represents the southern extension of Cordon B or at least one of the two red dunes observed south of the Mfolozi River flood plain (Figure IV.2). Further studies, however, are required to confirm this hypothesis.

The narrow width of Cordon B in the Nhlabane area may be due to overlap with the present coastal dune cordon (Cordon A or 1). Cordon B would thus, at least partly, underlie the present coastal dune cordon.

#### IV.2.2. Dune Class 2: inland dunes

Dune Class 2 comprises relatively low lying inland dunes. These are the oldest dunes recognised in the coastal dune cordon and extend almost continuously along the most inland part of the cordon (Figure IV.2). They have been affected by erosion that has altered their original shape, lowered their elevation or simply smoothed their crests. No surface water induced gullies were identified. It is difficult to determine whether their present shape represents a slightly altered original form or a new shape produced by complete reworking and later weathering. The inland dunes are all characterised by a dark orange - brown colour, and by a substantial clay content (Figure IV.3). This dune class can be subdivided into two regional subclasses, as discussed below.

The central region of the study area (between N600 and N1500) is characterised by inland dunes with a low-lying topography, and a typical elevation of 60 - 70 m above msl or 35 - 45 m above the surrounding flat to undulating plateau (Figures IV.2 and IV.4). Their present shape is interpreted as a mixture of parabolic, hairpin parabolic and wind-rift dune types (after Tinley, 1985). They suggest a southwesterly effective wind direction during their formation, and possibly an additional northeasterly wind during later reworking (Figure IV.2).

North and south of the central portion, the inland dunes rise up to 100 metres above sea level. The crest pattern appears irregular and chaotic, however parabolic dunes seem to have played a reworking or building role at some time during their formation (Figure IV.2). South of N600, the effective wind had a south – southwesterly direction (Figure IV.2).

Exposures of Dune Class 2 are only visible on mining faces when not covered by slump sands. These present thick cross-beds at N330 (Mining Pond C, August 1998) showing laminations with azimuth dip directions between 280° and 350°, and with a consistent 28° to 35° dip. These lamination orientations are expected to be present in a south – southwesterly arm of a parabolic dune (Figure IV.2). One 3 m thick cross-bed developed locally under the two palaeosols had laminations with an azimuth dip direction of 155° and a dip of 20°, possibly indicating a temporary reworking by a northwesterly effective wind. The steep slopes on the western side of Dune Class 2 near Lake Nhlabane reach a maximum of 30°. This can either be interpreted as dune slipfaces (see above) or as steepening due to later erosion by the Nhlabane River. Two palaeosols (ca. 1 m thick) are exposed close to the top of Dune Class 2 at N330, MPC (Figure IV.3). Both contain terrestrial gastropod shells, but no evidence for human activity in the form of clay pottery shards. A similar palaeosol was observed at MPD in August 1998 at N810.

### IV.2.3. Dune Class 3: linear parallel dunes

The linear parallel morphology of Dune Class 3 is only identified in the northern part of the area under study (from N800) (Figure IV.2). North of N1950 the very steep slopes on both side of the dunes attest to intense (basal) reworking by both north – northeast and south – southwest winds.

Between N800 and N1950, up to four linear and parallel dunes rise up to 120 m above msl, and are characterised by a light orange colour (Figure IV.4). Their landward slope is generally steeper (up to 32°) than the broader seaward slope (Figure IV.1). Many bidirectional to unidirectional blowouts and small parabolic dunes have superficially reworked the original dune forms (see bared dune locations in 1937, Figure IV.2). This superficial reworking is thought to have partly contributed to the steepening of the landward slope (see below) and the formation of sinuous dune crests (Figure IV.2). Fockema (1986) interpreted the linear parallel dunes of Dune Class 3 (and the hairpin parabolic dunes of Dune Class 2) as seif dunes, also called longitudinal dunes. However several elements (Section IV.1.2.1) exclude this hypothesis (see also McKee *et al.*, 1964; Folk, 1971). Two different hypotheses are presented below in regard of the formation of the linear parallel dunes of Dune Class 3.

Between N1000 and N2100, a large bare field of buttress transverse dunes stretches along the shore, where the beach and foredunes act as the sediment supply (Figure IV.2). On the inner margin of this dune field, simple and compound transgressive parabolic dunes have formed, with an oblique north – northeast direction to the shoreline. By analogy with this recent process, successive parabolic dunes could have formed the linear parallel dunes of Dune Class 3. In this case, only their landward arm would have been preserved, the seaward arm being absent or reworked by a younger parabolic dune. The absence of a terminal nose in this dune form would classify them as wind-rift dunes (Section IV.1.2.2).

In the second hypothesis, the linear parallel dunes can be interpreted as crests of giant transverse dunes, or rather as successive (partially) vegetated noses of complex parabolic dunes (Figure IV.5). This hypothesis implies a lowered sea level and a strong effective wind from the east – southeast (Figure IV.2). However, the presence of a predominant east – southeasterly palaeo-wind has not been identified by earlier studies, unless this wind direction was a combination of the present northeast and south winds (Figure II.2). These hypotheses can not be discriminated using only geomorphologic evidence and further analysis is presented in Section IV.3.



**Figure IV.3.** Orange-brown inland dune (Dune Class 2) as exposed in Mining Pond C (N330). Note the two dark brown palaeosols at the top of the dune, characterised by a relatively resistant sub-horizontal layer. A single palaeosol at the base of the dune (on the right) presents a red alteration profile (see Figure IV.2 for location and orientation).

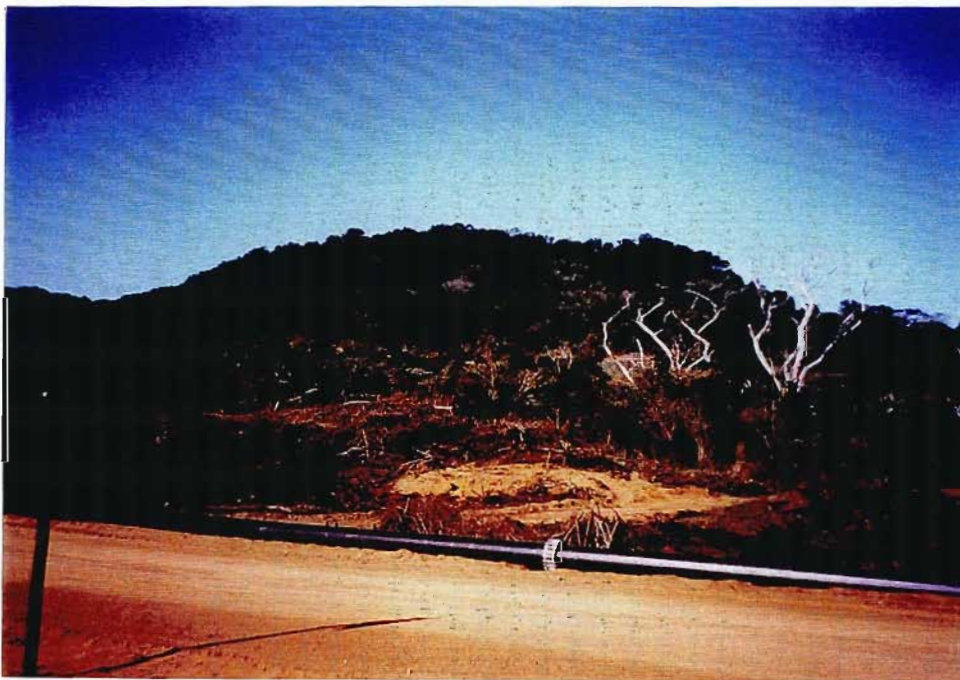


**Figure IV.4.** Landward side of the most inland dune of Dune Class 3, and plateau separating it from the inland dune (Dune Class 2). The foreground is dominated by an access road to Mining Pond E. Bottom part of the linear dune: narrow road where sample RBM1 was collected for luminescence dating (see Figure IV.2 for location and orientation).

## IV.2.4. Dune Class 4: large scale parabolic dunes

The large scale parabolic dunes of Dune Class 4 form large imposing features with relatively unaltered shape. Their characteristics define them as accretion ascending parabolic dunes (Section IV.1.2.2). Simple, complex and compound parabolic dunes are represented and are often transitional between end-members (Figure IV.5). The large dimensions of these parabolic dunes suggest they formed by a combination of a high wind velocity and voluminous sand supply. This suggestion has to be considered with caution, as the vegetation cover and humidity during the formation of these dunes are not known. The orientation of Dune Class 4 suggest that anticyclonic north – northeasterly winds were not instrumental in their formation, and that the south – southwesterly winds predominated. The anticyclonic winds were probably attenuated or deflected due to the coastal barrier north of Cape St.-Lucia, where they built very high (up to 180 m) parabolic dunes (Figure IV.2).

South of N600 Dune Class 4 does not present an arcuate morphology as the coastal arm of the complex parabolic dune has been reworked or truncated by younger dunes. However, an absence of development of the coastal arm cannot be ruled out.

The internal features of Dune Class 4 were observed at MPC in August 98. The dunes are typically light orange in colour, however, northward the sand colour has not been recorded. Since this dune class is defined primarily on the dimension of the parabolic dunes, they may have formed over a considerable time period representing different weathering stages. This interpretation is supported by the presence in 1937 of a large bare transgressive dune field (Figure IV.2, N250 – E1000, and Figure IV.6) that would have naturally evolved (if not stabilised by afforestation) into a fixed parabolic dune by a self-stabilisation process (Section IV.1.2.2) or by a decrease of the rate of advancement allowing vegetation to stabilise the dune. Nevertheless, these large scale parabolic dunes (Dune Class 4) must post-date the development of both the inland dunes (Dune Class 2) and linear parallel dunes (Dune Class 3) north of N800, and post-date at least the inland dunes (Dune Class 2) to the south.

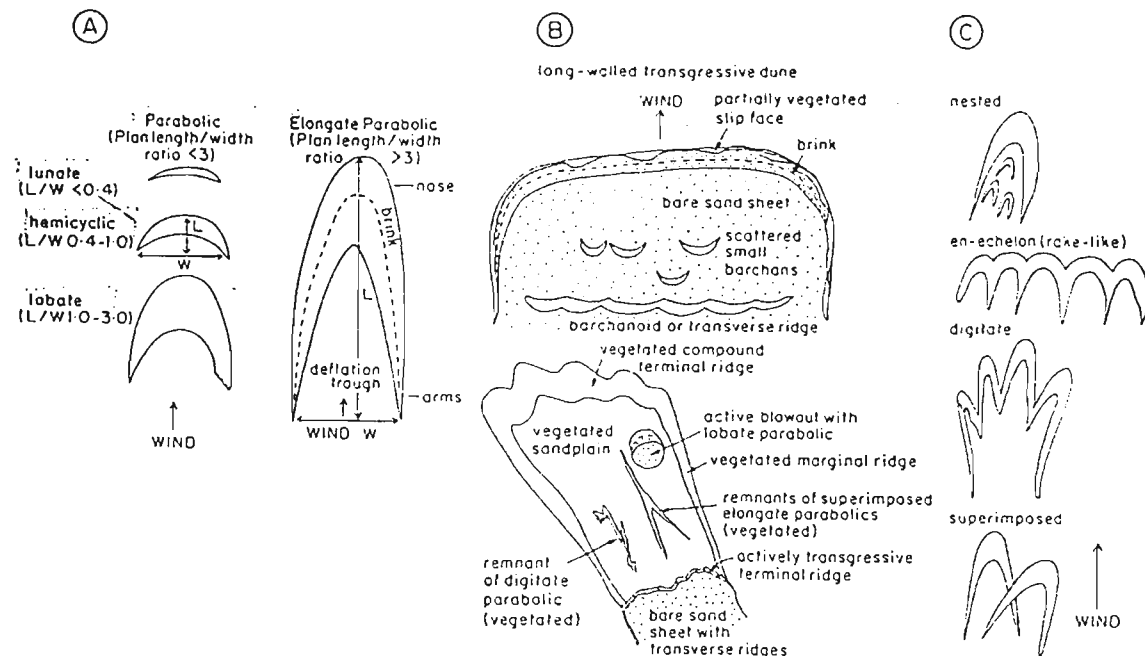
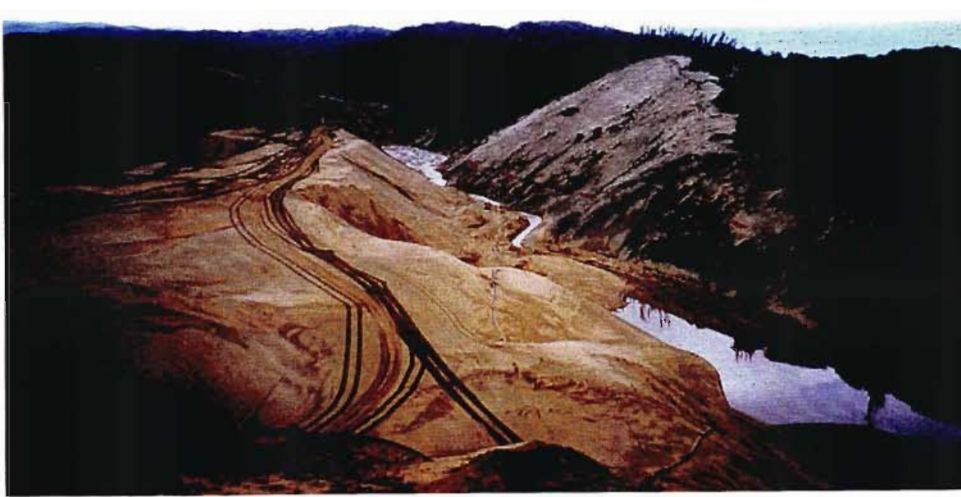


Figure IV.5. Morphological variants of parabolic dunes. A: Simple dunes. B: Complex dunes. C: Compound dunes (Pye, 1993).



**Figure IV.6.** View from Mining Pond C looking northeast (August 1998). The orange sand in the foreground is mine tailings. The coastal dune (right of view) comprises recent sediment and was bare in 1937. At the base of this dune is a palaeosol (dotted red line), which is underlain by Dune Class 4 that continues inland (left of view). The undulating morphology in the middle background are small scale parabolic dunes of Dune Class 5 (see Figure IV.2 for location and orientation).

#### IV.2.5. Dune Class 5: small scale parabolic dunes

The small scale parabolic dunes of Dune Class 5 are the youngest dunes identified (Figure IV.2). Dune Class 5 can be subdivided into an inland sub-class and a coastal sub-class, as discussed below.

Inland, bi- and unidirectional parabolic dunes and blowouts superficially rework underlying sands (Figure IV.2). Despite large areas being affected by reworking, the thickness of Dune Class 5 is insignificant. As noted by Tinley (1985), wind direction is greatly affected by local topography. This can be seen by the range of directions expressed by these small parabolic dunes and blowouts, even though the general trend is northeast – southwest. Tinley (1985) showed that human activity can also initiate this reworking process (deforestation, slash and burn and footpaths).

The presence of coastal unidirectional parabolic dunes south of N850 suggest that the most recent dune forming event contributed to a net onshore sediment transport (Figure IV.2 and Figure IV.6). The bare dune fields adjacent to the beach (at N250 and between N1000 to N2100) and bare dunes observed in the 1937 photographs are very recent analogues (Figure IV.2). As recorded on coastal outcrops, the young sand within Dune Class 5 contains low abundances of fine sediment, high heavy mineral content and is pale yellow to light grey in colour, similar to the present foredune colour (Figures IV.7 and IV.8). Aeolian dunes are

unlikely to climb the steep coastal cliffs present along that portion of the study area. Therefore the onset of the coastal parabolic dunes within Dune Class 5 must predate subsequent shoreline erosion. The present position of the coastal dunes of Dune Class 5 defines them as cliff-top dunes (Figure IV.7).

According to Pye (1993), only unidirectional winds (or with a slight variation of direction) create parabolic dunes with a high length/width ratio such as those observed here (note that their original length must have been greater prior to shoreline retreat). The modest dimension of these coastal dunes suggests formation from relatively lower wind velocity and/or greater vegetation cover compared to the conditions prevailing during the development of the large parabolic dunes of Dune Class 4 (Figure IV.2). A decrease of sand supply due to coastal erosion and cliff formation may have stopped their migration. Many factors can induce coastal erosion: longshore currents associated to specific coastline configuration (Section IV.1.1), sea level rise, strengthening of wind and wave regimes, reduction of sand supply to the beach system (Komar, 1976; Cooper, 1991).

### IV.3. Luminescence dating

Two samples from the coastal dune cordon have been dated using the luminescence of quartz and feldspar. These samples were selected to support an ongoing study by Botha (1998, pers. comm.). The study by Botha aims to identify the age of diverse features along the northern KwaZulu-Natal plain and coastal areas. The coastal dunes selected by Botha in Mining Pond C appear to represent Dune Class 2 and 4. In order to complete the dating of all dune classes present in the coastal dune cordon, the author carried out luminescence dating of Dune Classes 3 and 5.

The luminescence dating method is based on the accumulation of crystalline damage caused by radiation from trace levels of radioactive uranium, thorium and potassium that naturally occur in the minerals that make up the sediment, as well as a constant bombardment by cosmic radiation (Woodborne & Collett, 1999). The damage is annealed when the sediment is exposed to sufficient heat or light. When the damage is annealed the sand grains release energy in the form of light that is known as *luminescence*. It is normally assumed that the process of wind transport exposes the sand grains to sufficient sunlight to zero the luminescence signal. Once the dune has formed the buried sand grains gradually begin to accumulate the radiation damage. The date of the last exposure to light can be determined by measuring the radiation dose rate in the dune, and comparing the radiation dose accumulated by the minerals (quartz and feldspar).

The luminescence signal in quartz grains is stimulated by heat and is called thermoluminescence (TL). The luminescence signal in feldspars can also be stimulated by heat, but it can also be stimulated by exposure to infrared light. The latter technique is called infrared stimulated luminescence (IRSL). The thermodynamic qualities of the IRSL and TL signals differ, in particular the IRSL signal is rapidly zeroed after minutes of exposure to sunlight while the TL signal requires several days of exposure. Thus IRSL and TL dating methods can identify both depositional and reworking ages of an aeolian dune. Both methods, including dating results, are detailed in the report compiled by Woodborne & Collett (1999) from the CSIR (Appendix A).



**Figure IV.7.** Retreating shoreline north of Dawson's Rock. The steep cliffs show older orange sands overlain by younger sand from the (cliff-top) small scale parabolic dunes of Dune Class 5. Differential erosion at Dawson's Rock headland leads to reworking and slumping of the younger sand. Note also the abundant beach placers on the backshore (see Figure IV.2 for location and orientation).

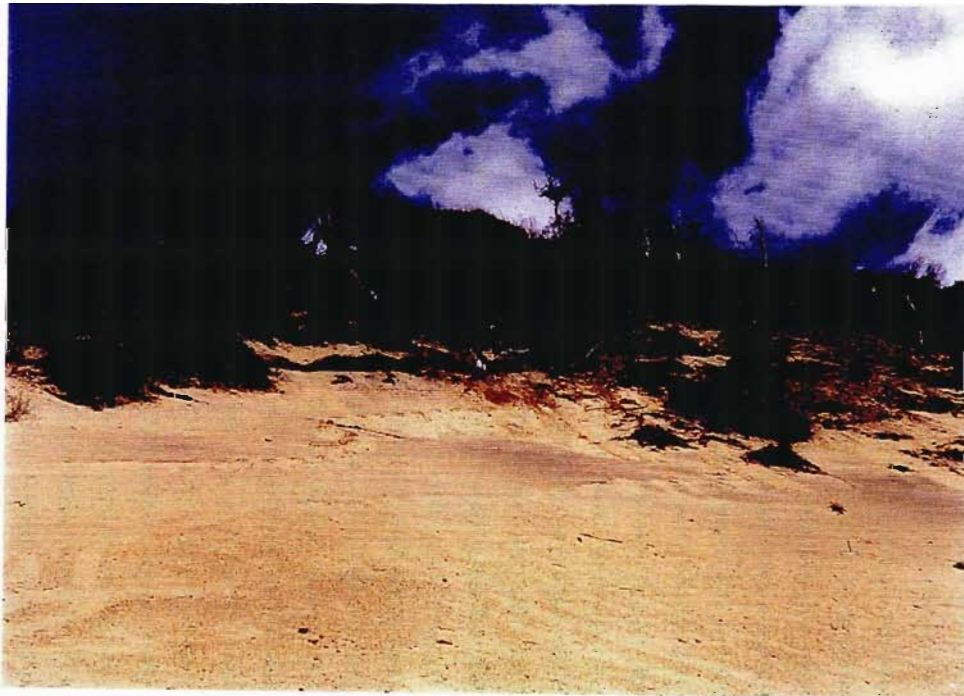


**Figure IV.8.** Outcrop at Dawson's Rock of a small parabolic dune (Dune Class 5, Unit E) separated from the underlying sand (Unit E as well) by a palaeosol. Stephan Woodborne stands where sample RBM 2 has been collected for luminescence dating (centre of the photograph). D'Rock 1 sample was collected under the present soil of the parabolic dune (upper right of the photograph) (see Figure IV.2 for location and orientation).

### IV.3.1. Results

Luminescence dating of sample RBM 1 (Figures IV.2 and IV.4) gave a depositional age of  $12\,800 \pm 2100$  B.P. (oxygen isotope Stage 2) (Appendix A). Thus, the linear parallel dunes of Dune Class 3 were formed during the marine transgression following the last glaciation (Figure II.9 and Section II.4). At this time the sea level was between -50 to -100 m below present (Figure II.9), placing the coastline 3 to 8 km offshore (Figure II.1). The sediment constituting the linear parallel dunes during this time migrated inland at least 4 km from the former shoreline. Luminescence dating of sample RBM 1 also indicates a short reworking event at an age of  $6500 \pm 450$  B.P. (Appendix A). These considerations discount the first hypothesis and confirm the second hypothesis presented in Section IV.2.3. Between 15 000 and 11 000 B.P., sand migrated inland for more than 3 km, probably as bare dune fields derived from the palaeocoastline. At ca. 6500 B.P. these dune fields were reworked and, due to dense vegetation cover, were converted into successive complex parabolic dunes that created the present linear parallel morphology (Figure IV.2). Final superficial reworking steepened the landward slope and formed the sinuous dune crests of Dune Class 3.

Sample RBM 2 (Figure IV.2) was collected directly under a palaeosol that is located within a coastal parabolic dune of Dune Class 5 (Figures IV.8). Luminescence dating of this sample gave a depositional age of  $7400 \pm 2600$  B.P. and indicated a reworking event at an age of  $2100 \pm 142$  B.P. (Appendix A). The depositional age given above for the sediment underlying the palaeosol unfortunately implies a wide range of associated sea levels between ca. -19 m below msl and 1.5 m above msl (Figure II.10). The reworking age given above attributes the palaeosol to a maximum age of 2100 B.P. Thus the latest depositional events forming the coastal parabolic dunes occurred within the last 2000 years or probably within the last 1500 years as voluminous onshore aeolian transport of sand is likely to take place during regressive sea levels (Figure II.10). In summary, the formation of the coastal parabolic dunes of Dune Class 5 is restricted to the Holocene.

## V. SOUTHERN ZULTI NORTH ORE BODY (NORTHING LINE 380)

### V.1. Introduction

The geomorphology study led to the subdivision of the Zulti North ore body into southern and northern parts, with a transitional boundary between N600 and N800. The southern part of the ore body is composed of three of the five dune classes defined in Chapter IV (Figure V.1): the inland dunes of Dune Class 2, the large scale parabolic dunes of Dune Class 4, and the small scale parabolic dunes of Dune Class 5. In addition an interpretation of the geomorphology suggests that Dune Class 1 (older dune cordons) underlies the inland portion of the study area. The aim of this chapter is to establish a geological cross-section for Northing Line 380, which is considered to represent the southern Zulti North ore body (Section V.6).

Three boreholes from Line 380 were selected for analysis. They are located on the crest of parabolic dunes representing Dune Classes 2, 4 and 5. For practical reasons, the three boreholes studied (380/B/1, 380/G/1 and 380/M/1) are referred to as boreholes S1, S2 and S3 respectively, representing the “inland”, “central” and “coastal” dunes (Figure V.1).

A great variety of analytical data is needed to unravel the structure and characteristics of the dune cordon as it is mainly composed of relatively homogeneous unconsolidated sand. The data sets analysed comprise details of mineralogy and absolute heavy mineral content, heavy mineral abundance ratios, bulk sample geochemistry, grain size, and SEM images and chemistry of quartz grain surfaces. Each method gives useful data, but only comparison and integration of all data sets can lead to a detailed and consistent understanding of the study area. Due to the complexity of palaeosols and the effect of a 6 m sampling interval, a “best-fit” approach is often used to define and characterise sedimentological units.

If not specified, interpretations discussed in the following sections are based on the assumption that the characteristics of the sediment supplied to the dune cordon by longshore drift have been consistent with time.

#### V.1.1. RBM grid reference, borehole and sample numbering

RBM uses a unique grid as a reference system for the location of boreholes. Although this grid is oblique to the geographical positioning system (latitudes and longitudes), it makes use of “north” and “east” terms. If not specified, geographical positions mentioned in the following sections refer to the RBM reference system. The “Northing Lines” were defined to be perpendicular to the coastline, and the “Easting Lines” parallel to it (Figures IV.1 and V.1). While the Northing axis is a metric scale, the Easting axis is characterised by a numerical and alphabetical system. According to this reference system, a borehole located at Northing 380 and Easting 200 is denominated as 380/B. Boreholes were drilled by RBM every 50 m along Northing and Easting Lines separated by 100 m. The prefix 380/B/1 refers to a borehole located on Easting 250. If not specified below, all borehole samples studied are bulk archive splits

labelled GEN in the RBM storage room. GER is the prefix given to boreholes that were redrilled.

### V.1.2. Sample location and description

Borehole S3 is located at Northing 380 and Easting 1250 (Table V.1). The collar elevation is 72 m above msl and drilling ceased -3 m below msl (Figure V.2). Thirteen samples were collected at a 6 m interval from Borehole S3. The uppermost sample is defined as "sample 69", while the deepest sample at -1 m below msl ("sample -1") incorporates 5 m as drilling is often hampered and finally stopped by harder lithologies (compacted clays or cemented sand).

The RBM storage room contains thousands of archived dune samples. These were searched extensively by the author and two research assistants to find a complete suite of samples. Despite this samples are missing from some boreholes. In the case of borehole S3, sample 8 could not be found.

All boreholes and their samples follow the principles outlined above. The reader is directed to Table V.1 for details pertaining to boreholes S1 and S2.

**Table V.1.** Nomenclature, location and characteristics of boreholes S1, S2 and S3 from Line 380.

Borehole	S3	S2	S1
RBM nomenclature	380/M/1	380/G/1	380/B/1
Location	N380, E1250	N380, E750	N380, E250
Top elevation	72 m above msl	67 m above msl	92 m above msl
Bottom elevation	-3 m below msl	-3 m below msl	-2 m below msl
Number of samples	13	12	16
Missing samples	sample 8		

#### *Foredune samples*

Sample F-dune 4 was collected 3 m above msl from a foredune 2.5 km south of Dawson's Rock (Figure V.1). This foredune acted as a sediment source for the dune field active before 1937. Sample F-dune 1 was collected 3 m above msl from a foredune 3.6 km north of Dawson's Rock (Figure IV.2). No foredunes are developed between Dawson's Rock and N800 because of the erosive character of that portion of the coast. F-dune 1 sample represents the first foredunes encountered north of Dawson's Rock. Sample F-dune 2 was collected 3 m above msl from a foredune 7.5 km north of Dawson's Rock (Figure IV.2). This foredune acted as a sediment source for the buttress dune field active before 1937.

#### *Dawson's Rock field samples*

D'Rock 1 and RBM 2 samples were collected at Dawson's Rock on a coastal outcrop of Dune Class 5 (small scale parabolic dunes) (Figures V.1 and V.2). RBM 2 sample has been dated by luminescence and was located directly below a palaeosol (55 m above msl) (Figure IV.8). D'Rock 1 sample was collected 1 to 2 m under the present soil (Figure IV.8).

D'Rock 3 and 4 samples (Figures V.1 and V.2) were collected 200 m north of Dawson's Rock on a coastal outcrop of an old orange dune, which is the lateral equivalent of the calcretised orange dune constituting Dawson's Rock (Figure IV.7). The two samples, separated from each other by less than one metre, were collected 10 m below the top of the old orange dune. D'Rock 3 and 4 samples represent the base of an aeolian dune unit overlying a thick brown palaeosol.

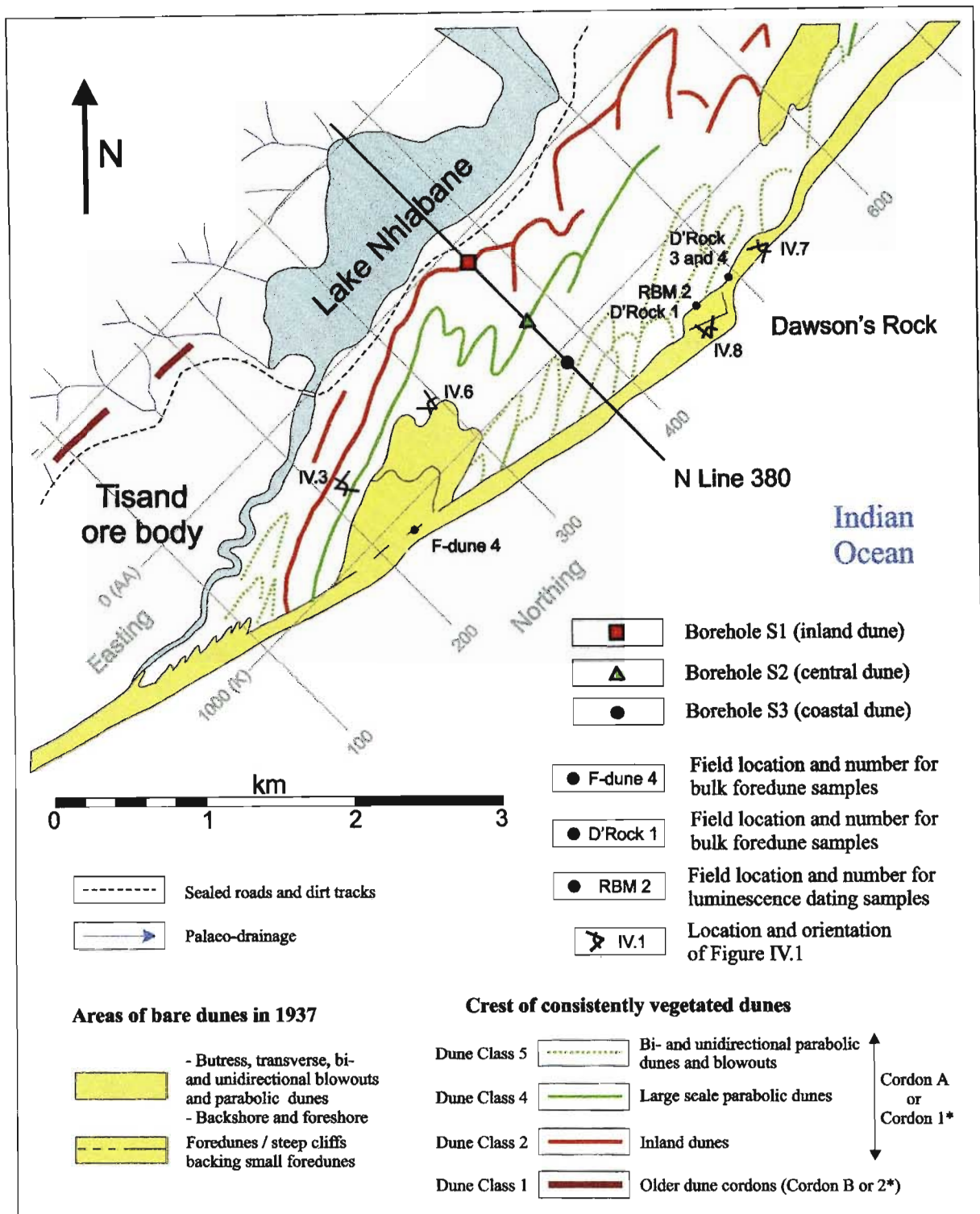


**Figure V.1.** Geomorphological map of the southern Zulti North ore body, showing the location of inland, central and coastal boreholes (S1, S2 and S3), which intercept Dune Classes 2, 4 and 5. \*Cordon A and B of Davies (1975), Cordon 1 and 2 of Wright (1999).

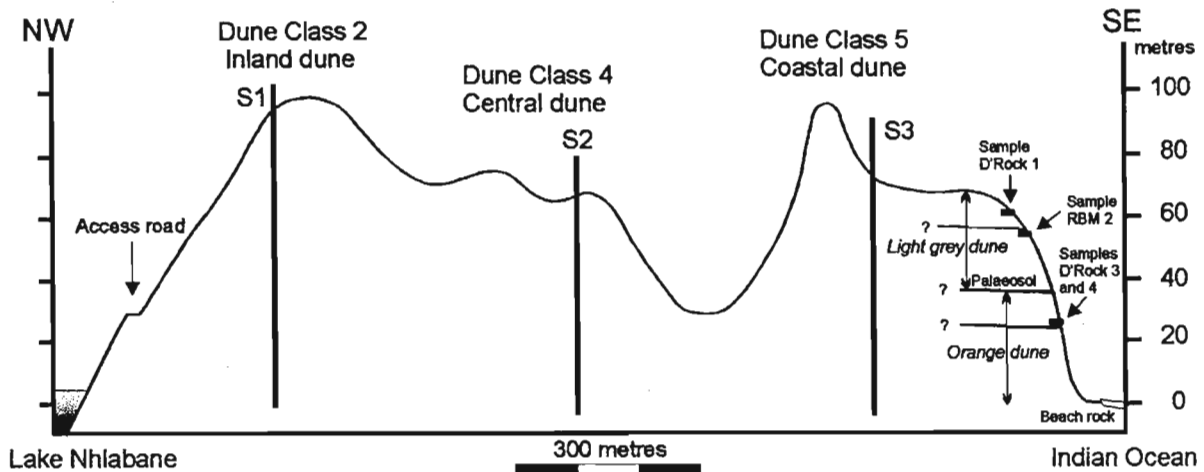


**Figure V.2.** Topographic section along Line 380, showing the morphology and location of the three boreholes studied. Field samples studied and coastal outcrops of palaeosols are projected onto Line 380 (see text and Figure V.1).

## V.2. Mineralogy

Boreholes S1, S2 and S3 are characterised by the same overall mineral assemblage of quartz, feldspar, carbonate grains, rock fragments, and a diverse heavy mineral suite. However, the relative abundance of these minerals can be used to subdivide the coastal dune cordon into distinct internal units.

Throughout the northern KwaZulu-Natal coast, the heavy mineral population of the coastal dune cordon comprises a mixture of stable and unstable minerals including amphibole (hornblende), pyroxene (augite), chromite, garnet (pyrope and some almandin), staurolite, kyanite, sphene, epidote, ilmenite, magnetite, rutile, zircon, leucoxene, hematite, goethite, pyrite, monazite, apatite and tourmaline (Fockema, 1986; Hugo, 1993). Recent aeolian dunes north of Richards Bay contain between 4 to 23 weight percent heavy minerals (Fockema, 1986).

Hugo (1993) was able to differentiate the Kosi Bay Formation, the "Berea-type red sand" and the recent coastal dunes (Sibayi Formation?) by analysing the heavy mineral content of 47 samples. No other similar studies have been applied to the present coastal dune cordon in order to characterise or further subdivide the coastal Sibayi Formation and the underlying deposits such as the KwaMbonambi Formation.

### V.2.1. Mineral point counting

Thirty borehole samples (Figures V.3, V.4 and V.5) and two field samples (F-dune 4 and D'Rock 1, Figure V.6) were point counted to identify mineral abundance variations within the dune cordon. Because the analytical error becomes significant for minor minerals, this analysis focuses on the variation of abundant minerals only. Mineral abundance below 1 percent should be considered as qualitative information only.

Terminology and mineral characteristics observed under microscopy are outlined below.

- Quartz: monocrystalline, rarely polycrystalline quartz.
- Feldspar: mainly potassic feldspar, minor plagioclase.
- Carbonate: mainly broken marine shells (bivalves and gastropods, rare brachiopods), and rare red algae, foraminifera, bryozoans and echinoderms. Grains commonly show dissolution or recrystallisation toward the base of the boreholes.
- Pyroxene and amphibole: coarse in recent sand and decreasing grain size with depth.
- Opaque grains: very well rounded ilmenite and other minor opaque minerals.
- Zircon and rutile: subhedral shape to moderately rounded.
- Garnet: rounded and generally as coarse grained as pyroxene and amphibole.
- Rock fragments: mafic igneous (dolerite?) and sandstone clasts, which are altered in old sands.
- Volcanic glass: microcrystalline igneous clasts (possibly basalts, fine dolerites and rhyolites).
- Completely altered grains: unidentified highly weathered minerals (possibly feldspar and pyroxene).
- Cement: very fine grained calcite (fragments or overgrowth) resulting from the breakdown of a weak cement.
- Iron hydroxide: very fine grained semi-translucent brown material (fragments or as grain coating), which is abundant towards the bottom of each borehole.
- Others: unspecified heavy minerals, including rare homogeneous and microcrystalline glauconite.

Quartz content varies between 40 to 90 % and presents an average of 70 % (Figure V.3 to V.6). Almost all samples studied contain a minimum of 2 % feldspar, whose abundance correlates with that of quartz (Figures V.3 to V.6). Samples enriched in heavy minerals (see opaque grains), and consequently depleted in quartz, contain 1 to 2 % feldspar.

Pyroxene (1 to 10 %), amphibole (3 to 8 %) and carbonate grains (0 to 6 %) present a decreasing trend down boreholes S2 and S3 (Figures V.4 and V.5). Borehole S1 is characterised by a consistently low content of pyroxene and amphibole (0.5 to 2 %), and by an absence of carbonate grains in the lower 35 m portion (Figure V.3).

Samples 21 and 27 of borehole S3 show high volcanic glass abundances (4 to 7 %), whereas other studied samples contain a maximum of 2 % (Figures V.3 to V.6).

In order to document the significant information given by the point count data, the following sections will describe important minerals and group of minerals by comparing their abundance between boreholes and field samples.

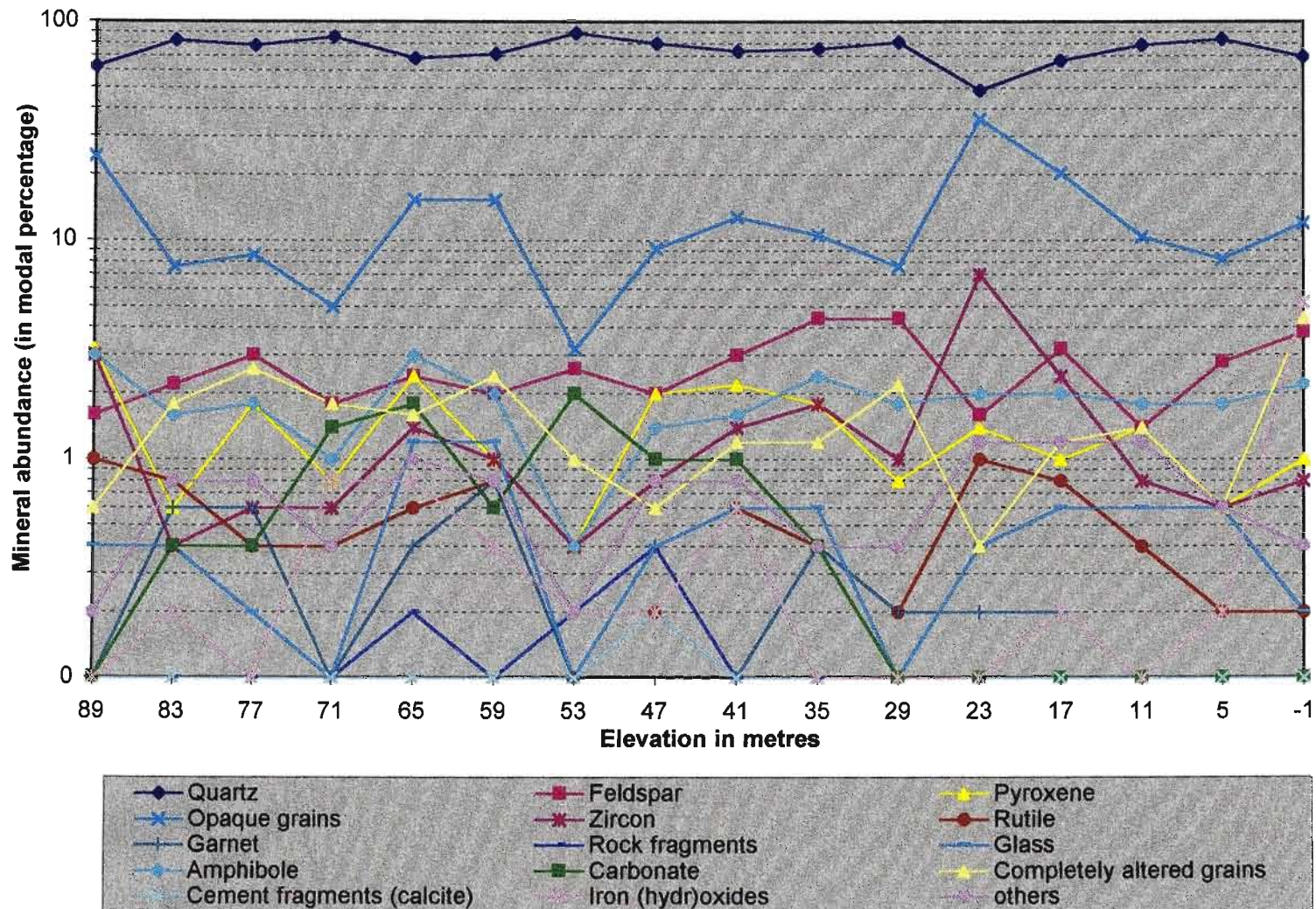
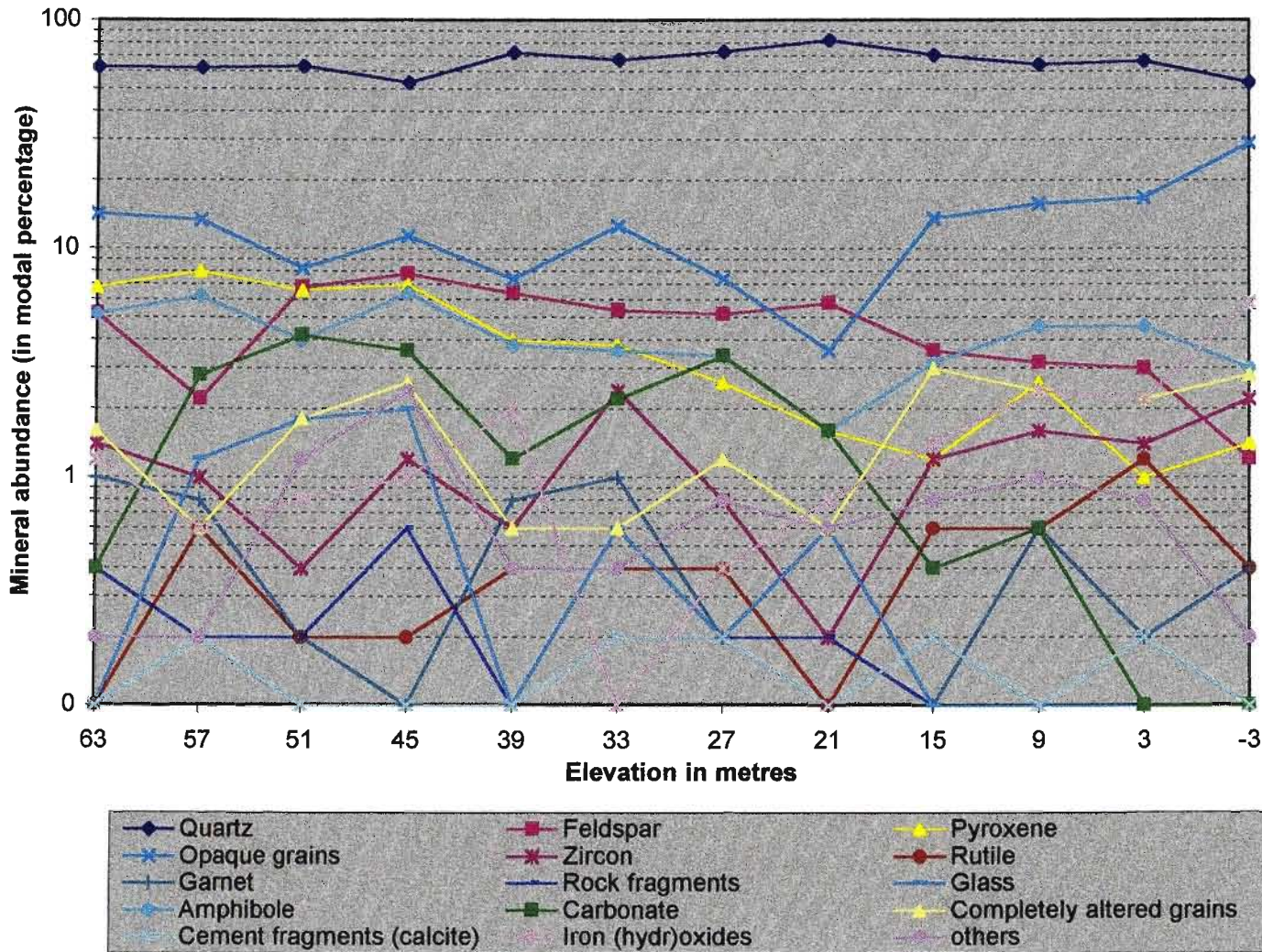
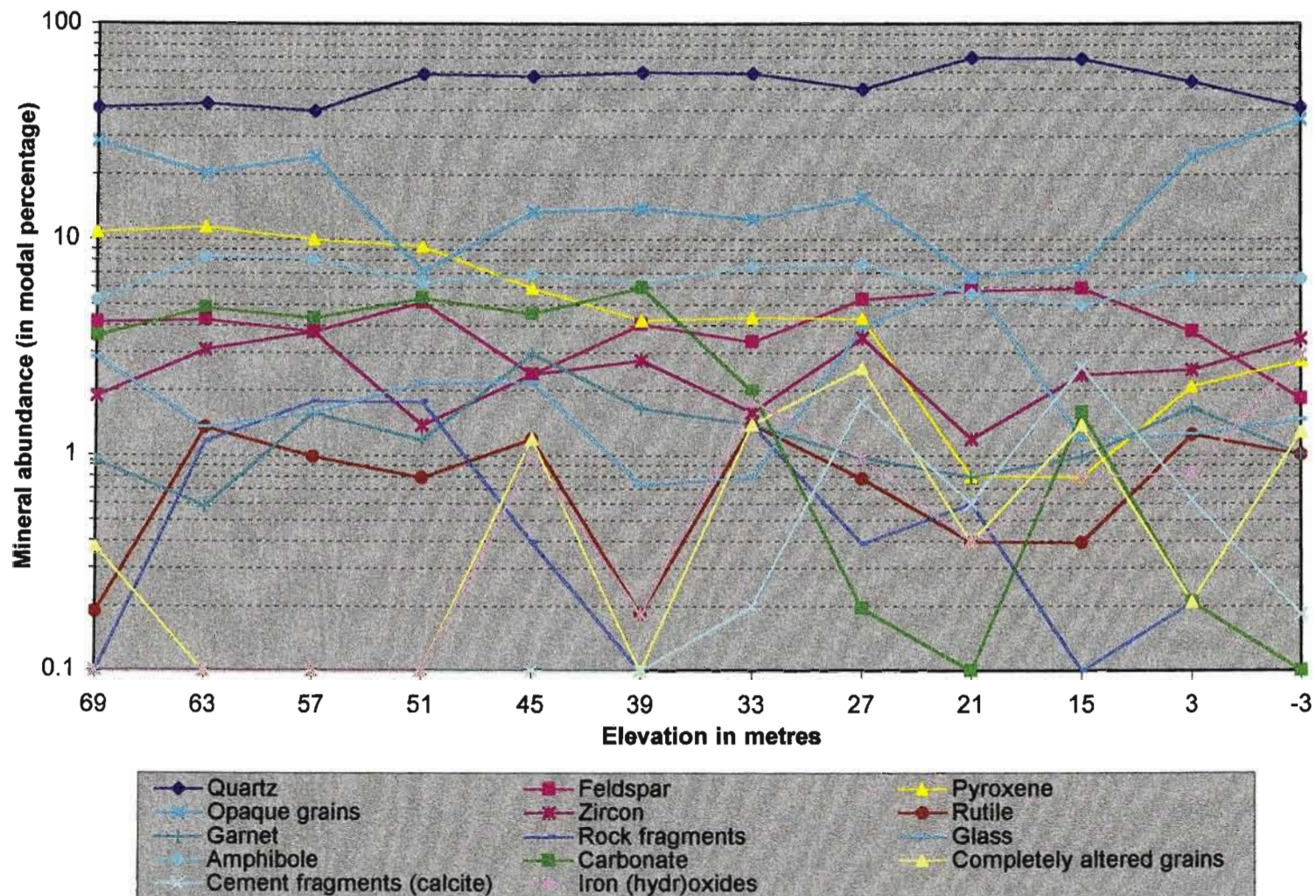


Figure V.3. Mineral abundance of the Line 380 borehole S1. See Section V.2.1 for an explanation of terminology.



**Figure V.4.** Mineral abundance of the Line 380 borehole S2. See Section V.2.1 for an explanation of terminology.



**Figure V.5.** Mineral abundance of the Line 380 borehole S3. See Section V.2.1 for an explanation of terminology.

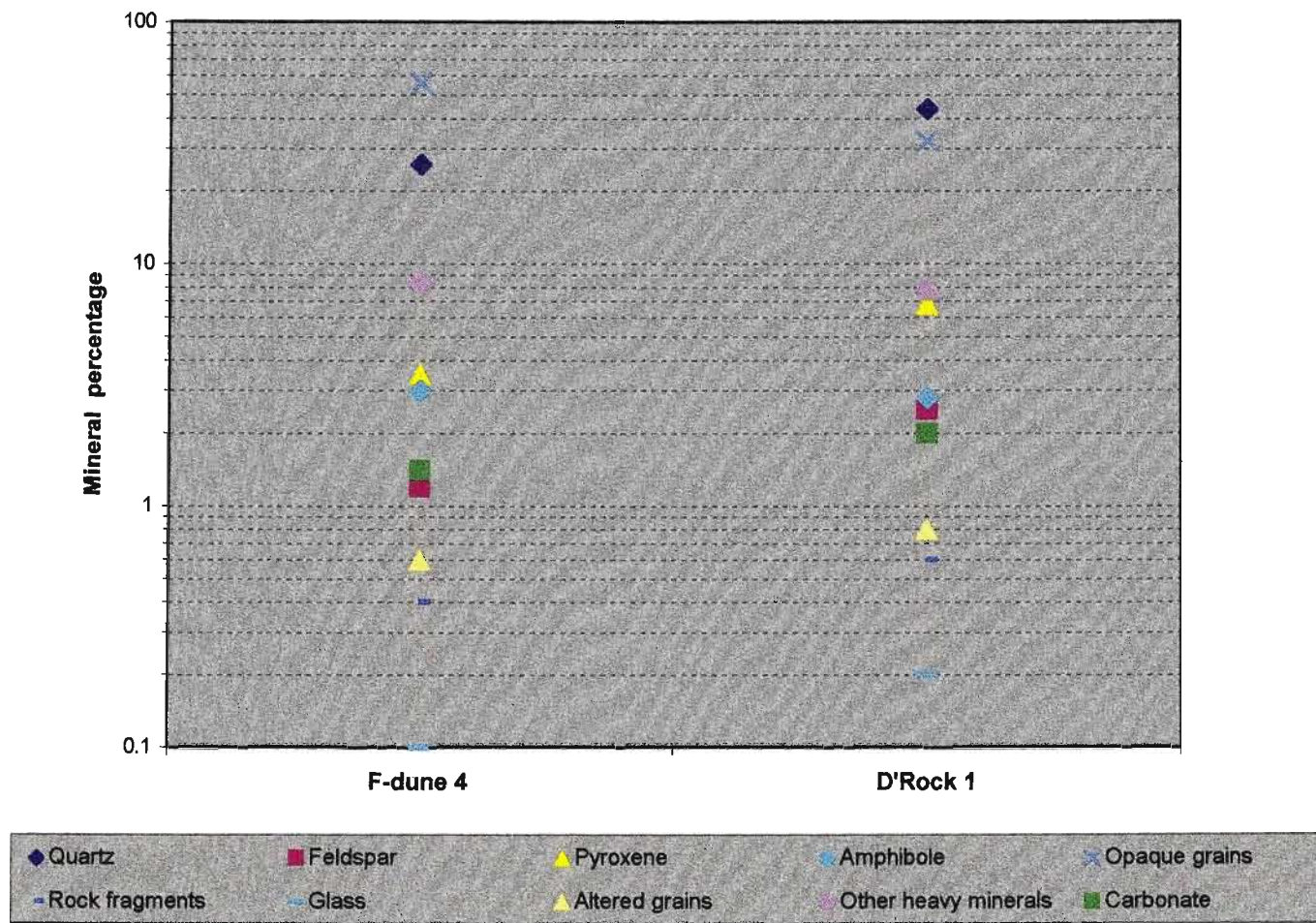


**Figure V.6.** Mineral abundance of D'Rock 1 and F-dune 4 field samples. See Section V.2.1 for an explanation of terminology

### V.2.1.1. Heavy mineral variation

The heavy mineral content in boreholes S1 to S3 varies from a low of 5 modal % to more than 50 modal % (Figure V.7). Heavy mineral abundance given by point counting is generally 3 to 5 times higher than those obtained by RBM's standard mineral separation techniques (Section I.3). However, their relative variation is almost identical for the two techniques (compare with Figure V.10).

Borehole S1 has a relatively low heavy mineral abundance throughout the borehole. The top sample represents the modern soil horizon and has significantly higher abundance values. The same is true for samples 23 and 17, which are nevertheless not interpreted as palaeosols but as sediments that were derived from nearby foredunes (see following sections).

Borehole S2 has a generally higher heavy mineral content and two distinct trends with depth are recognised. From the top of the borehole to ca. 20 m there is a regular decrease of heavy mineral content. This trend reverses at ca. 20 m and the values increase towards the bottom of the borehole.

Borehole S3 displays the same trend with depth (changing trend at 14 m) but with slightly higher heavy mineral values. The upper part of the borehole (from 69 m to 14 m above msl) can also be subdivided into three sub-units with relatively consistent heavy mineral values. The upper 20 m portion of borehole S3 shows very high heavy mineral content and is defined here as Unit E (Figure V.7).

The two field samples F-dune 4 and D'Rock 1 show very high heavy mineral content. The abundance of heavy minerals in sample D'Rock 1 correlates with the top three samples of borehole S3, which are considered to be derived from a beach – foredune system (Section V.2.2.1). The higher heavy mineral content of F-dune 4 compared to D'Rock 1 and the top three samples of borehole S3 suggest that aeolian transport is not as efficient at concentrating the heavy minerals as beach swash. This suggests a decrease of heavy mineral content from the foredune – beach system to purely aeolian dunes further inland.

### V.2.1.2. Rock fragments and carbonate grains

Sandstone and mafic igneous clasts dominate the diverse rock fragment assemblage found in the dune cordon. These rapidly weather into their constituent minerals due to in situ weathering and mechanical breakdown during transport. Since all samples are free-flowing sands, it can be deduced that ground water in the area is, at least during recent periods, undersaturated with calcium carbonate. In these conditions, marine carbonate grains are highly unstable and dissolve rapidly.

One means of assessing the weathering state of samples is to plot the sum of rock fragment and carbonate grain abundance (Figure V.8). Their abundance increases from the bottom to the top of each borehole, and from inland (borehole S1) towards the coast (borehole S3). As rock fragments and carbonate grains belong to the light fraction of the sand (in opposition to the heavy minerals), their abundance given in Figure V.8 should be multiplied by a factor of 3 to 5 to find their true abundance (see previous section). It should also be noted that carbonate grains are far more abundant than rock fragments, so that Figure V.8 would show similar trends at slightly lower values if only carbonate grains were considered.

In the upper 35 m portion of borehole S3 and the upper 40 m portion of borehole S2, the rock fragment and carbonate abundance is relatively high (> 2.5 %) compared to the lower portions of boreholes S2 and S3. The upper portions of boreholes S2 and S3 are here interpreted

as an individual sediment package, which includes Unit D and the heavy mineral rich Unit E (Figure V.8). One more unit, Unit B, is defined in this way by the upper 55 m of borehole S1.

Note that Unit B contains more carbonate grains than the bottom units of boreholes S2 and S3 (Figure V.8, and Figures V.3 to V.5). This observation will be of importance for later correlation (Sections V.3.1.4 and V.6).

The upper samples of boreholes S1, S2 and S3 show relatively low rock fragment and carbonate grain abundance. These samples are within the current soil horizon, where alteration is the most intense. Sample 39 of Unit D, borehole S2, shows a similar feature and is interpreted to be a buried palaeosol (Sudan *et al*, 1999). The two field samples present strikingly low rock fragments and carbonate abundance. D'Rock 1 was collected directly beneath the present soil and may have been altered by pedogenic processes. The high heavy mineral content of F-dune 4 could partly explain the low rock fragments and carbonate abundances.

### V.2.1.3. Pyroxene and amphibole

The pyroxene and amphibole fraction of the northern KwaZulu-Natal coastal dune cordon is mainly composed of augite and hornblende (Fockema, 1986). These mineral are, after carbonate grains, the least stable minerals of the assemblage present in the dune cordon (Goldich, 1938; Pettijohn, 1957). Furthermore augite is suspected to be more rapidly altered and reduced in grain size than hornblende (Berner & Schott, 1982).

Pyroxene abundance variations are best investigated using the ratio of pyroxene/total heavy minerals (pyroxene/thm) as heavy mineral content varies greatly throughout the dune cordon (Figure V.9). This ratio can be used as a proxy for weathering as unaltered sediments have relatively high values and increased weathering depletes the pyroxene fraction of the total heavy minerals, producing lower values.

The upper units of boreholes S2 and S3 (Units D and E) clearly show higher (>0.15) ratio values than the upper unit of borehole S1 (Unit B), which in turn presents, on average, higher values than the bottom of each borehole.

D'Rock 1 sample is depleted in pyroxene (2.5 %) compared to Unit E (6 %), which is its most likely lateral equivalent (Section V.2.1.1). Once again, its position beneath the present soil could explain this relatively more weathered state. The pyroxene/thm ratio value of F-dune 4 suggests that the foredunes are strongly weathered compared to Units B, D and E, and as weathered as samples from the base of the dune cordon. The reasons for this will be explained in the following section.

The Amphibole/thm ratio values for most samples are similar and have the same trends as the pyroxene/thm ratio values, and are not presented in detail here. Only borehole S3 shows some discrepancies between these two ratios (Figure V.9). Samples 15 and 21 of borehole S3 are characterised by a substantial increase in relative abundance of amphibole and are strongly decalcified. They are thus regrouped in Unit C (from 5 m to 30 m above msl in borehole S3), which comprises sample 27 because of its decalcification state. As it will be demonstrated in the following sections, Unit C always presents characteristics that are significantly different from the rest of the sediment in the study area.

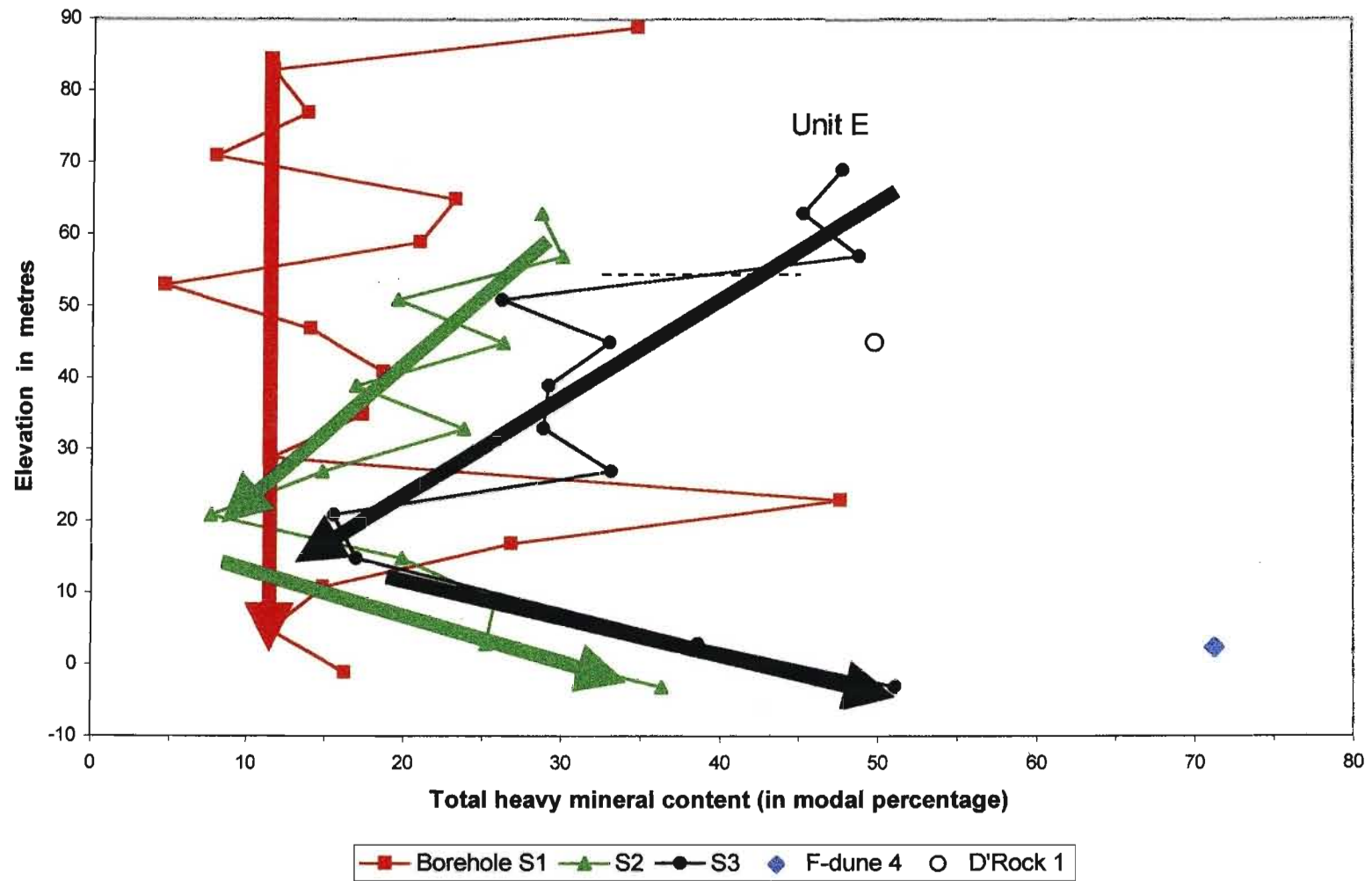


**Figure V.7.** Heavy mineral content of samples from boreholes S1, S2, S3 and field samples, plotted against the elevation above msl. Dashed line = unit boundary.

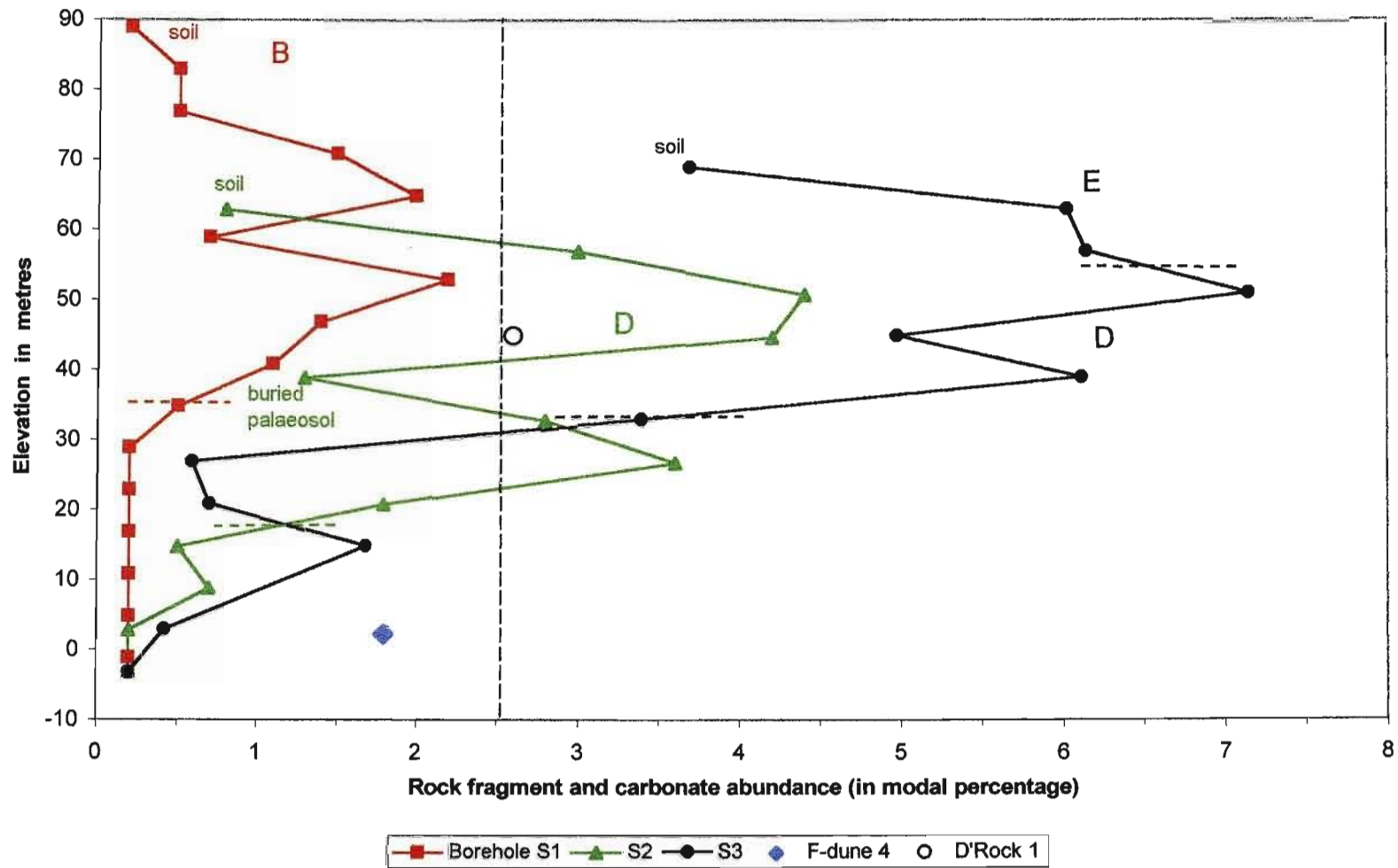
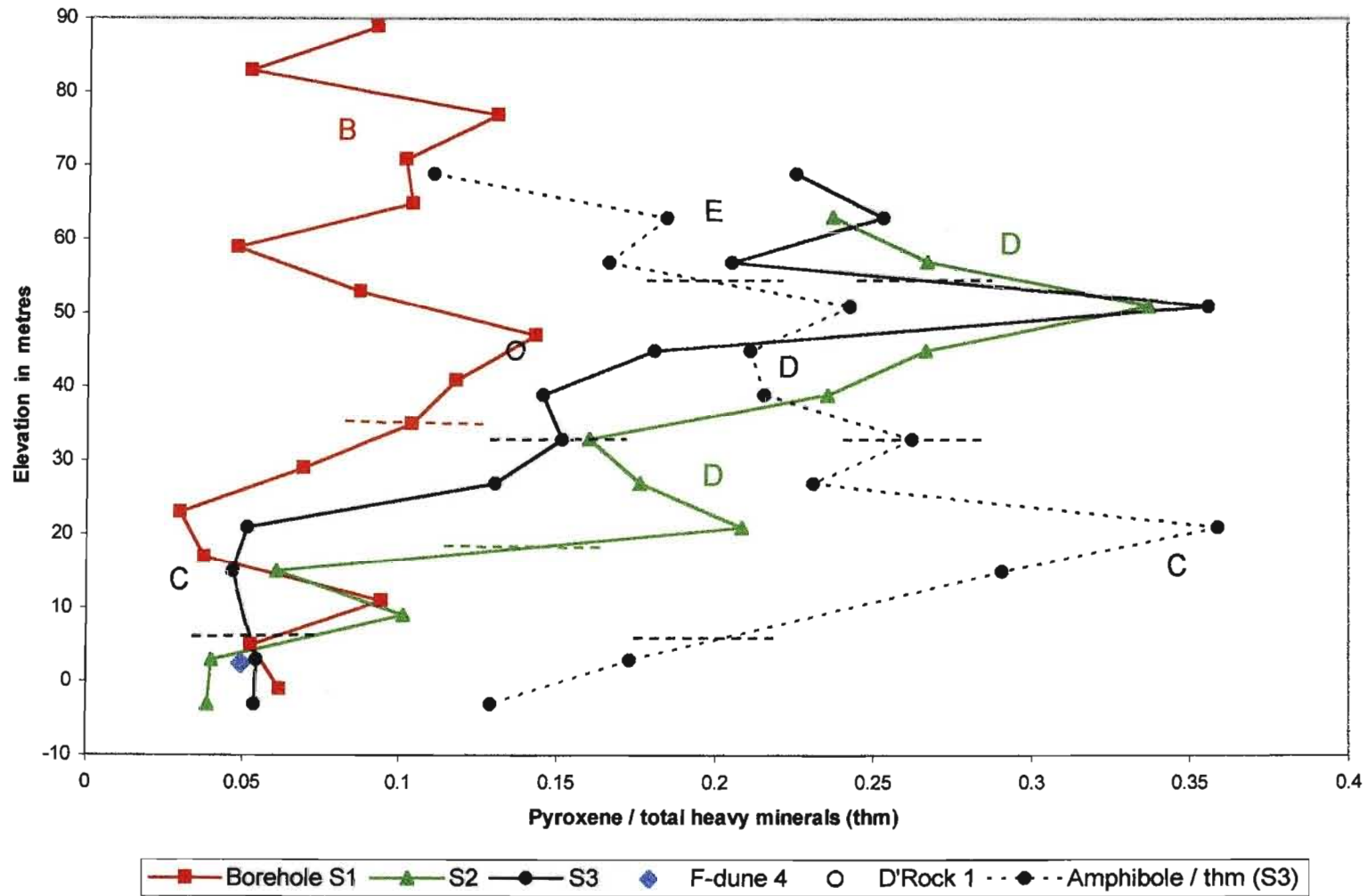


Figure V.8. Rock fragment and carbonate grain abundance of samples from boreholes S1, S2, S3 and field samples. Dashed lines = unit boundaries.



**Figure V.9.** Ratio of pyroxene divided by the total heavy mineral abundance for samples from boreholes S1, S2, S3 and field samples. Note that Unit D is found in boreholes S2 and S3.

## V.2.2. Heavy mineral abundance

Heavy mineral abundance (mass) ratios, obtained by magnetic separation techniques (Section I.3), are studied in order to define and characterise sedimentological units and to assess their relative degree of weathering. They are compared with data from other authors, especially from Hugo (1993).

Each mineral species presents a varying range of magnetic susceptibility due to solid solutions and intergrowths with other minerals and/or their alteration state (Hugo, 1993). Lätti (1997), Hugo & Cornell (1991) and Dawson (1997) studied the mineral occurrence amongst the different magnetic fractions obtained by a Carpco HIDMS magnetic separator. Their results are applied here to assess the mineralogy of the magnetic fractions given by RBM. If not specified below in brackets, mineral species are attributed to the magnetic fraction where they are most abundant.

- "Magnetite": mainly magnetite; and other Fe (Ti) – oxides such as iron rich chrome spinel.
- "Magnetics": ilmenite and altered ilmenite (95 % of total ilmenite content); remaining Fe (Ti) - oxides (> 60 % of total Fe (Ti) - oxides); up to 30 % of the total garnet; chromite; and possibly minor silicates.
- "Magnetic others": amphibole; pyroxene; garnet; epidote; remaining ilmenite (mainly altered and highly altered); staurolite; tourmaline; monazite; sphene; (leucoxene).
- "Non magnetic others": apatite; kyanite (Al-silicates); pyrite; leucoxene; (sphene).

Hugo (1993) classified the ilmenite grains found on the east coast of South Africa into "ilmenite", "altered ilmenite" and "highly altered ilmenite – leucoxene". Hugo (1993) showed that the ilmenite recovered in the "magnetics" fraction is composed of both "ilmenite" and "altered ilmenite". Therefore the ilmenite obtained by XRF at RBM correlates to the "ilmenite" plus "altered ilmenite" contents of Hugo (1993).

It must be noted that the ilmenite abundance given by RBM is possibly overestimated, for altered ilmenite has a higher TiO<sub>2</sub> content (more than 50 %). However, Hugo (1993) showed that recent dunes contain far more unaltered and homogeneous ilmenite than heterogeneous ilmenite (the latter showing by the way TiO<sub>2</sub> content less than 50 %) and ilmenite alteration products. Ilmenite abundance calculated by RBM is thus considered to be reliable.

### V.2.2.1. Absolute heavy mineral content

The absolute heavy mineral content in samples from boreholes S1, S2 and S3 has been recalculated by dividing the ilmenite abundance (obtained from RBM) by the ilmenite/total heavy mineral ratio (ILM/THM) (Figure V.10). The heavy mineral contents between 2 to 18 wt% are comparable to those given by Fockema (1986) for the dunes south of Lake Nhlabane. They are thus considered to express the true heavy mineral content compared to the point counting results. Even though variation trends are similar to those obtained by mineral point counting (Section V.2.1.1), the absolute abundances are significantly reduced and are discussed in this section.

The heavy mineral content of sediment offshore of Richards Bay can be as low as 0.8 wt%, but shows a mean of 3.7 wt% due to the presence of local placers that contain up to 15 wt% heavy minerals (Fockema, 1986). Most of the sediment under study contains between 2 to 7 wt% heavy minerals and is most likely derived from a beach - foredune environment (Figure V.10), which is one of the most efficient means of concentrating heavy minerals (Force, 1991).

Heavy mineral contents of 18 to 27 wt% have been observed in beaches at the Tugela River mouth and show a decreasing trend northward (Jordaan, 1996).

Heavy mineral content in dune sediment decreases with time, as unstable heavy minerals are weathered and finally leached away. This process explains why the upper unit of borehole S1 (Unit B) contains relatively low heavy mineral abundance compared to the upper units of boreholes S2 and S3 (Units D and E) (Figure V.10). It is assumed here that Units B, D and E were derived from beach – foredune systems. Interpretations for lower units will be dealt in the following sections.

By comparison, the Kosi Bay Formation contains significantly lower concentrations of heavy minerals (Singh & Dunlevey, 1997): less than 3.5 wt% for the white sand, and 3 to 6 wt% for the upper thin red-brown units. The KwaMbonambi Formation is characterised by similar heavy mineral content as those of the study area (Fockema, 1986).

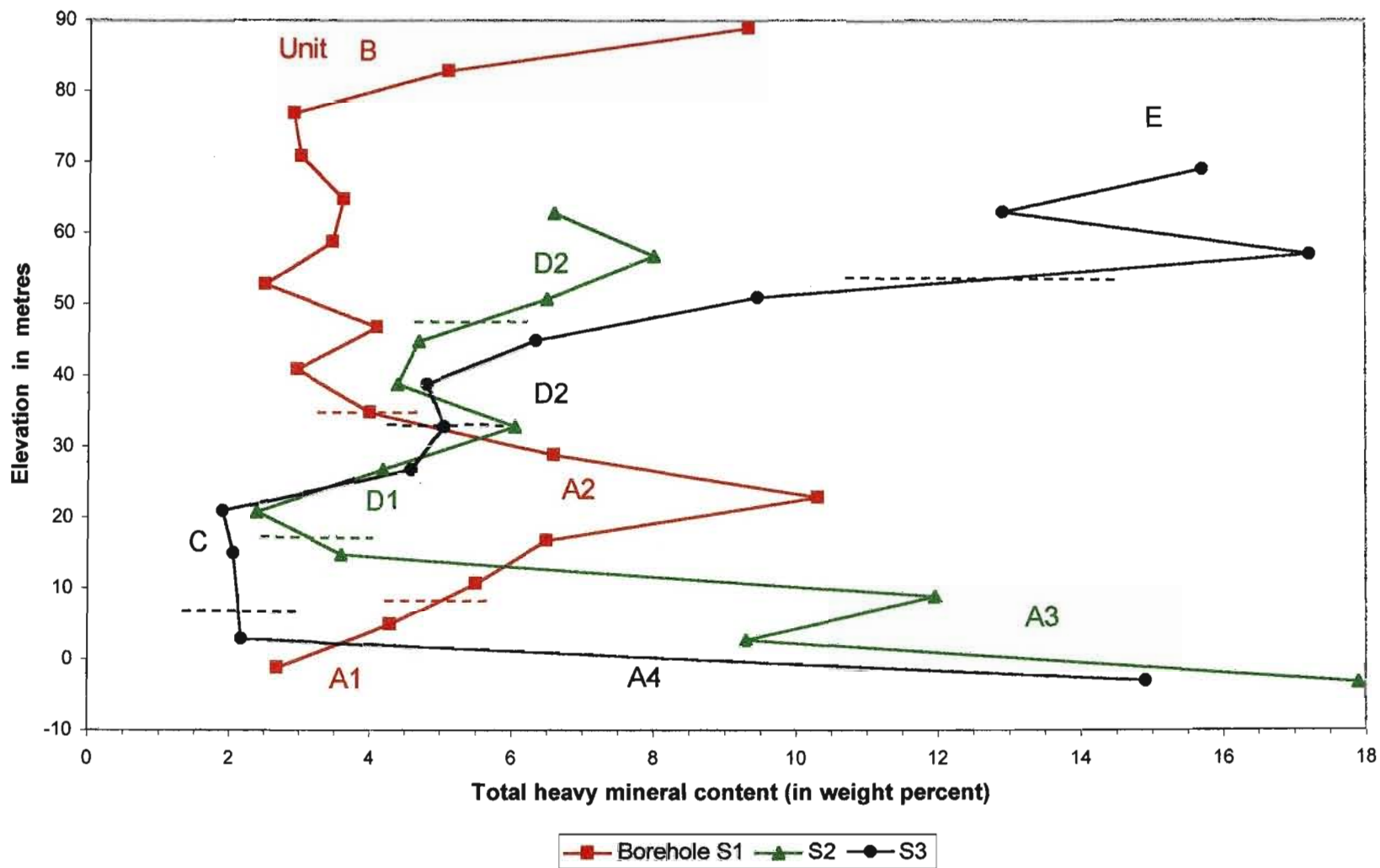
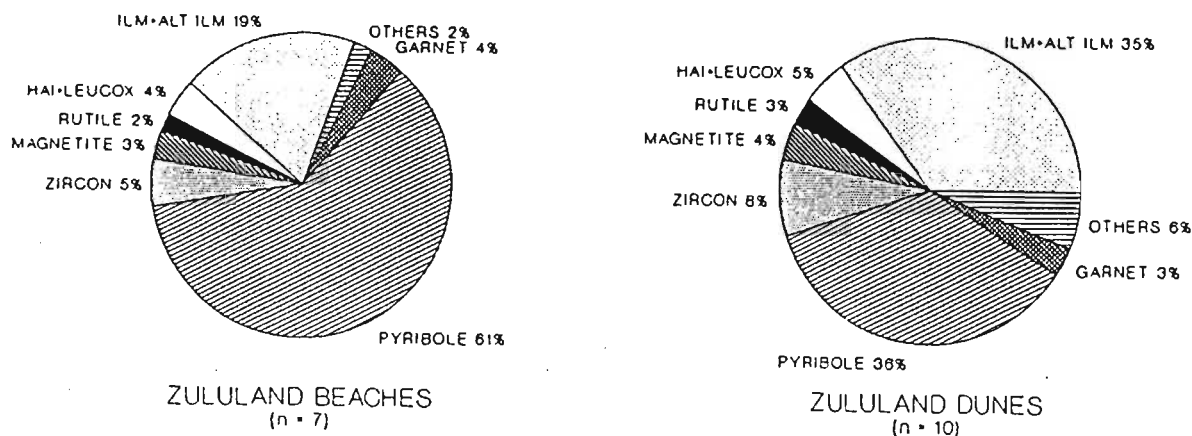


Figure V.10. Heavy mineral content for samples from boreholes S1, S2 and S3 (recalculated from RBM heavy mineral ratios). Dashed lines = unit boundaries.

## V.2.2.2. IRZ / OHM ratio

The most informative ratio values for discriminating dune units based on their heavy mineral abundance is provided by the ratio of ilmenite, rutile and zircon divided by other heavy minerals (IRZ/OHM). This ratio can be used as a proxy for weathering as ilmenite, rutile and zircon are the most resistant of the heavy mineral suite encountered (Force, 1991; Dill, 1998). Given a relatively consistent supply of heavy minerals during dune formation, high IRZ/OHM values indicate relatively weathered samples and high maturity of sand. Other factors, in addition to alteration, may also influence this ratio. These include grain size and shape, differential mineral sorting by wind and aqueous environments, and the proximity of the shoreline during dune formation. Force (1991) and Hamilton & Collins (1998) detailed all these processes, which will be discussed below.

The mean heavy mineral proportions of northern KwaZulu-Natal beaches and undifferentiated coastal dunes have been investigated by Hugo (1993; Figure V.11) who suggests that the difference in ratios between the beach and the dune is due to the difference of grain size (Figure V.12): ilmenite, zircon and rutile are fine grained compared to the pyriboles (amphibole and pyroxene) and are thus more abundant in the aeolian environment than in the coarser grained beach sediment. As discussed below the author disagrees with this interpretation and suggests that the difference in mineralogy between these two environments is due to an increase in the average maturity (age) of the dune sediments.



**Figure V.11.** Average heavy mineral proportions in northern KwaZulu-Natal beaches and coastal dunes (Hugo, 1993). n = number of samples. "Beach" samples were collected in the upper foreshore and on the beach berm.

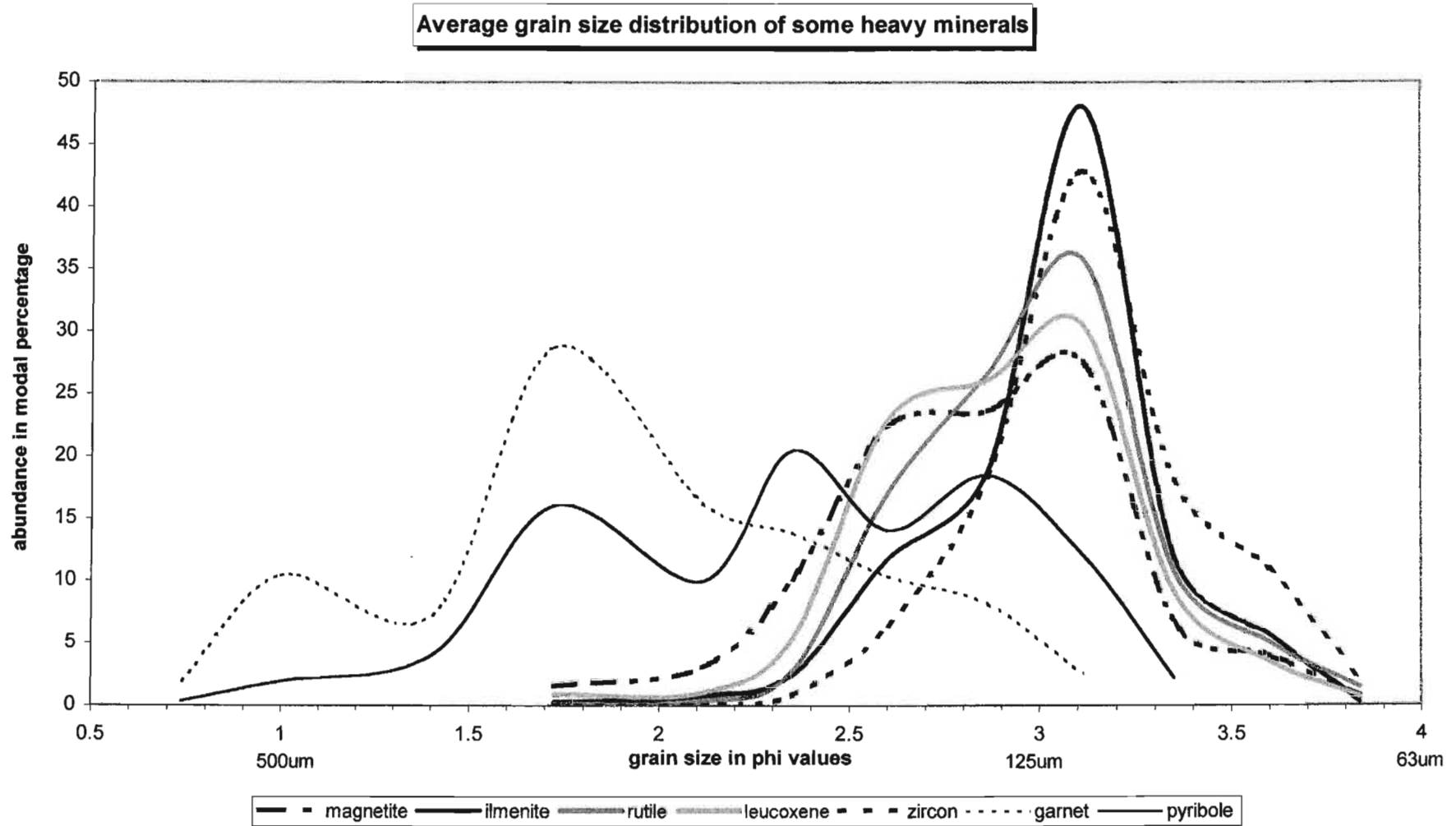


**Figure V.12.** Average grain size distribution of selected heavy minerals from coastal dunes near Richards Bay (data from Fockema, 1986 and Hugo, 1993).

In order to assess the maturity of diverse samples from the study area, IRZ/OHM ratios of local sediments have been obtained by recalculation of data from Hugo (1993) and Jordaan (1996). These ratios (Figure V.13) are derived from beach berm and swash zone deposits from the central and northern KwaZulu-Natal coast, between the Tugela River mouth and Sodwana Bay. Hugo (1993) studied a weathered red dune 1.5 km south of Lake Nhlabane; his HZ30 sample is considered to represent Dune Class 1 (Figure V.1 and Chapter IV) and has been thus renamed here "Dune Class 1" sample.

Beach sediments located close to the Tugela River mouth have lower IRZ/OHM values and are interpreted to be immature compared to those further north (Figure V.13). The somewhat restricted number of beach analyses presented in Figure V.13 suggests that Richards Bay beaches contain the most mature sediment along the northern KwaZulu-Natal coast. This suggests that northward longshore drift of immature fluvial sediment is gradually dispersed into a larger volume of mature shelf sediment. It also suggests that the fluvial sediment (Mfolozi and Mkuze Rivers) supplied to the St.-Lucia estuary system is already more mature than the Tugela River sediment (Figures III.2 and V.13). Unfortunately no fluvial and shelf ratio data are available to confirm these hypotheses.

The IRZ/OHM ratio values in the upper part of each borehole (Units B, D and E) are relatively consistent and decrease from inland towards the sea (Figure V.13). This supports the relationships shown on the geomorphological map (Figure V.1), in which dune age decreases from inland towards the sea. Unit D1 (from 20 m to 50 m above msl in borehole S2) is here defined by its higher ratio values compared to the overlying Unit D2 (upper 20 m of borehole S2) (Figure V.13).

The sediment of Unit E is believed to be derived from a beach – foredune environment (Section V.2.2.1). However, its IRZ/OHM ratio is lower than the average ratio for surrounding beaches (Figure V.13). This observation contradicts the hypothesis of Hugo (1993). It is believed that the lower ratio values (greater immaturity) of the coastal dune is due to selective transport of "OHM" (other heavy minerals) rather than relatively small and dense ilmenite, rutile and zircon (IRZ) during onshore aeolian transport from the coastline. The "entrainment equivalence" law, one of many summarised by Force (1991), governs mineral segregation during the transfer from beach to dune and during aeolian transport. In southeast Australia, Hamilton & Collins (1998) noted that "large, less dense grains such as garnet and hornblende are visibly more abundant in dunes farthest from the sea, while ilmenite and zircon are more abundant near the foredune". These authors also showed that aeolian dunes contained relatively more garnet than the beach.

An alternative hypothesis has to be considered. The possibility that Unit E was formed at a time when the beach had a lower IRZ/OHM ratio value and the sediment supplied to the dune was relatively immature such as the present beach at the mouth of the Tugela River. Immature sediment supplying Unit E would thus have been derived from the Tugela and possibly Nhlabane Rivers by longshore drift. In more recent times erosion, concomitant to the shoreline retreat, of older deposits such as the Kosi Bay Formation, caused the beach sand of the southern part of the KwaZulu-Natal coastal plain to become more mature (see below). Additional analysis presented below makes this hypothesis unlikely.

The mean IRZ/OHM ratio value for samples of Units B, D and E is greater than the mean value for northern KwaZulu-Natal beaches (Figure V.13). This finding is consistent with that of Hugo (1993) who showed that the mean beach sand is less mature than the mean aeolian sand of the present dune cordon (Figure V.11). However, it has been shown that the evolution with time of the IRZ/OHM ratio is more complicated. Dunes are initially less mature than their source environment (adjacent beaches) because of aeolian sorting processes. They then become increasingly mature with time as alteration proceeds, until their IRZ/OHM ratio values surpass those of adjacent beaches. This interpretation contrasts with that of Hugo (1993) (see above).

A striking feature of borehole S3 is low IRZ/OHM ratio values for Unit C (Figure V.13). These values are similar to ratio values for the overlying Units D2 and E, however, Unit C contains very few carbonate grains (Figure V.8). For Units E, D and B decalcification normally correlates to an increase in the IRZ/OHM values (compare Figures V.8 and V.13). IRZ/OHM values for the highly decalcified Unit C should therefore be higher than observed. It was shown in Section V.2.1.3 that this unit is characterised by an abnormally high amphibole content, which could explain the low IRZ/OHM ratio values.

In each of the boreholes studied relatively high IRZ/OHM values (ratio > 1) are located in the lower portion of each borehole (Figure V.13). This indicates that the dune cordon is underlain by an old unconsolidated sand substratum defined here as Unit A.

Dune Class 1 sample ("Berea-type red sand" facies) shows a similar high ratio value. This supports the interpretation of the geomorphology study (Sections IV.2.1 and V.1) that an older dune cordon (Dune Class 1) underlies the present coastal dune cordon. Unit A will be further subdivided in the following sections, to more precisely document internal characteristics.

Samples of other "Berea-type red sand" facies (HZ19, HZ18, HZ27 of Hugo, 1993) present IRZ/OHM values of 3.2, 3.55 and 3.55 respectively. HZ 18 and 27 were collected in Mtunzini, and HZ19 represents the red units of the Kosi Bay Formation, between Richards Bay and Lake Nhlabane. This suggests two different weathering states and possibly ages, supporting the finding that the "Berea-type red sand" is only a facies type, and does not constitute a single formation as noted by Botha (1997a).

Samples from the white coloured units of the Kosi Bay Formation have IRZ/OHM ratio values ranging from 2.5 to 6.2 (samples HZ21, 22, 23, 51, 52 of Hugo, 1993), all collected around Richards Bay). These ratio values are higher than all samples from the coastal dune cordon (Figure V.13). This suggests that the Kosi Bay Formation is absent from the southern part of the study area.

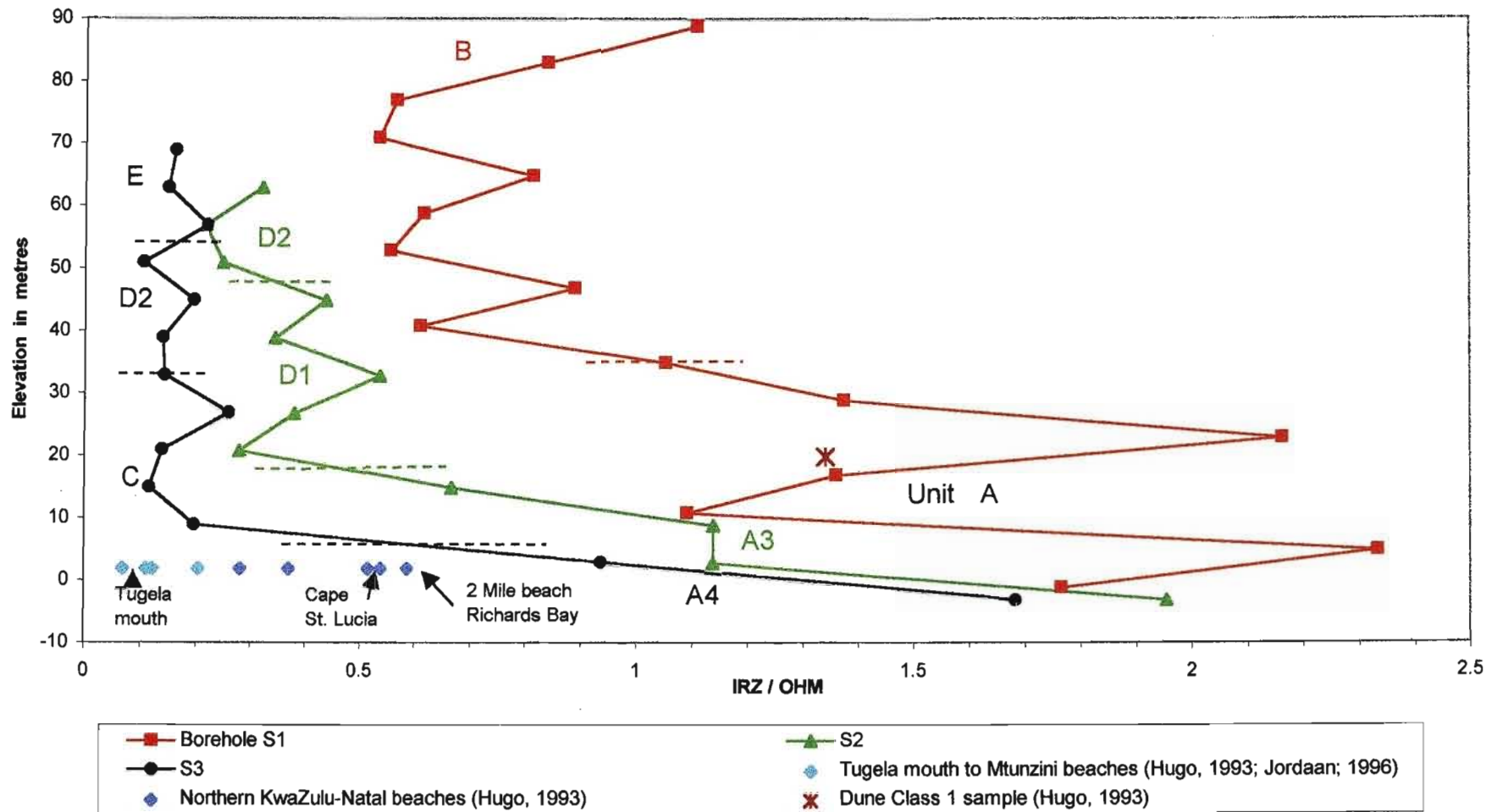


**Figure V.13.** Ratio of ilmenite, rutile and zircon divided by other heavy minerals (IRZ/OHM) for samples from boreholes S1, S2, S3 and field samples. Note that Unit D2 is found in boreholes S2 and S3.

### V.2.2.3. Magnetite / THM ratio

Hugo (1993) showed that magnetite (spinel group) found in the coastal environment of southeastern Africa presents a complex internal structure and composition. This mineral is sometimes partly enclosed in pyroxene grains and its chemical composition varies between magnetite and ulvöspinel. This study finds that ca. 70 % of magnetite in beach and dune sediment close to river mouths is homogenous (single mineral grains). This figure increases to more than 80 % away from river mouths, due to the break down of composite grains during marine reworking. This complexity results in a wide range of magnetic susceptibility for grains where magnetite is present. It is however assumed that the "Magnetite" fraction contains a majority of homogenous magnetite, few composite grains in which the magnetite mineral is dominant and minor iron rich chrome spinel (Hugo, 1993; Lätti, 1997).

For practical reason, the minerals from the "Magnetite" magnetic fraction will be referred to as magnetite. It should be noted that up to 30 % of the heterogeneous magnetite grains may be separated into other magnetic fractions.

Magnetite is generally less stable than ilmenite, rutile and zircon, and is more resistant to weathering than pyroxene, amphibole and some other silicate heavy minerals (Goldich, 1938; Dryden & Dryden, 1946; Pettijohn, 1957). Therefore the Magnetite/THM ratio should yield similar results to those obtained from the IRZ/OHM ratio. This relationship holds for the relatively young sand with increasing values of the Magnetite/THM ratio from Units E to D to B (Figure V.14). The ratio values for Unit E are similar or slightly lower than those for the present adjacent beaches and much lower than beach samples between the Tugela River mouth and Mtunzini.

If the sediment supplied to Unit E was mainly derived from the Tugela River (via longshore drift), the aeolian transport would have decreased the magnetite abundance by a minimum factor of 3 (Figure V.14). On the other hand, no mineral segregation would have effected the ilmenite, rutile and zircon abundances (see Figure V.13). This is unexpected, as these minerals are unlikely to be selectively sorted. Therefore Unit E sediment was derived from beaches whose ratio values (IRZ/OHM and Magnetite/THM) were similar to those of the present adjacent beaches. Further information will be given in the next section.

Unit A does not present a coherent variation in Magnetite/THM value compared to the IRZ/OHM ratio values. This suggests that Unit A is not homogeneous and it is divided into 4 units. Unit A1 (10m) and Unit A2 (25m) represent the lower 35 m of the borehole S1. Units A3 and A4 comprise the lower 25 m and 10 m of boreholes S2 and S3 respectively. To fully understand the reasons of the observed variations, Magnetite/Ilmenite ratio has to be considered (see next section).

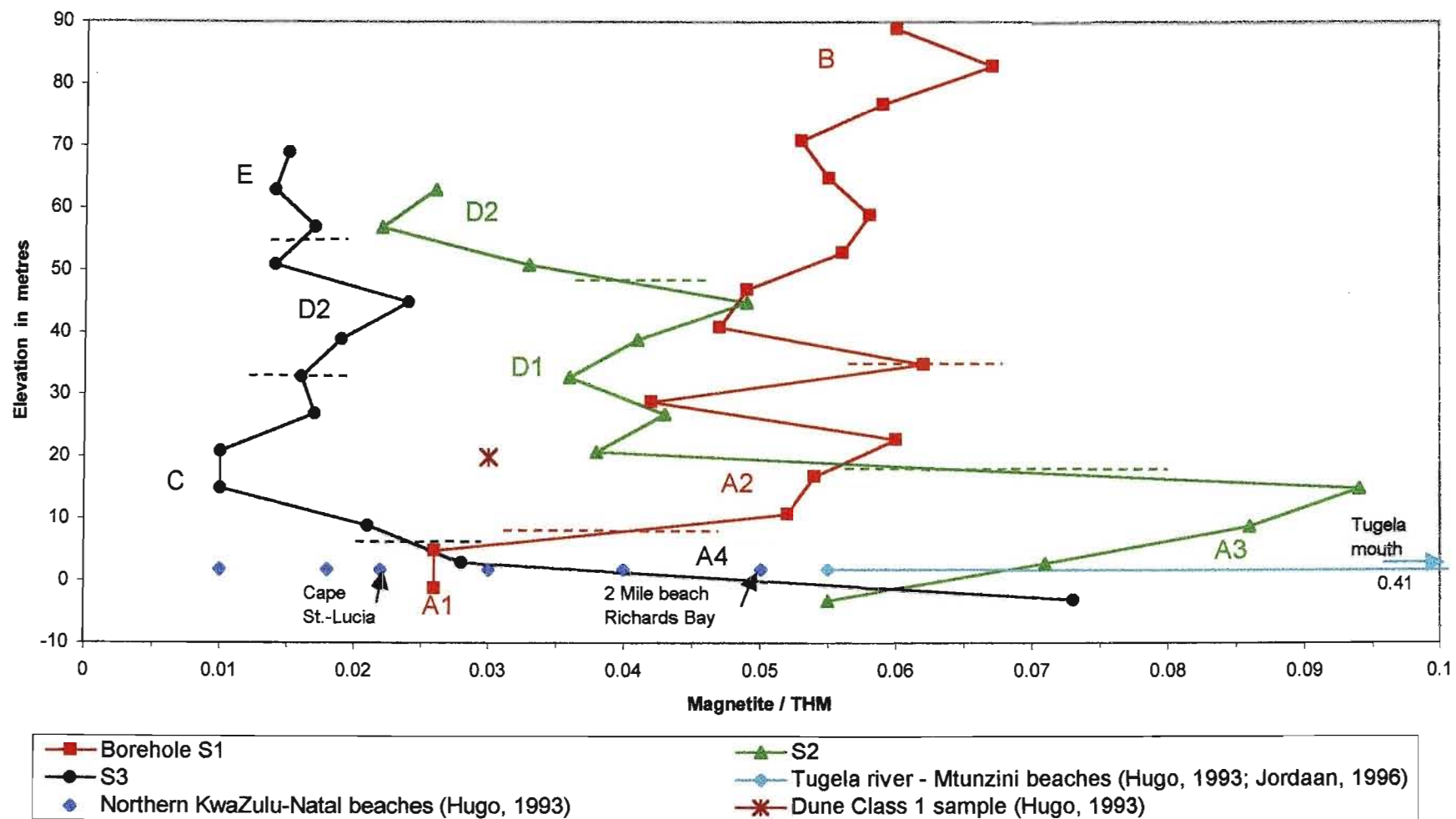
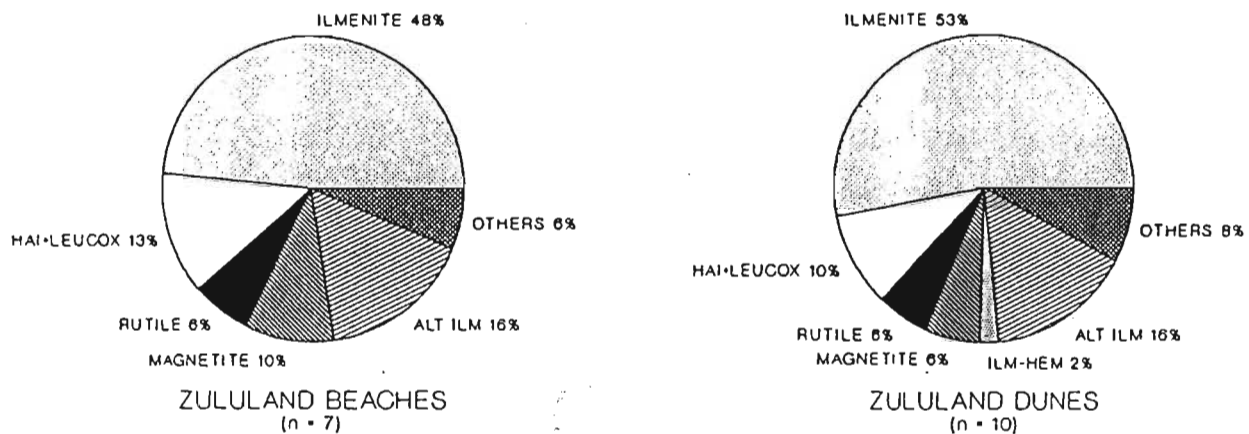


Figure V.14. Ratio of Magnetite divided by total heavy mineral content (Magnetite / THM) for samples from boreholes S1, S2, S3 and various field samples.

#### V.2.2.4. Magnetite / Ilmenite ratio

Hugo (1993) indicated that there is little proportional difference in iron-titanium oxide (as minerals) abundance between beach and dune sediments along the northern KwaZulu-Natal shoreline (Figure V.15). This is due to the absence of selective sorting by wave or wind action, as these minerals have similar densities and grain sizes (Figure V.12). The relative abundance of magnetite is, however, slightly lower in dunes than in beaches (Figure V.15). This difference can be explained by a higher weathering state of the average coastal dunes, further suggesting that the grain size influence is insignificant compared to alteration when the dune cordon is considered as a whole (Section V.2.2.2).



**Figure V.15.** Average iron-titanium oxide proportions in northern KwaZulu-Natal beaches and coastal dunes (Hugo, 1993). n = number of samples.

Beach sediment from central and northern KwaZulu-Natal shows a wide range of Magnetite/Ilmenite ratio values that decrease northward from the Tugela River mouth (Figure V.16). Possible explanations for this phenomenon are grouped below into three hypotheses.

a.) Magnetite-rich fluvial sediment is supplied to the coast by the Tugela River, at a Magnetite/Ilmenite ratio greater than 3 (Figure V.16). Mechanical breakdown of composite grains and/or dissolution of magnetite in the marine environment leads to a progressive decrease of ratio values during northward longshore drift (Hugo, 1993; Ramsay, 1999, pers. com.). This hypothesis is unlikely as magnetite is believed to be as stable as ilmenite in the marine environment (Dimanche & Bartholome, 1976), and because at the Tugela River mouth 70 % of magnetite grains are homogeneous (Hugo, 1993).

b.) Differential sorting of magnetite and ilmenite during longshore transport causes decreasing ratio values northwards from the Tugela River mouth. In this case, magnetite does not migrate northward at the same rate as ilmenite, and is concentrated close to the source sediment. This hypothesis is unlikely because magnetite and ilmenite are not expected to be preferentially sorted; magnetite is slightly more dense than ilmenite (5.2 cf. 4.7) but is slightly coarser (Figure V.12). These two differences are expected to compensate for each other and imply similar behaviour for both mineral during hydraulic transport (Force, 1991).

c.) Sediment from the continental shelf offshore of KwaZulu-Natal has a relatively low Magnetite/Ilmenite ratio. Shelf sediment is relatively impoverished in magnetite and unstable minerals such as amphibole and pyroxene (Ramsay, 1999, pers. comm.). Magnetite-rich sediment from the Tugela River is increasingly mixed with shelf sediment during the longshore drift, which decreases the ratio values northward. This hypothesis is supported by the work of

Hugo (1993) on ilmenite, its alteration products and their distribution along the southeastern coast of South Africa.

In conclusion, the beach sediment surrounding the study area appears to be a mixture of immature fluvial sediment (mainly from the Tugela River) transported northward by longshore currents and relatively mature sediment from the continental shelf. It is further suggested that extensive mixing occurs north of Mtunzini. This is explained by two factors. Firstly the coast between the Tugela River mouth and Mtunzini is the only prograding shoreline observed in KwaZulu-Natal (McCarthy, 1988), and its beach sediment is therefore more likely to store the immature fluvial sand. On the other hand, coastal erosion in the north supplies to the beach additional mature sediment from the Kosi Bay Formation and older deposits. Secondly, the break in the coastline direction at Mtunzini (Figures II.1 and III.2) hampers the northward longshore drift, reducing the immature sediment transfer to the beaches of the northern KwaZulu-Natal coastal plain. Luepke (1980) observed similar heavy mineral segregation at headlands of the Californian coast.

Magnetite/Ilmenite is not a reliable discriminate of relatively young sediments, as evidenced by overlapping values for Units B, D and E (Figure V.16). This ratio can, however, distinguish older units, as magnetite alteration and leaching proceeds more rapidly than ilmenite alteration. Consequently Magnetite/Ilmenite ratio values decrease from young Units B, D and E to older Unit A and the Kosi Bay Formation. The Dune Class 1 sample correlates well with Unit A1, suggesting that Unit A1 is the coastal extension of Dune Class 1.

The relative stratigraphy proposed here has to be considered with caution, as the ratio values are not only influenced by the alteration state of the sediment, but also by the initial maturity of the source sediment. Samples from Unit A3 and the base of Unit D from borehole S2 exhibit abnormally high values for Magnetite/Ilmenite. This implies relatively high magnetite or low ilmenite abundances compared to the adjacent beach and the rest of the samples analysed (Figure V.16). The high ratio values may reflect derivation from an immature sediment source such as observed at the Tugela River mouth. This can be explained by either a more effective northward longshore drift from the Tugela River mouth sediment, or a direct supply of immature sediment from surrounding rivers (Nhlabane River or Mlhatuze River). The mineralogy characterising these rivers is unfortunately unknown.

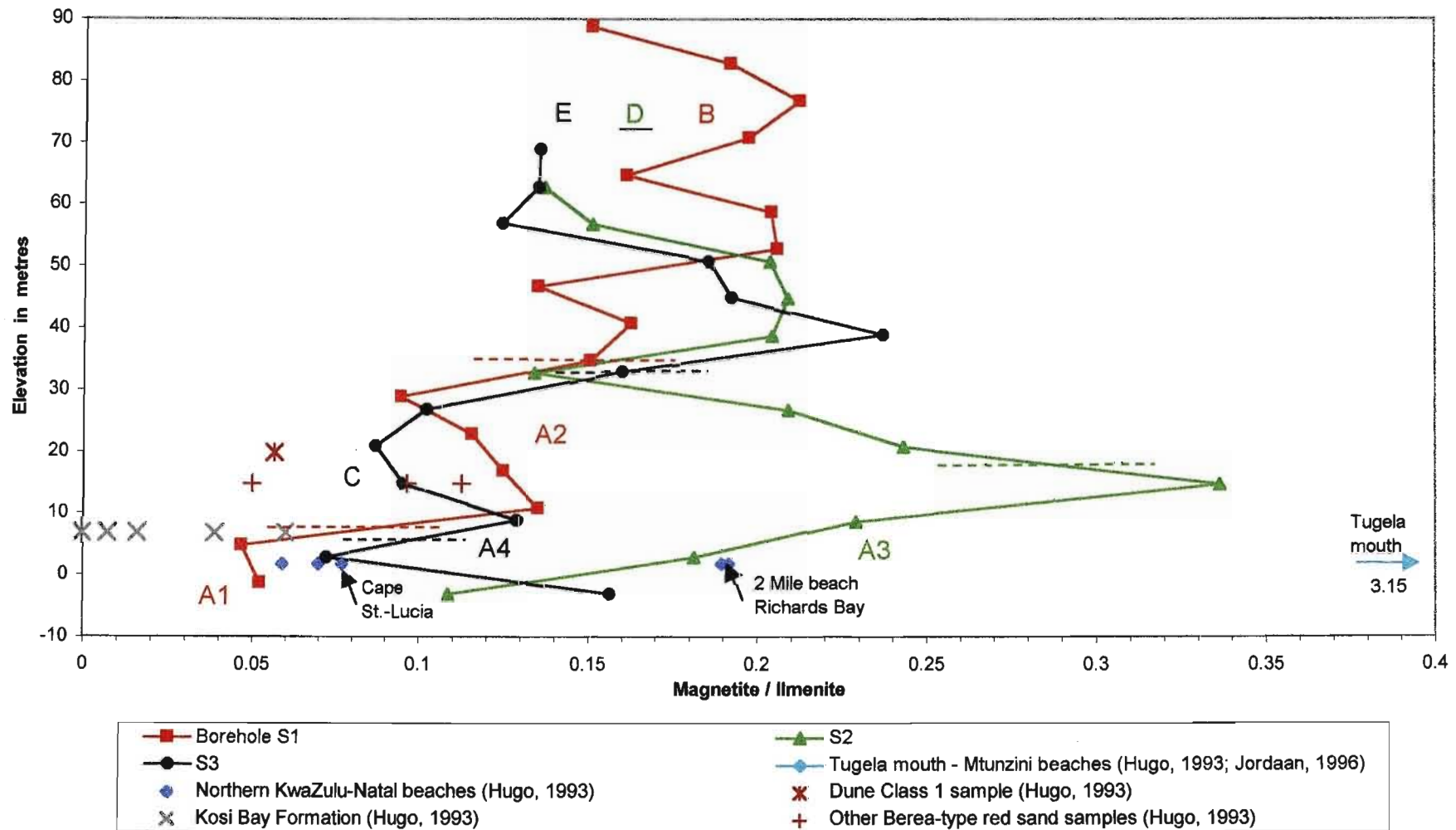


Figure V.16. Ratio of Magnetite divided by ilmenite (Magnetite / Ilmenite) for samples from boreholes S1, S2, S3 and various field samples.

## V.3. Geochemistry

### V.3.1. General description

Forty samples from boreholes S1, S2, S3 and two foredune samples (F-dune 4 and F-dune 2) were analysed by X-ray fluorescence for major and trace elements (Appendix B). The abundance of major elements in these samples is plotted without silica in Figures V.17, V.18, V.19 and V.20. SiO<sub>2</sub> content varies between 81 to 95 weight percent, and shows an antipathetic variation with heavy mineral content. Previously defined sedimentological units are marked on Figures V.18 to V.20, to help identify distinct geochemical signatures.

For the following discussion and interpretations, it will be assumed that the TiO<sub>2</sub> and Zr concentrations in dune sands has not altered, as these two elements are considered to be the most stable elements under terrestrial weathering (Augustithis, 1983). Their abundance is interpreted to reflect the relative abundance of titanium oxides and zircon respectively. If not specified otherwise the TiO<sub>2</sub> and Zr abundance is used as a relative and indirect measure of the original heavy mineral content.

#### V.3.1.1. Foredunes

F-dune 4 and F-dune 2 samples represent foredunes in two different environments. Cliffs that are currently being eroded by wave attack (Section V.1.2 and Chapter IV) surround F-dune 4. The foredune where F-dune 2 has been sampled is located on a shoreline portion that is stable or maybe prograding. Coastal erosion of unconsolidated sand is known to supply a considerable amount of sediment to a beach system (Komar, 1976). In the study area this sediment is altered (very high IRZ/OHM ratio) and decalcified. This could explain why F-dune 4 presents relatively high titanium and surprisingly low magnesium content compared to sample F-dune 2 (Figure V.17). It will be seen in Section V.3.2.1 that the MgO content is mainly related to the silicate heavy minerals (amphibole, pyroxene) and that its variation due to carbonate abundance is only secondary. In order to verify this hypothesis more foredunes need to be sampled, as many different mineral segregation processes affect the beach and nearshore environments.

F-dune 4 and F-dune 2 contain relatively high TiO<sub>2</sub> (2 to 3 wt%) abundance (Figure V.17), reflecting concentration of total heavy minerals in the adjacent beach environment. For the discussion below, samples with TiO<sub>2</sub> abundance greater than 3 wt% will be interpreted as a beach – foredune deposit.

#### V.3.1.2. Borehole S3 (coastal)

Calcium is incorporated into various minerals within the coastal dune cordon. These include Ca-feldspar (anorthite), carbonate and silicate heavy minerals. The relative abundance of CaO and L.O.I. (Lost On Ignition) values in borehole S3 correlates well with carbonate abundance from point count data (Figures V.18 and V.5). The uppermost Unit E is defined by a high CaO (6 to 7 wt%) and L.O.I. (4 wt%) content (Figure V.18), indicating a very high carbonate content. The top sample represents the present soil and is characterised by relatively low CaO and L.O.I content. Relatively high TiO<sub>2</sub>, Fe<sub>2</sub>O<sub>3</sub>, MnO and MgO (Al<sub>2</sub>O<sub>3</sub> in a lesser extent)

abundances indicate a high total heavy mineral abundance for Unit E (Sections V.2.1.1 and V.2.2.1).

Unit D2 is characterised by 4 wt% CaO, 3 wt% L.O.I and relatively low TiO<sub>2</sub> (0.5 to 0.9 wt%) content. The uppermost sample 52 of Unit D2 shows higher values for both CaO (5.5 wt%) and L.O.I (ca. 4 wt%), which are similar to Unit E. This suggests that sample 52 belongs to Unit E. However, Unit E is richer in total heavy minerals than sample 52 of Unit D2, as indicated by respective TiO<sub>2</sub> content (Figure V.18).

Unit C is characterised by a relatively high Al<sub>2</sub>O<sub>3</sub> content, which ranges from 3 to 4 wt% and is significantly more abundant than any other major element (after the silica). Unit C is the only sediment package from the study area with this trend. Moreover, the P<sub>2</sub>O<sub>5</sub> content of 0.9 to 1.3 wt% in Unit C is also the highest encountered in the dune cordon under study (Appendix B).

The basal Unit A4 exhibits very high TiO<sub>2</sub> and Fe<sub>2</sub>O<sub>3</sub> abundances at its base, much higher than the foredunes (compare Figures V.17 and V.18). This suggests that its depositional environment was a beach, at least for the bottom sample. The top sample of the unit is considered as an aeolian dune because of its relatively low TiO<sub>2</sub> content. Unit A4 is further discussed in Section V.3.1.3.

### V.3.1.3. Borehole S2 (central)

Borehole S2 shows similar downhole geochemical variation to borehole S3 (Figure V.19). A higher CaO and L.O.I. content (carbonate content) distinguishes Unit D2 from Unit D1. Unit D2 of borehole S2 contains similar CaO (4 wt%), L.O.I. (ca. 3 wt%) and total heavy mineral content (TiO<sub>2</sub> = 0.7 to 1 wt%) to Unit D2 of borehole S3 (Figure V.10).

Sample 63 at the top of Unit D2 has been affected by soil alteration and consequently shows a very low CaO and L.O.I. content. The comparative lower abundances of CaO and L.O.I. in the present soil of Unit D2, borehole S3, compared to the present soil of Unit E, borehole S2, suggests that the latter soil is younger and less affected by alteration and soil development. This interpretation is consistent with the geomorphology study; the central dune (Dune Class 4) is considered to have formed before the coastal dune (Dune Class 5) (Chapter IV).

Unit A3 contains elevated abundances of Fe<sub>2</sub>O<sub>3</sub> (5 to 10 wt%) and TiO<sub>2</sub> (2 to 6 wt%) reflecting relatively high concentrations of iron and titanium oxides and other heavy minerals. The bottom sample of Unit A3, like Unit A4, is therefore considered to have been deposited in a beach environment, which underlies an associated foredune (two middle samples) and an aeolian dune (top sample).

Strikingly, the TiO<sub>2</sub> content and IRZ/OHM values increase rapidly with depth in Units A3 and A4 (compare Figures V.18, V.19 and V.13). This suggests that the high IRZ/OHM ratio values found at the bottom of Units A3 and A4 are not due to an increased alteration state (older age), but due to a significant mineral segregation leading to the selective concentration of iron and titanium oxides (IRZ) relative to other heavy minerals (OHM). Such mineral segregation is commonly observed in the swash zone of a beach, where wave swash and backwash tend to concentrate small, dense grains (IRZ) by a combination of "settling" and "entrainment" or by shear sorting (Sallenger, 1979; Collins & Hamilton, 1989). The thickness of these swash zone placers can reach 10 m or more (Force, 1991), and can contain more than 40 % heavy minerals (Jordaan, 1996; Hamilton & Collins, 1998). Variations of the IRZ/OHM ratio values for Units A3 and A4 are also linked to the grain size characteristics (Section V.4.2).

Units A3 and A4 are interpreted to represent a transition from beach sediments at sea level overlain by aeolian deposits. A representative IRZ/OHM value for these units is that for the uppermost aeolian sample at 15 m above msl in borehole S2 and 3 m above msl in borehole S3 (Figure V.13). A representative aeolian value must be used to allow sample comparison without

being influenced by depositional environment. Therefore the IRZ/OHM value for Units A3 and A4 is between 0.6 and 1 (Figure V.13). The IRZ/OHM value between 0.6 and 1 for Units A3 and A4 is similar to the IRZ/OHM value for Unit B (Figure V.13). This suggests that the sediments of Units B, A3 and A4 are of similar age. However, Unit B is interpreted to be reworked from Units A3 and A4 with unaltered sediment, as point counting revealed relatively high carbonate abundance for Unit B (Section V.2.1.2). Thus only Units A3 and A4 are considered to be true lateral equivalents.

#### V.3.1.4. Borehole S1 (inland)

Unit B of borehole S1 contains relatively low CaO concentration and L.O.I. values, correlating with low carbonate grain abundances (Section V.2.1), compared to Units D and E (Figure V.20). This suggests an older age for Unit B compared to Units D and E. Whereas L.O.I. values are lower than CaO content for Units D and E, these values are similar for Unit B (Figures V.18 to V.20). This suggests that Ca-feldspar and silicate heavy mineral abundances are considerably reduced by weathering in Unit B.

The top sample of Unit B is characterised by high TiO<sub>2</sub> content and associated heavy mineral abundance (Figures V.10 and V.20), which could be related to the presence of the modern soil and palaeosols described in Section IV.4.2.2. Soil and vegetation are known to selectively trap heavy minerals relative to light minerals (Bagnold, 1941; Tinley, 1985).

The TiO<sub>2</sub> content of Unit B presents an average of 0.75 wt%, which is similar to Unit D. This observation suggests that Unit B was originally richer in total heavy minerals, and that the inland dune sediment was derived from a beach – foredune system (Section V.2.2.1).

From these observations and the previous section it appears that Unit B derives from the beach – foredune system of Units A3 and A4. However, a relatively higher carbonate content in Unit B (Section V.2.1.2) suggests that the inland dune was formed by a later reworking that added some immature and calcareous sediment.

Unit A2, borehole S1, is relatively enriched in Fe<sub>2</sub>O<sub>3</sub> and TiO<sub>2</sub>, indicating a high original heavy mineral content (Figure V.20). By showing a TiO<sub>2</sub> content of 3 wt%, sample 23 sediment may represent a foredune or was a transgressive aeolian dune deposited very close to the associated palaeo-shoreline. Its high IRZ/OHM ratio value (Figure V.13) is therefore interpreted to be due to its palaeogeographical position rather than to an older age, as discussed in the previous section. The homogeneity of the Magnetite/Ilmenite ratio (Figure V.16) further suggests a similar age for all samples of Unit A2.

The lowermost samples (Unit A1) of borehole S1 exhibit low CaO abundance and relatively high L.O.I. and Al<sub>2</sub>O<sub>3</sub> values (Figure V.20). This is interpreted to reflect intense dissolution of carbonate bioclasts and other Ca-bearing minerals, and precipitation of aluminium – iron hydroxide grains (Figure V.3) and grain coatings (Walker, 1967; Dunlevey, 1997). Bulk sample analysis of “Berea-type red sand” from a dune at Mtunzini (Dunlevey, 1997) showed significantly higher Fe<sub>2</sub>O<sub>3</sub>, Al<sub>2</sub>O<sub>3</sub> and L.O.I. abundances than the dune cordon samples under study. This can be explained by the loss of fine fraction in the borehole samples from the RBM storage room (Section I.3).

### Geochemistry of F-Dune 2 and F-Dune 4

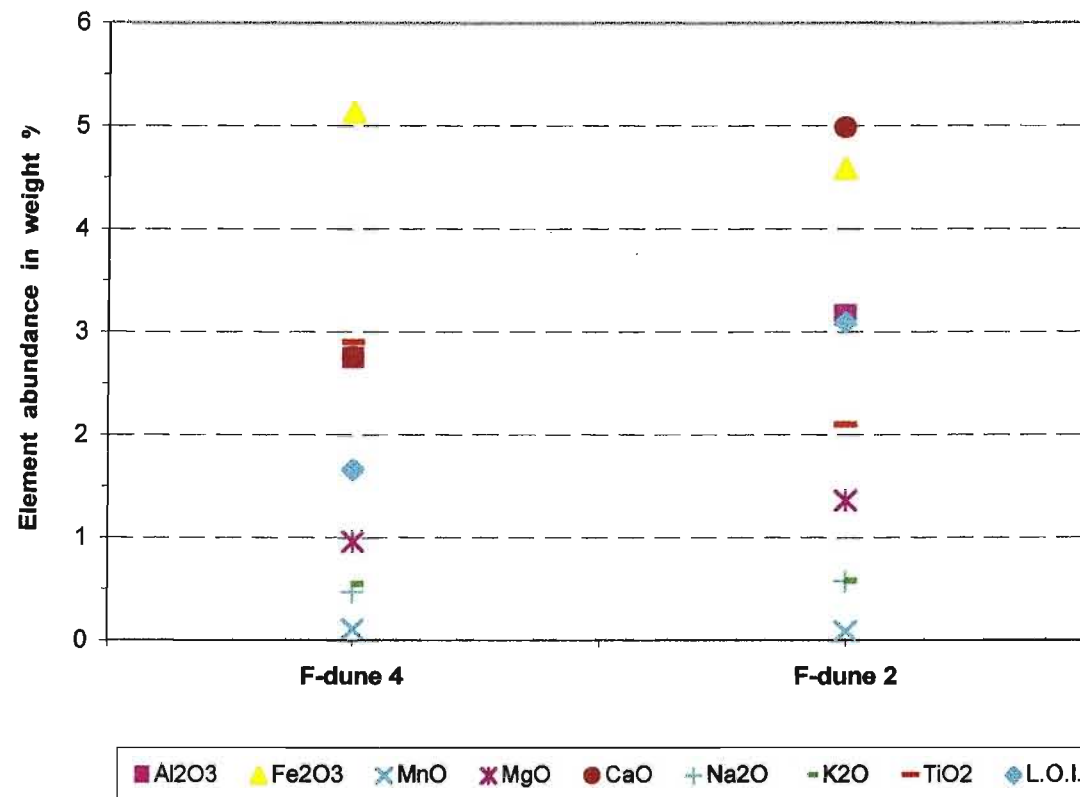
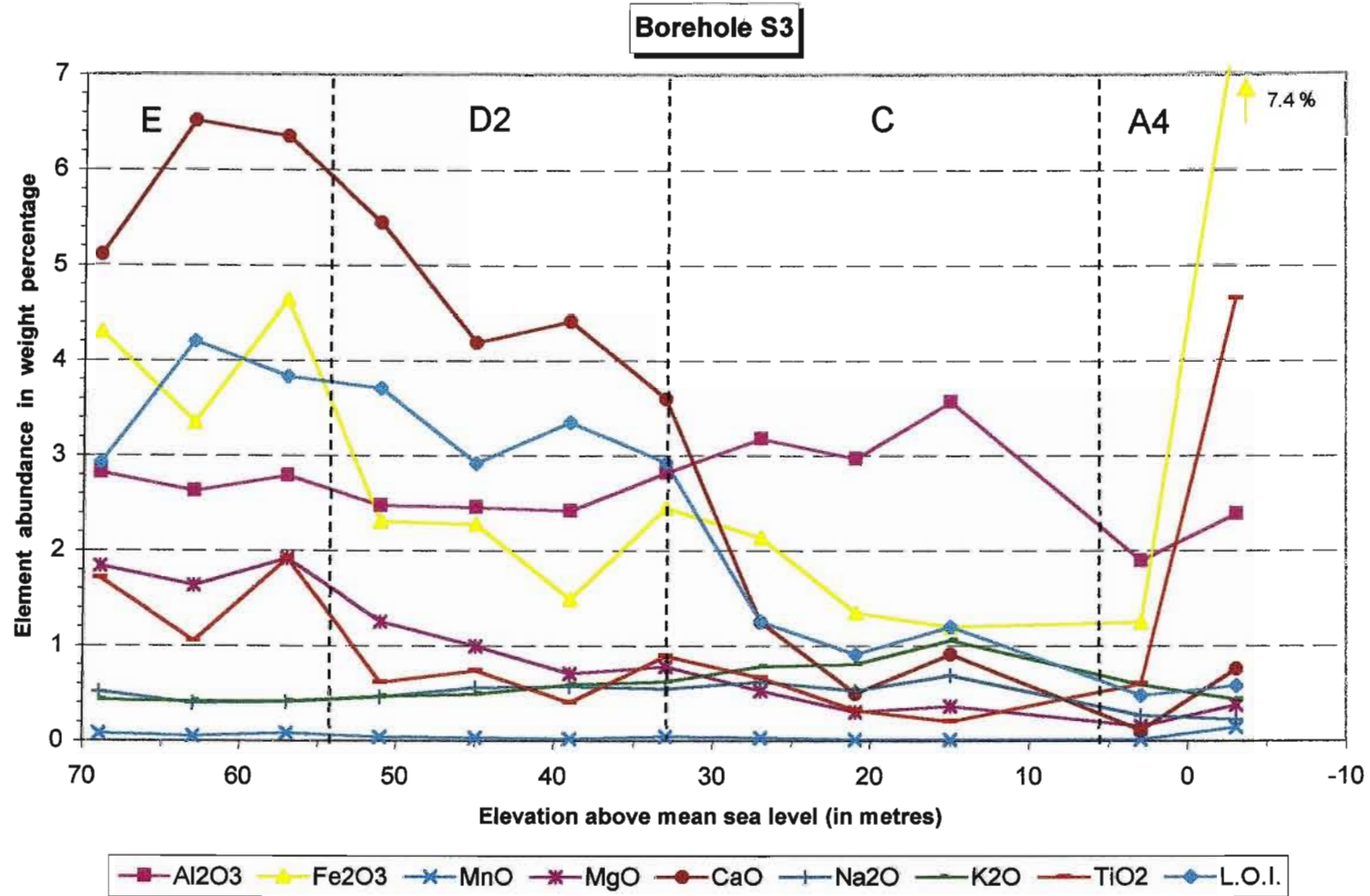
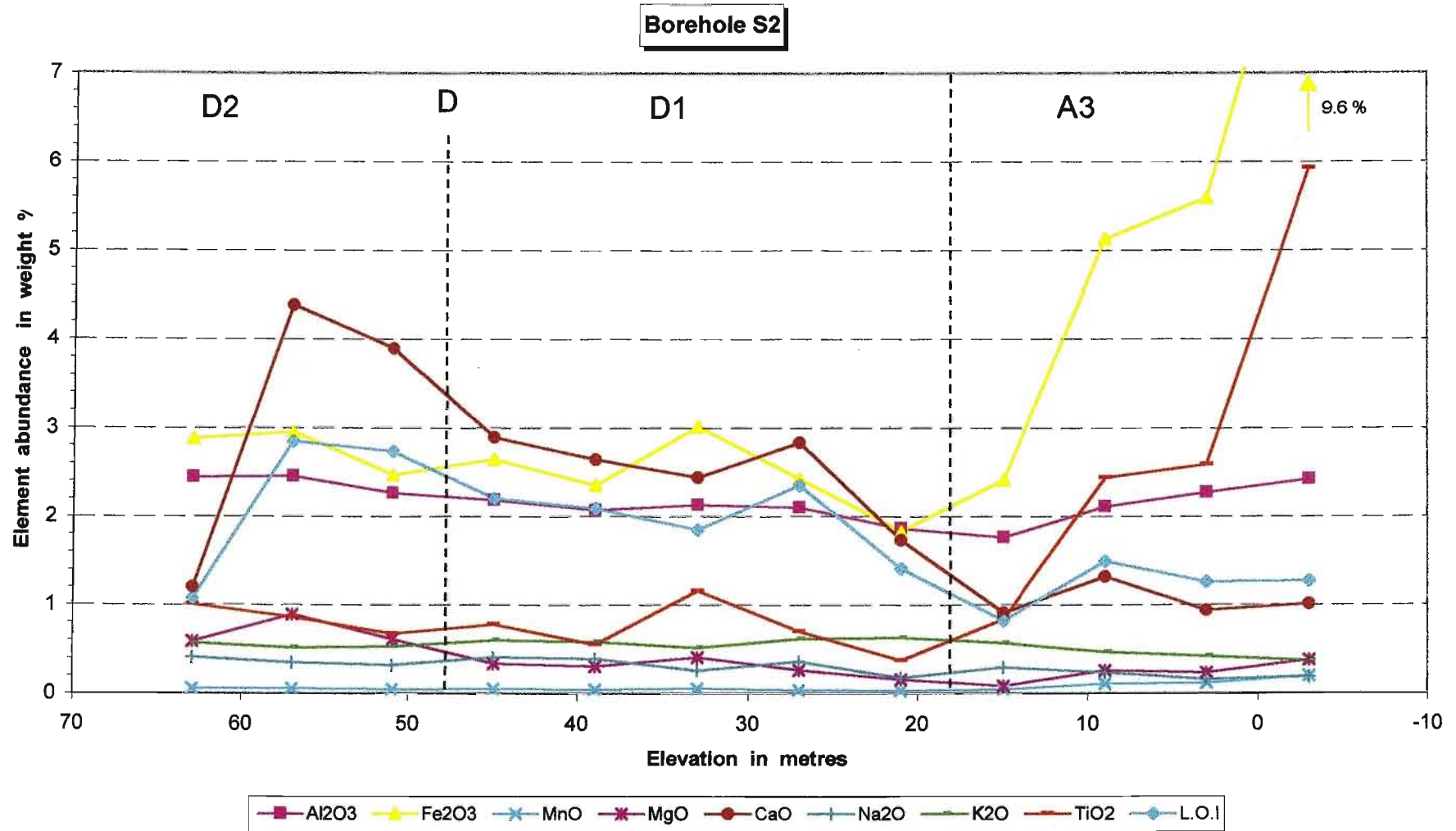


Figure V.17. Major element abundance (excluding for SiO<sub>2</sub>) for the foredune samples F-dune 2 and F-dune 4.



**Figure V.18.** Major element abundance (excluding SiO<sub>2</sub>) for samples from borehole S3, showing sedimentological units defined in the previous sections.



**Figure V.19.** Major element abundance (excluding SiO<sub>2</sub>) for samples from borehole S2, showing sedimentological units defined in the previous sections.

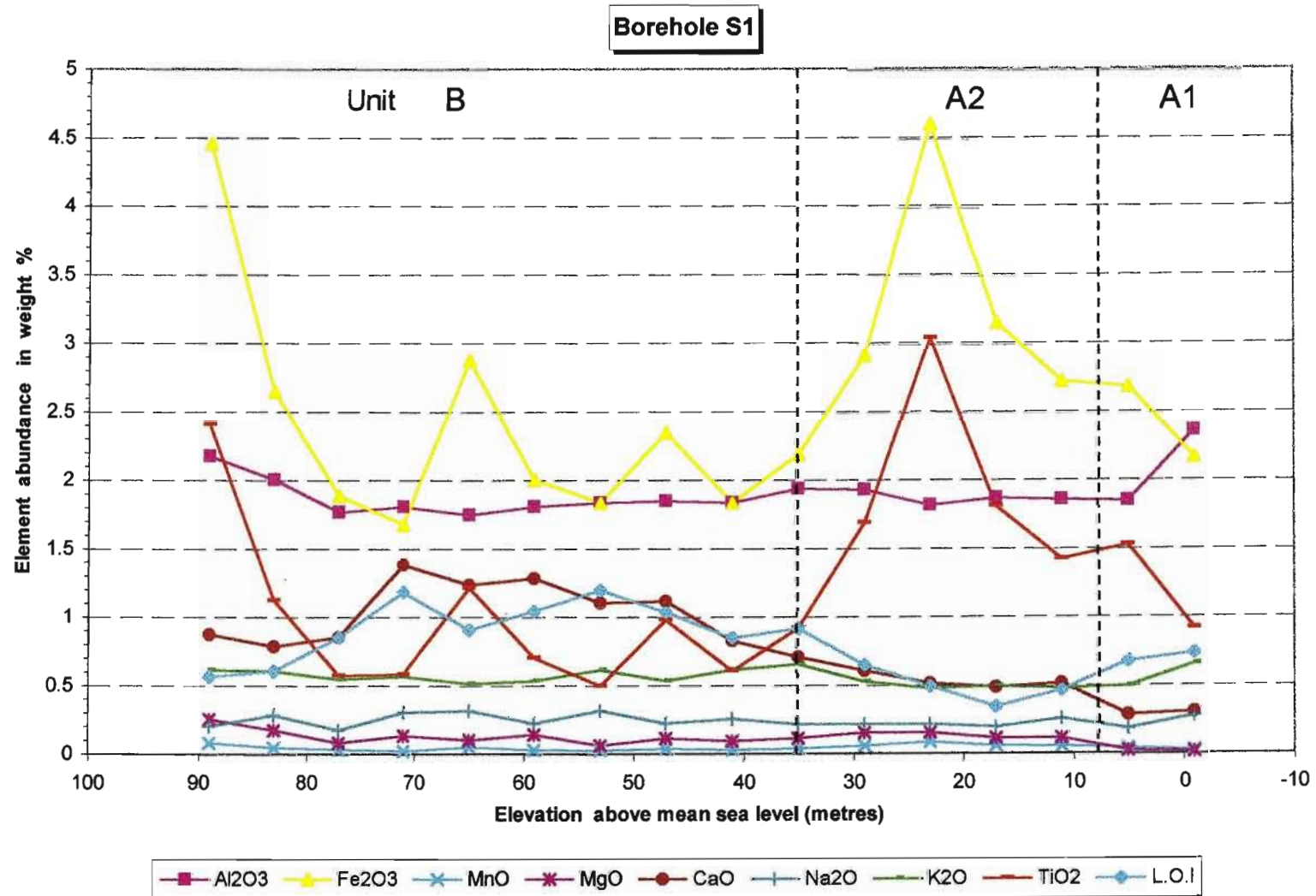


**Figure V.20.** Major element abundance (excluding SiO<sub>2</sub>) for samples from borehole S1, showing sedimentological units defined in the previous sections.

## V.3.2. Chemical element ratios

### V.3.2.1. $\text{TiO}_2$ / MgO ratio

Titanium is incorporated in various minerals. However, given the mineral suite of the study area ilmenite, rutile (and sphene) are the major hosts for Ti element. In most cases  $\text{TiO}_2$  is considered an immobile element and is often accumulated even in the most weathered zone of a soil profile (Minarik *et al.*, 1983). In contrast to this MgO and CaO are the most labile elements, reflecting the relative instability of their host minerals (carbonate, pyroxene, amphibole and other silicates) (Henderson, 1982). MgO and CaO can nevertheless be fixed on and in structural sites of neo-formed clays such as montmorillonite and chlorite (Minarik *et al.*, 1983). These clays are absent in the samples studied except as thin grain coating.

The  $\text{TiO}_2$ /MgO ratio (Figure V.21) can therefore be used as a proxy for the alteration state of the sediment, and is expected to show similar trends to the IRZ/OHM ratio (Figure V.13).

Units C, D and E show  $\text{TiO}_2$ /MgO ratio values similar to the foredune represented by F-dune 2 (Figure V.21). F-dune 4 sample appears to be more altered than F-dune 2, indicating the erosive nature of the coastline surrounding F-dune 4 (Section IV.1.1). Units A and B show significantly higher  $\text{TiO}_2$ /MgO ratio values, suggesting a considerably older age.

Unit C, D2 and E, borehole S3, present similar ratio values (Figure V.21), yet Unit C is strongly depleted in carbonate compared to Unit E. This suggests that the MgO content in carbonate is insignificant and that variation of this mineral does not influence the  $\text{TiO}_2$ /MgO ratio as much as the silicate heavy minerals.

Unit B shows ratio values much greater than Units D and E, but similar to Units A3 and A4 (Figure V.21), supporting the finding that the sediment of Unit B is partially reworked from Units A3 and A4.

Unit A1 is clearly distinguished from Unit A2 by much higher  $\text{TiO}_2$ /MgO ratio values. The IRZ/OHM ratio is not able to discriminate these two units (Figure V.13). This suggests that Unit A1 is strongly depleted in Mg-bearing heavy minerals (mainly pyroxene and amphibole), but retains more resistant minerals of the OHM group (garnet, staurolite, epidote, tourmaline, apatite, monazite and kyanite).

### V.3.2.2. Chemical Index of Alteration

Various index of alteration exist in the literature. The Chemical Index of Alteration (CIA), as defined by Nesbitt & Young (1982), is used here to assess the alteration state of the sediments under study. The CIA plots the ratio value of  $\text{Al}_2\text{O}_3$ , which is considered to be one of the most stable element during weathering (Henderson, 1982), against the labile elements sodium, calcium and potassium (Figure V.22). Thus a strongly altered sediment would present an index value close to 100.

The three boreholes studied have generally increasing CIA values with depth, except for the uppermost samples that illustrate the alteration state of the present soils and possible buried palaeosols (Figure V.22). Unit C presents high CIA values compared to Units D and E, suggesting it is more intensively altered. F-dune 4 sample presents a higher CIA values than F-dune 2, suggesting a greater alteration state (see previous section).

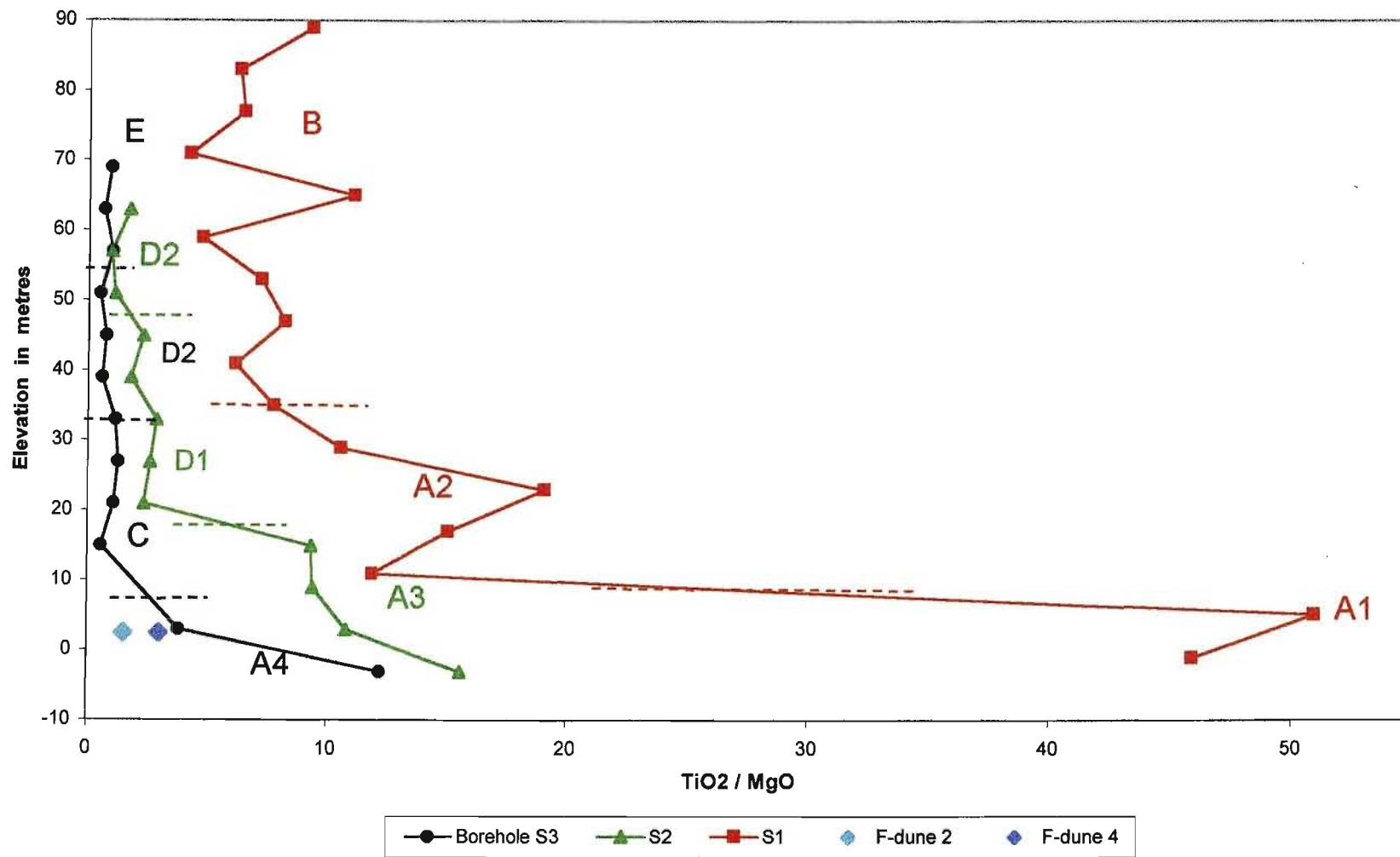


**Figure V.21.**  $TiO_2 / MgO$  ratio values for samples from boreholes S1, S2, S3 and the two foredune samples (F-dune 2 and 4).

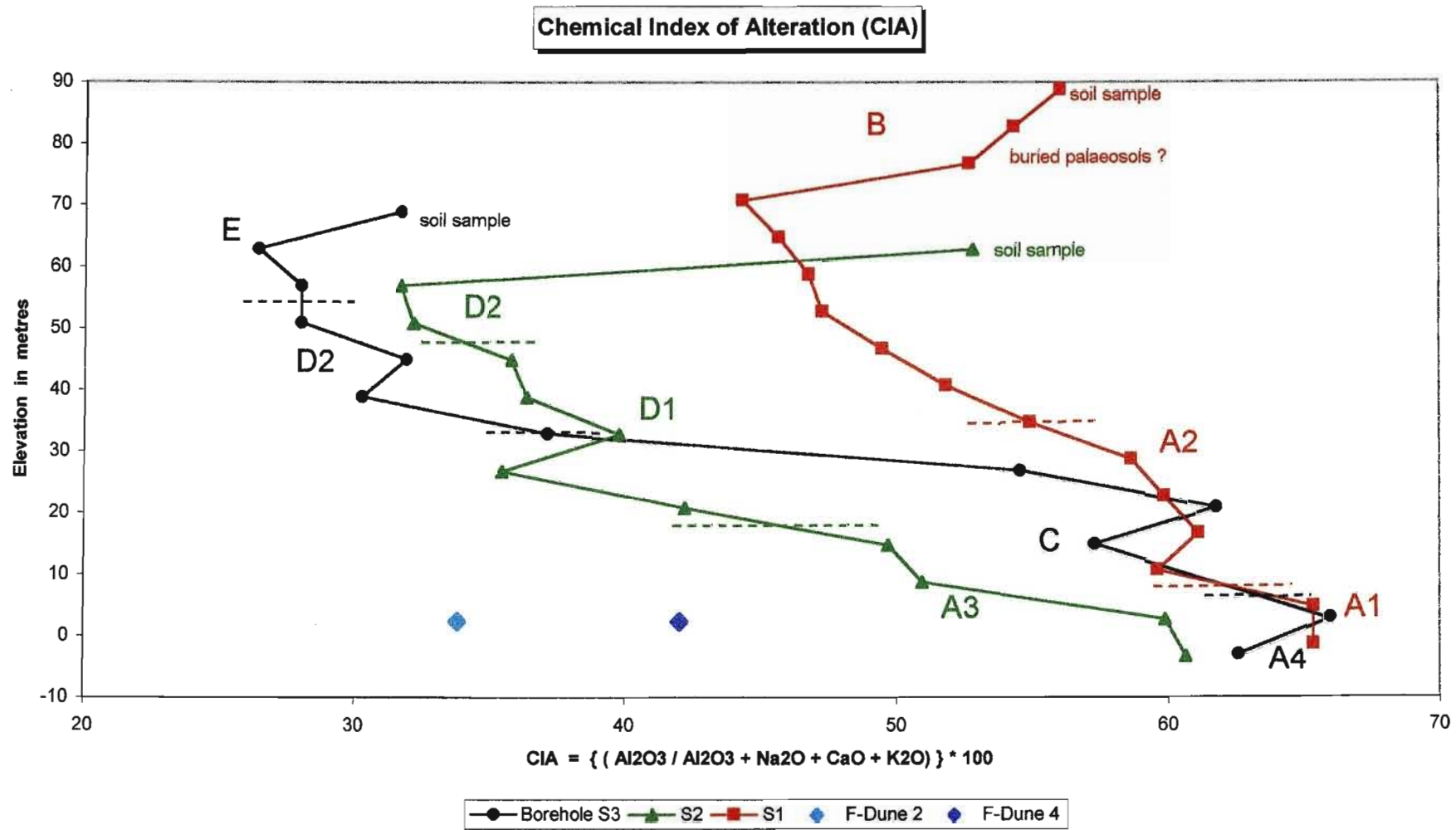


**Figure V.22.** Chemical Index of Alteration for samples from boreholes S1, S2, S3 and the two foredune samples (F-dune 2 and 4).

### V.3.2.3. Trace element ratios and Unit C characteristics

Numerous element ratios present characteristic features concerning Unit C. These elements are ratioed with titanium or zirconium abundance, in order to compare samples with varying heavy mineral abundances and to assess their weathering state.

Unit C is distinguished from the overlying and adjacent units by higher ratio values of  $\text{TiO}_2$ , Th, (La+Ce) and  $\text{P}_2\text{O}_5$  versus Zr, along with Th and  $\text{P}_2\text{O}_5$  versus  $\text{TiO}_2$  (Appendix B). These data are exemplified by the ratio  $\text{P}_2\text{O}_5/\text{Zr}$  (Figure V.23). The  $\text{P}_2\text{O}_5/\text{Zr}$  ratio values decrease from both the coast inland and downhole (Figure V.23). This decrease may be due to the greater instability of phosphorus (monazite, apatite) compared to zirconium (zircon) in the weathering environment. Unit C is defined by very high  $\text{P}_2\text{O}_5/\text{Zr}$  ratio values (Figure V.23). This trend is also identified for element ratios noted above (Appendix B). Higher  $\text{P}_2\text{O}_5/\text{Zr}$  and  $\text{P}_2\text{O}_5/\text{TiO}_2$  ratio values for Unit C suggest that this unit is enriched in monazite and/or apatite. Unit C is also distinguished by ratio values for NMO/THM (Section I.3). Unit C has values for NMO/THM close to 0.1 while all other samples vary between 0.02 and 0.05. This suggests that Unit C is relatively enriched in one or more of the following minerals: apatite, kyanite (Al-silicates), pyrite, leucoxene and sphene (Section V.2.2).

Conversely Unit C presents relatively low values for  $\text{Nb}/\text{TiO}_2$  and  $\text{Nb}/\text{Zr}$ , which are constantly higher for the other units (Appendix B). Niobium has been found in rutile along the northern KwaZulu-Natal coast (Hugo, 1988). The low  $\text{Nb}/\text{TiO}_2$  values for Unit C could be related to a dilution of rutile by ilmenite and other titanium oxides. On the other hand, it is possible that the ilmenite/rutile ratio is identical in Unit C to other studied samples, indicating a lower niobium content in the rutile of Unit C.

Unit C presents element ratios fundamentally different from all the other units. This finding is reflected in results from the mineral point counting (see Section V.2.1), as well as with the high  $\text{Al}_2\text{O}_3$  content observed in this unit (Section V.3.1.2).

In summary Unit C is interpreted to be relatively enriched in volcanic glass, amphibole, apatite, monazite, kyanite (and aluminosilicates?), ilmenite (possibly sphene and leucoxene) and may be depleted in rutile. Facies interpretation of Unit C is discussed at a later stage. Further information concerning Ti-minerals and zircon in Unit C will be given in Section VII.1.1.

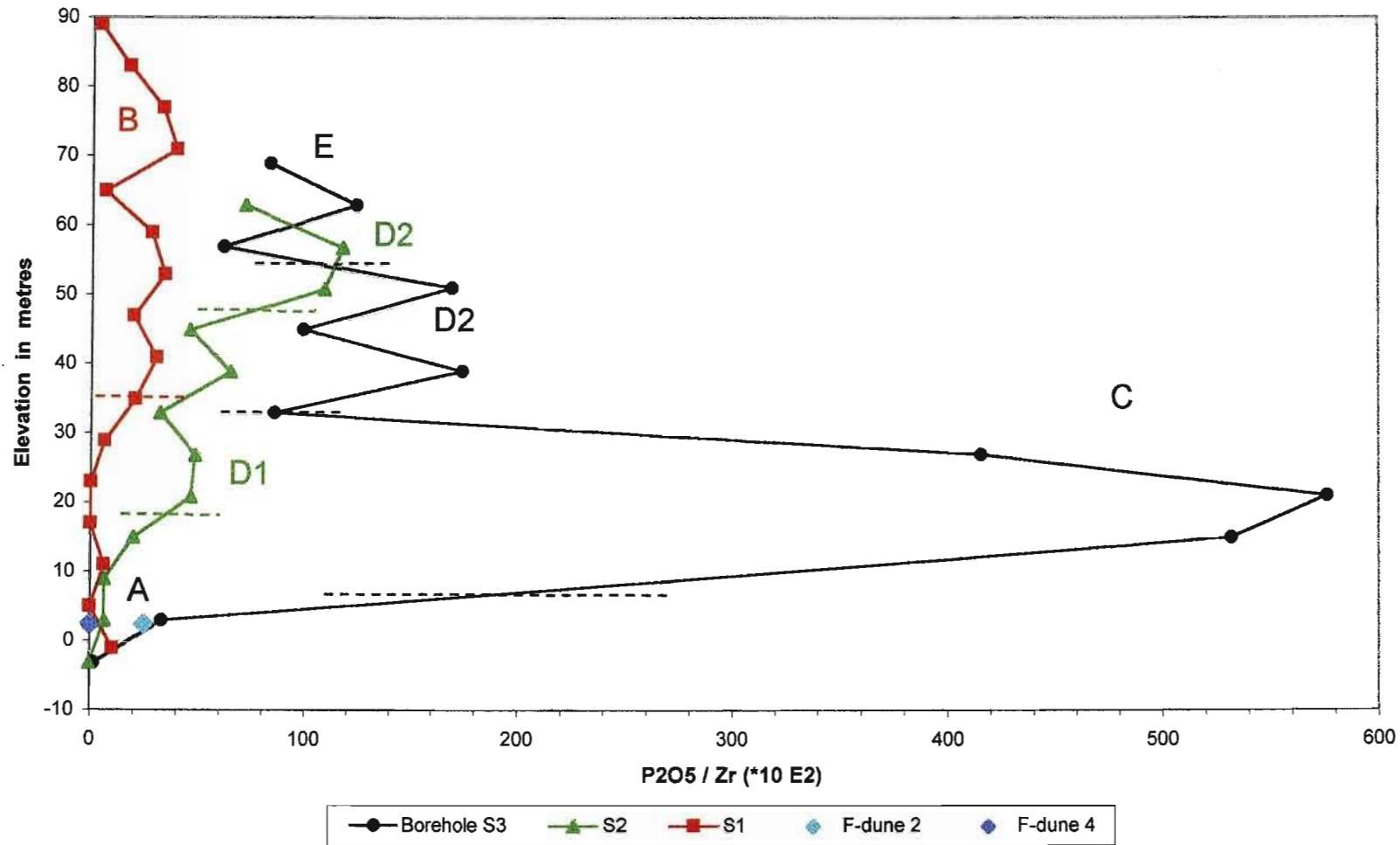


**Figure V.23.**  $P_2O_5 / Zr$  values for samples from boreholes S1, S2, S3 and the two foredune samples (F-dune 2 and 4). For practical reasons,  $P_2O_5 / Zr$  values are multiplied by a factor of 100.

## V.4. Grain size

### V.4.1. Introduction

Mason & Folk (1958), Friedman (1961; 1979), Moiola & Weiser (1968) and Visher (1969) successfully differentiated sedimentary environments (river, beach, coastal dune and inland dune sands) by combinations of various textural parameters (Section I.3).

Results from these authors were applied to all samples from the study area. This laborious work unfortunately led to few discoveries. This is explained by many factors that limit the resolution and discrimination power of the textural parameters. These factors include the presence of at least two distinct grain populations (light and heavy minerals); mixture of different depositional beds in each sample (6 metre interval sampling); alteration which changes the abundance of select grain size fractions and loss of fines during laboratory manipulations.

The loss of fine sediment during sample treatment at RBM is borne out by comparing the silt and clay contents of bulk samples with those from the RBM storage room. Slime content (<45 $\mu$ m) given by RBM for the three boreholes ranges between 2 to 12 weight percent. Silt and clay content (<63 $\mu$ m) of the samples from the RBM storage does not exceed 2 %, and most of the samples present values below 0.4 %. It is evident that a significant loss of fine sediment occurred, and could be due to the drying method used by RBM (Pietersen, 1999, pers. comm.).

Relevant information obtained from the textural analysis is presented during discussion of the grain size distribution curves (Section V.4.3). The summary of grain size textural parameters is presented in Appendix C. Mean grain size is treated in detail as this parameter provides a useful discrimination between the recognised units (Section V.4.2).

### V.4.2. Mean grain size

Most of the sedimentological units defined in the previous sections can be differentiated using the mean grain size of their constituent sediment (Figure V.24). Three field samples of aeolian dunes (D'Rock 1, 3 and 4) and three field samples of foredunes (F-dune 1, 2 and 4) have been integrated in this study (see Section V.1.2 for description). Most samples are medium grained sands with mean values between 1 and 2 phi (500 to 250  $\mu$ m).

Hugo (1993) showed that, for any dune or beach sample along the eastern coast of South Africa, the mean grain size of the heavy mineral suite is positively related to the mean grain size of the bulk sediment. This statement cannot be verified here, as mineral grain size has not been studied. However, the present study reveals that the grain size of the bulk sample is closely related to the heavy mineral abundance with fine grained sediment containing higher abundances of heavy minerals (Figures V.24 and V.10). Units A1 and A2 differ from this observation, as intense alteration has significantly reduced the original heavy mineral content.

Borehole S1 can be divided into the relatively coarse grained (ca. 1.5 phi) upper Unit B and comparatively finer lower Units A1 and A2 (1.8 phi). Borehole S2 can be subdivided into the relatively coarse grained (ca. 1.5 phi) upper Unit D and comparatively finer Unit A3. Unit A3 is characterised by a marked coarsening upward trend from the bottom sample, which is the only fine sand (2.05 phi) encountered in the Northing Line 380. Borehole S3 exhibits complex

downhole trends in mean grain size. The uppermost Unit E shows consistently fine grain size (1.9 phi). Unit D2 of borehole S3 fines upwards from 1.4 to 1.7 phi. This unit is generally finer grained than Unit C but it seems that the boundary between these two units is transitional. Unit C is the coarsest grained unit from Northing Line 380, and is characterised by a marked fining upward trend from sample 15 (possibly from sample 8, which is missing and not analysed), which is the only coarse sand sized sample (0.95 phi) encountered from Northing Line 380. Unit A4, like Unit A3, is characterised by a marked coarsening upward trend.

IRZ/OHM ratio values for Unit A3 and Unit A4 correlate well with the mean grain size (Figures V.13 and V.24). Force & Stone (1990) demonstrated that, for a common supply, the proportion of a given heavy mineral in the sediment is dependent on the grain size of that mineral in comparison to the grain size of the sediment. In other words iron-titanium oxides (fine grained minerals) will be more abundant in a fine grained sediment, whereas other heavy minerals (coarser grained) will be more abundant in a medium to coarse grained sediment. Therefore it is suggested that the observed increase of the IRZ/OHM ratio is due to a decrease of the mean grain size of the bulk sediment. Variations of the IRZ/OHM ratio values for Units A3 and A4 are further discussed in Section V.3.1.3.

D'Rock 1 sample is slightly finer than Unit E, which is in turn much finer than the three foredune samples studied. D'Rock 3 and 4 samples were collected because of their coarser grain size compared to other aeolian sands observed in the field. However, both samples are finer than the base of Unit C (sample 15) (Figure V.24). Friedman (1961) studied 114 aeolian dunes of various origins (coastal, inland, river and lake dunes) from around the world. He found a maximum limit for the mean grain size of 1.49 phi. Mean values of the study area decrease this limit to 1.35 phi (note however that the original samples contained greater abundances of fine sediments that would shift the mean towards finer grain sizes). Thus sample 15 of Unit C appears to be too coarse to be entirely aeolian, given the maximum limit of Friedman (1961). In contrast to this McKee (1966) found some dune samples to be as coarse as sample 15. The study of the grain size distribution curves for Unit C will provide additional information (Section V.4.3).

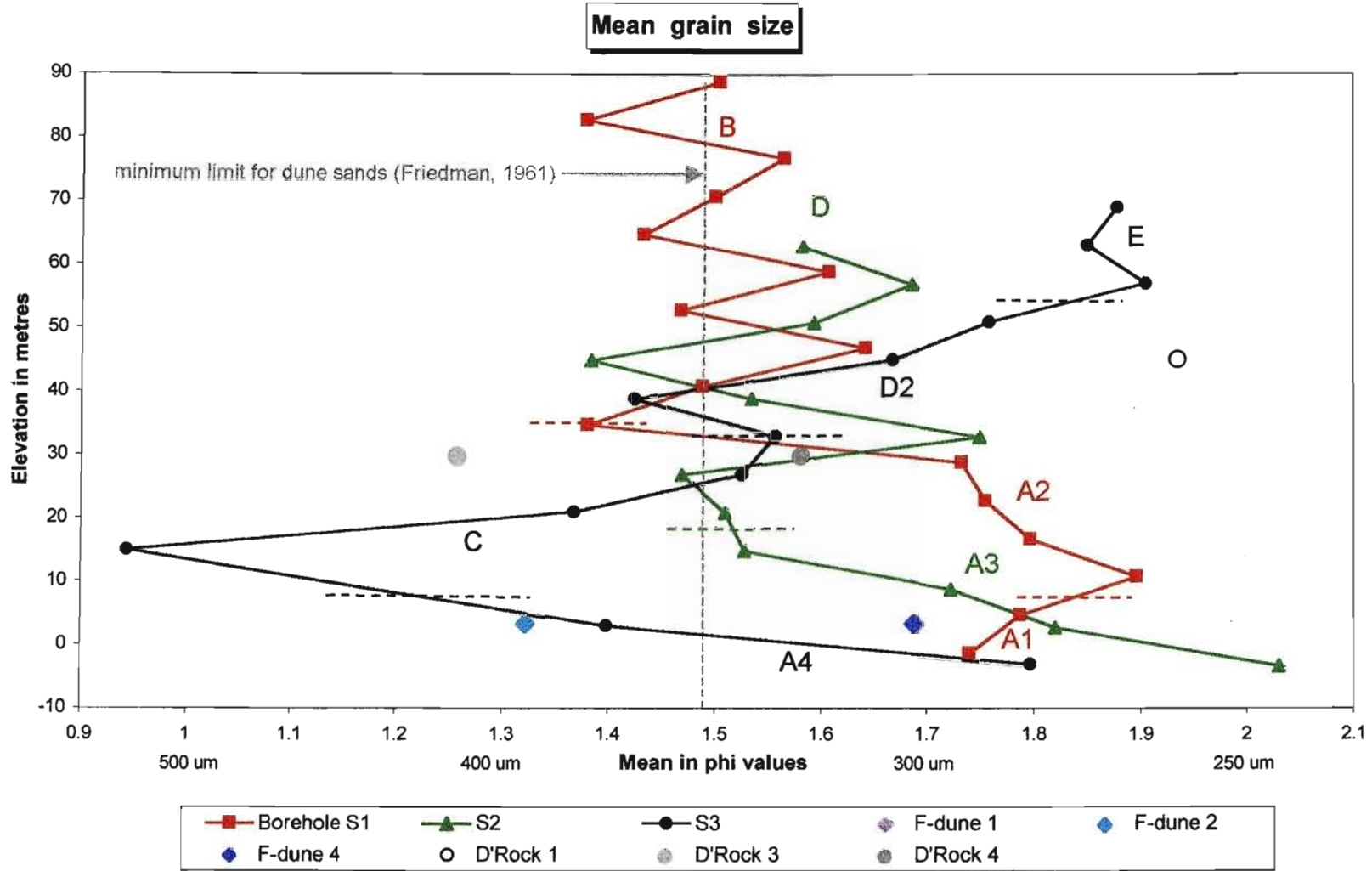


Figure V.24. Mean grain size for samples from boreholes S1, S2, S3 and field samples. Dashed lines = unit boundaries.

### V.4.3. Distribution curves

Textural parameters (Appendix C), with the exception of the mean grain size, are generally not as useful as frequency distribution curves for discriminating sedimentological units. In order to present a broader view of each sample, the frequency distribution curve for each sample has been plotted in Figure V.25 to V.28. It was noticed that most of the units can be recognised and differentiated in this manner, and samples were therefore regrouped into their respective units.

Units B of borehole S1 and D of borehole S2 present a generally symmetrical and moderately well sorted distribution curve. The two top samples of Unit B, as well as sample 35, show relatively broad curves indicating a poor sorting possibly related to reworking or to observed palaeosols (Section IV.2.2).

Grain size distribution curves for Units A1, A2, A3, A4 and E are weakly asymmetrical and moderately well to well sorted. The coarse tails are truncated, and no grains coarser than 0.25 phi (840  $\mu\text{m}$ ) are present in these units. Moreover a coarse population seems to be present between 0.5 and 1.1 phi (460 to 700  $\mu\text{m}$ ). The fine tails are characterised by relative depletion of grains with size between 2.6 to 3 phi and a minor mode at 2.9 to 3.7 phi. The high grain abundance at ca. 70 to 130  $\mu\text{m}$  is considered to reflect economic heavy minerals, which have their mean grain sizes in this range (Figure V.12). Depletion in the 2.6 to 3 phi range (125 to 160  $\mu\text{m}$ ) is marked for old sands such as Units A1 and A2, possibly due to leaching of fine grained pyroxene and amphibole (Figure V.12). Distribution curves of sample 3 of Unit A4, borehole S3, and sample 15 of Unit A3, borehole S2, are anomalous as they are similar to curves characteristic of Units B and D. These two samples are coarser grained than other samples of Units A1, A2, A3, A4 and E (Figure V.24). The characteristic feature of the fine tail described above seems to be thus related to the fine grained character of Units A1, A2, E and the lower portions of Units A3 and A4 (mean grain size finer than 300  $\mu\text{m}$ , Figure V.24).

Unit C presents similar grain size distribution curves to those of Units B and D, with the exception of sample 15 (borehole S3). The asymmetrical shape and moderate sorting of this sample suggests that two or more different grain populations are present (Figure V.27). The well sorted grain population with a mode of 0.9 phi (525  $\mu\text{m}$ ) can be interpreted as a coarse grained aeolian sand. The fine fraction of the curve is comparatively coarse grained and is characterised by the absence of grains smaller than 2.6 phi (165  $\mu\text{m}$ ). The coarse fraction (>750  $\mu\text{m}$ ) is not observed in other distribution curves. Unit C contains 55 % coarse sand (0 to 1 phi, 500  $\mu\text{m}$  to 1 mm) and 10 % very coarse sand (-1 to 0 phi, 1 to 2 mm). Wind usually transports the medium and fine sand, as coarser grains are left behind as a lag or winnowed deposits (Bagnold, 1941). Folk (1971) noticed that wind ripples and traction load of wind deposits are characterised by coarse grains, but are nevertheless well sorted. Further interpretations would need detailed sampling inside the 6 m of sand intercepted by sample 15. However, a non-aeolian origin for part of sample 15 (borehole S3) is considered likely.

Foredune samples F-dune 1 and 4 and sample D'Rock 1 present weakly asymmetrical and well sorted distribution curves (Figure V.28). The fine tails of the distribution curves for these three samples are characterised by relative depletion of grains with size between 2.6 to 3 phi and a minor mode at 3 to 3.1 phi. The coarse tails are truncated and no grains coarser than 0.3 phi (810  $\mu\text{m}$ ) are present in these samples. F-dune 1, F-dune 4 and D'Rock 1 samples have thus similar grain size distribution curves to those of Unit E, borehole S3 (see above). F-dune 2 distribution curve is moderately well sorted and similar to samples 3 and 21 of Unit A4, borehole S3 (Figure V.27).

D'Rock 3 and 4 were collected just above a palaeosol, and therefore represent the base of an aeolian dune. Their distribution curves clearly differ from sample 15 of Unit C (borehole S3) by an approximately symmetrical shape and the relatively low abundance of coarse and very coarse sands. Thus, sample 15 of Unit C (borehole S3) is unlikely to represent a coarse basal portion of an aeolian dune. This is again suggestive of a non-aeolian origin for part of sample 15.

The coarse grain size population observed from Units A1, A2, A3, A4, E, F-dune 1 and 4 curves between 0.5 and 1.1 phi (see above) and the remaining samples (including F-dune 2) for phi values less than 0.5 phi is of unknown origin. It could be related to lag deposits of coarse to very coarse sand by winnowing of medium sands. McKee (1966) and Fryberger & Ahlbrandt (1979) noted that dunes close to their source origin are less sorted and contain more coarse grains than dunes located further downwind. In term of transport distance, coastal dunes can be considered as proximal dunes and are therefore likely to contain coarse grain populations.

From the textural parameter values given in Appendix C, it can be concluded that the sand of the study area is moderately to moderately well sorted ( $\sigma = 0.47$  to  $0.68$ ), and can be either negatively or positively skewed ( $\alpha_3 = -0.1$  to  $1.05$ ;  $\alpha_s = -0.3$  to  $0.15$ ). The borehole samples are poorly sorted compared to the foredunes, as indicated by higher values of standard deviation ( $\sigma$ ) and cubed deviation ( $\sigma^3$ ) (Appendix C). This is probably due to the mixing of different depositional sets that reduce the sorting quality of borehole samples. The lower parts of Units A3 and A4 were interpreted as beach deposits (Sections V.3.1.2 and V.3.1.3) and should thus present negative skewness values or at least lower skewness values than aeolian deposits (see review by Folk, 1971). On the contrary they show the highest positive values for both the statistical ( $\alpha_3$ ) and simple measure ( $\alpha_s$ ) of the skewness (Appendix C). Their exceptionally high content of fine heavy minerals is believed to increase the skewness. Felhaber (1984) also noticed high positive skewness values for heavy mineral rich nearshore sand north of the Tugela River mouth.

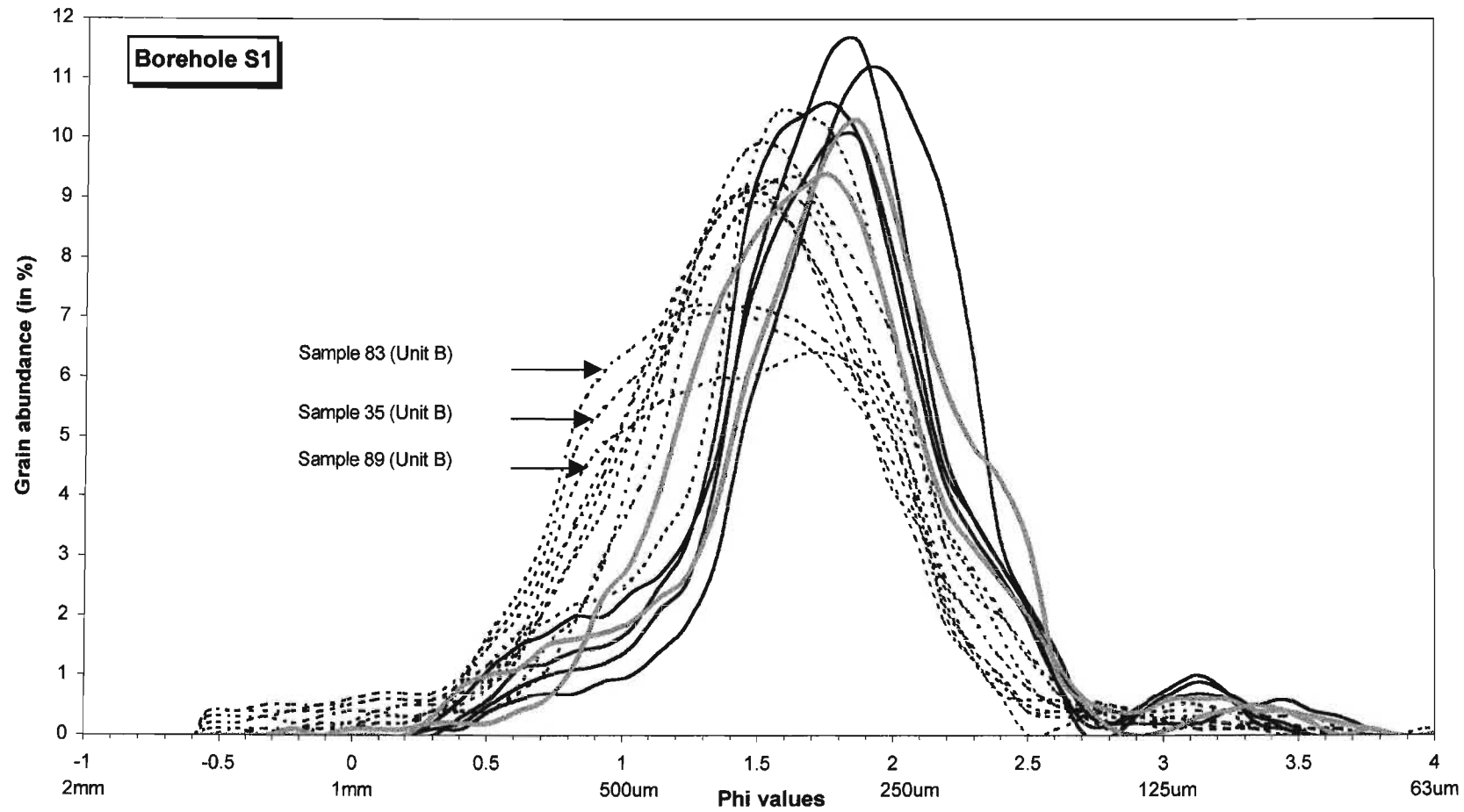


**Figure V.25.** Grain size distribution curve for samples from borehole S1. Dashed lines = Unit B, black lines = Unit A2, grey lines = Unit A1.

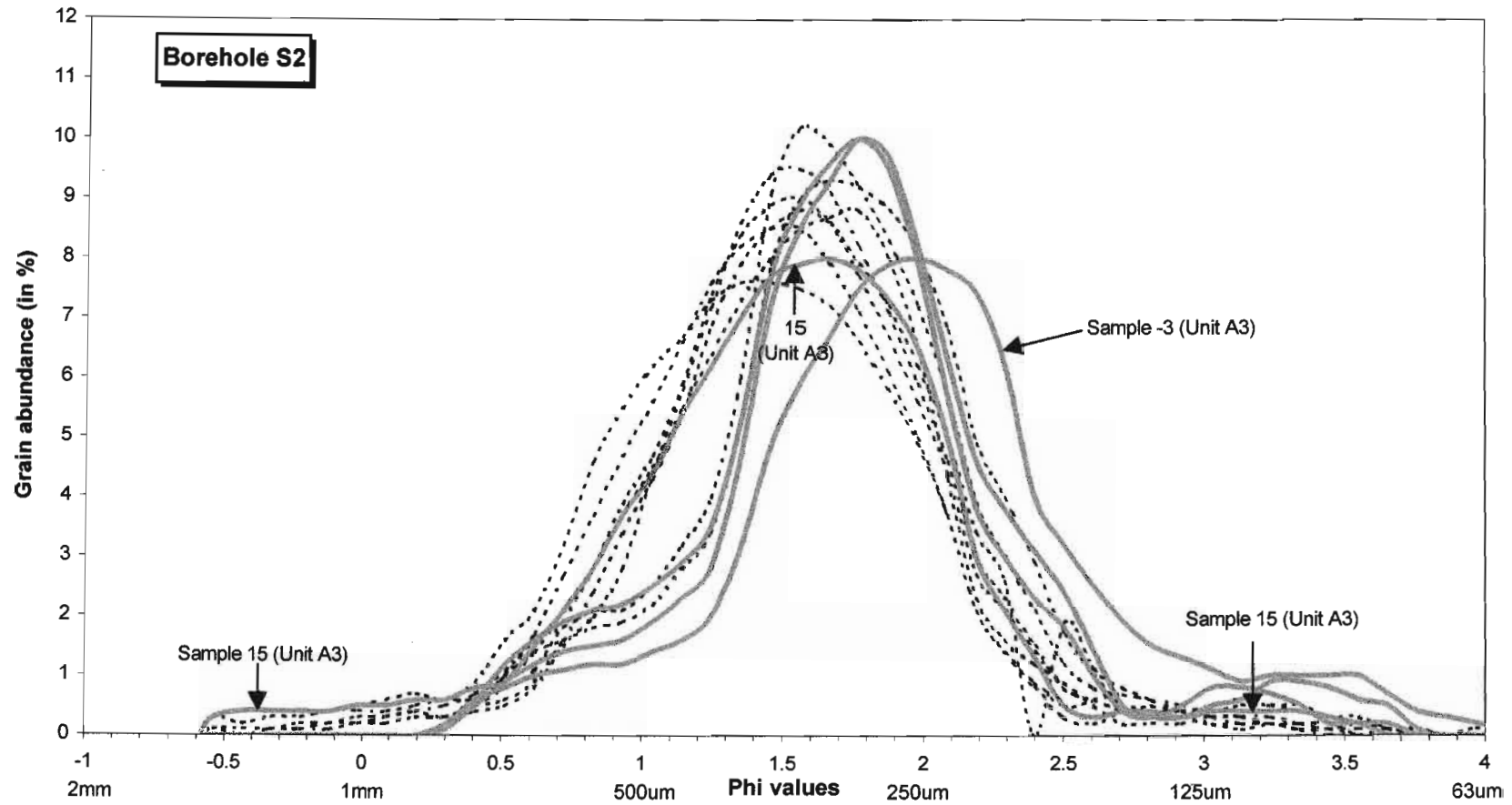


**Figure V.26.** Grain size distribution curve for samples from borehole S2. Dashed lines = Unit D, grey lines = Unit A3.

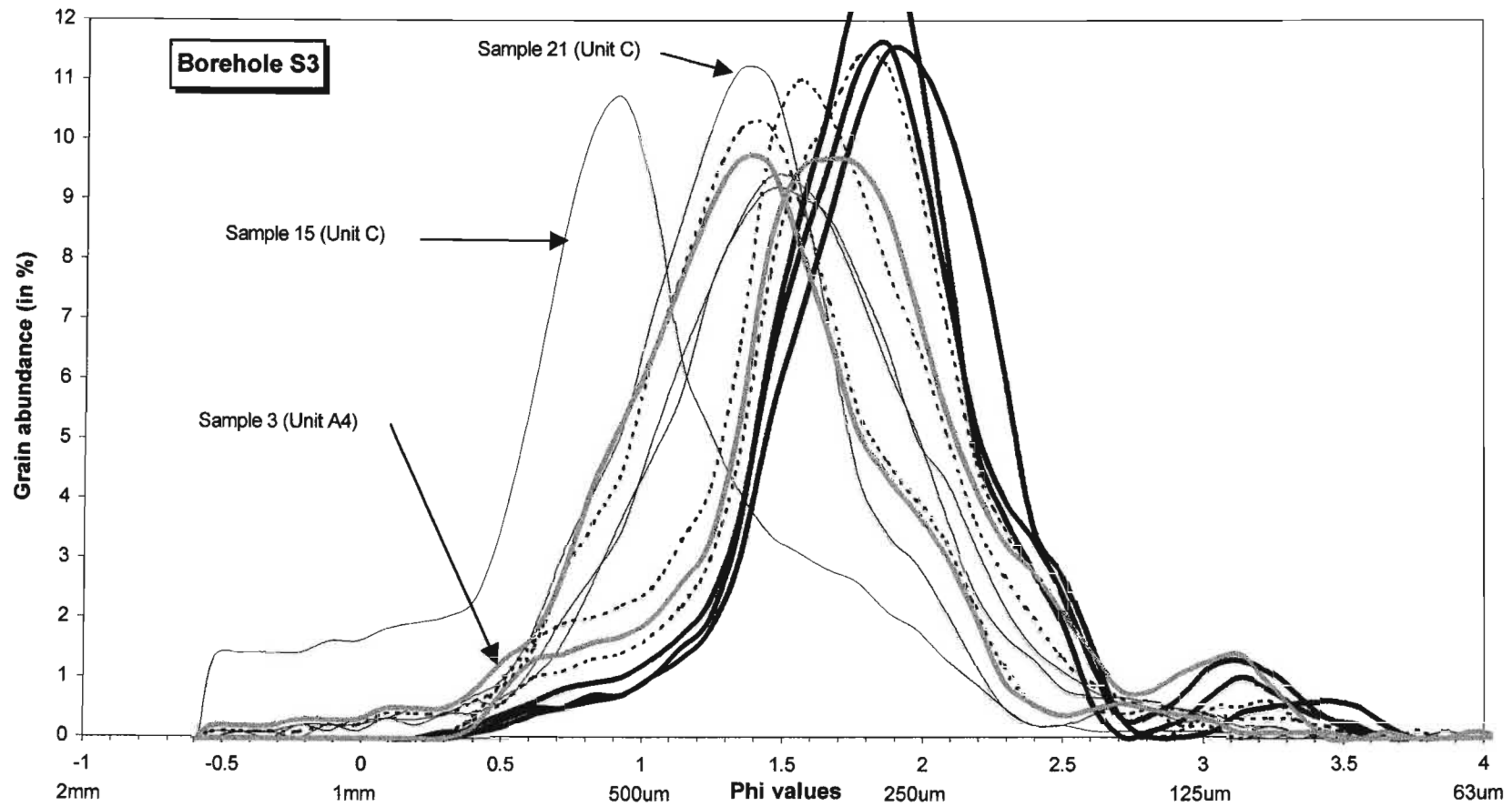
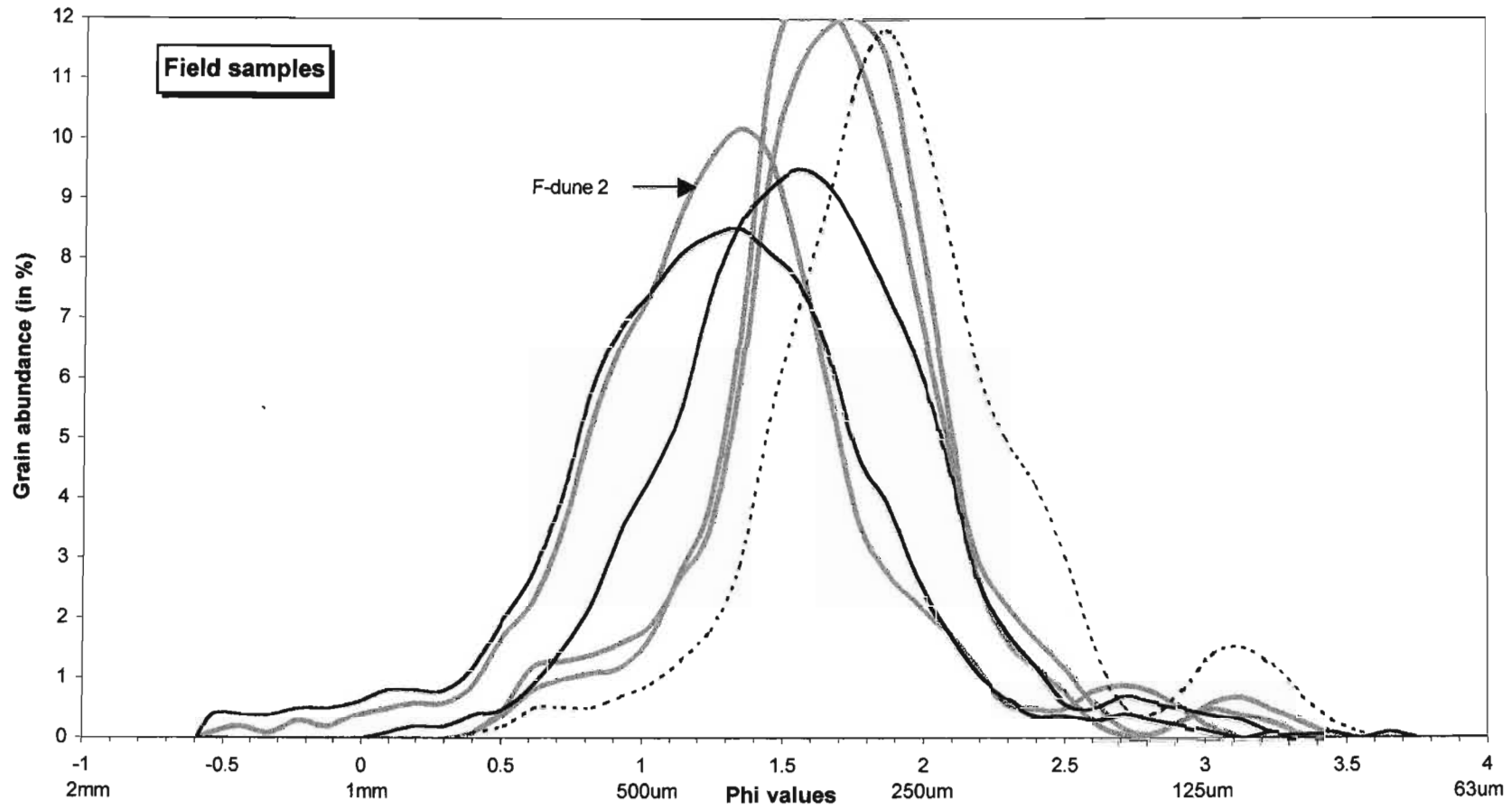


Figure V.27. Grain size distribution curve for borehole S3. Thick black lines = Unit E, dashed lines = Unit D2, thin black lines = Unit C, grey lines = Unit A4.



**Figure V.28.** Grain size distribution curve for the field samples. Dashed line = D'Rock 1, black lines = D'Rock 3 and 4, grey lines = F-dune 1, 2 and 4.

## V.5. SEM studies on quartz grains

Scanning electron microscopy (SEM) of the surface of quartz sand grains is a useful tool for differentiating ancient sedimentary environments and transport mechanisms. Abrasion of quartz produces mechanical textures that are characteristic of specific environments; features due to chemical action can also be distinguished by means of SEM and a number of criteria are available to separate these mechanical and chemical features (Krinsley & Doornkamp, 1973).

Since most of the aeolian sand in the study is derived from a beach – foredune system, quartz grains from this environment were initially investigated in order to identify their primary surface features. Sand samples from Line 380 were subsequently analysed from the youngest units to the oldest based on results from the previous sections. This allows changes in grain shapes and surface features due to alteration and environmental changes to be observed, and provides useful information concerning the sedimentary history.

### V.5.1. Foredunes

Quartz grains in the foredune samples (F-dune 1, 2 and 4) have a characteristic low sphericity, reflecting a short distance of transport from the source rock (euhedral to subhedral shape, Figure V.29a) or due to destructive impacts during high energy transport in the surf zone (Figure V.29b). Some of these grains show slightly sub-rounded surfaces due to abrasion in the beach foreshore (Friedman & Sanders, 1978) (Figure V.29a). Grain surface features typically indicate a beach and nearshore origin for the quartz. Conchoidal fracture patterns (Krinsley & Donahue, 1968) and marine dissolution (Le Ribault, 1978) create very clear surfaces (Figure V.29b). Semi-quantitative chemical analysis shows that these surfaces are almost entirely composed of  $\text{SiO}_2$  (> 90 wt%).

At higher magnification the surface of these grains shows geometric solution features and fine pitting; dissolution holes located on edges are typical of an infratidal marine environment (Le Ribault, 1978) (Figure V.29c). Inter-granular collision in the beach and surf zones mark the grain surface by V-shaped indentations (Figure V.29d) (Krinsley & Donahue, 1968; Nordstrom & Margolis, 1972; Lin *et al.*, 1974; Le Ribault, 1978 and Kaldi *et al.*, 1978).

From the above observations it can be concluded that the quartz grains from the foredunes present surface features indicating a littoral environment (beach and nearshore). Thus the short aeolian transport from that environment to the foredunes was not sufficient to erase the previous surface features. It must however be kept in mind that not all quartz grains present the shapes and surface features described above. Littoral sand of the study area is a mixture of mature and immature sediments (Section V.2.2). It is therefore, normal to observe grain features showing a complex sedimentary history. This is illustrated in Figure V.29b by an amphibole grain exhibiting structurally oriented dissolution and rounding, followed by a phase of grain coating that was later partly removed by a high energy event.

### V.5.2. Aeolian Units B, D and E

As shown in previous sections, Unit E is a transgressive dune derived from a beach - foredune system. It is also interpreted to be the youngest unit in the study area. Compared to the foredune samples, the quartz grains in Unit E are characteristically more spherical and rounded (Figure V.29e). Aeolian transport is known to cause such shape changes (Kransley & Doornkamp, 1973; Kransley & McCoy, 1978). However, the grain surfaces became rough (Figure V.29e), due to grain collisions and production of "upturned plates", which are responsible for the frosted opaque surface visible with a binocular microscope (Kransley & McCoy, 1978; Friedmann & Sanders, 1978), and to the deposition or neo-formation of fine particles (Figures V.29c and V.29f). These silt and clay sized particles are sometimes found only in depressions of the quartz grain surface, which usually indicates a vadose environment (Le Ribault, 1978) (Figure V.29g). Semi-quantitative chemical analysis revealed the presence of calcium carbonates (calcite), unidentified clays and "globular silica deposits or layers" (Le Ribault, 1978) (see below). The chemical composition of the grain rimming silica layers in Unit E are variable, yet show a characteristically high iron and calcium contents (Table V.2).

The silica layers are formed by successive diagenetic cycles of dissolution and precipitation, which eventually smooths the surface of the quartz grain (Le Ribault, 1978). Despite a gradual transition from young to old aeolian sediments, quartz grains from older units such as Unit B tend to be almost entirely covered by silica layers (Figure V.29h). Dunlevey (1997) has described this type of grain coatings for "Berea-type red sand" grains as "amorphous aluminium-iron hydroxides". Quartz grains from the upper half of borehole S1 (Unit B) are coated with silica layers that are rich in iron and depleted in calcium compared to the upper unit of borehole S3 (Unit E). The lower calcium content can be explained by the fact that calcium is a labile element and is rapidly leached by weathering. Increasing iron content with age may indicate a greater thickness of the silica layer in older sediments.

**Table V.2.** Semi-quantitative chemical analysis of a globular silica layer on a quartz grain of Unit E (sample 57 of borehole S3).

Elmt	Spect. Type	Element %	Atomic %
O	K ED	17.64	33.49
Na	K ED	0.22	0.29
Mg	K ED	0.56	0.69
Al	K ED	2.29	2.57
Si	K ED	31.03	33.55
P	K ED	0.65	0.64
K	K ED	1.02	0.79
Ca	K ED	11.61	8.80
Ti	K ED	1.68	1.07
Fe	K ED	33.30	18.11
Total		100.00	100.00

\* = <2 Sigma

### V.5.3. Units A and C

Most quartz grains from Units A1 and A2 are well rounded and often cemented together to form rock fragments (Figure V.29i). A thick silica layer covers the grain surface and dissolution

holes, due to chemical etching, are common (Figure V.29j). The chemical composition of the silica layers in Units A1 and A2 is dominated by iron (> 40 wt%) and aluminium (Table V.3).

Rare irregular shaped quartz grains from Unit A1 indicate a non-aeolian origin. Unfortunately a thick silica layer around the grain most often prevents identification of the grain or its surface features (Figure V.29k). Sample 23 of Unit A2 (borehole S1), which is thought to be derived from a beach – foredune system (Section V.3.1.4), does not show such characteristics (irregular shapes), illustrating the masking effect of a thick silica layer.

Units A3 and A4 contain a large amount of subhedral and broken quartz grains that have a clear surface (Figure V.29l), confirming the hypothesis that these units were deposited in a beach – foredune environment (Sections V.3.1.2 and V.3.1.3). Grain coatings in Units A3 and A4 are characterised by relatively pure quartz with a relatively low iron content (max 6 wt%). This suggests that the formation of the silica layer occurs preferentially on aeolian quartz grains. The presence of upturned plates on aeolian grain surfaces could thus favour the dissolution of the grain surface. Grains recognised as aeolian in origin are present, even at the base of the dune cordon, and suggest that sediment mixing is active in the beach – foredune environment.

Unit C contains two types of quartz grain surfaces. Typical aeolian grains are present, as evidenced by spherical and rounded grain shapes, upturned plates, and polygonal cracks (Kransley & McCoy, 1978; Figure V.29m), all of which are characteristic of this environment. The occurrence (ca. 20 to 30 %) of subhedral and broken grains with clean surfaces suggests a non-aeolian origin for part of Unit C (Figures V.29n and V.29o).

#### V.5.4. Other features

Deposition or neoformation of fine particles (calcite, clays) and silica layers does not occur exclusively on the surfaces of quartz grains. Heavy minerals are also affected by these processes. Ilmenite may be coated by thick silica layers and various fine particles (Figure V.29p). A zircon grain from Unit A2 was analysed with a grain coating of 14 wt% iron and 1 wt% aluminium.

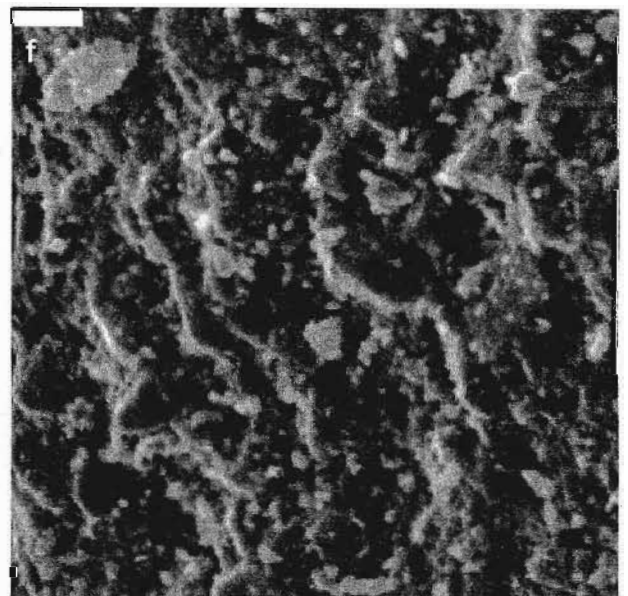
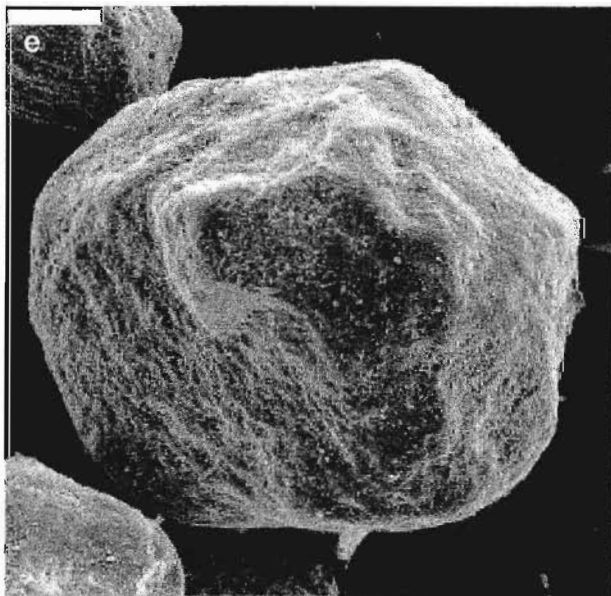
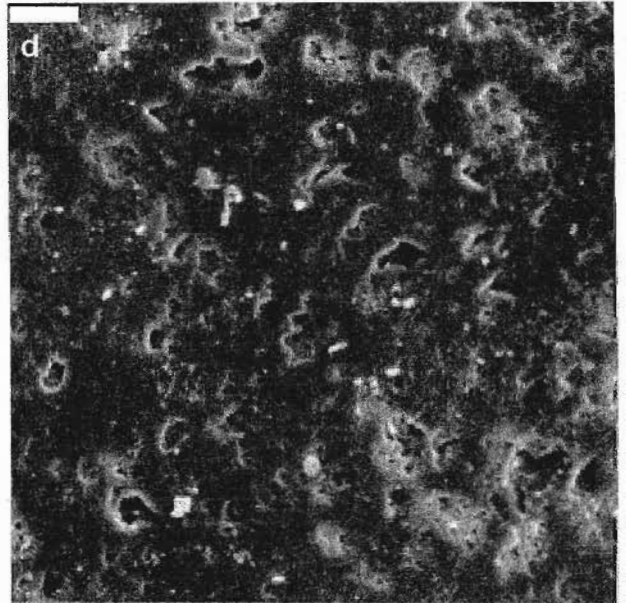
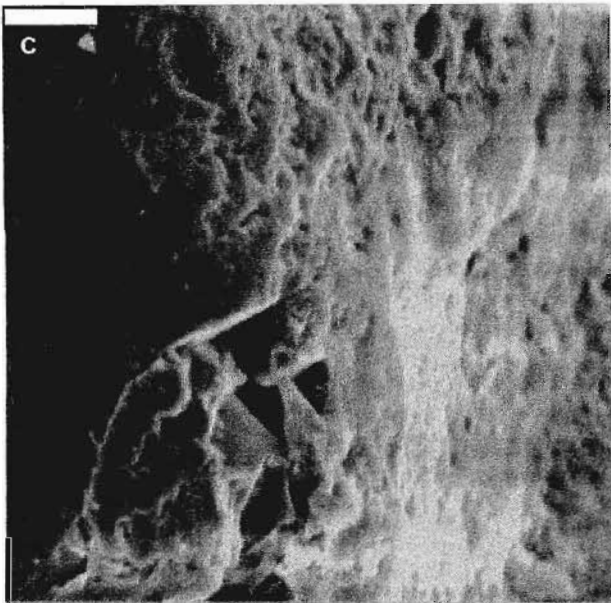
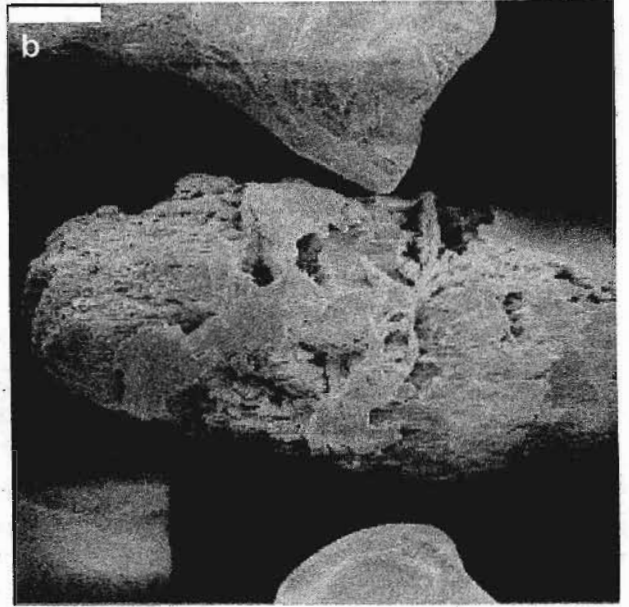
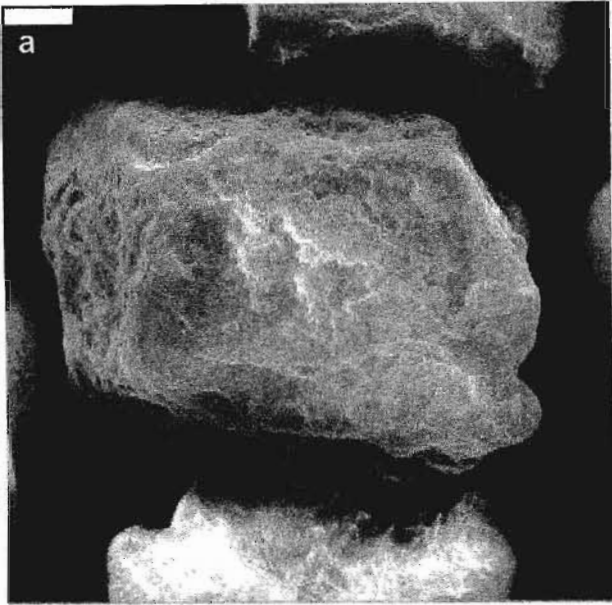
**Table V.3.** Semi-quantitative chemical analysis of a globular silica layer on a quartz grain of Unit A1 (sample -1), reflecting the average chemical composition of silica layers for Units A1 and A2.

Elmt	Spect. Type	Element %	Atomic %
O K	ED	11.43	23.70
Al K	ED	6.94	8.54
Si K	ED	31.64	37.37
K K	ED	1.11	0.94
Ca K	ED	0.70	0.58
Ti K	ED	2.47	1.71
Fe K	ED	45.70	27.15
Total		100.00	100.00

\* = <2 Sigma

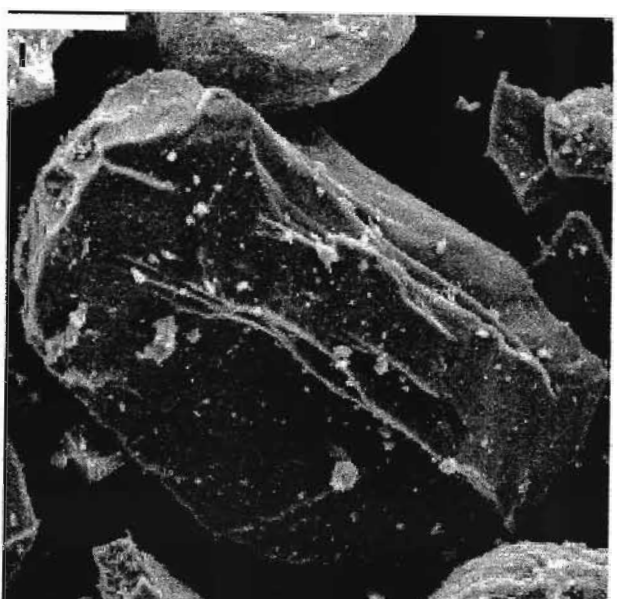
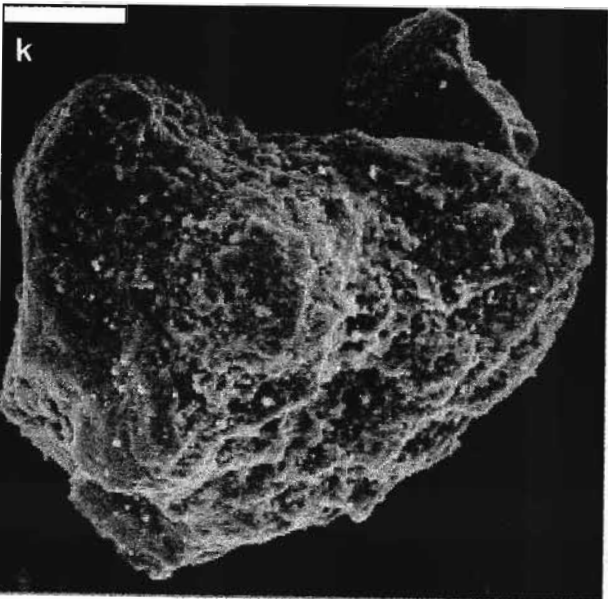
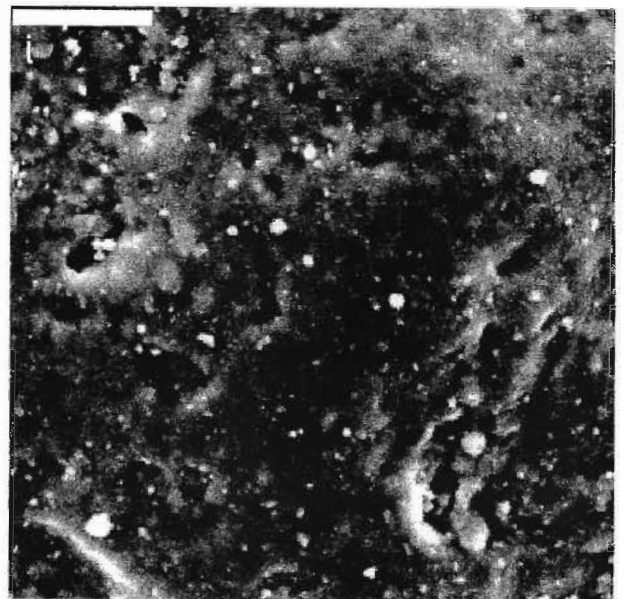
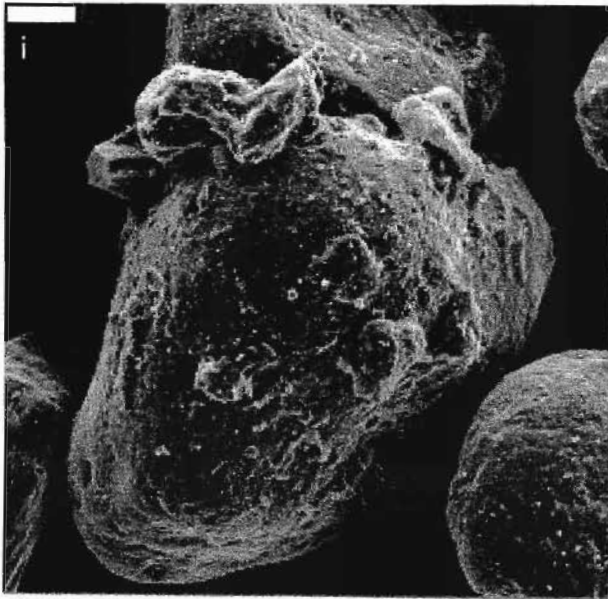
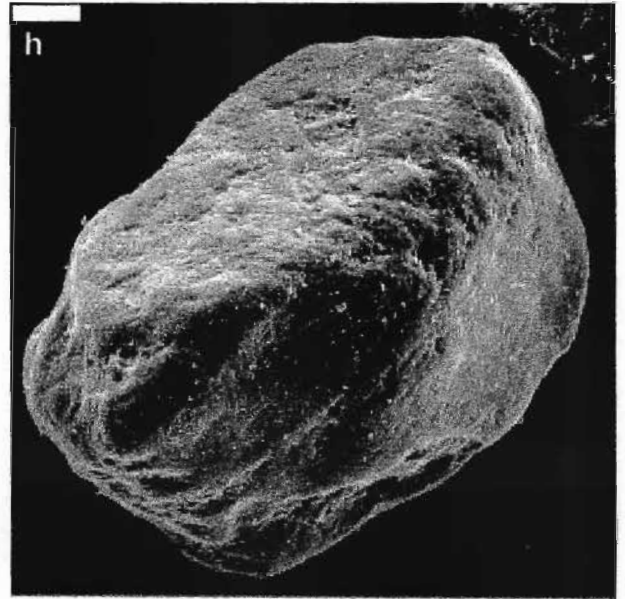
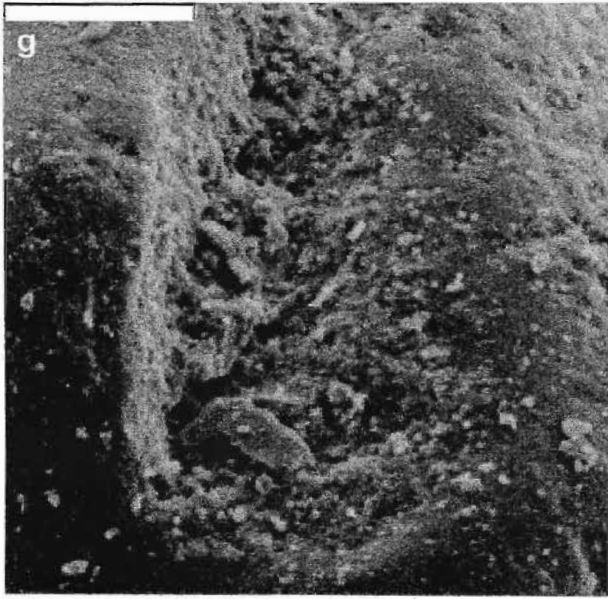
**Figure V.29 (a-f).** Physical and chemical features on quartz grain surfaces from marine, aeolian and diagenetic environments, as observed by SEM (scanning electron microscopy).

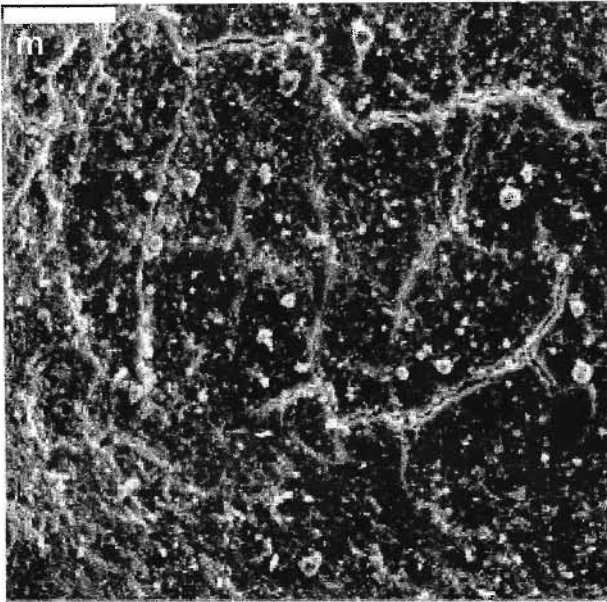
- a.) Subhedral quartz grain with slightly abraded edges. The surface appears more or less clean. F-dune 1 sample. Scale bar length: 50  $\mu\text{m}$ .
- b.)
  1. Quartz grain showing conchoidal fracture patterns and a very clear surface due to marine etching (top of photograph).
  2. Amphibole grain showing a complex sedimentary history: rounding; chemical etching along fractures; at least three generations of grain coating later destroyed partially by a high energy event; and structurally oriented chemical etching. F-dune 2 sample. Scale bar length: 50  $\mu\text{m}$ .
- c.) Quartz grain surface showing geometric solution features (oriented triangles) and fine pitting (upper left of the photograph) that are located on edges, indicating an infratidal marine environment. In the upper right of photograph: upturned plates indicating an aeolian environment. F-dune 2 sample. Scale bar length: 5  $\mu\text{m}$ .
- d.) V-shaped indentations (mechanical "V's") on a clean surface of a quartz grain, indicating a beach – surf zone environment. Note that most of these features have been enlarged and modified by chemical etching. F-dune 4 sample. Scale bar length: 5  $\mu\text{m}$ .
- e.) Moderately well rounded aeolian quartz grain with a spherical shape. The surface appears rough because of the presence of upturned plates and neof ormation or deposition of fine particles (see Figure V.29f). Upper left of the photograph: bryozoan. Sample 57 of borehole S3: Unit E. Scale bar length: 50  $\mu\text{m}$ .
- f.) Parallel ridges called "upturned plates" (Krinsley & McCoy, 1978) on the surface of a quartz grain, indicating an aeolian environment. Many fine particles (calcite and clays) are stuck on the surface. Sample 57 of borehole S3: Unit E. Scale bar length: 5  $\mu\text{m}$ .



**Figure V.29 (g-l).** Physical and chemical features on quartz grain surfaces from marine, aeolian and diagenetic environments, as observed by SEM (scanning electron microscopy).

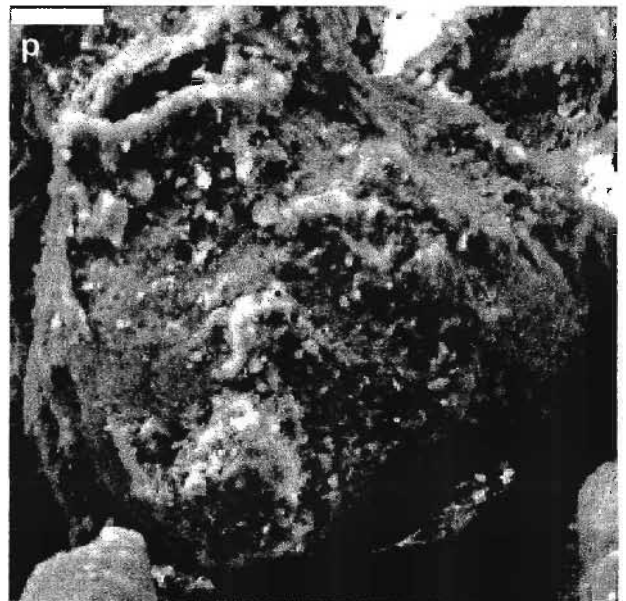
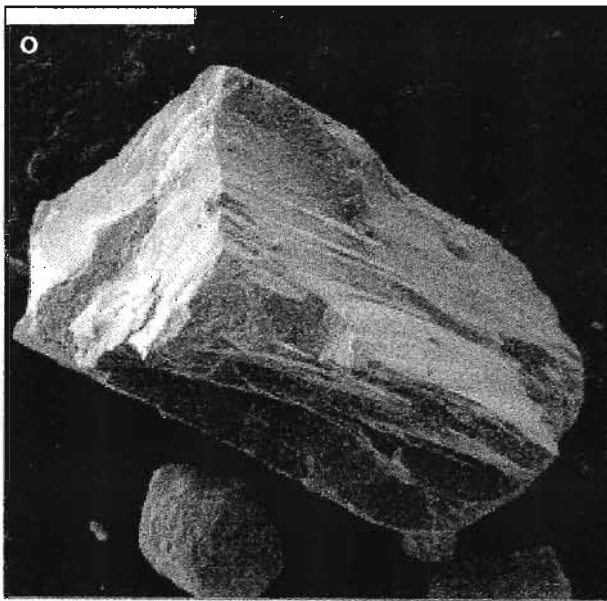
- g.) Fine particles (calcite, clays, silica deposits and unidentified minerals) within a depression on a quartz grain surface, indicating a vadose sedimentary environment. Sample 57 of borehole S3: Unit E. Scale bar length: 20  $\mu\text{m}$ .
- h.) Well rounded quartz grain with a surface smoothed by a thick layer of silica deposits. Sample 47 of borehole S1: Unit B. Scale bar length: 50  $\mu\text{m}$ .
- i.) Well rounded quartz grains with a smooth surface due to a thick layer of silica deposit. Various small minerals are cemented on their surface by silica deposits. Sample 5 of borehole S1: Unit A1. Scale bar length: 50  $\mu\text{m}$ .
- j.) Enlargement of previous photograph focussed on the central quartz grain. The original surface is completely covered by a globular silica layer, which has been subsequently chemically etched. Sample 5 of borehole S1: Unit A1. Scale bar length: 20  $\mu\text{m}$ .
- k.) Angular quartz grain that has been extensively coated by silica deposits, suggesting a non-aeolian environment. Sample 5 of borehole S1: Unit A1. Scale bar length: 50  $\mu\text{m}$ .
- l.) Subhedral and broken quartz grains that show a more or less clean surface, indicating a non-aeolian environment. Sample -2 of borehole S2: Unit A3. Scale bar length: 50  $\mu\text{m}$ .





m.) Polygonal cracks on a quartz grain surface, indicating an aeolian environment. Note also the upturned plates on the left part of the photograph and the thin or absent silica deposits. Sample 21 of borehole S3: Unit C. Scale bare length: 20  $\mu\text{m}$ .

n.) Broken quartz showing a clear surface with conchoidal fracture patterns, indicating a non-aeolian environment. Sample 21 of borehole S3: Unit C. Scale bare length: 50  $\mu\text{m}$ .



o.) Subhedral sodic feldspar grain showing a clear surface and sharp edges, suggesting a short transport distance from the source area before sedimentation. Sample 21 of borehole S3: Unit C. Scale bare length: 200  $\mu\text{m}$ .

p.) Titanium oxide grain (ilmenite?) thickly coated by silica layers and unidentified small particles (clays). Sample -3 of borehole S3: Unit A4. Scale bare length: 20  $\mu\text{m}$ .

**Figure V.29 (m-p).** Physical and chemical features on quartz grain surfaces from non-aeolian, aeolian and diagenetic environments, as observed by SEM (scanning electron microscopy).

## V.6. Summary: geological section of Northing Line 380

Eight sedimentological units can be identified from boreholes S1, S2 and S3 through Northing Line 380: Units A1, A2, A3/A4, B, C, D1, D2 and E. In contrast to this the geomorphological study recognised three different dune classes in the southern part of the study area: Dune Classes 2, 4 and 5. Thus the geomorphological study only identifies superficial units that have built upon older units. This illustrates that the present topography of the study area does not accurately reflect the internal structure of the dune cordon.

Lateral extension of the units identified from 3 boreholes from Line 380 has been investigated using heavy mineral ratios and the ilmenite content determined by RBM for all boreholes from this line (Figure V.30). The main units can be identified in this way, however further subdivision requires additional observations. The inland dune borehole (S1) comprises two stratigraphic units; a basal Unit A divided into two sub-units, Units A1 and A2, and an overlying Unit B. Unit A1 is considered to be the lateral equivalent of the old dune cordon present inland (Dune Class 1). The central dune borehole (S2) is subdivided into a lower Unit A3, which contains basal beach placers, and an overlying Unit D that is divided into Units D1 and D2. Recognition of the spatial distribution of Units D1 and D2, which are separated from each other by a palaeosol (Sudan *et al*, 1999), was assisted by field observations at MPC in August 1998 and January 1999 (Figure IV.6). The coastal dune borehole (S3) comprises four units. Unit A4, which contains basal beach placers, is considered to be a lateral equivalent to Unit A3 (borehole S2). The coastal extension of the overlying Unit C, borehole S3, has been correlated to the orange dune that outcrops south and north of Dawson's Rock (Figure IV.7). The upper portion of borehole S3 is divided into Unit D2 and the uppermost Unit E (Figure V.30). As observed on a coastal outcrop at Dawson's Rock (Figures IV.7), Unit E contains at least one buried palaeosol and may be subdivided into sub-units (Figure IV.8).

The following description presents a geological history based on Figures V.30 and V.31. If not specified, ages mentioned below are interpretative and are based on the relative values of IRZ/OHM (Section V.2.2.2). Units E and D are calcareous, have IRZ/OHM ratio values below 0.5 and are Late Pleistocene to Holocene in age (oxygen isotope Stages 2 and 1) as confirmed by luminescence dating (see below). Beach deposits associated to Unit A3/A4 reflect a high sea level, have IRZ/OHM ratio values between 0.5 and 1 (see last paragraph in Section V.3.1.3) and are considered to have formed during the last interglacial (last high sea level period, oxygen isotope Stage 5). Units A1 and A2 also reflect a high sea level period (see below), show even greater IRZ/OHM ratio values (above 1.2) and are thus considered to be of penultimate interglacial age (penultimate high sea level, oxygen isotope Stage 7).

Unit A1 is the oldest deposit of the dune cordon in the southern part of the study area. Aeolian sand, mixed probably with marine and/or fluvial sediments, composes this unit. Unit A2 consists exclusively of aeolian sand derived from a nearby beach – foredune system (Figure V.31a). It originally contained a high total of heavy mineral content and now contains the highest ilmenite content observed in aeolian sediment of the Line 380. Unit A2 is believed to be of similar age to Unit A1 or slightly younger. Unit A2, and Unit A1 in a lesser extent, were thus deposited at a high sea level and are interpreted to represent sediments from the penultimate interglacial period, during the oxygen isotope Stage 7 (Figure V.31a). The possibility of Units A1 and A2 representing two distinct interglacials cannot be ruled out.

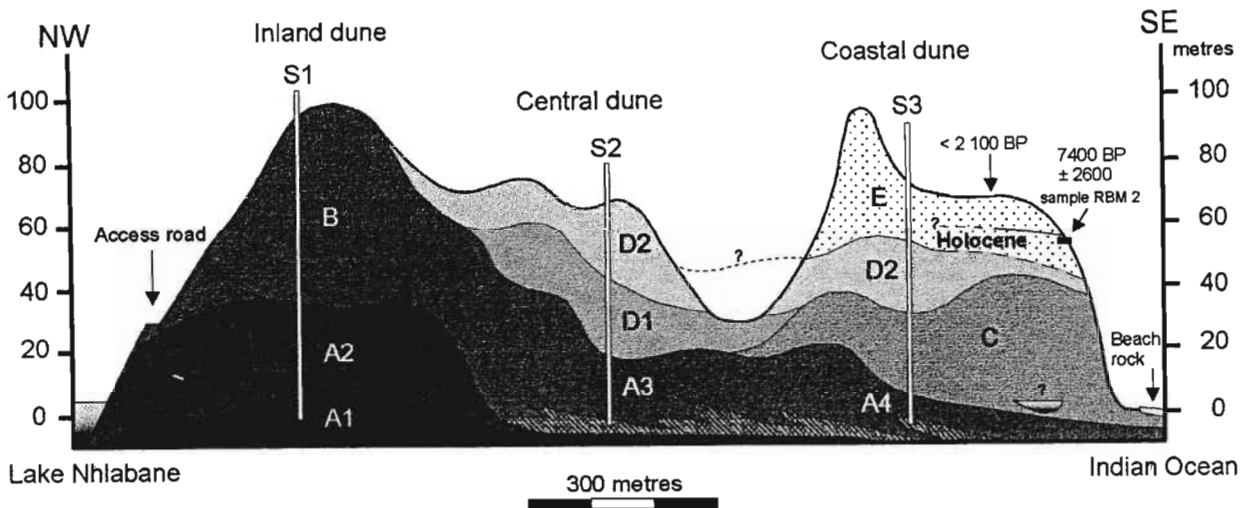


**Figure V.30.** Geological section of Northing Line 380, showing the lateral extension of the height units defined in Chapter V and the location of the sample RBM 2 dated by luminescence (Figure IV.8). Hatched patterns illustrate beach placers. The symbol in Unit C represents a river bed (Nhlabane River?) during the early phase of the last glaciation. The exact location of that river bed is unknown and could actually be located in a more southwestern direction (see text).

Aeolian reworking characterised the penultimate glacial period (oxygen isotope Stage 6) (Figure V.31b). Marine transgression following the penultimate glaciation eroded the old dune cordon, resulting in the formation of steep cliffs similar to those observed on the present shoreline (Figures V.30 and V.31c). Sea level still-stands and regressive phases during the last interglacial (oxygen isotope Stage 5) induced the progradation of the associated beach – foredune system illustrated by abundant beach placers at the base of the present dune cordon (Figures V.30 and V.31c). Transgressive aeolian dunes with relatively low heavy mineral content subsequently covered these littoral deposits (Figure V.31c).

Sediment at the base of Unit C, borehole S3, has distinctive characteristics suggesting that it is derived from a non-aeolian environment, that is to say fluvial or marine. A marine origin is unlikely as this would imply a sea level at more than 18 m above msl, a point not reached during the last interglacial period (Ramsay, 1997). For the same reasons, a fluvial origin is improbable. The most likely scenario is that a nearby river (Nhlabane River?) deposited sediments that were reworked by proximal aeolian dunes (Figure V.31d). This would explain the immature state, distinct mineralogy and low heavy mineral content of Unit C (see Sections V.2.2.2 and V.3.2.3).

Marine regression to -130 m below msl during the last glacial maximum (18 000 B.P., oxygen isotope Stage 2) induced fluvial erosion of the inland portion of the dune cordon (Units A1 and A2, and possibly Unit B), resulting in steepening the westward facing dune slope (Figures V.30 and V.31e-f). The sediment characteristics of Unit B suggest that this unit is a mixture of material reworked from Unit A3/A4 with a minor amount of younger calcareous sediments (Section V.2.1.2). Unit B is interpreted to have formed during oxygen isotope Stage 2

(Figure V.31e-f). The geomorphological equivalent to Unit B is the inland dune (Dune Class 2). Spatial distribution (elevation and thickness) of Units A3/A4 and B also suggests significant reworking (Figure V.30). Units A3/A4 and B generally contain more abundant ilmenite than the overlying units, except for the youngest coastal sediment of Unit E.

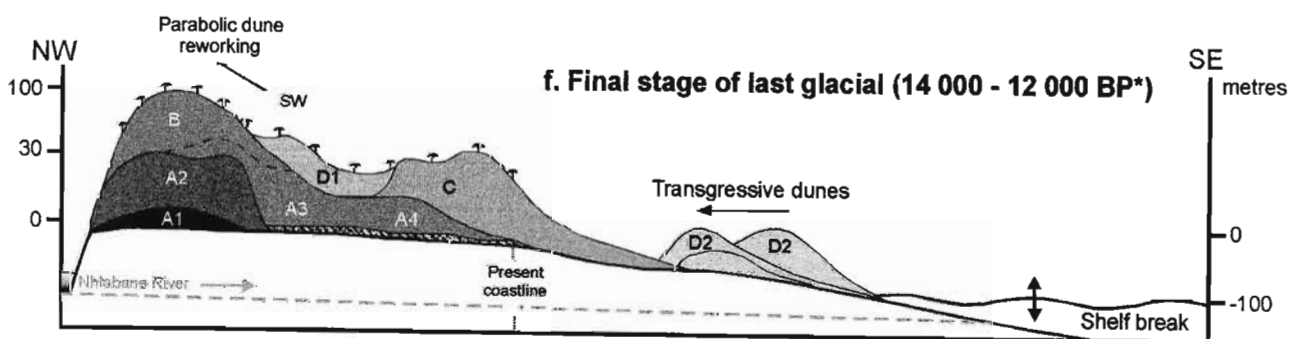
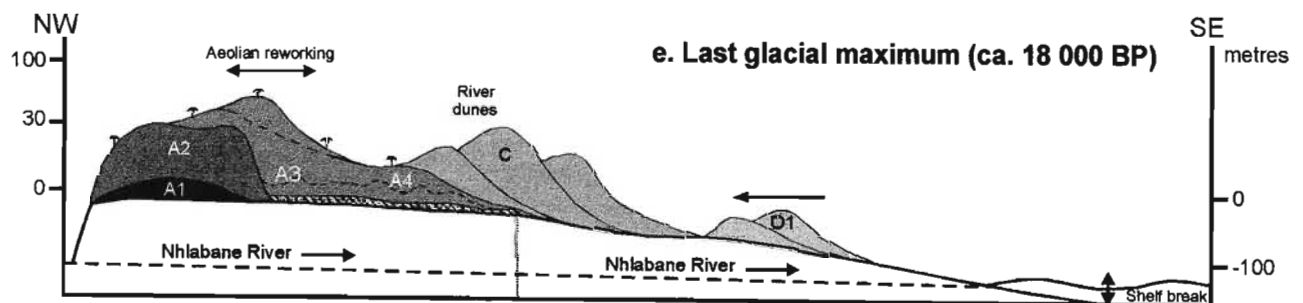
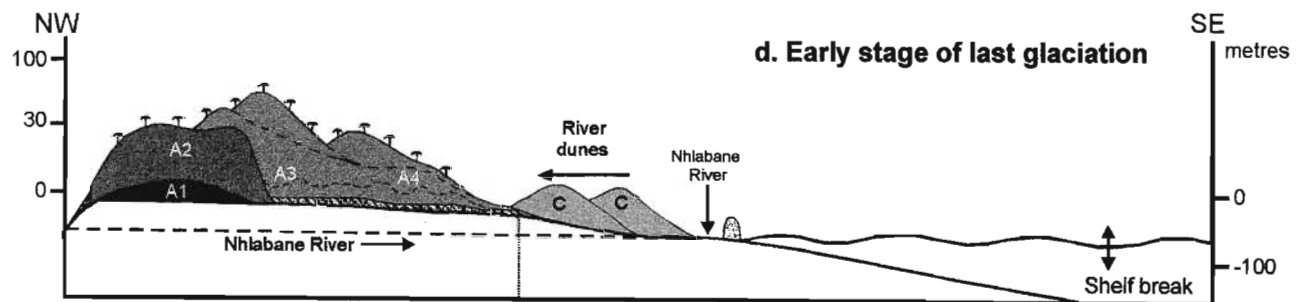
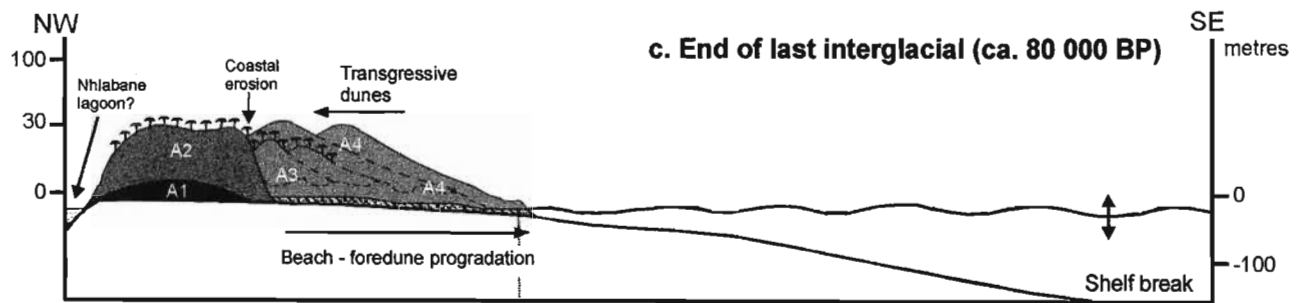
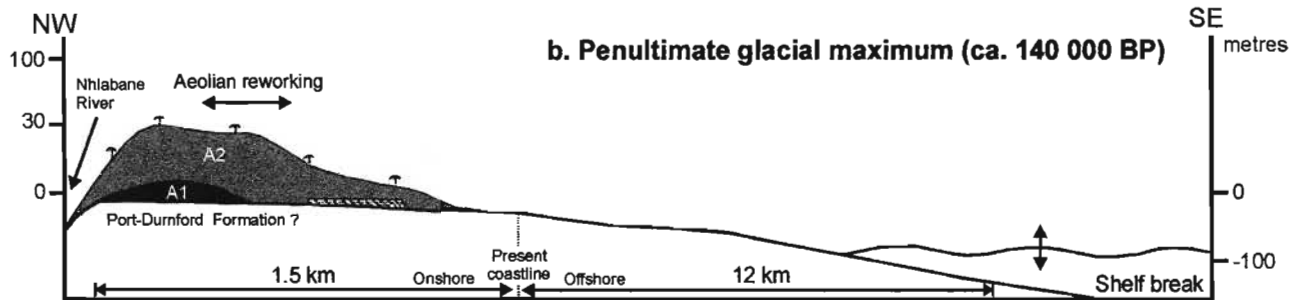
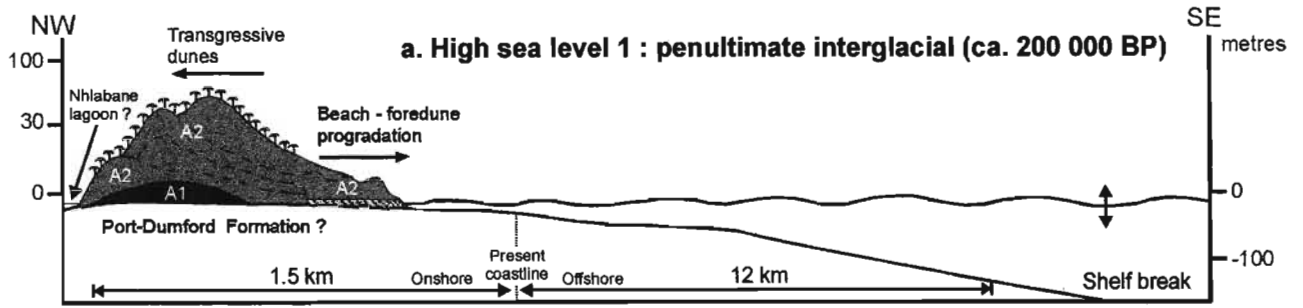
Aeolian Units D and E are the only deposits that contain large amount of detrital bioclastic grains (up to 6 %). Unit D1 is characterised by a more advanced alteration state determined from heavy mineral ratios (pyriboles) and bioclastic content. The suggested older age for Unit D1 compared to Units D2 and E may be apparent, as reworking of older deposits (Units B – A3 – A4 system) might have provided more mature sediment.

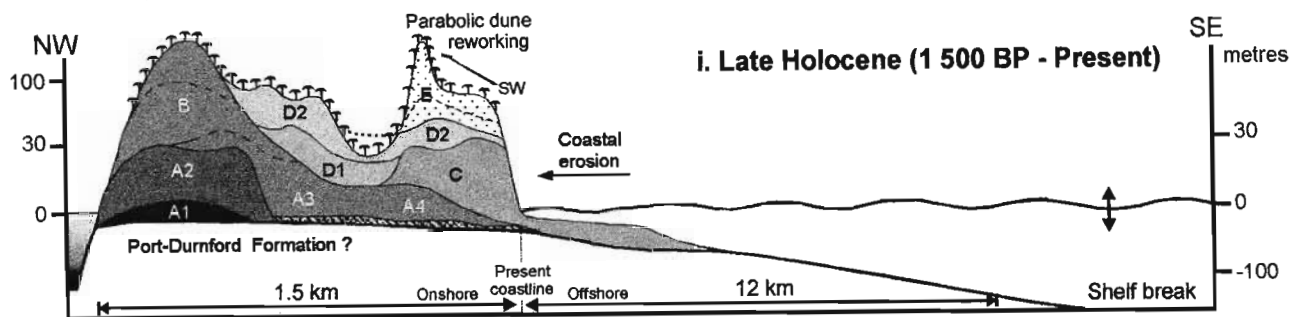
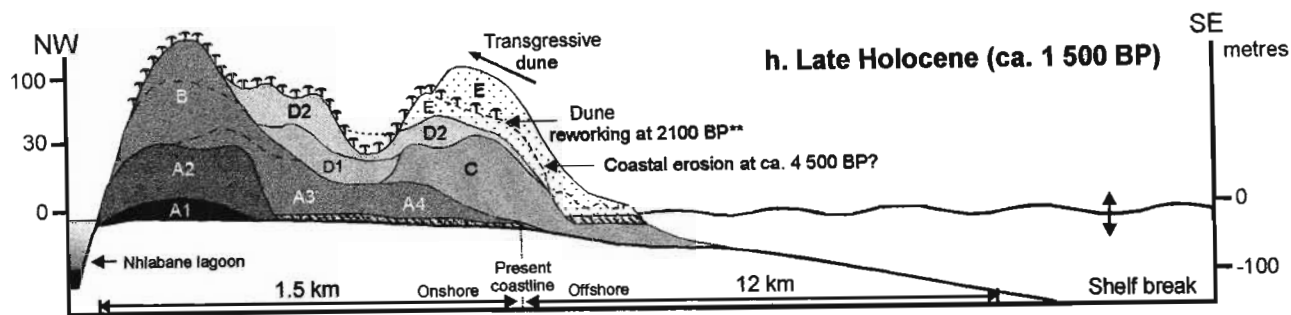
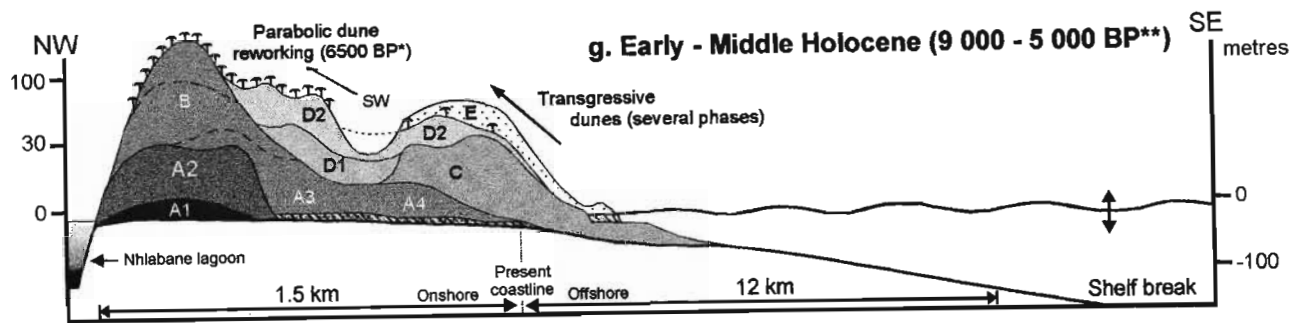
The relatively low heavy mineral content for Unit D2 suggests that the sediment has migrated a considerable distance from the beach – foredune system it originated from. These units (with Unit D1?) would thus have overlain the dune cordon as transgressive dune fields, and were later reworked into parabolic dunes (Figures V.30 and V.31e-g). Depositional and reworking ages of sample RBM 1 (Section IV.2.3) are applied here to Unit D2 for the southern part of the study area (Figure V.31f-g). Unit D2 is further discussed in Section VI.6.

Unit E is characterised by a high heavy mineral content, indicating that it was formed during a high sea level period and that the sediment did not travel a long distance from the associated shoreline. The associated coastline is interpreted to have been located close to the present coastline (Figure V.31g-h). Luminescence dating of sample RBM 2 (Section V.1.2) indicates a depositional age of  $7400 \pm 2600$  B.P. and a reworking event at  $2100 \pm 142$  B.P. This Early Holocene depositional age unfortunately implies a wide range of associated sea levels between ca. -50 m below msl and 1.5 m above msl (Figures II.9 and V.31). However, as Unit E did not travel a long distance, it is assumed here that this unit formed less than 9 000 B.P., when sea level was not lower than -10 m below msl (Figure V.31g). The reworking age (Figure V.31h) attributes a maximum age of 2100 B.P. for the palaeosol within Unit E (Figure IV.8). Thus the latest depositional event(s) occurred within the last 2000 years or probably within the last 1500 years as voluminous onshore aeolian transport of sand is likely to take place during stable or regressive sea levels (Figures V.30 and V.31h).

Finally recent sea level rise or a decrease of sand supply to the beach caused coastal retreat and formed cliffs by erosion of Units C, D2 and E (Figures V.30 and V.31i). Episodic still stand periods were recorded as beach rocks (Figure V.30). It is possible that these beach rocks were formed at an earlier stage, prior to the deposition of at least Unit E, as sea level change during this time is not precisely known.

The proposed geological evolution differs from that of Fockema (1986, Figure III.5, section C-D). No units matching the Kosi Bay Formation have been identified and it is suggested that the latter formation probably lies inland (compare Figures V.30 and III.5). Units D and E can be regrouped into the Sibayi Formation on the basis of their high carbonate content (Section III.4.1.7). Therefore Units A, B and C should be attributed to the KwaMbonambi Formation. However, their facies style, complexity and age do not match the informal definition of the formation (Section III.4.1.6). This suggests that the Kosi Bay Formation is older than initially thought, possibly as old as or rather older than the penultimate interglacial period (oxygen isotope Stage 7, ca. 200 000 years B.P.). The present regional stratigraphy as described in Chapter III appears thus to be too simple and will no doubt be revised in due course.





Sea level curves

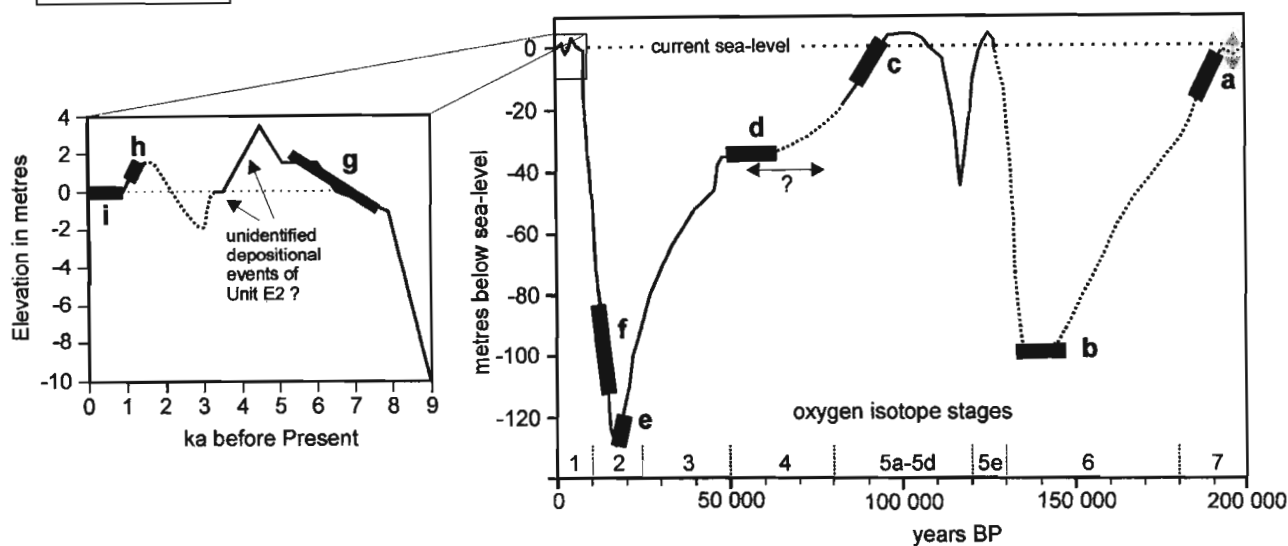


**Figure 31 (a-i).** Evolutionary model for the southern cross-section (Line 380), showing the depositional and reworking events correlated with time and sea level fluctuations. Single and double asterisks refer to luminescence dates from samples RBM1 and RBM2 (see text). Each cartoon is labelled a to i, which correspond to periods marked on the sea level curves. Sea level curves from Ramsay (1995; 1997).

## VI. NORTHERN ZULTI NORTH ORE BODY (NORTHING LINE 1200)

### VI.1. Introduction

Results from the geomorphology study suggest that the Zulti North ore body can be divided into southern and northern portions, with a transitional boundary between N600 and N800 (Chapter IV). The northern portion of the ore body is composed of four dune classes and may well be underlain by Dune Class 1, as identified to the south.

Five boreholes from Northing Line 1200 were selected for analysis. The boreholes are located on the crest of a hairpin parabolic dune of Dune Class 2, two linear dunes of Dune Class 3 and on the crest of one parabolic dune of Dune Class 4 (Figure VI.1). Thus, at least the upper section of each borehole represents one of three dune classes. For practical reasons, the five boreholes, from inland to the coast, will be referred to as boreholes N1, N2, N3, N4, and N5. Two boreholes (N5a and N5b) from the coastal parabolic dune have been studied to gain a relatively complete data set for this geomorphic feature. Samples from borehole N5a were not found in the RBM sample archives. Only data supplied by RBM on these samples are presented. Additional samples from borehole N5b are utilised to characterise the coastal parabolic dune.

Similar analyses to those presented for the southern part of the study area (Chapter V) were applied to samples from Line 1200. The reader is thus referred to Chapter V for description of the methods used, and a discussion of their reliability. The following chapter focuses on the definition of sedimentological units in the Northing Line 1200, and correlation of these units with those identified for Line 380.

Sixty-one samples from 6 boreholes have been analysed for grain size, heavy mineral abundance and recalculated heavy mineral ratios. Only twenty-six selected samples have been analysed for mineral point counting and bulk geochemistry.

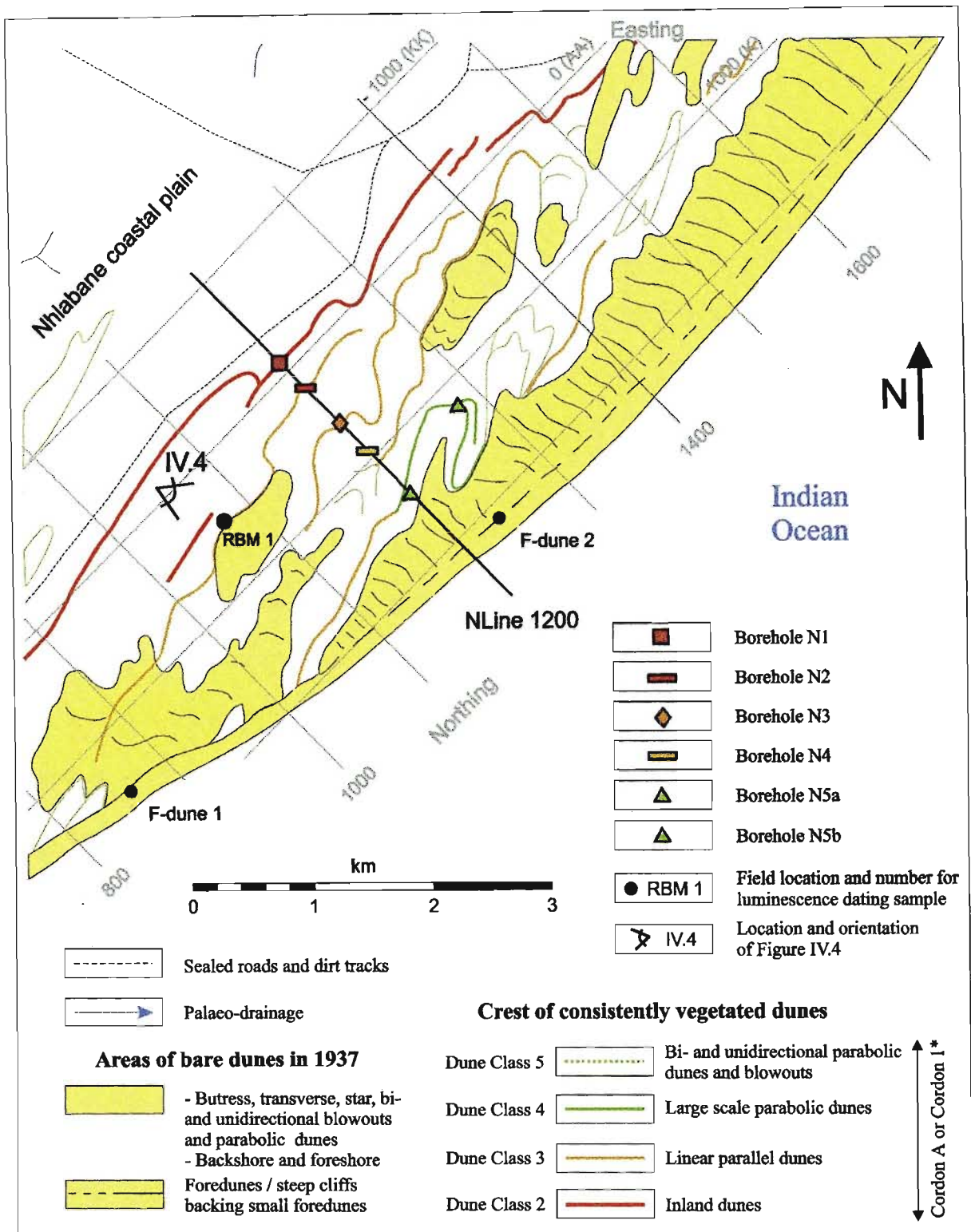


**Figure VI.1.** Geomorphological map of the northern Zulti North ore body, showing the location of boreholes N1, N2, N3, N4, N5a and N5b, which intercept Dune Classes 2, 3 and 4. \*Cordon A of Davies (1975), Cordon 1 of Wright (1999).

### VI.1.1. Sample location and description

The location and characteristics of the six boreholes N1, N2, N3, N4, N5a and N5b are presented in Table VI.1; the reader is directed to Section V.1.1 for explanations. The five boreholes N1, N2, N3, N4 and N5a located along Line 1200 are shown in Figure VI.2.

**Table VI.1.** Nomenclature, location and characteristics of the six boreholes N1 to N5b from Line 1200. Asterisk = samples selected for mineral point counting and bulk geochemistry.

Borehole	N1	N2	N3	N4	N5a	N5b
<b>RBM nomenclature</b>	1200/BB/1	GER/1200/B	1200/E/1	1200/H/1	1200/R	GER1280/M
<b>Location</b>	N1200 E-150	N1200 E200	N1200 E550	N1200 E850	N1200 E1500	N1280 E1200
<b>Top elevation</b>	62 m above msl	109 m above msl	88 m above msl	49 m above msl	63 m above msl	105 m above msl
<b>Bottom elevation</b>	17 m above msl	7 m above msl	-12 m below msl	-17 m below msl	-23 m below msl	51 m above msl
<b>Number of samples</b>	8	17	17	11	15	10
<b>Missing samples</b>		106, 88, 76, 70, 28	55		15	
<b>Selected samples*</b>	53, 41, 23 and 18	94, 82, 52, 34, 16, 10	73, 61, 37, 19, 1, -5, - 10	40, 28, 10, 4, -8		96, 78, 60, 48

#### *RBM 1 field sample*

RBM 1 sample was collected on the flank of the most inland of the linear parallel dunes (Dune Class 3) at N1075 and E450 (Figures VI.1, VI.2, IV.4). It was sampled below the present soil at an elevation of 85 m above msl.

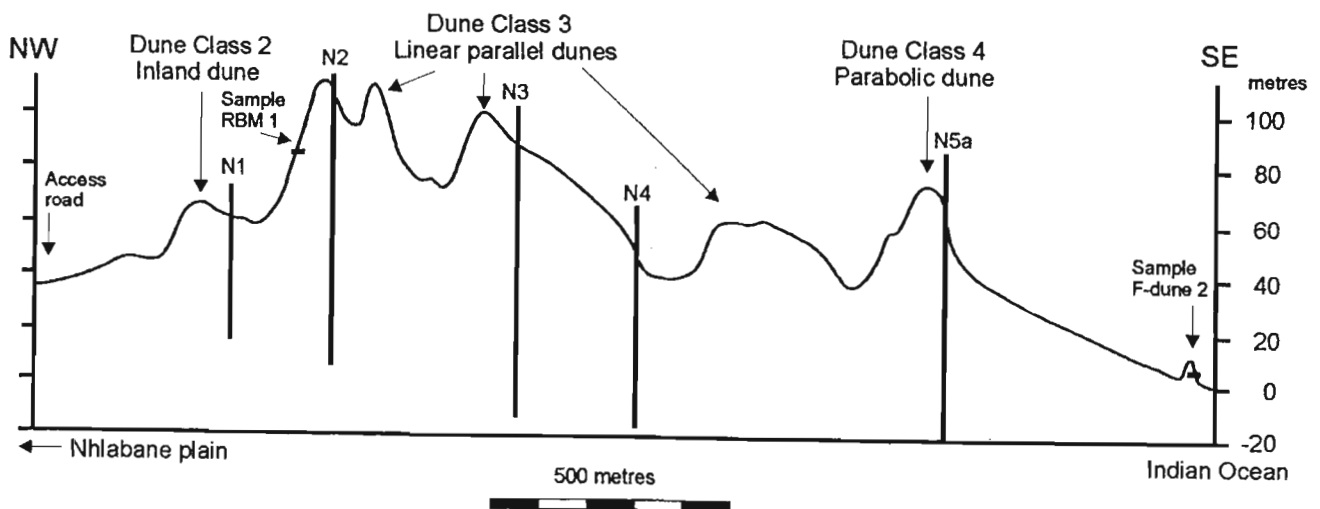


**Figure VI.2.** Topographic section along Line 1200, showing the morphology and the location of the five boreholes and field samples studied. RBM1 field sample has been dated by luminescence (see text and Figure VI.1).

## VI.2. Mineralogy

### VI.2.1. Mineral point counting

Point counting of thin sections made from bulk sediment significantly lowers the accuracy of abundance data for rare minerals such as zircon, rutile and garnet (Section V.2.1). For the analysis of Line 1200 these minerals are grouped into a "remaining heavy minerals" category. As the point count data for "iron hydroxides" and "cement fragments" were not useful in the study of Line 380, these two categories have been discarded and will only be mentioned below when relevant.

In order to focus on the significant information from the mineral point count data, the following sections will describe important minerals or group of minerals by comparing their abundance variations between boreholes and field samples. The complete point count data is presented in Appendix D. Terminology and petrological characteristics are described in Section V.2.1.

#### VI.2.1.1. Rock fragments and carbonate grains

The abundance of rock fragments and carbonate grains can be used to subdivide the study area into relatively immature (young) and mature (old) sediments (Figure VI.3). The upper 40 to 60 m of boreholes N2 and N3, and the entire borehole N5b are characterised by abundant (1.5 to 8 %) calcareous bioclasts and rock fragments. Similar abundances were recorded for Units D and E in Line 380 (Figure V.8). Sediments located below ca. 50 m above msl are strongly depleted in carbonate grains and rock fragments.

#### VI.2.1.2. Pyroxene and amphibole

Pyroxene/thm (Figure VI.4) and amphibole/thm ratios present similar trends, and thus only the former ratio has been considered and compared with that for Line 380 (Figure V.9).

Units D and E in the southern cross-section are characterised by pyroxene/thm ratio values greater than 0.15. This relationship is also observed for Units D and E in Line 1200 (Figure VI.4). Samples with values less than 0.15 are defined here as Unit A. A break in pyroxene/thm values at 0.05 is used to divide the lower Unit A2 in boreholes N2, N3 and N4 from the overlying Unit A4.

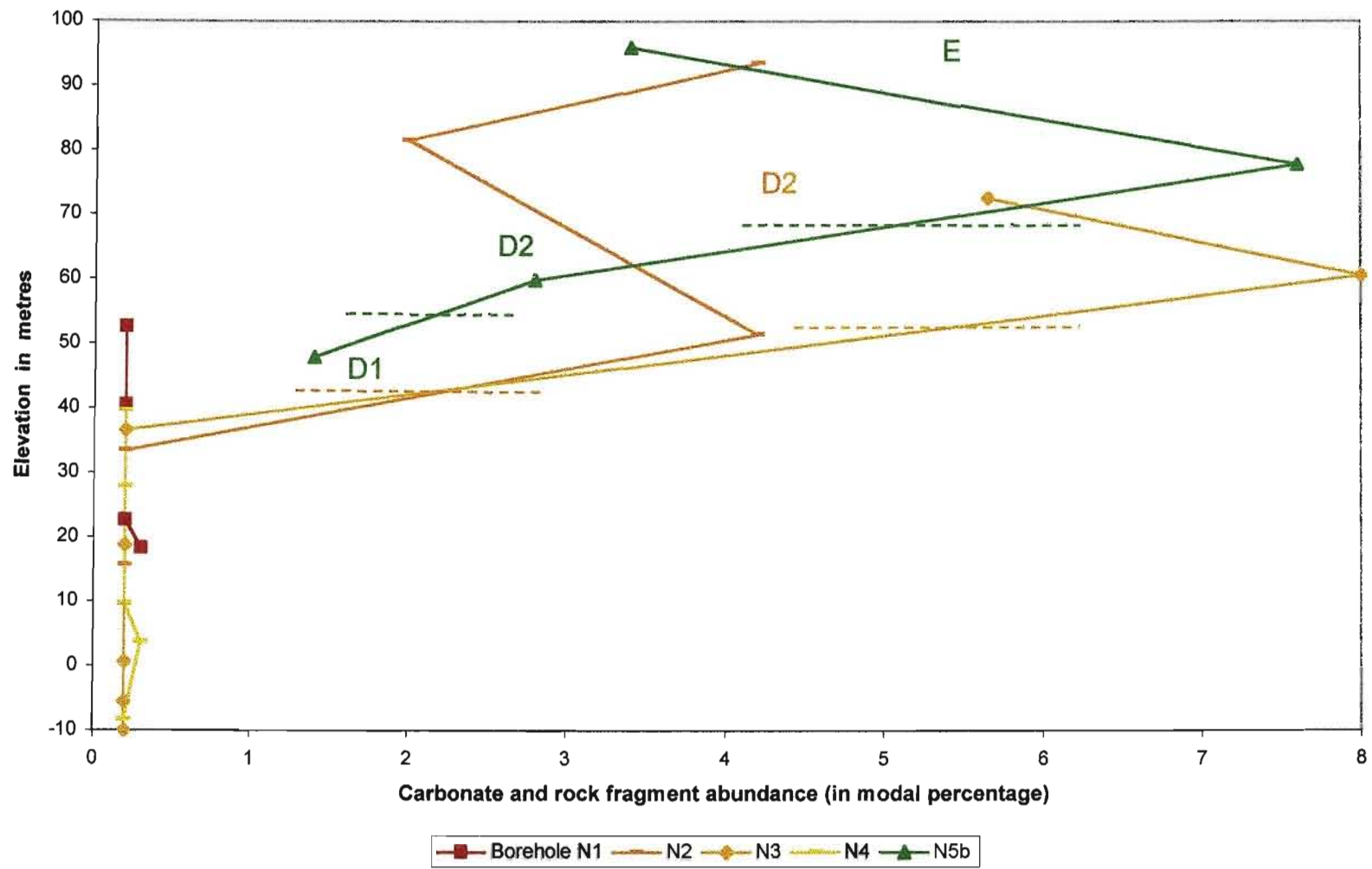
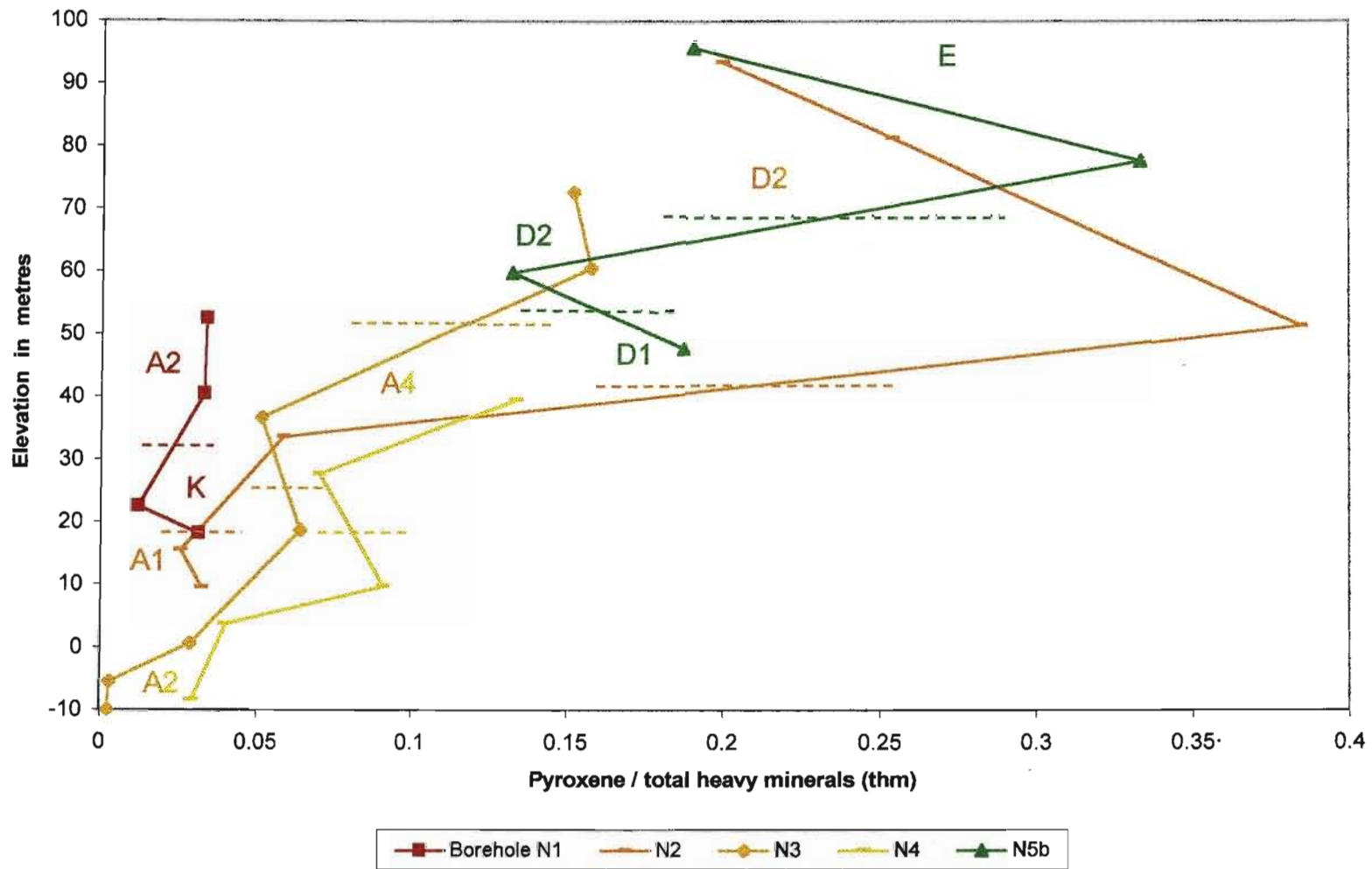


Figure VI.3. Rock fragment and carbonate grain abundance for samples from Line 1200 boreholes. Dashed lines = unit boundaries. Note that Unit D2 is found in boreholes N2, N3 and N5b.



**Figure VI.4.** Ratio of pyroxene divided by total heavy mineral for samples from Line 1200 boreholes. Note that Units A2 and A4 are found in boreholes N2, N3 and N4.

## VI.2.2. Heavy mineral abundance

### VI.2.2.1. Absolute heavy mineral content

The heavy mineral content in samples from Line 1200 is relatively homogeneous and presents a decreasing trend with depth (Figure VI.5). An interesting feature presented in Figure VI.5 is the presence of 10 samples at the base of the dune cordon containing less than 2 wt% total heavy minerals. This is unexpected as all samples from the southern cross-section (Line 380) are characterised by heavy mineral content higher than 2 wt% (Figure V.10).

Two units can be distinguished by very high heavy mineral content. Unit E incorporates the upper 45 m of borehole N5a, in which high heavy mineral abundances range between 9 to 32 wt%. These values are similar to Unit E in Line 380 (Figure V.10), for which the high heavy mineral content was interpreted to reflect proximity to the beach. The two basal samples of borehole N3 (bottom part of Unit A2) contain between 20 to 40 wt% heavy minerals, significantly higher than all other samples from the base of the dune cordon. This suggests that these two samples were deposited in a beach environment.

The upper 60 m and 35 m of boreholes N2 and N3 contain 2 to 8 wt% heavy minerals. This is similar to Unit D2 of Line 380, and a tentative correlation is made.

### VI.2.2.2. IRZ / OHM ratio

The IRZ/OHM ratio is a good proxy for the alteration state of the sediment. The IRZ/OHM ratio values for borehole samples from Line 1200 show an increasing trend with depth and from the coast towards the inland portion of the dune cordon (Figure VI.6).

Boreholes N5a and N5b and the upper portion of boreholes N2 and N3 (Unit D2) are characterised by low IRZ/OHM values (Figure VI.6), similar to the upper Units D and E of the central and coastal boreholes of Line 380 (Figure V.13). This is consistent with the high carbonate, rock fragment and pyroxene abundance observed in these sands (Section VI.2.1.1). The basal 40 m of borehole N5a is characterised with slightly higher IRZ/OHM values, similar to Unit D1 in Line 380, and is thus defined here as Unit D1.

High heavy mineral content defines the occurrence of Unit E in borehole N5a (Section VI.2.2.1). The proximity of the beach – foredune system might be responsible for the higher IRZ/OHM values presented by the top four samples of Unit E, borehole N5a (Figure VI.6).

Samples between 20 to 45 m above msl of boreholes N2, N3 and N4 (Unit A4) present similar IRZ/OHM ratio values to the upper portions of Units A3 and A4 in Line 380 (compare Figures VI.6 and V.13).

The basal 35 m of boreholes N3 and N4 and the upper 30 m of borehole N1 are defined as Unit A2 due to their intermediate to high IRZ/OHM ratio values, which are similar those of Unit A2 along Line 380. Note that the beach deposits at the base of borehole N3 show elevated IRZ/OHM values, yet are considered to be contemporaneous to the other samples in Unit A2. The elevated IRZ/OHM values for the beach deposits are considered to be due to mineral segregation in the beach and nearshore environment as described in Chapter V (Sections V.2.2.2 and V.3.1.3).

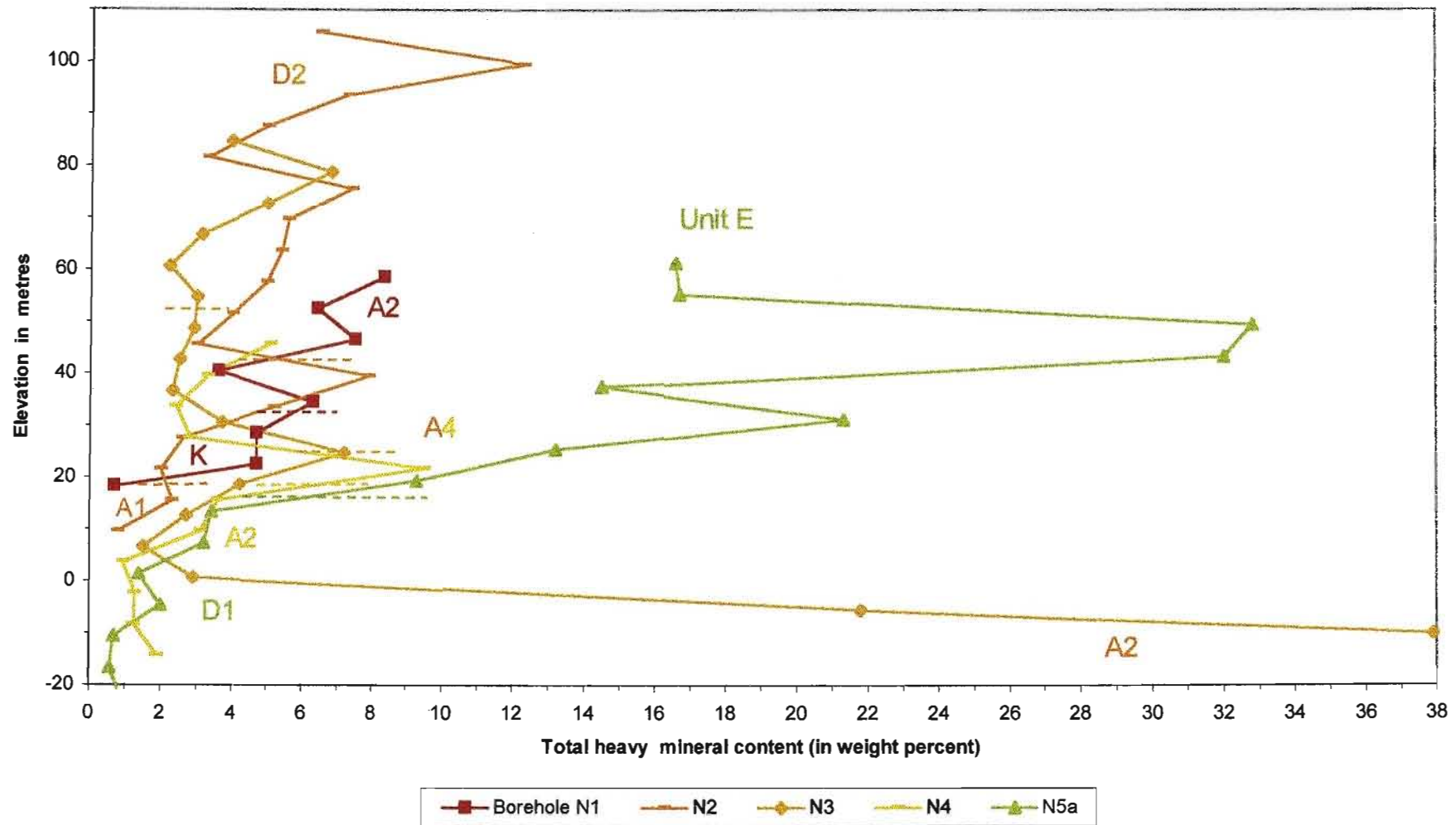
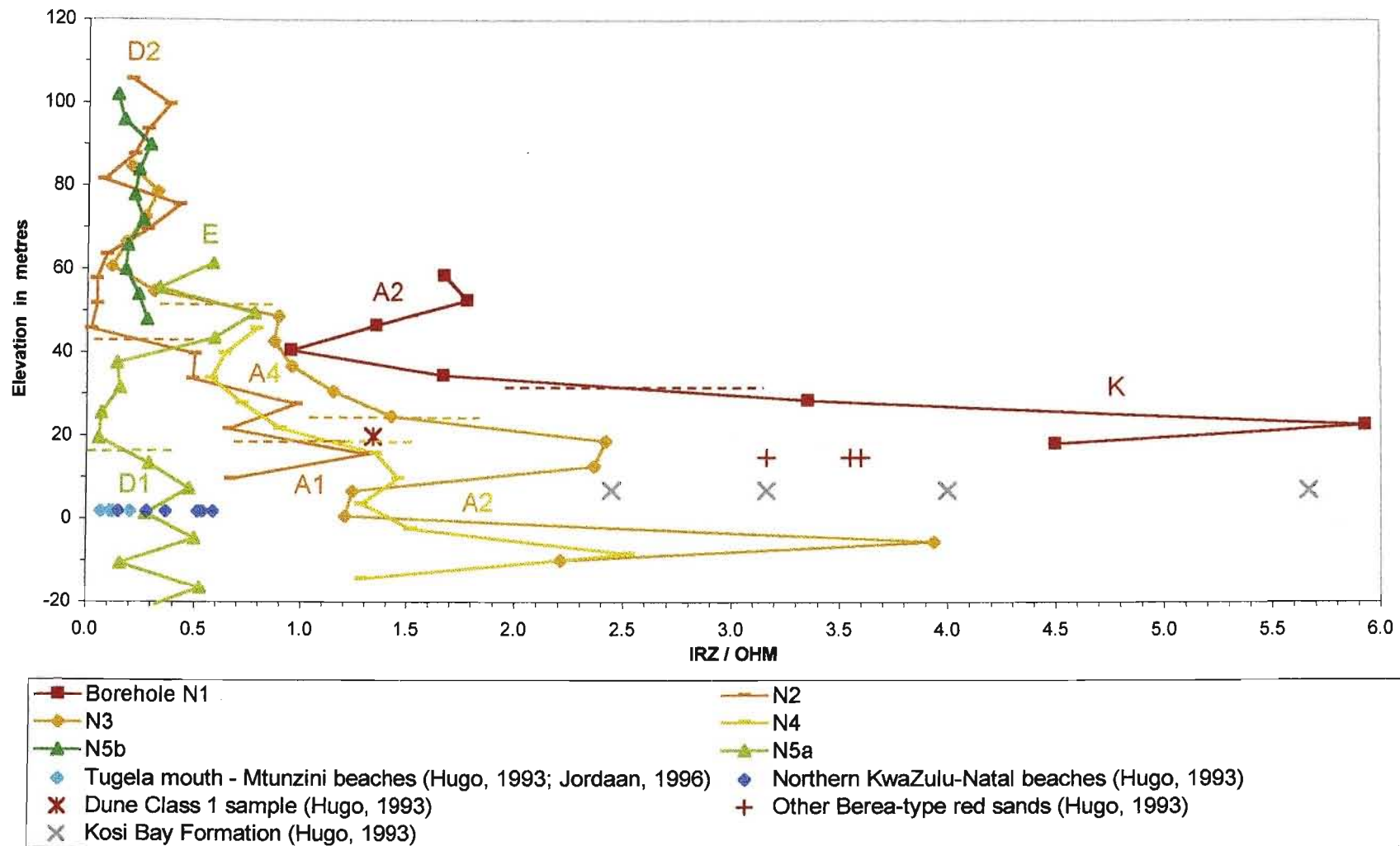


Figure VI.5. Heavy mineral content for samples from Line 1200 boreholes (recalculated from heavy mineral ratios and ilmenite content determined by RBM).



**Figure VI.6.** Ratio of ilmenite, rutile and zircon divided by other heavy minerals (IRZ/OHM) for Line 1200 borehole and field samples.

The beach and associated aeolian sediments of Unit A2 from the northern cross-section present higher IRZ/OHM values than the beach and associated aeolian sediments identified in Units A3, A4 and B to the south (Figure V.13). This suggests that the beach and associated aeolian deposits in the northern part of the study area (Unit A2) are older than those in the southern part (Units A3, A4 and B). This interpretation is based on the assumption that the sediment is derived from the Tugela River and has migrated more than 100 km by northward longshore drift (Section II.3.3 and Figure III.2). During transport this sediment is expected to be thoroughly mixed with shelf sediment before reaching the study area. In this context, a significant increase in maturity for marine sediments between Lines 380 and 1200, which are separated by less than 8 km, is unlikely (see also Section V.2.2.2).

The basal 10 m of borehole N2 is defined as Unit A1. As discussed in Chapter V, Unit A1 is believed to be as old or older than Unit A2 and should contain higher IRZ/OHM ratio values. It is not fully understood why this unit (especially the bottom sample) shows relatively low IRZ/OHM ratio values (Figure VI.6). However, it has been shown that the IRZ/OHM ratio is less sensitive for discriminating old sediment compared to Magnetite/THM and Magnetite/Ilmenite ratios.

The very high IRZ/OHM values of the basal 15 m of the inland borehole N1 led to the definition of a new unit, Unit K (Figure VI.6). The IRZ/OHM value for this unit varies between 3 to 6 and closely matches that for the Kosi Bay Formation (Figure VI.6).

### VI.2.2.3. Magnetite / THM

The evolution of the Magnetite/THM ratio (Figure VI.7) through time is complex, and initial values may be influenced by palaeogeography and the magnetite content of the source sediment (Chapter V.2.2.3). Magnetite/THM values for borehole N5a are irregular and they are not discussed. The coastal parabolic dune is thus represented in Figure VI.7 by borehole N5b only.

The entire borehole N5b and the upper portions of boreholes N2 and N3 (Unit D2) present Magnetite/THM values comprised between 0.15 and 0.3. A similar value range characterises Units D2 and E in the southern cross-section (Figure V.14).

Unit A2 is brought out by the highest Magnetite/THM values (Figure VI.7). This may be due to alteration of pyroxene and amphibole within the THM fraction. However, the very high ratio values for the basal five samples of Unit A2, borehole N3, suggest an input of immature sediment (rich in magnetite). Unit A3 from the southern cross-section presents similar overall trends and ratio values.

Unit A1 is distinguished from Units A2 and A4 by low Magnetite/THM ratio values (Figure VI.7). This suggests that the sediment of Unit A1 is more mature than Units A2 and A4, a conclusion that could not be obtained from the IRZ/OHM ratio values.

Unit K presents the lowest Magnetite/THM values for the study area. Only samples of the Kosi Bay Formation show similar ratio values.

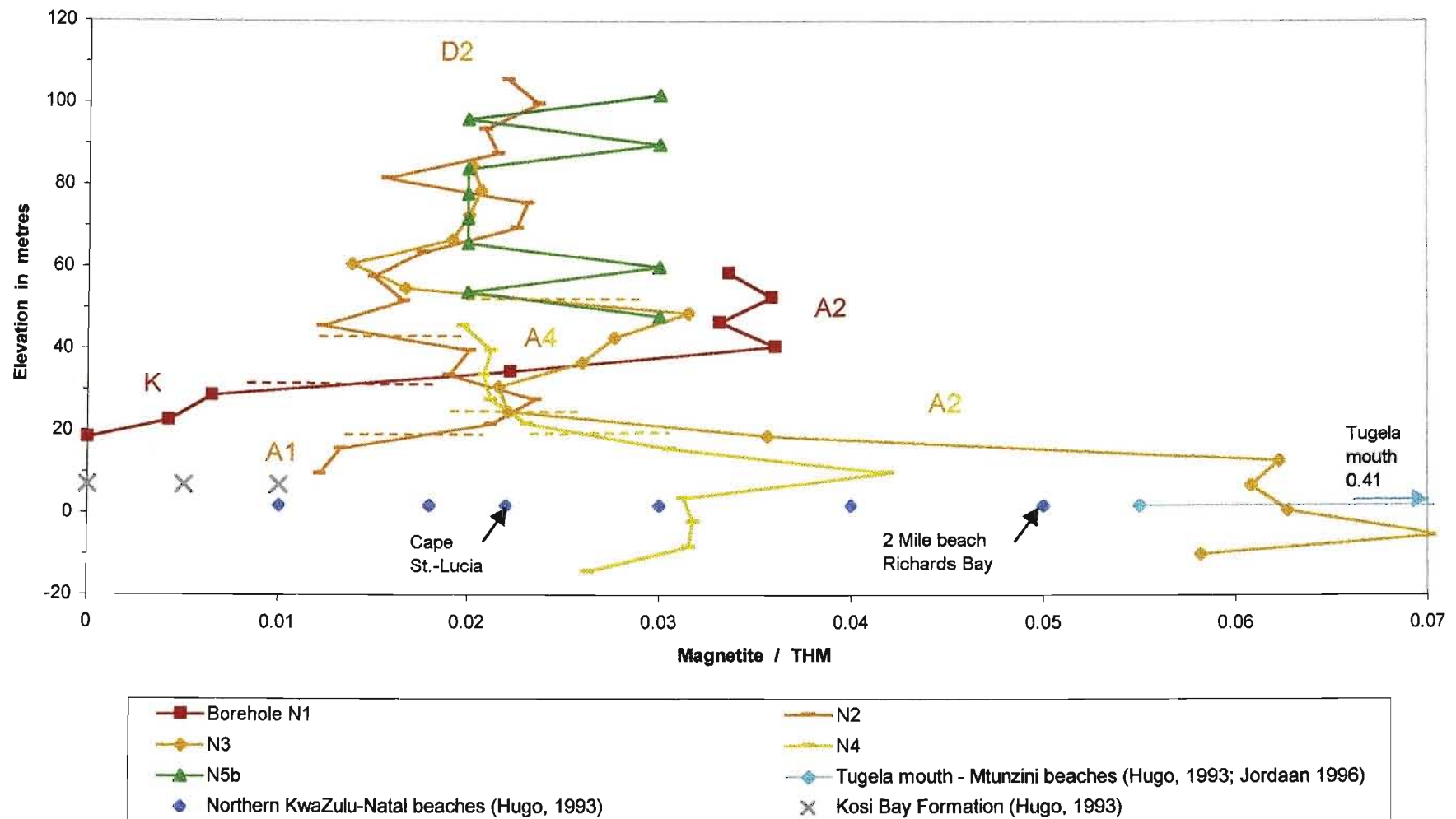


Figure VI.7. Ratio of Magnetite divided by total heavy mineral content (Magnetite / THM) for Line 1200 borehole and field samples.

#### VI.2.2.4. Magnetite / Ilmenite

Magnetite/Ilmenite ratio values (Figure VI.8) have been shown to decrease with increasing age. Borehole N5a presents similar ratio values to Unit D2 and to borehole N5b. The coastal parabolic dune is represented in Figure VI.8 by borehole N5b, in order to avoid the confusion due to too many samples.

Boreholes N5a, N5b and the upper portions of boreholes N2 and N3 present a relatively wide range of Magnetite/Ilmenite values comprised between 0.10 and 0.25 (Figure VI.8). The lower 40 m of borehole N5a, which has been identified as Unit D1, is characterised by the lowest Magnetite/Ilmenite values within this range.

The lower 25 m of Unit D2, borehole N2, is characterised by extremely high Magnetite/Ilmenite values. The sediments forming Unit D2 in the northern part of the study area migrated a long distance onshore from the continental shelf, during the post-glacial marine transgression (Section IV.3). These extremely high values are interpreted to reflect input of immature and magnetite rich sediment from a local river such as the Nhlabane or Mhlatuze Rivers. River sampling needs to be undertaken for further discussion of this hypothesis.

Samples between 20 to 50 m above msl of boreholes N2, N3 and N4 are characterised by intermediate Magnetite/Ilmenite values between 0.05 and 0.12. This unit is defined here as Unit A4, as Units A3 and B from the southern cross-section show higher values (Figure V.16). In addition Units A2 and A4 from Line 1200 (Figure VI.8) show overlapping Magnetite/Ilmenite values as identified in the southern cross-section. Higher Magnetite/Ilmenite values for the five basal samples of borehole N3 (Unit A2) support the hypothesis of a local input of immature sediment rich in magnetite.

Units A1 and K are distinguished from the remaining Line 1200 samples by extremely low Magnetite/Ilmenite values ( $< 0.05$ ). Unit A1 ratio values are identical for both the northern and southern cross-sections, and similar to the Dune Class 1 sample identified from the geomorphological study (see Chapter IV and Section VI.1). Unit K is defined by Magnetite/Ilmenite values less than 0.02, which match the values for the Kosi Bay Formation.

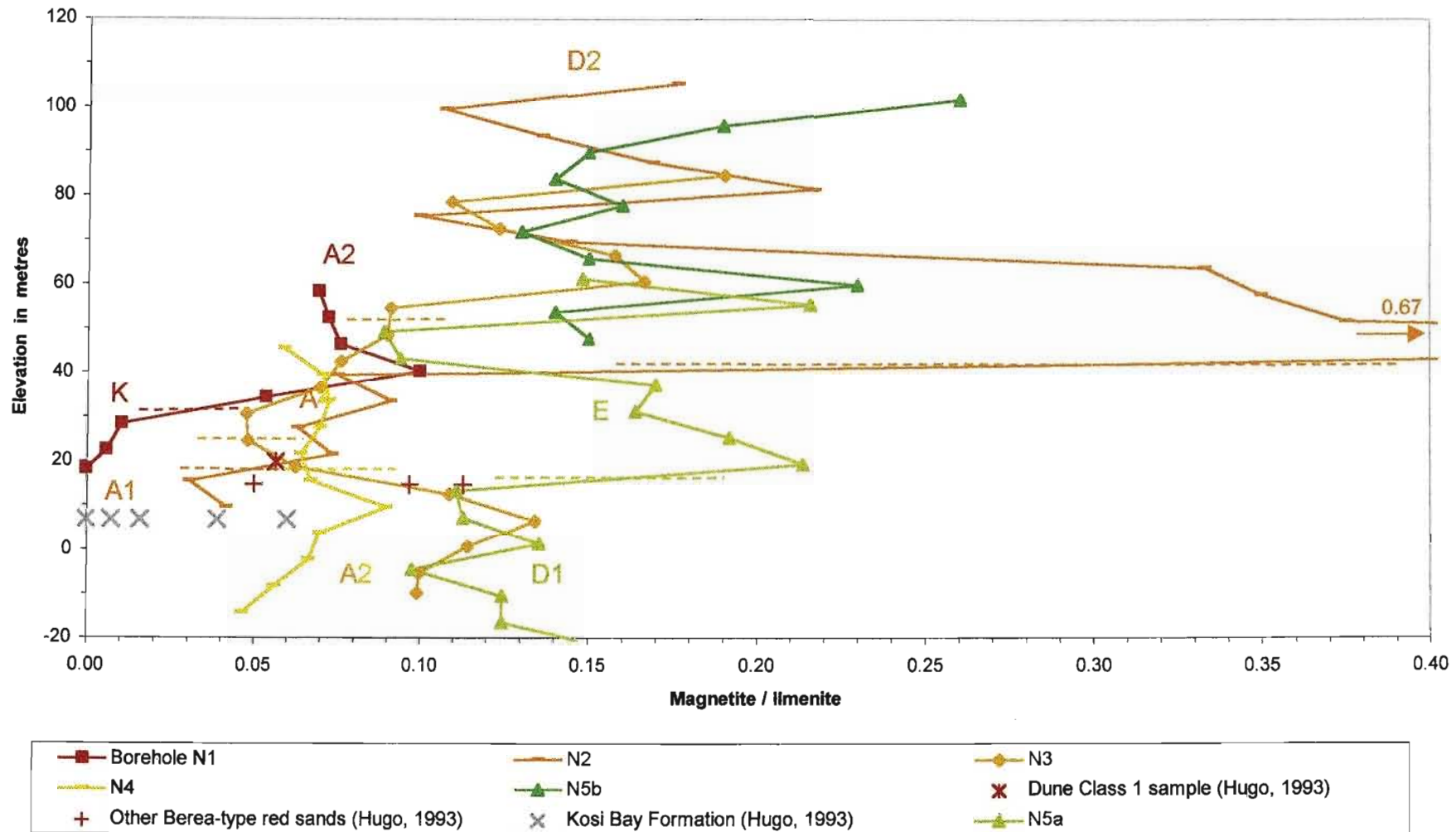


Figure VI.8. Ratio of Magnetite divided by ilmenite (Magnetite / Ilmenite) for samples from Line 1200 boreholes and various field samples.

## VI.3. Geochemistry

### VI.3.1. General description

The geochemical study presented below was carried out to characterise the sedimentological units defined from mineral abundance and heavy mineral ratio values. Relatively few analyses have been made as previous work has shown that bulk geochemistry provides valuable information, but is not a primary tool for discriminating sedimentological units. Full results are presented in Appendix B.

#### VI.3.1.1. Borehole N5b

Borehole N5b is divided into the lower Unit D and upper Unit E at 68 m above msl (Figure VI.9). Unit E, characterised by samples 96 and 78, contains high CaO (> 6 wt%), L.O.I. (4 wt%), MgO (1.5 to 2 wt%) and TiO<sub>2</sub> (1 to 3 wt%) contents, which correlate with values for Unit E (Figure V.19). Unit D can be subdivided into the lower Unit D1 with low CaO (2 wt%) and L.O.I. (2 wt%) contents and the upper Unit D2 with 3.3 wt% CaO and 3 wt% L.O.I.

#### VI.3.1.2. Borehole N4

The upper 30 m of borehole N4 has been defined as Unit A4, whereas Unit A2 comprises the lower 35 m from -15 m below msl to 18 m above msl. Unit A4 is distinguished from Unit A2 by a lower L.O.I. (< 1 wt%), Al<sub>2</sub>O<sub>3</sub> and K<sub>2</sub>O values, and by a higher content of CaO, MgO and MnO (Figure VI.10). The relative concentration of aluminium and dilution of labile elements (calcium, magnesium and manganese) suggests a greater maturity for Unit A2, hence a greater age. The higher content of potassium (generally considered as a labile element) in Unit A2 can be explained by fixation into and on clays, whose presence is also suggested by higher Al<sub>2</sub>O<sub>3</sub> and L.O.I. values compared to Unit A4.

In terms of original heavy mineral content (related to the TiO<sub>2</sub> content), Unit A2 in this borehole is characterised at its bottom by a relatively low grade sediment (TiO<sub>2</sub> = 0.5 to 0.75 wt%). This is unexpected as Unit A2 in both the northern and southern cross-sections has a high original heavy mineral content (> 1.5 wt% TiO<sub>2</sub>) (see below).

#### VI.3.1.3. Borehole N3

The two upper samples of borehole N3 (samples 61 and 73) contain a high CaO (5 wt%) content, low total heavy mineral (< 0.5 wt% TiO<sub>2</sub>) abundances, and show high L.O.I. (3 to 4 wt%) values (Figure VI.11). The high CaO and L.O.I. contents illustrate the high carbonate abundances (Section VI.2.1.1). The geomorphic position, heavy mineral abundance and ratio data, and CaO (5 wt%) and L.O.I. (3.5 to 4 wt%) values correlate the upper 35 m of borehole N3 with Unit D2 defined in the southern cross-section (Figures V.18 and V.19).

Units A2 and A4 comprise the lower and middle portions of borehole N3 from -10 m below msl to 55 m above msl. The lower 35 m thick Unit A2 is distinguished from the overlying 30 m thick Unit A4 by a higher L.O.I.,  $\text{Al}_2\text{O}_3$ ,  $\text{Fe}_2\text{O}_3$  and  $\text{TiO}_2$  contents. This reflects higher abundances of heavy minerals and clay, both free and as grain coatings. The two basal samples (samples -5 and -10) of Unit A2 contain ca. 10 wt%  $\text{TiO}_2$ , indicating that they were deposited in a beach environment. This basal beach deposit is ca. 9 m in thickness.

#### VI.3.1.4. Borehole N2

The three upper samples of borehole N2 (samples 94, 82 and 52) contain a high CaO (4 to 4.5 wt%) content, low total heavy mineral (< 0.5 wt%  $\text{TiO}_2$ ) abundances, and show high L.O.I. (3 to 3.5 wt%) values (Figure VI.12). The geomorphic position and composition correlate the upper 60 m of borehole N2 with Unit D2 (Figure VI.12). Unit D2 in the northern cross-section (upper portions of boreholes N2 and N3) is characterised on average by a lower  $\text{TiO}_2$  content compared to Unit D2 of the southern cross-section (compare Figures VI.11, VI.12 with Figures V.18 and V.19). This suggests a lower total heavy mineral for Unit D2 in the northern part of the study area and may be due to the long distance travelled by the sediment of the northern Unit D2 (Section IV.3).

The middle portion of borehole N2 (from 18 to 45 m above msl) has been defined as Unit A4 and is characterised by sample 34 (Figure VI.12). This sample contains 1.9 wt%  $\text{TiO}_2$  and is interpreted to have had a high original heavy mineral content. This is unexpected as Unit A4 in other boreholes from Line 1200 have a moderate original heavy mineral content (0.6 to 0.9 wt%  $\text{TiO}_2$ ) (Figures VI.10 to VI.12).

The basal 10 m of borehole N2 has been defined as Unit A1. Units A1 and A4 are decalcified (Section VI.2.1.1). Optical microscopy of these units identified more abundant clays and grain coatings in Unit A1 compared to Unit A2. This observation is supported by relatively higher L.O.I. values in Unit A1 and by higher  $\text{Al}_2\text{O}_3$  content in the basal sample of Unit A1. At the base of borehole N2 within Unit A1 the  $\text{Fe}_2\text{O}_3$  abundance shows a relative increase while  $\text{TiO}_2$  decreases. This is the opposite to the relationship normally observed for these elements and further suggests the presence of abundant clay and Fe-OH grain coatings.

#### VI.3.1.5. Borehole N1

The upper 30 m of borehole N1 have been defined as Unit A2, which is characterised by samples 41 and 52 (Figure VI.13). These two samples contain 1.5 to 2.5 wt%  $\text{TiO}_2$  and are interpreted to have had a high original heavy mineral content.

Unit K comprises the lower portion of borehole N1 from 18 to 33 m above msl. This unit is characterised by higher  $\text{TiO}_2$  (0.6 to 1.6 wt%) abundance compared to  $\text{Fe}_2\text{O}_3$  (Figure VI.13). This feature is only observed in Unit K. Furthermore, the bottom sample presents the lowest  $\text{Fe}_2\text{O}_3$  (0.6 wt%) abundance encountered. An intense leaching of the iron must have thus occurred. That phenomenon is believed to be responsible for the light grey to white colour observed in this unit. Higher  $\text{Al}_2\text{O}_3$ ,  $\text{K}_2\text{O}$  and L.O.I contents suggest the presence of abundant clay in the bottom sample of Unit K (Figure VI.13). Ware (in prep.) identifies abundant kaolinite at the base of a borehole located ca. 1 km northeast of borehole N1.

*Inland dunes and beach placer relationships*

Unit A2, borehole N1, represents the inland dune in the northern cross-section. Sample 52 from this unit contains 2.5 wt% TiO<sub>2</sub> (Figure VI.13). Except for sample 41, other samples from this unit are considered to contain a similar TiO<sub>2</sub> content as they contain similar heavy mineral abundances (see Figure VI.5). Thus, Unit A2 of borehole N1 is characterised by an average TiO<sub>2</sub> content greater than 2 wt%. These values are similar to that of the foredunes (Figure V.17).

The sediment constituting the inland dune (Dune Class 2) in the northern cross-section is therefore derived from a beach – foredune system and did not migrate a long distance from the palaeo-shoreline. This observation suggests that the sediment of the inland dune in the northern cross-section is associated with the beach sediment found at the base of Unit A2, borehole N3. This correlation is confirmed by similar alteration state for Unit A2 of boreholes N1 and N3 (Section VI.2.2.2).

The inland dune (Dune Class 2) in the southern cross-section is represented by Unit B and contains on average less than 1 wt% TiO<sub>2</sub> (Figure V.20). This suggests that the northern inland dune originally contained twice the abundance of total heavy minerals compared to the southern inland dune. A similar relationship is observed between the northern (10 wt% TiO<sub>2</sub>) and southern (4.5 to 6 wt% TiO<sub>2</sub>) beach deposits (Figures V.18, V.19 and VI.11). By definition, a greater alteration state characterise Unit A2 compared to Unit B. This indicates that the northern inland dunes are older than the southern inland dunes, and that Unit B is restricted to the south. The subdivision of Dune Class 2 into northern and southern subclasses was already suggested in the geomorphology study (Section IV.2.2).

In summary, the northern beach deposits and associated inland dunes are older and contained higher original heavy mineral abundances than the southern inland dunes and associated beach deposits.

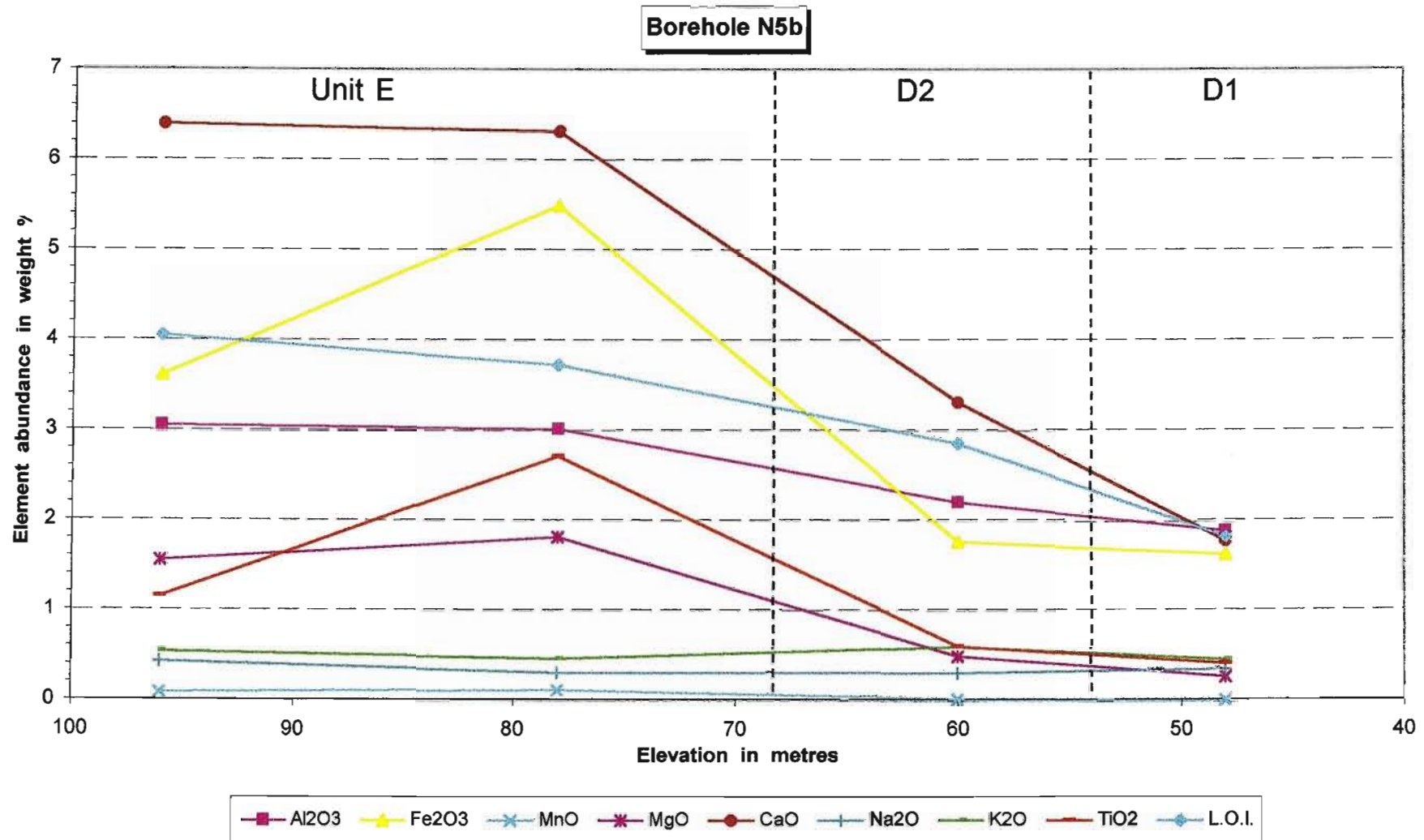


**Figure VI.9.** Major element abundance (excluding SiO<sub>2</sub>) for samples from borehole N5b, showing sedimentological units defined in the previous sections.

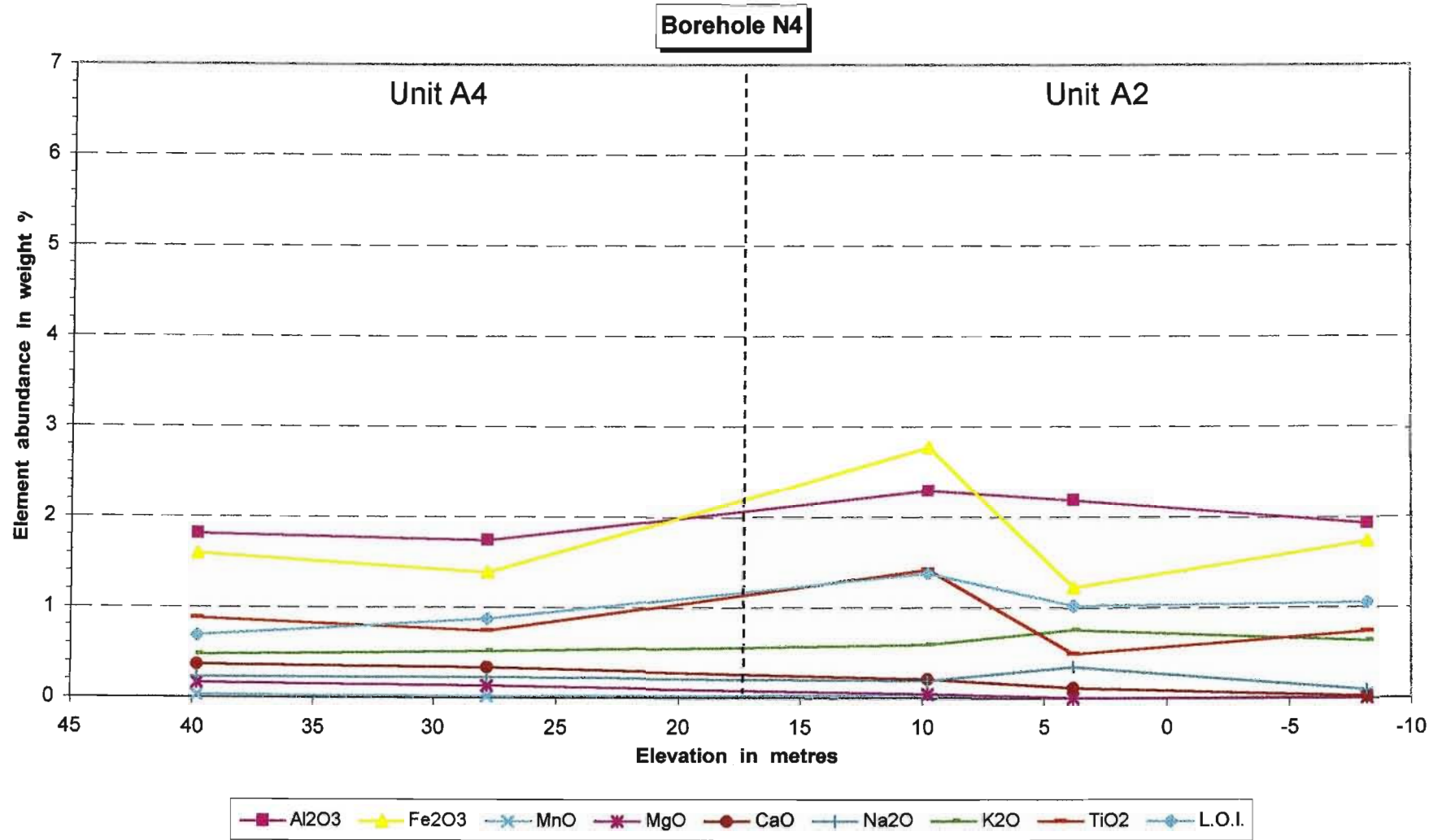


**Figure VI.10.** Major element abundance (excluding SiO<sub>2</sub>) for samples from borehole N4, showing sedimentological units defined in the previous sections.

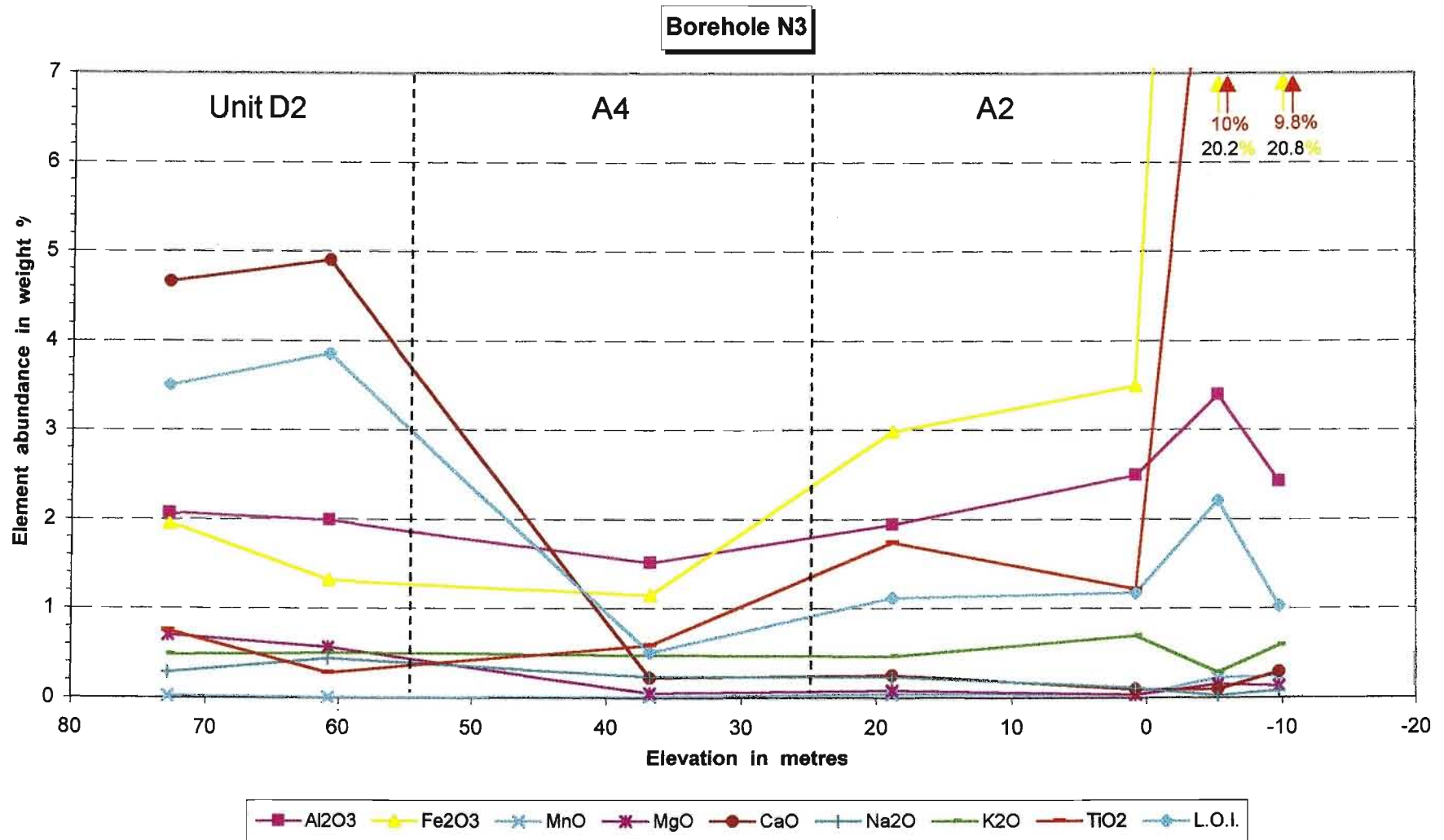


**Figure VI.11.** Major element abundance (excluding SiO<sub>2</sub>) for samples from borehole N3, showing sedimentological units defined in the previous sections.

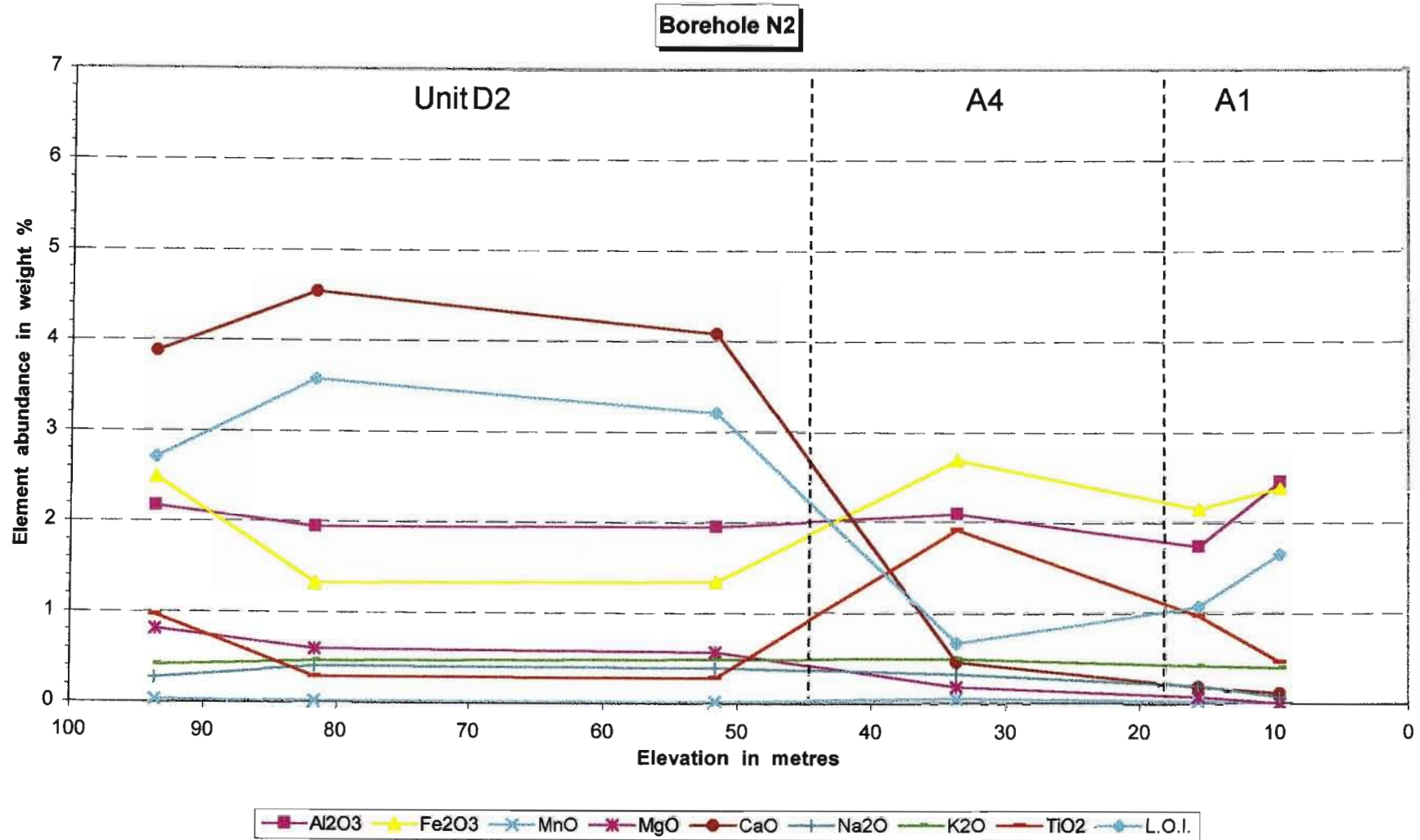


**Figure VI.12.** Major element abundance (excluding SiO<sub>2</sub>) for samples from borehole N2, showing the sedimentological units defined in the previous sections.

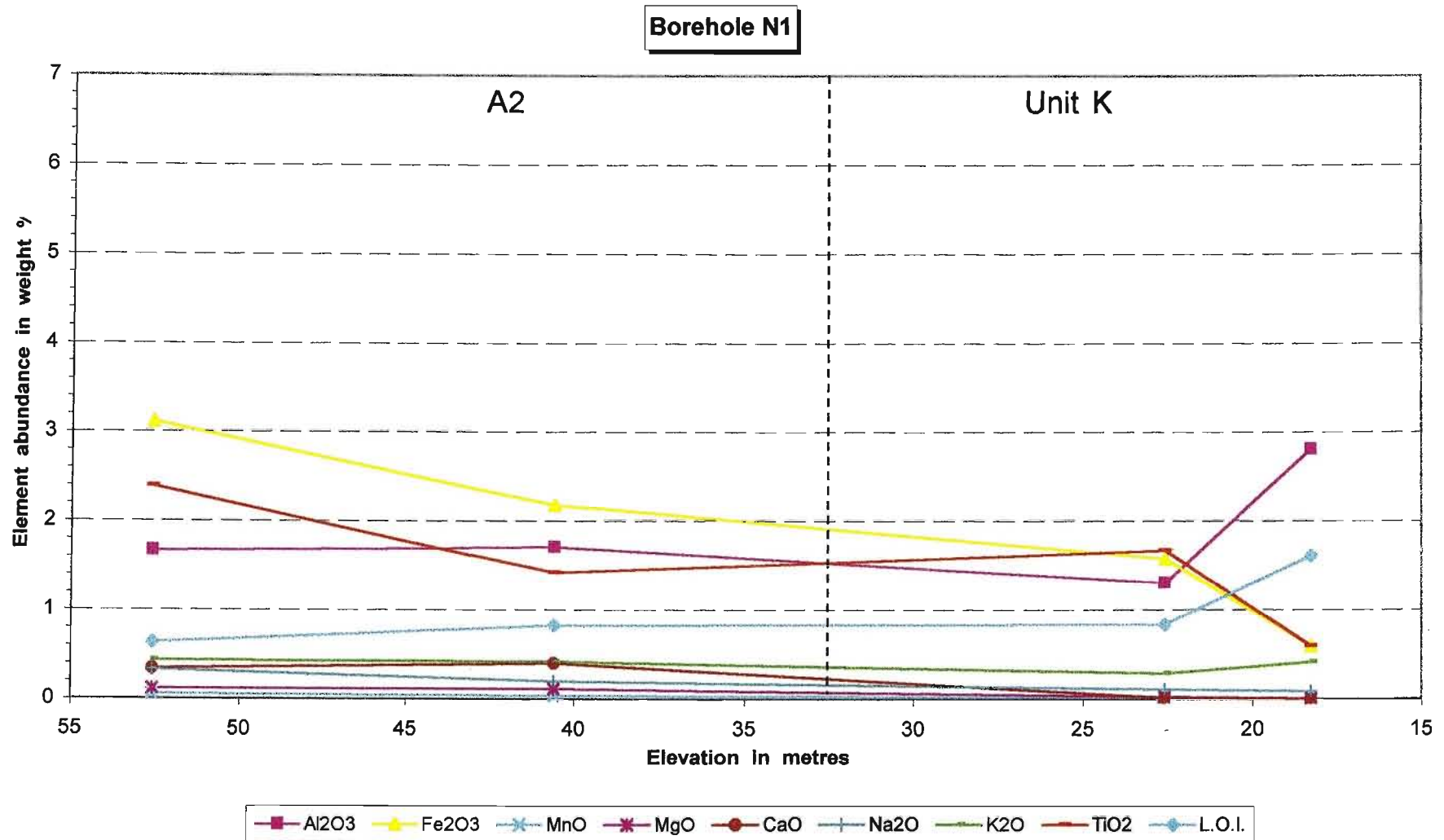


**Figure VI.13.** Major element abundance (excluding SiO<sub>2</sub>) for samples from borehole N1, showing sedimentological units defined in the previous sections.

## VI.3.2. Chemical element ratios

### VI.3.2.1. $\text{TiO}_2 / \text{MgO}$ ratio

The  $\text{TiO}_2/\text{MgO}$  values increase with depth for all boreholes, with significantly increasing values for all samples less than 50 m above msl (Figure VI.14).

The upper 40 to 50 m of boreholes N2 and N3 have very low  $\text{TiO}_2/\text{MgO}$  values (<2) and define Unit D2. Borehole N5b, which comprises Units E, D2 and D1, has similar  $\text{TiO}_2/\text{MgO}$  values.

Unit A4 in boreholes N2, N3 and N4 show consistent  $\text{TiO}_2/\text{MgO}$  values comprised between 4 and 11 (Figure VI.14), similar to the ratio values for the aeolian sediment in Units A3, A4 and B from the southern cross-section (Figure V.21).

Unit A2 in boreholes N1, N3 and N4 is characterised by  $\text{TiO}_2/\text{MgO}$  values higher than 11 (Figure VI.14). Unit A2 in the southern cross-section is defined by  $\text{TiO}_2/\text{MgO}$  values between 11 and 20 (Figure V.21). The elevated  $\text{TiO}_2/\text{MgO}$  values at the base of boreholes N3 are considered to be due to mineral segregation that typically occur in a beach environment (Section VI.2.2.2).

The northern inland dune (Unit A2 in borehole N1) has higher  $\text{TiO}_2/\text{MgO}$  values than the southern inland dune (Unit B). This suggests a greater maturity for the northern inland dune.

Unit A1 is characterised by low  $\text{TiO}_2/\text{MgO}$  values compared to Unit A1 from the southern cross-section. These relatively low values could be due to fixation of magnesium on abundant clay and iron hydroxide minerals, as indicated by the high  $\text{Fe}_2\text{O}_3$ ,  $\text{Al}_2\text{O}_3$ , L.O.I. values and past work of Singh (1995) on the bulk geochemistry of samples from the Kosi Bay and KwaMbonambi Formations near Richards Bay.

### VI.3.2.2. Chemical Index of Alteration

The Chemical Index of Alteration (CIA) values for the northern boreholes clearly discriminate mature and immature sediments (Figure VI.15). The foredune samples and all samples of Units D and E are characterised by index values below 42. This upper limit is also observed for Units D and E in the southern cross-section (Figure V.22). However, this index does not readily discriminate sub-units within mature units (compare with Figure V.22).

Bulk samples from the Kosi bay Formation and the overlying KwaMbonambi Formation near Richards Bay (data from Singh, 1995) have CIA values comprised between 75 and 98, which are higher than most samples from the dune cordon under study. The higher CIA values for these two Formations may be due to the high clay content of the bulk samples, which greatly modify the element abundance (e.g.  $\text{Al}_2\text{O}_3$  content is higher than 20 wt% (Singh, 1995), resulting to a higher CIA value).

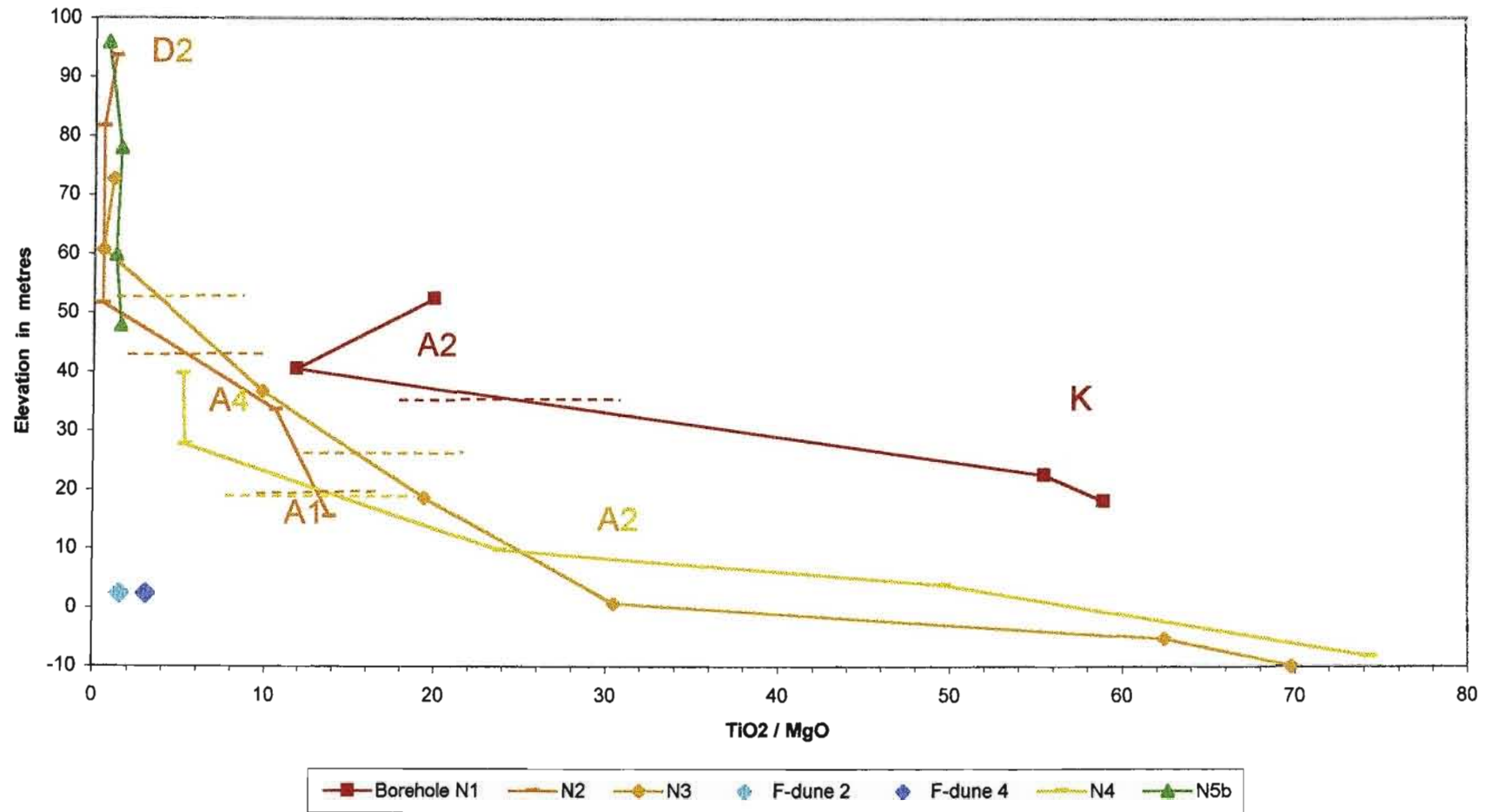
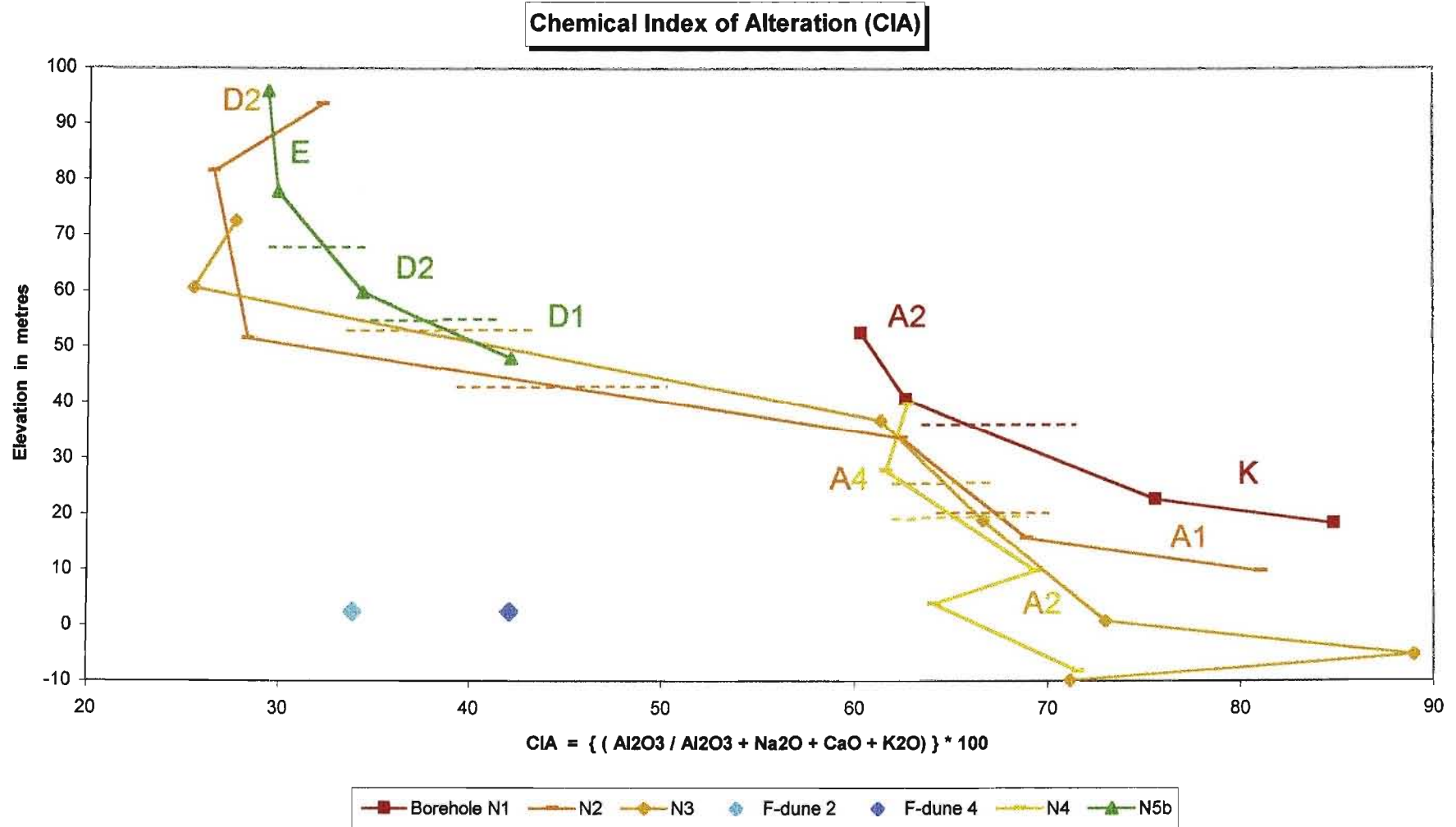


Figure VI.14.  $TiO_2 / MgO$  values for samples from Line 1200 boreholes and foredune samples.



**Figure VI.15.** Chemical Index of Alteration for samples from Line 1200 boreholes and foredune samples.

## VI.4. Grain size

### VI.4.1. Mean grain size

All samples from the northern cross-section are medium grained sands with mean size between 1 to 2 phi (500 to 250  $\mu\text{m}$ ) (Figure VI.16). Sample -5, borehole N3, has been interpreted as a beach deposit and is characterised by fine grained sand.

The sedimentological units show a wide range of mean grain size values. Furthermore, most units present different values in the southern and northern portions of the study area (compare Figures V.24 and VI.16). This is not surprising as the mean grain size depends on many factors, such as the mean grain size of the source sediment, the vegetation cover, wind velocity, horizontal and vertical transport distance and sample treatment.

Except for borehole N5b, a weak fining upward trend is observed for the northern cross-section (Figure VI.16). Unit E (upper 35 m of borehole N5b), interpreted to have been derived from a beach – foredune system, is finer grained than the adjacent foredune (sample F-dune 2). This suggests that accreting dunes became finer grained during their growth as greater energy is required to propel sand to elevations in excess of 70 m above msl. The fining upward trend within Unit D2 (from ca. 50 m to 100 m above msl in boreholes N2 and N3) supports this interpretation. The opposite trend is observed for Unit E. This may be due to progressive sea level rise during deposition, however more data is required to support this.

### VI.4.2. Distribution curves

Grain size analysis for the southern cross-section showed that the frequency distribution curves are more useful in discriminating units than any single textural parameter (Section V.4). The frequency distribution curves for each borehole have been plotted in Figures VI.17 to VI.21, and have been regrouped into their respective units defined in the previous sections. Values of the textural parameters for the northern cross-section are presented below only when they differ from that expressed for the southern cross-section (Section V.4.1 and Appendix C).

Unit D2 comprises the upper portions of boreholes N2 and N3 correlates to the linear parallel dunes of Dune Class 3. This unit is characterised by very well sorted aeolian sand as indicated by the leptokurtic shape (lit.: more peaked than a normal distribution curve) of the frequency distribution curve (Figures VI.18 and VI.19). Samples from Unit D2 in these two boreholes show standard deviation values ( $\sigma$ ) between 0.40 and 0.47 and cubed deviation values ( $\sigma^3$ ) between 0.06 and 0.1. These values indicate that, of all samples analysed, Unit D2 from the northern cross-section is characterised by the most consistently well sorted sediment. This is believed to be due to the long distance travelled by the sediment of Unit D2 (Section IV.3). Note that Unit D2 in the southern cross-section is characterised by moderately well sorted sediment (Section V.4.3 and Figure V.26). This suggests that the southern Unit D2 migrated a shorter distance than the northern Unit D2.

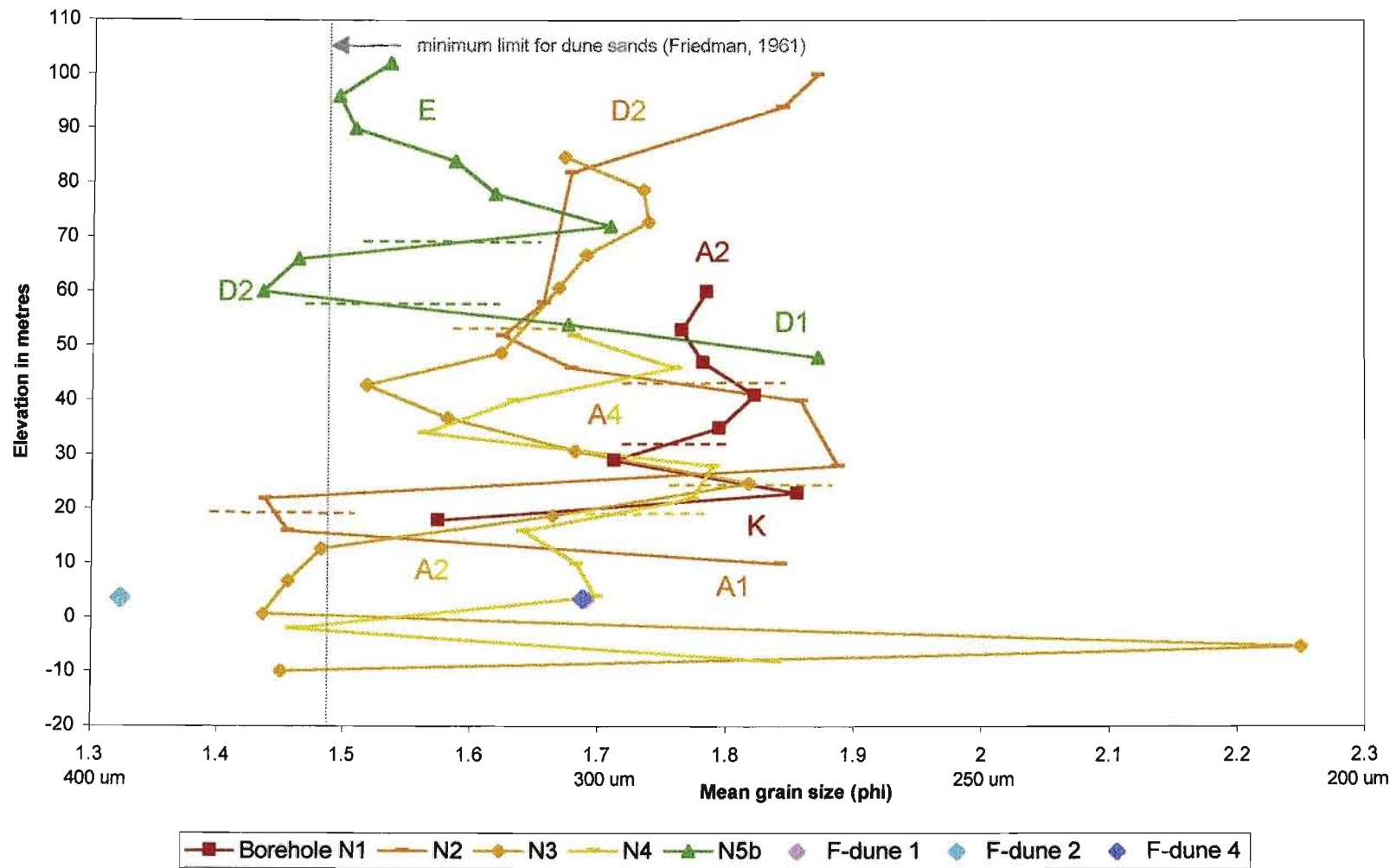


Figure VI.16. Mean grain size for samples from Line 1200 boreholes and foredune samples. Dashed lines = unit boundaries.

Unit A2 in the upper 30 m of borehole N1, representing the inland dune (Dune Class 2), is also characterised by very well sorted sand (Figure VI.17), suggesting that the sediment of the inland dune has travelled a considerable distance. This is characteristic of hairpin parabolic dunes (Section IV.1.2.2), which constitute the northern inland dunes (Section IV.2.2).

Unit E in the upper 35 m of borehole N5b, representing the coastal parabolic dune, is characterised by moderately well sorted sand. The distribution curves for this unit are broader and the modal peak is lower than that of Unit D2 (borehole N2 and N3) and Unit A2 (borehole N1) (Figures VI.17 and VI.21). This is considered to indicate a short aeolian transport.

Unit A4 in the lower 30 m of boreholes N2, N3 and in the upper 40 m of borehole N4 is moderately well to well sorted (Figures VI.18 to VI.20), suggesting both short and long transport distances.

Unit A2 in the lower 35 m of boreholes N3 and N4 contains aeolian sand, which is underlain by beach sediment in borehole N3. The three bottom samples from borehole N3 (samples -10, -5 and 1) have high standard deviation values ( $\sigma$ ) between 0.79 and 0.96, cubed deviation values ( $\sigma^3$ ) between 0.49 and 0.89, skewness ( $\alpha_3$ ) values between 1.92 to 2.02 (but sample -10 = 0.5), and mean-cubed deviation values ( $\alpha_3\sigma^3$ ) between 0.42 and 1.71. Thus they show the poorest sorting and are the most positive skewed of all samples analysed (Figure VI.19). The only similar samples are from the base of Unit A3 in the southern cross-section (Appendix C), which also represent beach sediment.

The bottom sample (sample -8) of Unit A2, borehole N4, shows a mesokurtic distribution curve, with significant amounts of fine and very fine sand (Figure VI.20). Sample -8 is poorly sorted with a standard deviation value ( $\sigma$ ) of 0.80 and a cubed deviation value ( $\sigma^3$ ) of 0.51. However, this sample has not been identified as beach sediment. These observations suggest the presence of marine or fluvial sediment, possibly mixed with aeolian sand, at the base of Unit A2 from borehole N4.

The basal 10 m of borehole N2 (samples 10 and 16) has been defined as Unit A1 and show mesokurtic distribution curves (Figure VI.18) and consequently a relatively poor sorting. Unit A1 is characterised by significant amounts of coarse and very coarse sand (sample 16) or very fine sand (sample 10). These observations may suggest the presence of non-aeolian sediments in Unit A1, mixed with aeolian sand.

Unit K comprises the lower 15 m of Borehole N1. This unit is interpreted to represent the Kosi Bay Formation and is characterised by moderately sorted sand with a mode of 1.7 to 1.9 phi (Figure VI.17). The bottom sample (sample 18) of Unit K seems to be constituted of at least two grain populations; one with a mode of 1 phi (500  $\mu\text{m}$ ), and a finer grain population with a mode of 1.9 phi (265  $\mu\text{m}$ ) (Figure VI.17). Sample 18 contains significant amounts of coarse (17 %) and very coarse (5 %) sand that is unlikely to be aeolian in origin. Only sample 15 from Unit C (Line380) shows similar characteristics (Section V.4.3 and Figure V.27).

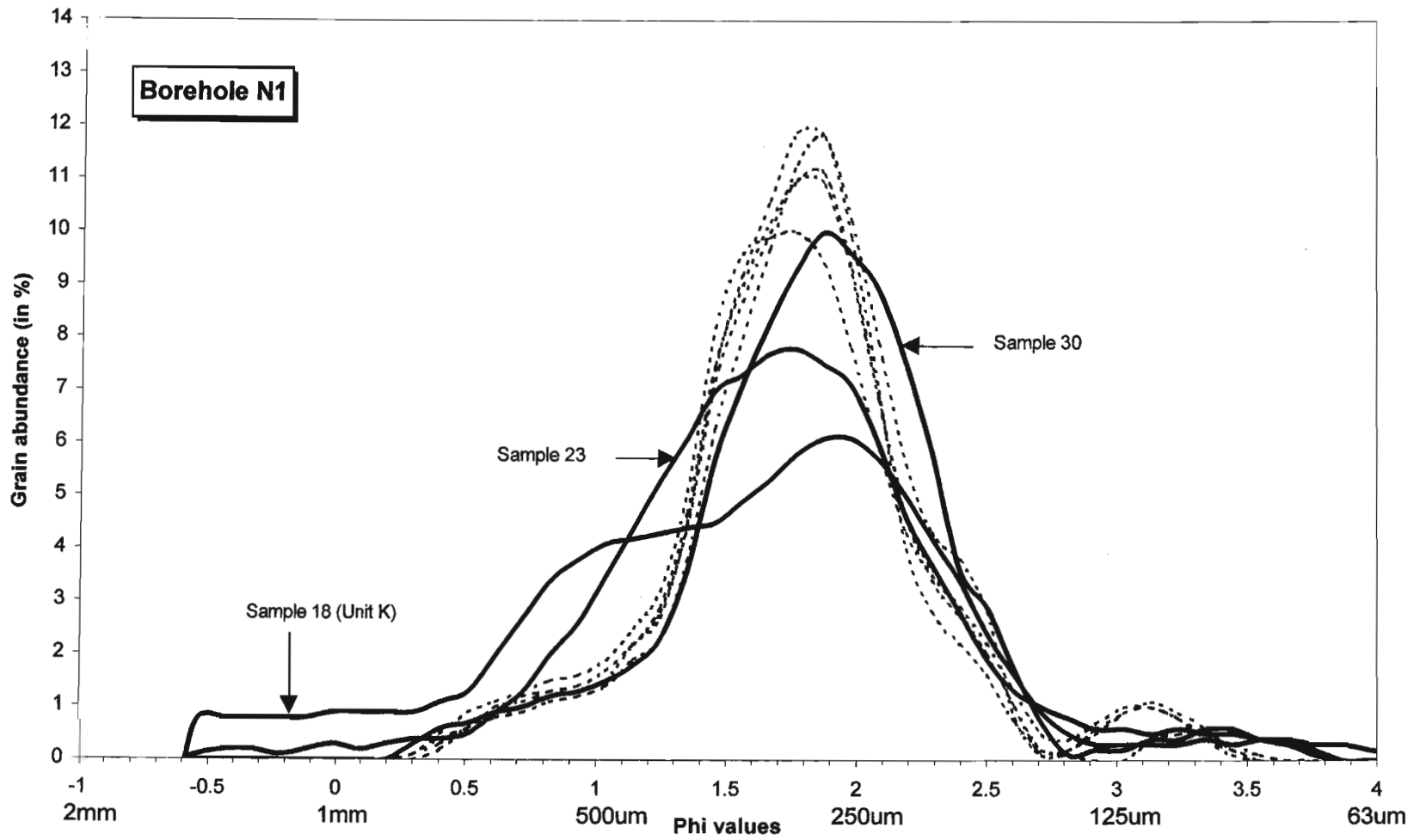


**Figure VI.17.** Grain size distribution curves for samples from borehole N1. Dashed lines = Unit A2, black lines = Unit K.

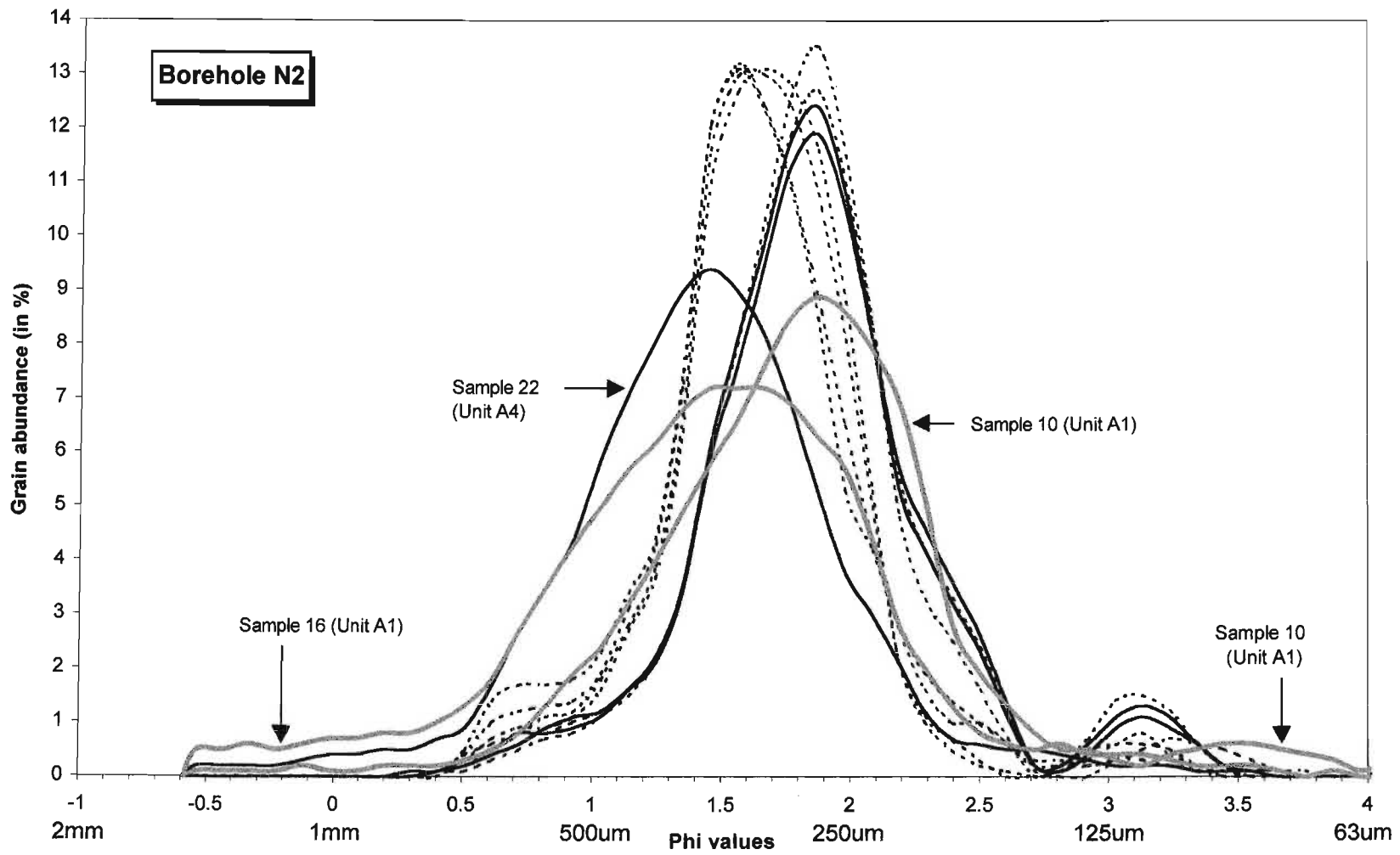


**Figure VI.18.** Grain size distribution curves for samples from borehole N2. Dashed lines = Unit D2, black lines = Unit A4, grey lines = Unit A2.

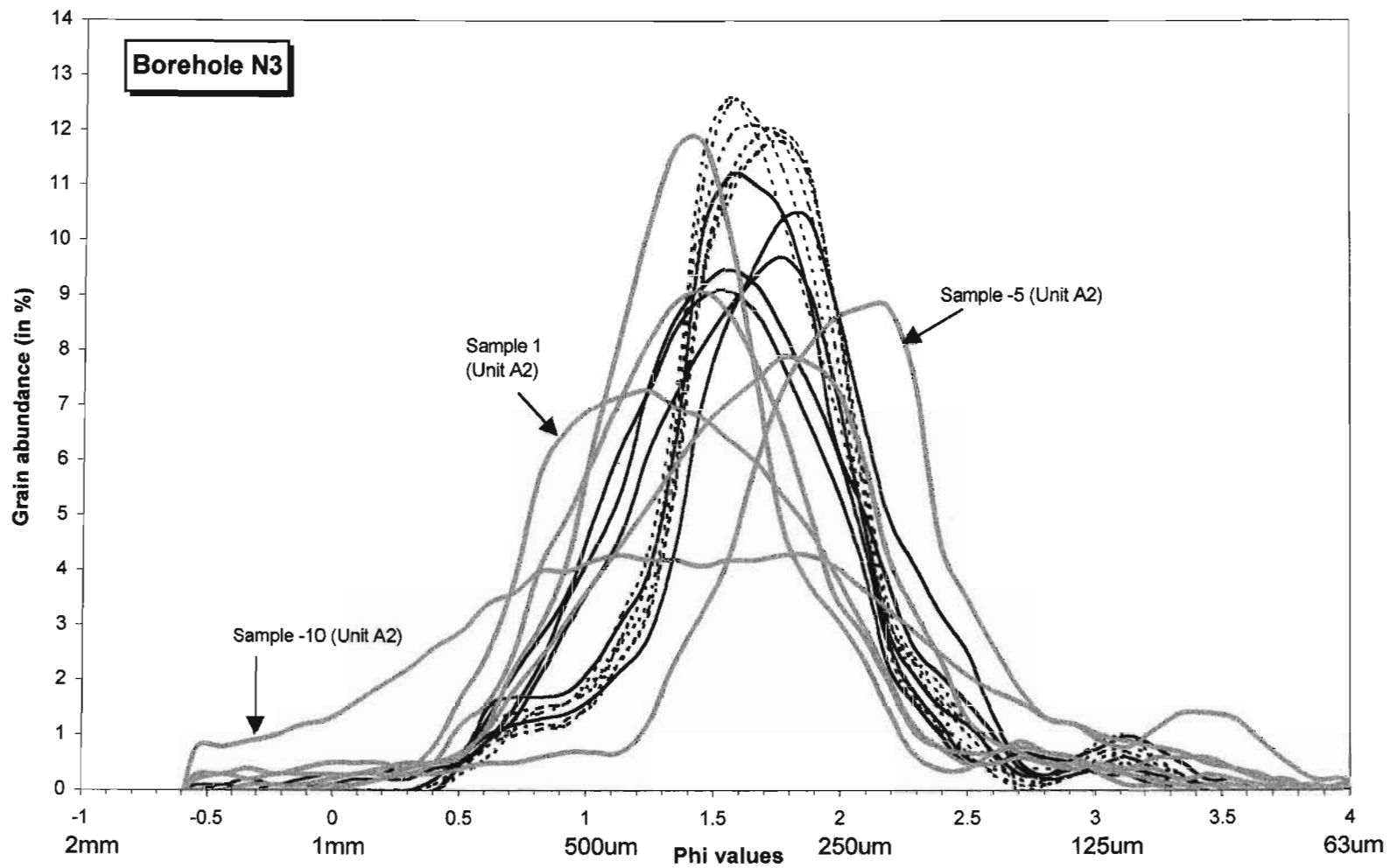


**Figure VI.19.** Grain size distribution curves for samples from borehole N3. Dashed lines = Unit D2, black lines = Unit A4, grey lines = Unit A2.

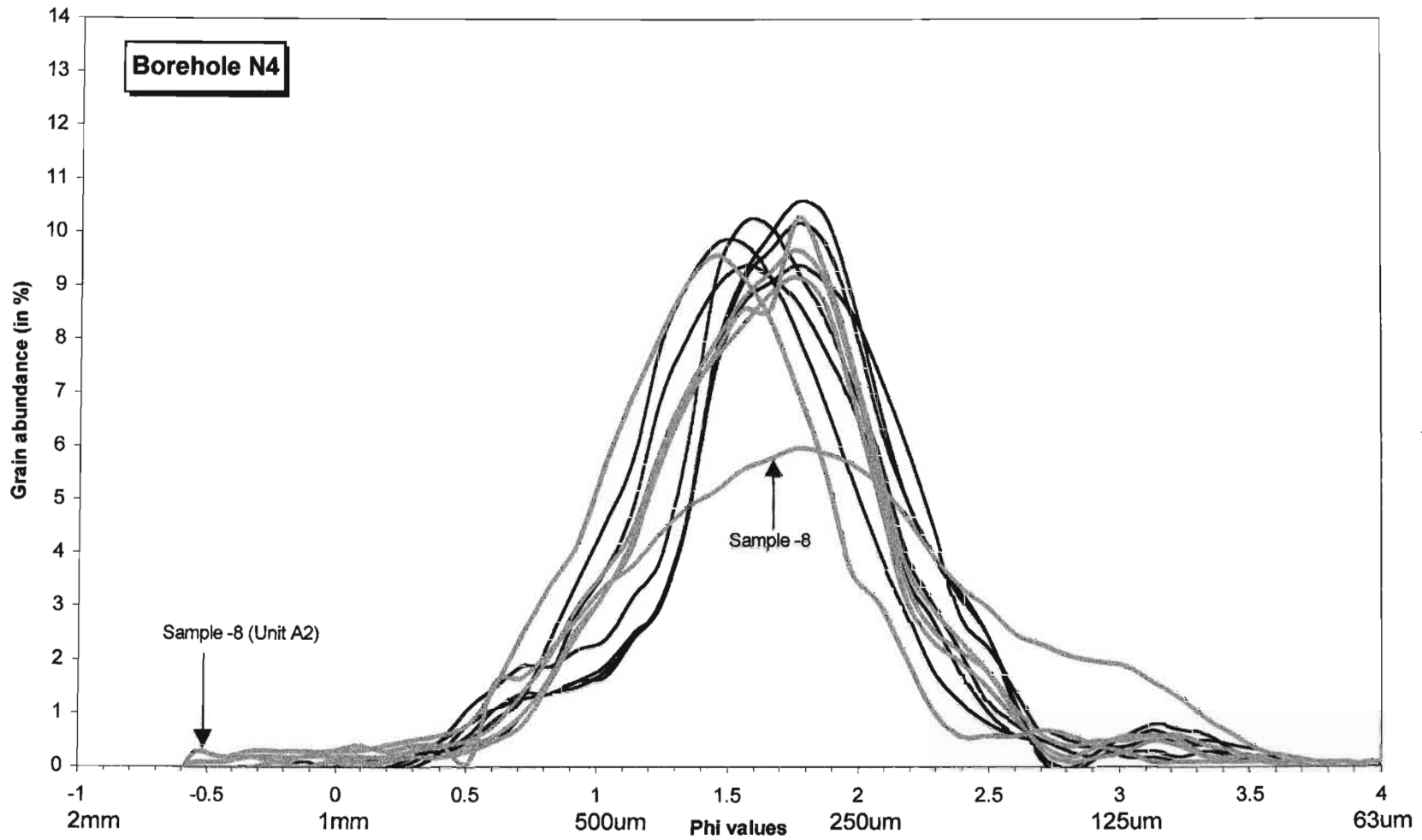


**Figure VI.20.** Grain size distribution curves for samples from borehole N4. Black lines = Unit A4, grey lines = Unit A2.

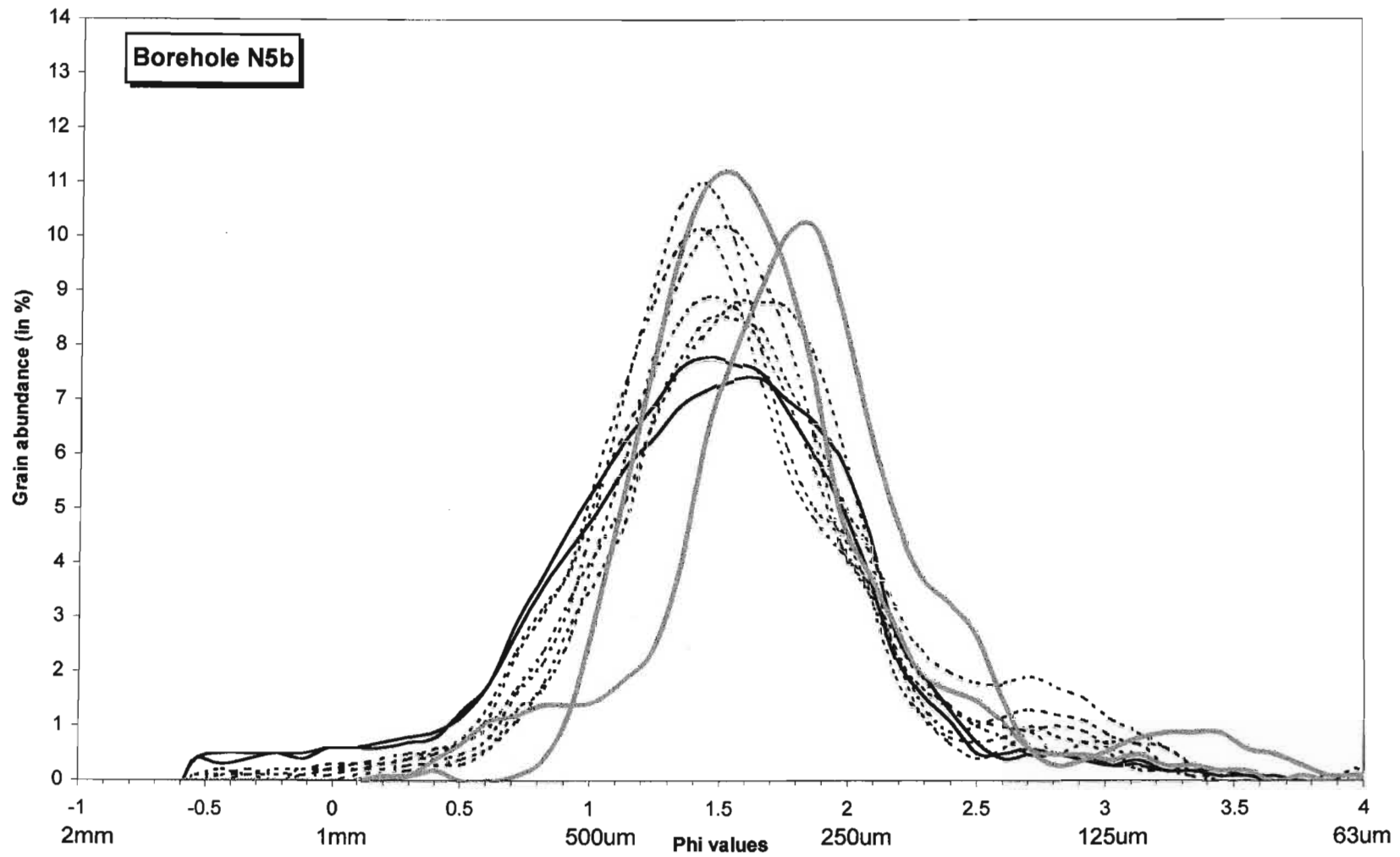


**Figure VI.21.** Grain size distribution curves for samples from borehole N5b. Dashed line = Unit E, black lines = Unit D2, grey lines = Unit D1.

## VI.5. SEM studies on quartz grains

SEM studies on quartz grains from Line 1200 samples were mainly focussed on Unit K, as this new unit was not recognised from Line 380 (Section V.5). The bottom samples of boreholes N2, N3, N4 and N5b have also been investigated in order to identify potential non-aeolian sediments.

Two different types of quartz grains have been observed in samples 18 and 23 (borehole N1), which represent the base of Unit K.

Typical aeolian grains (Section V.5) are abundant and may preserve two distinct grain coatings (Figure VI.22). The first is a relatively thick silica layer as shown by surface indentations (Figure VI.22), and overall smooth grain surface. This initial grain coating contains low amounts of iron (1 to 4 wt%), and a high aluminium content (up to 14 wt%) (compare with Tables V.2 and V.3). The second generation of grain coating is heterogeneous and localised to depressions on the grain surface (Figure VI.22). Chemical analyses of the second grain coating identifies 6 to 8 wt% aluminium, ca. 5 wt% titanium, < 0.5 wt% calcium and 17 to 25 wt% iron. This composition is similar to silica layers on quartz grains from Units A1 and A2, Line 380 (Table V.3). However Units A1 and A2, Line 380, are characterised by higher iron (45 wt%) and lower titanium (2.5 wt%) abundances in silica layers. Potassium is present in both generations of layers (ca. 2 wt%), in a slightly greater amount than found in other units (ca. 1 wt%) (compare with Tables V.2 and V.3). Rare clay particles identified as Kaolinite have been observed in samples from Unit K, and can be 15  $\mu\text{m}$  in width.

Typical non-aeolian quartz grains comprises ca. 20 wt% of sample 18 and 10 wt% of samples 23. This suggests the presence of fluvial, beach or marine sediments in part of Unit K, probably at its base some 17 m above msl. These non-aeolian deposits correspond to relatively coarse and poorly sorted samples, and are possibly related to the grain population with a mode of 1 phi identified in sample 18 (Figure VI.17, Section VI.4.2).

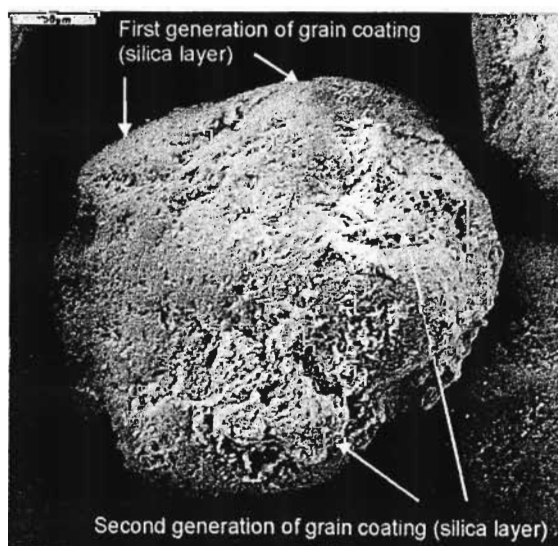


**Figure VI.22.** Aeolian quartz grain of Unit K, showing two generations of silica layers (sample 18 of borehole N1). Scale bar length: 50 $\mu\text{m}$ .

Unit A2 in borehole N4 is characterised by moderately well to well rounded quartz grains with well developed grain coatings (silica layers), indicating an aeolian environment.

Unit A2 in borehole N3 contains similar grains amongst fractured quartz showing conchoidal cleavage and thin or absent grain coatings. The latter quartz grains indicate a non-aeolian environment, supporting the hypothesis of a beach origin for the base of Unit A2 in borehole N3 (Section VI.3.1.3).

Unit A1 at the bottom of borehole N2 contains relatively low amounts of non-aeolian quartz grains as described above, suggesting the presence of fluvial, beach or marine deposits. A beach origin is unlikely, as Unit A1 had originally low heavy mineral abundances (Section VI.3.1.5).

## VI.6. Summary: geological section of Northing Line 1200

Six sedimentological units previously defined from Line 380 and one new unit (Unit K) can be identified for the northern Line 1200: Units K, A1, A2, A4, D1, D2 and E. Lateral extension of these units along Line 1200 has been investigated using the heavy mineral ratios and ilmenite content given by RBM (Figure VI.23). The interpretation presented in Figure VI.23 incorporates diverse data, which, while not being conclusive, provide a consistent, geologically plausible interpretation.

This section describes the geological section presented in Figures VI.23 and proposes a geological history (Figure VI.24). If not specified, ages mentioned below are interpretative. In the northern part of the study area one sample (sample RBM 1, Figure VI.23) has been dated by luminescence (Section IV.3) and provides chronological control on the geological history presented below.

Unit K is interpreted as the Kosi Bay Formation. It is largely of aeolian origin with minor marine, beach or fluvial sediments at the base of borehole N1. The thickness of Unit K is not known. This unit disappears abruptly toward the coastline, suggesting later erosion during a period of relatively high sea level (Figures VI.23 and VI.24a).

Unit A1, characterised by only two samples that present ambiguous characteristics is believed to be a highly altered aeolian dune with a high clay content. It is possible that these two samples are actually of similar age to Unit A2 (discussed below), representing an aeolian dune deposited just before the high sea level period associated with Unit A2 (Figures VI.23 and VI.24a). Grain size and SEM analyses indicate that the two samples are partly constituted of non-aeolian sediment. Further sampling is needed to clarify the stratigraphy in this part of the dune cordon.

Unit A2 in Line 1200 is characterised by beach placers at the base of borehole N3 (Figure VI.23). This sediment type is not encountered in boreholes to the southeast and the narrow width of the placer suggests that the nearshore morphology was relatively steep or that the placer was truncated by later erosion (Figure VI.24a). Overlying heavy mineral rich aeolian sand (Figure VI.24b) appears to have been subsequently reworked given the spatial distribution of this unit (Figures VI.23 and VI.24c). Unit A2 is interpreted to have formed during the penultimate interglacial (oxygen isotope Stage 7) or possibly during an older interglacial period (Section V.6).

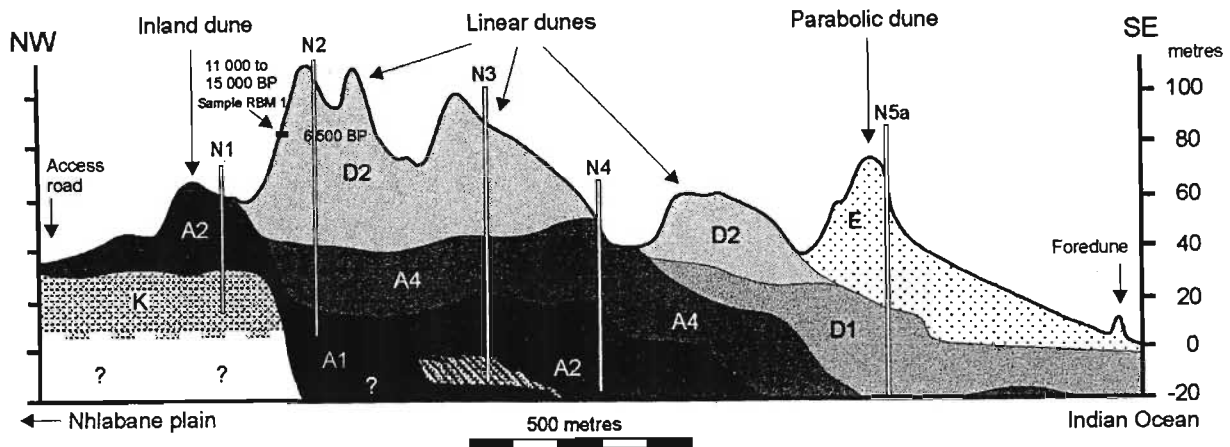


**Figure VI.23.** Geological section of Northing Line 1200, showing the lateral extension of the seven units defined in Chapter VI and the location of sample RBM 1 dated by luminescence. Hatched patterns illustrate beach placers.

Unit A4 is of aeolian origin and its deposition post-dates reworking of Unit A2 (Figure VI.23). It has been suggested that Units A2 and A4 (and associated Units A3 and B) represent high stand deposits during the penultimate (oxygen isotope Stage 7) and the last (oxygen isotope Stage 5) interglacial periods. Given this depositional environment, beach placers (indicating a high sea level) may be present at the base of Unit A4. Beach deposits are identified in this position in Line 380 but have not been identified in Line 1200 (Figure VI.23). This can be explained in two ways.

Firstly, the physical conditions (sediment supply, wave regime, nearshore morphology) were not favourable for beach placer formation or these deposits were later reworked.

Secondly, Units A2 and A4 were formed during the same interglacial period. In this hypothesis Unit A4 would have been deposited during the early stage of the last marine regression (oxygen isotope Stage 4 or 5a). However, several samples of Unit A4 present a high original heavy mineral content (Figure VI.5 and Section VI.3.1). This suggests that the dunes represented by these heavy mineral rich samples were formed during a high sea level period and were deposited very close to the palaeoshoreline. Furthermore Unit A4 has been shown to be significantly less altered than Unit A2, supporting the hypothesis of two distinct interglacial periods. A possible depositional history of Unit A4 is illustrated in Figure VI.24c to Figure VI.24e.

During the last glacial maximum (oxygen isotope Stage 2), increased wind activity combined with sparse vegetation cover (Section II.4) induced aeolian reworking of Units A4 and A2 (Figure VI.24f). It is believed that Unit A2 was reworked by hairpin parabolic dunes at this time, forming the present morphology of the inland dunes (Section IV.2.2, Figures VI.1 and VI.24f).

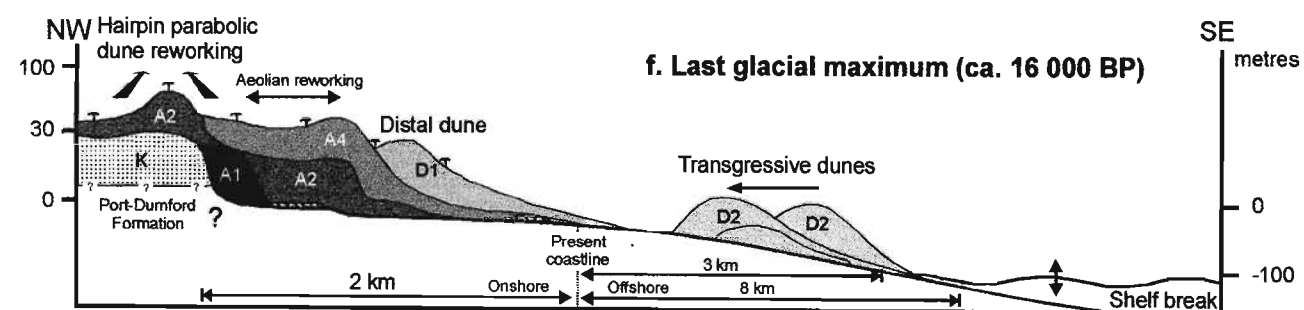
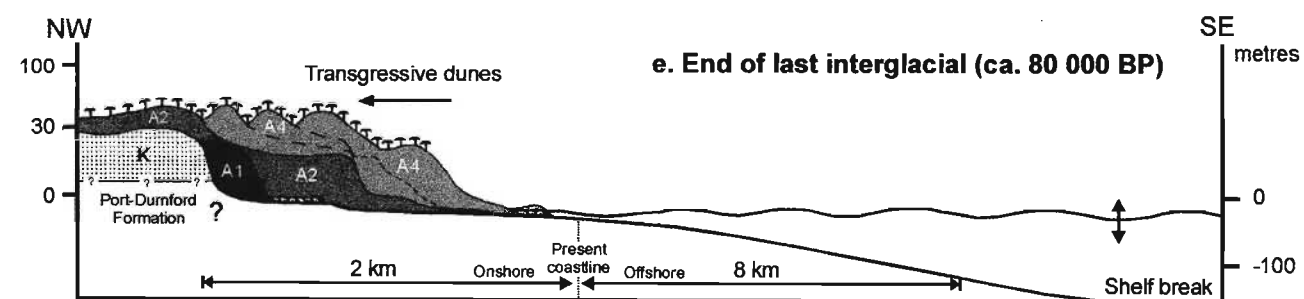
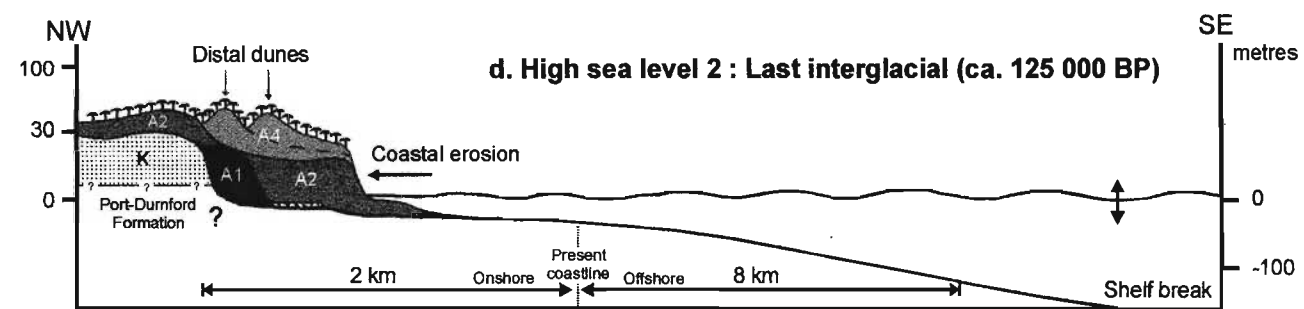
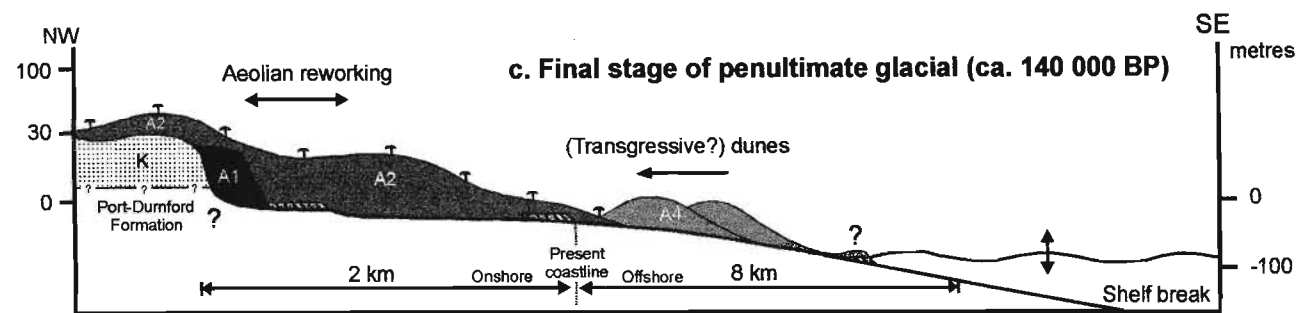
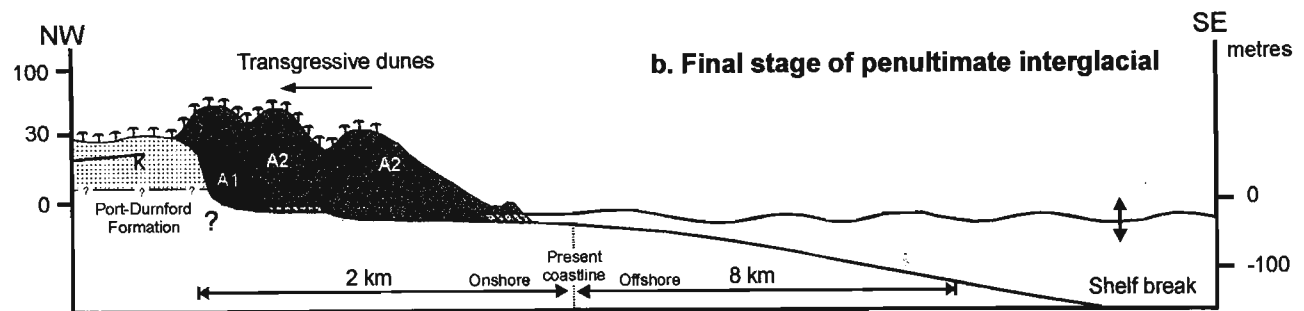
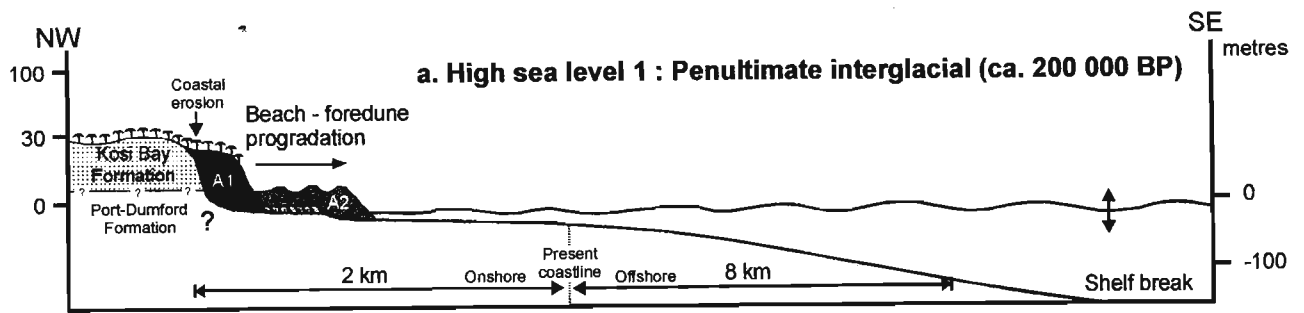
The very well sorted (Section VI.4.2) aeolian sediment constituting Unit D2 contains abundant unaltered bioclasts (Section VI.2.1.1), suggesting a marine sediment source with negligible reworking of older sands during aeolian transport. Units D1 and D2 are relatively unaltered and contain low abundances of heavy minerals (Figure VI.5), suggesting a prolonged aeolian transport. Luminescence dating of Unit D2 (sample RBM 1) gave a depositional age of

12 800 ± 2100 B.P. (Figure VI.23). Thus Unit D2 was formed during the marine transgression (oxygen isotope Stages 2 to 1 boundary) following the last glaciation (Figure VI.24f and VI.24g). The sea level during the formation of Unit D2 was between -50 to -100 m below present (Figures VI.24), placing the coastline between 3 to 8 km offshore (Figure II.1). Therefore the sediment comprising Unit D2 is interpreted to have migrated several kilometres inland (Figure VI.24f). Note that the aeolian sediment of Unit D2 in the southern cross-section is moderately well sorted (Section VI.4.2) and contains slightly higher abundances of heavy minerals (Section VI.3.1.4). This suggests that the southern Unit D2 formed at a higher sea level and is presumably younger than the northern Unit D2 (compare Figures VI.24f and V31f).

Luminescence dating of the northern Unit D2 (sample RBM 1) also indicated a short reworking event at an age of 6500 ± 450 B.P (Section IV.3). These reworking events, described in Section IV.2.3, are thought to be responsible for the linear parallel morphology of Dune Class 3 (Figures VI.1 and VI.24h).

In the southern part of the study area, the first depositional events of Unit E were of Early Holocene age (Section V.6). It is assumed that the Early Holocene deposits of Unit E are also present in the northern part of the study area (Figure VI.24g). During the Holocene, and possibly during the Middle (4500 B.P.) or Late (1500 B.P.) Holocene high stands, a transgressive event eroded Unit E and/or Units D1 and D2 (Figures VI.23 and VI.24h). Later, as sea level regressed, the shoreline prograded and heavy mineral rich Unit E was deposited, forming the coastal parabolic dune (Figure VI.24i). No beach placers have been identified underlying Unit E (Figure VI.23). This may be due to constrained deposition or later reworking.

Units D and E contain 2 to 8 % carbonate bioclasts and can be grouped into the Sibayi Formation (Section III.4.1.7). Unit K has been attributed to the Kosi Bay Formation. Therefore Unit A should be attributed to the KwaMbonambi Formation. However, the variety of facies (marine, beach and aeolian) and age does not match the current informal definition of this formation (Section III.4.1.6). The age of Unit A2 suggests that the Kosi Bay Formation is older than the penultimate interglacial period (oxygen isotope Stage 7, ca. 200 000 years B.P.). Giving the non-aeolian sediments constituting the base of Unit K, this unit is interpreted to have formed during a high sea level period and might be as old or older than the interglacial represented by the oxygen isotope Stage 9 (Section II.4). This suggested age for the Kosi Bay Formation is older than considered by previous studies.



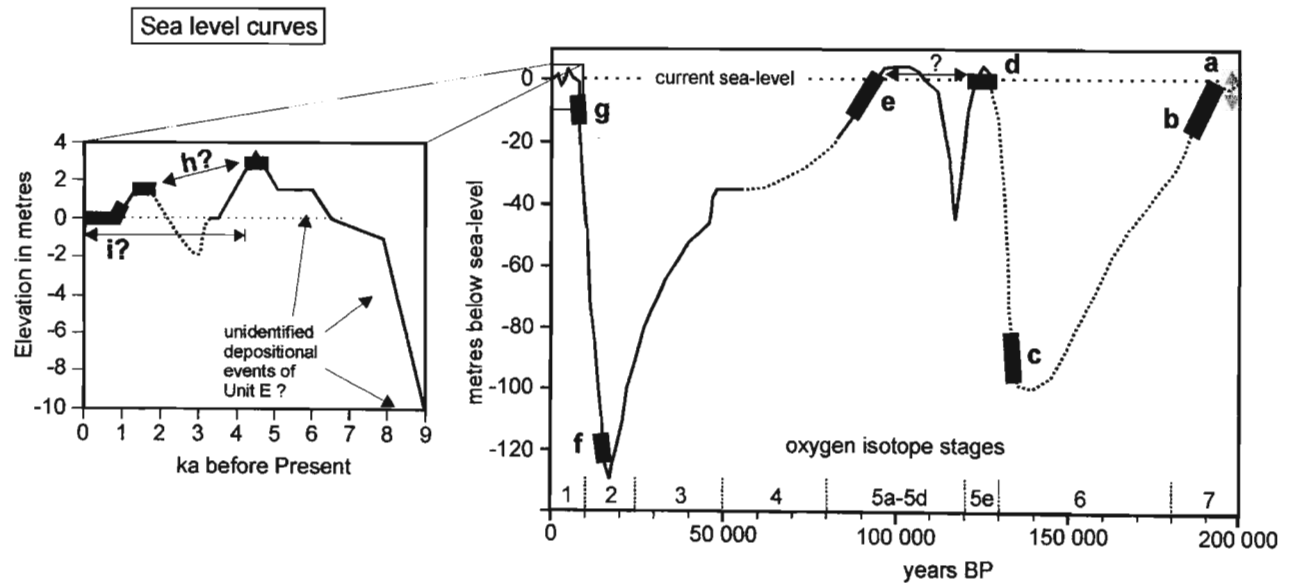
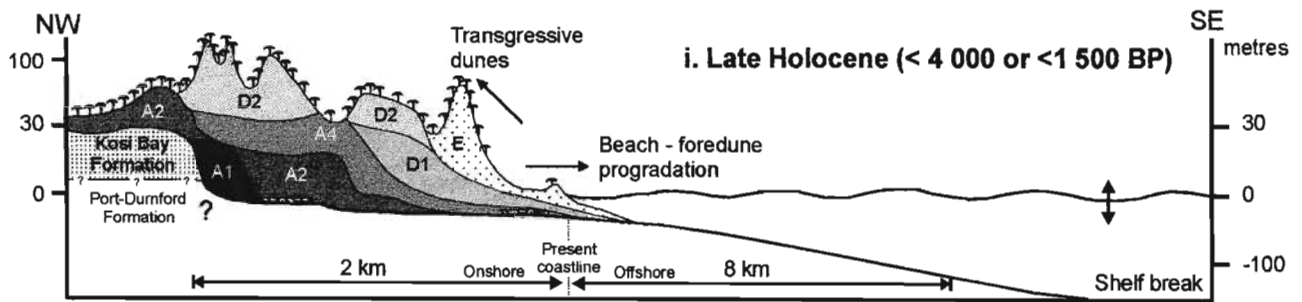
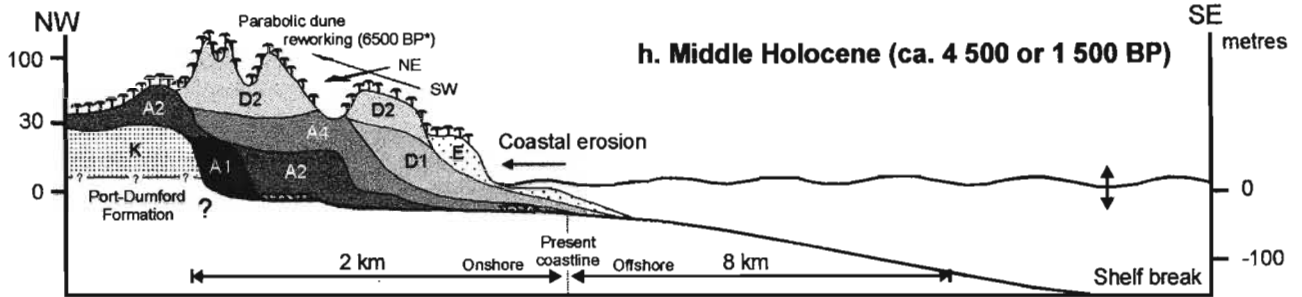
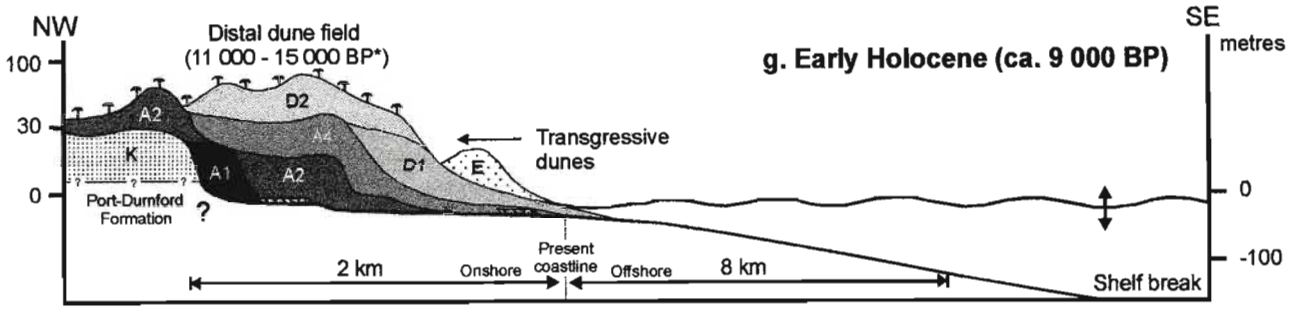


**Figure VI.24.** Evolutionary model for the northern cross-section (Line 1200), showing the depositional and reworking events correlated with time and sea level fluctuations. Asterisk refers to luminescence dates from sample RBM1. Each cartoon is labelled a to i, which correspond to periods marked on the sea level curves. Sea level curves from Ramsay (1995; 1997).

## VII. STRUCTURE AND GEOLOGICAL HISTORY OF THE ZULTI NORTH ORE BODY

### VII.1. Unit characteristics

Characteristics that discriminate the nine sedimentological units defined in the present study of the Zulti North ore body are presented in Table VII.1 and summarised with additional interpretation in Table VII.2. Study of the weathering state of the sediment (IRZ/OHM, Magnetite/ilmenite and other mineral ratios, carbonate content, and sand colour to a lesser extent) is the chief element used to define units, and thus to establish the structure of the coastal dune cordon.

Each criteria studied gives useful information, however, only the combination of all data sets is able to attribute samples to the defined units. Values given in Table VII.1 represent the value range observed in Lines 380 and 1200, and overlap of these values between units is common. However, detailed study of all characteristics makes each unit unique. The reader is referred to Chapters V and VI for the discussion of these considerations.

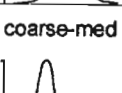
Ages given in Table VII.2 for the sedimentological units are interpretative, except for units D2 and E that have been dated by luminescence method. Depositional and reworking events are discussed in detail in Sections V.6 and VI.6, as well as summarised in Figure VII.1.

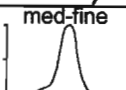
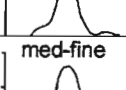
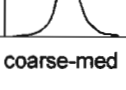
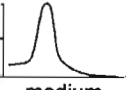
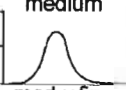
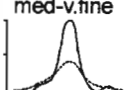
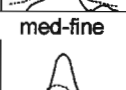
Sand colour noted in Table VII.1 refers to the colour observed in the field, when possible. Moreover each borehole sample has been attributed a colour using the Munsell colour chart (Rock-color chart committee, 1991). Colour variation is noticeable, but is subtle enough to be misleading and will no doubt differ from author to author. Absolute colour values should thus be regarded more as a relative indication of lightness and chroma saturation (Table VII.1).

It is interesting to note that a major colour change distinguishes Unit E from underlying units. The underlying units have a higher chroma value, giving the sand a light orange colour to orange-brown colour. In contrast to this Unit E has not been affected by any "reddening" process (Table VII.1) and shows a similar colour to the present foredunes. This leads to two conclusions. Firstly, since Unit E formed prior to the Holocene Climatic Optimum (4480 B.P.), the event was not long and/or intensive enough to alter the colour of dunes in the present study area. Secondly, the alteration process of Unit D2 to produce a light orange colour must have occurred at least before 4800 B.P. (prior to the youngest possible age of Unit E), and after its maximum depositional age of 15 000 B.P. (Table VII.2).

In tropical Northern Queensland (10° to 15° south), Pye (1981) noted that alteration and reddening of stabilised Holocene coastal dunes occurred within the past 7500 years. As the dune cordon under study is influenced by subtropical to temperate conditions (29° south, Chapter II), the light orange colour of Unit D2 probably formed over more than 7500 years. Therefore, the Holocene climatic conditions (interglacial) appeared to have played a minor role in sand reddening in the northern KwaZulu-Natal dune cordon.

**Table VII.1.** Discriminative characteristics for the nine sedimentological units defined in the Zulti North ore body. Dried sand samples from the RBM storage room were attributed a colour using a Munsell colour chart (Rock-color chart committee, 1991).

Units	IRZ / OHM	Magn / Ilm	Carbonate (modal %)	Titanium (weight %)	Grain size (medium sand)	Colour
E2	0.1 - 0.25	0.14-0.24	4 - 6	1.05 - 1.9 (2.7)	med-fine 	10YR 7/2-3
D2	0 - 0.4	0.12 - 0.24 (0.7)	(3) 4 - 6 (8)	(0.28) 0.4 - 0.75 (1)	med-fine 	10YR 7/4
D1	0.3 - 0.55	0.14-0.24	1.5 - 3.5	0.37 - 0.83 (1.16)	med-fine 	10YR 7/4-5
C	0.1 - 0.3	0.09-0.14	< 1 (1.5)	0.20 - 0.32 (0.66)	coarse-med 	10YR 6.5-7/4
B	0.55 - 0.9	0.14-0.24	0.5 - 2	0.5 - 1.22 (2.41)	medium 	10YR 6.5/4
A4 A3	0.5 - 1 (2)	0.05-0.16 (0.35)	< 1	0.6 - 5.9	med-v.fine 	10YR 6-7/4 Beach: 10YR 5/3
A2	1 - 2.5 (4)	0.05-0.14	0	1.4 - 1.8 (3.05) (north: 10)	med-v.fine 	10YR 4-7/4-6 Beach: 10YR 3/5, 6/7
A1	1.7 - 2.4	0.03-0.05	0	0.45 - 1.5	med-fine 	10YR 7/6
K	3.3 - 6	0-0.02	0	0.6 - 1.7	med-fine 	5Y 4-8/2

Units	IRZ / OHM	Magn / Ilm	Carbonate (modal %)	Titanium (weight %)	Grain size (medium sand)	Colour	Surface morphology	Facies interpretation	Age (BP)		Lithostratigraphy
									deposition	reworking	
E2	very low	very high	very high	high		Light grey to pale yellow	Parabolic dunes Dune Class 4/5	Aeolian dune transgressive proximal	Later events		Sibayi Formation
D2	very low	very high	very high	low		Light orange	Parabolic and Linear dunes Dune Class 4/3	Aeolian dune transgressive distal	± 7 500	± 2 000	
D1	low	very high	high	low		? Light orange	no surface expression	Aeolian dune transgressive distal	? 30 000 - 15 000		
C	very low	high	low	very low		Orange	Coastal cliffs near Dawson's Rock	Aeolian dune with proximal fluvial sediment input	? Last glaciation (95 000 - 30 000)		KwaMbonambi Formation
B	moderate	very high	mod-low	mod - high		Dark orange-brown	Parabolic dunes Dune Class 2	Aeolian reworked from units A3/4 and Unit (?) D1	as for units A3 - A4	? as for Unit D1	
A4 A3	mod (-high)	moderate	low	mod - high		? Dark orange-brown	no surface expression	- Aeolian transgr. proximal/distal - Beach/foredune	? Last interglacial (o/Stage 5) 125 000 - 80 000		
A2	high	moderate	0	high - very high		Dark orange-brown (red soils)	(north) Hairpin parabolic dunes Dune Class 2	- Aeolian transgr. proximal - Beach/foredune	? Penultimate interglacial (o/Stage 7) ca. 200 000		
A1	high	low	0	low - mod		? Dark orange-brown (red soils)	Inland older dune dordon Dune Class 1	- Aeolian transgr. proximal - Fluvial / marine?	? Penultimate or older interglacial (o/Stage 7)		
K	very high	very low	0	mod		Light olive to white	no surface expression	- Aeolian transgr. proximal - Fluvial / marine?	? As old or older than oxygen isotope Stage 9 interglacial (> 300 000)		Kosi Bay Formation

**Table VII.2.** Summary table of discriminative characteristics and interpretation of the nine sedimentological units defined in the Zulti North ore body. Colour refers to sand observed in the field.

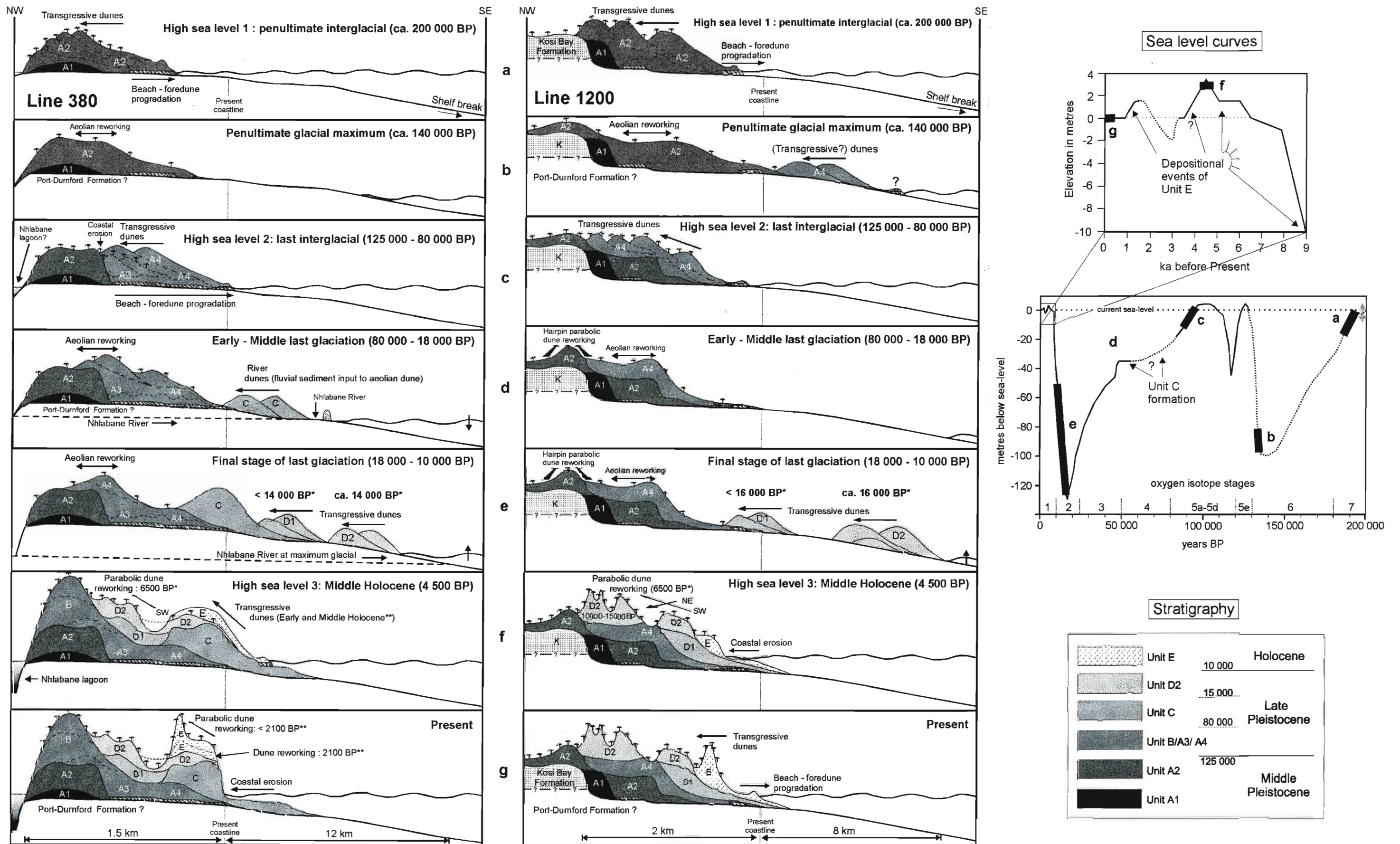


**Figure VII.1.** Schematic evolutionary model for part of the northern KwaZulu-Natal coastal dune cordon. Depositional and reworking events are correlated with time and sea level fluctuations. Single and double asterisks refer to luminescence dates from samples RBM1 and RBM2 (see Sections V.6 and VI.6 for detailed discussion). Each cartoon is labelled a to g, which correspond to periods marked on the sea level curves. Sea level curves from Ramsay (1995; 1997).

### VII.1.1. Sediment provenance based on Nb, Zr and Ti elements

Ratio values from combinations of Nb, Y, Zr and  $\text{TiO}_2$  are identical (within the analytical error range) for all samples of the study area except two samples from Unit C. These four elements have been chosen for further studies (see below) because they are known to be fairly immobile during weathering (Augustithis, 1983). They are thus useful in identifying provenance and mineral segregation processes.

$\text{TiO}_2/\text{Nb}$  and  $\text{TiO}_2/\text{Zr}$  ratios are investigated for all samples from the study area and of various fluvial and marine samples analysed by Felhaber (1984). Marine sediments were collected from the continental shelf between the Tugela River mouth and Mtunzini, while samples of the Tugela River represent the section between the N2 highway and the river mouth. Felhaber (1984) subdivided the continental shelf into three compartments: the nearshore environment (very fine sands with high heavy mineral content), the inner shelf (20 km wide) and the outer shelf (20 km wide) which are both composed of coarse to fine sands.

The  $\text{TiO}_2/\text{Nb}$  ( $\times 10^{-2}$ ) versus  $\text{TiO}_2/\text{Zr}$  values for all samples from the dune cordon under study show little variation and cluster towards the origin (Figure VII.2). Only samples 21 and 27 of Unit C have higher values for both ratios. To better interpret the ratio values given by these two samples, it is necessary to first describe and understand the reasons of the value variations for the other samples.

There is a gap in  $\text{TiO}_2/\text{Zr}$  values between 15 and 17 (Figure VII.2). Felhaber (1984) noted that the occurrence of titanium is relatively abundant in fine grained sand, and suggests that this is due to fixation of titanium on clays. The higher titanium content in fine grained sand could also be due to higher content of fine ilmenite that formed from the breakdown of intergrown iron – titanium oxides. The depletion in silts and clays (Section V.4.1) could explain the relatively low  $\text{TiO}_2/\text{Zr}$  values in the borehole samples (Figure VII.2). However, nearshore sand and foredune samples (F-dune 2 and 4), which constitute complete sediments, also have low ratio values (Figure VII.2). This suggests that loss of fine sediment in the borehole samples is not responsible for low  $\text{TiO}_2/\text{Zr}$  values. It is proposed here that nearshore and beach processes are responsible for the low ratio values observed ( $< 17$ ), possibly by removing the very fine ilmenite.

Samples 21 and 27 from Unit C show high  $\text{TiO}_2/\text{Zr}$  values and plot well away from the aeolian dune, beach and nearshore samples (Figure VII.2). These two samples plot within fields for river and shelf sediments. Further evidence that Unit C is derived from a fluvial source (Section V.6).

The majority of river, marine (nearshore and inner shelf) and borehole samples (beach and aeolian) are characterised by  $\text{TiO}_2/\text{Nb}$  ( $\times 10^{-2}$ ) values between 5 and 10 (Figure VII.2). Thus this ratio does not seem to reflect mineral segregation processes, possibly because Nb is included chiefly in iron – titanium oxides and rutile (Section V.3.2.3). Therefore the  $\text{TiO}_2/\text{Nb}$  values are considered to be influenced only by the provenance of the sediment source. If this is correct, the sediment of the coastal dune cordon between Lake Nhlabane and Cape St.-Lucia derives from the Tugela River, or from nearby rivers with similar ratios, and transported by northward longshore drift.

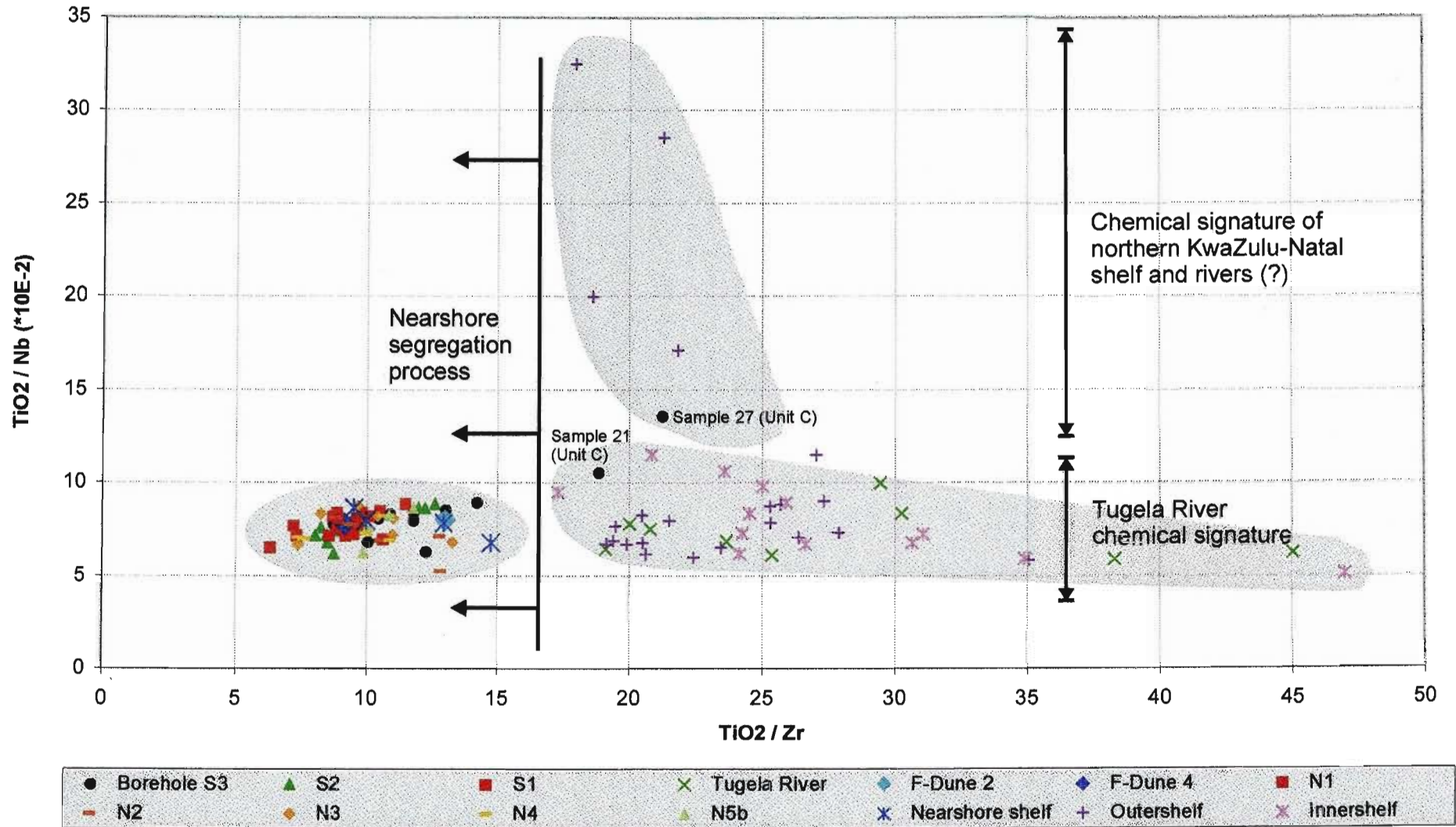


**Figure VII.2.**  $TiO_2 / Nb$  ( $\cdot 10^{-2}$ ) and  $TiO_2 / Zr$  ratio values for all samples of the present study and for various fluvial and marine samples near the Tugela River mouth, central KwaZulu-Natal (data from Felhaber, 1984). For graphical reasons, the  $TiO_2 / Nb$  values are divided by a factor of 100.

While most outer shelf samples plot with  $\text{TiO}_2/\text{Nb}$  ( $\cdot 10^{-2}$ ) values between 5 and 10, four to five samples from the outer shelf present higher  $\text{TiO}_2/\text{Nb}$  ( $\cdot 10^{-2}$ ) values (Figure VII.2). These samples (denominated TM029, TM030, TM083, TM101 and TM102 by Felhaber, 1984) are coarse to medium grained and were collected at the edge of the continental shelf to the east of Mtunzini. This part of the continental shelf is likely to be under the influence of the south flowing Agulhas Current, and thus its sediment may reflect the chemical characteristics of the continental shelf north of Mtunzini, and possibly rivers such as the Mfolozi River (Figure III.2). Therefore the high ( $> 10$ )  $\text{TiO}_2/\text{Nb}$  ( $\cdot 10^{-2}$ ) values are interpreted to reflect a distinct northern provenance (Figure VII.2). Further studies of the geochemistry of the continental shelf and regional rivers need to be undertaken to confirm this hypothesis.

Grain size and SEM analyses suggested that Unit C is a proximal aeolian dune reworked from non-aeolian sediments (Chapter V). Given this and the above discussion of the  $\text{TiO}_2/\text{Zr}$  and  $\text{TiO}_2/\text{Nb}$  ratios, it is suggested that samples 21 and 27 from Unit C contain aeolian sands reworked from local fluvial sediment rather than aeolian sands derived from the outer continental shelf, somewhere north of Richards Bay. The localised occurrence of Unit C, close to the Nhlabane River, also supports this finding.

Cr/Ti ratio values for the coastal dune cordon samples show little variation and does not discriminate any sedimentological units (Appendix B). This suggests that chrome is chiefly contained in stable iron-titanium oxides and that provenance studies using chromium may provide additional information. In contrast to this V/Ti and Ni/Ti values are consistently lower for older, altered samples. This indicates that vanadium and nickel are chiefly incorporated into unstable heavy minerals (Appendix B). Their abundance variation may be useful for discriminating sedimentological units.

## VII.2. Structure and geological history of the Zulti North ore body

The internal structure of the Zulti North ore body has been determined using the distribution of units in Lines 380 and 1200 with lateral correlation using the studies of Clark (1998) and Whitmore *et al.* (1999). These authors studied the spatial distribution of various heavy mineral ratios from RBM data. Unfortunately they do not present data north of Line 1000. Ilmenite grades from Line 750, determined by RBM, helped in constructing the spatial distribution of beach placers at the base of the dune cordon.

As noted in the previous section, mineral ratios alone are not sufficient to discriminate all of the defined units; young units (Units C, D and E) cannot be distinguished by this way. Therefore, results presented below must be considered cautiously.

### VII.2.1. Surface geology of the Zulti North ore body

The geomorphological map described in Chapter IV has been used to surimpose the surface distribution of sedimentological units (Figure VII.3). The northern KwaZulu-Natal dune cordon is often referred as a "Holocene dune cordon". This term is misleading, at least for the Zulti North ore body, as Unit E is the only Holocene dune and it represents a very small coastal portion of the dune cordon (Figure VII.3 and Table VII.1).

The inland and central section of the dune cordon is dominated by Pleistocene sediment, which extends to the coast between N600 and N1000. The sediment is believed to represent the outcrop of the last (Units B and A4) and penultimate (Unit A2) interglacial dune cordons (Figure VII.3). The sediment constituting the inland dunes (Dune Class 2) is older in the northern part of the ore body (north of N600 – N700) (Figure VII.3). Unit A2 is characterised on surface by hairpin parabolic dunes, which are considered to predate the formation of the parabolic dunes of Unit B to the south (Sections IV.2.2 and Figure VII.3).

### VII.2.2. Internal structure of the Zulti North ore body

The internal structure of the dune cordon under study is illustrated by two schematic geological maps along horizontal planes at 5 to 10 m and 30 to 35 m above msl (Figures VII.4 and VII.5).

Fockema (1986) suggests that the Kosi Bay Formation underlies the entire coastal dune cordon, as indicated by his geological cross-section at Dawson's Rock (Figure III.5). This interpretation is also suggested by the coastal distribution of the Kosi Bay Formation proposed by Hobday & Orme (1974) (Figure II.1 and Section III.4.1.3). However, the present study reveals that the Kosi Bay Formation (Unit K) is only present inland of the present coastal dune cordon, at the base of the inland dunes to the north (Figures VII.4 and VII.5). A high sea level event resulted in the erosion of this formation (Figure VII.4), which reappears on coastal outcrops south of the Nhlabane estuary.

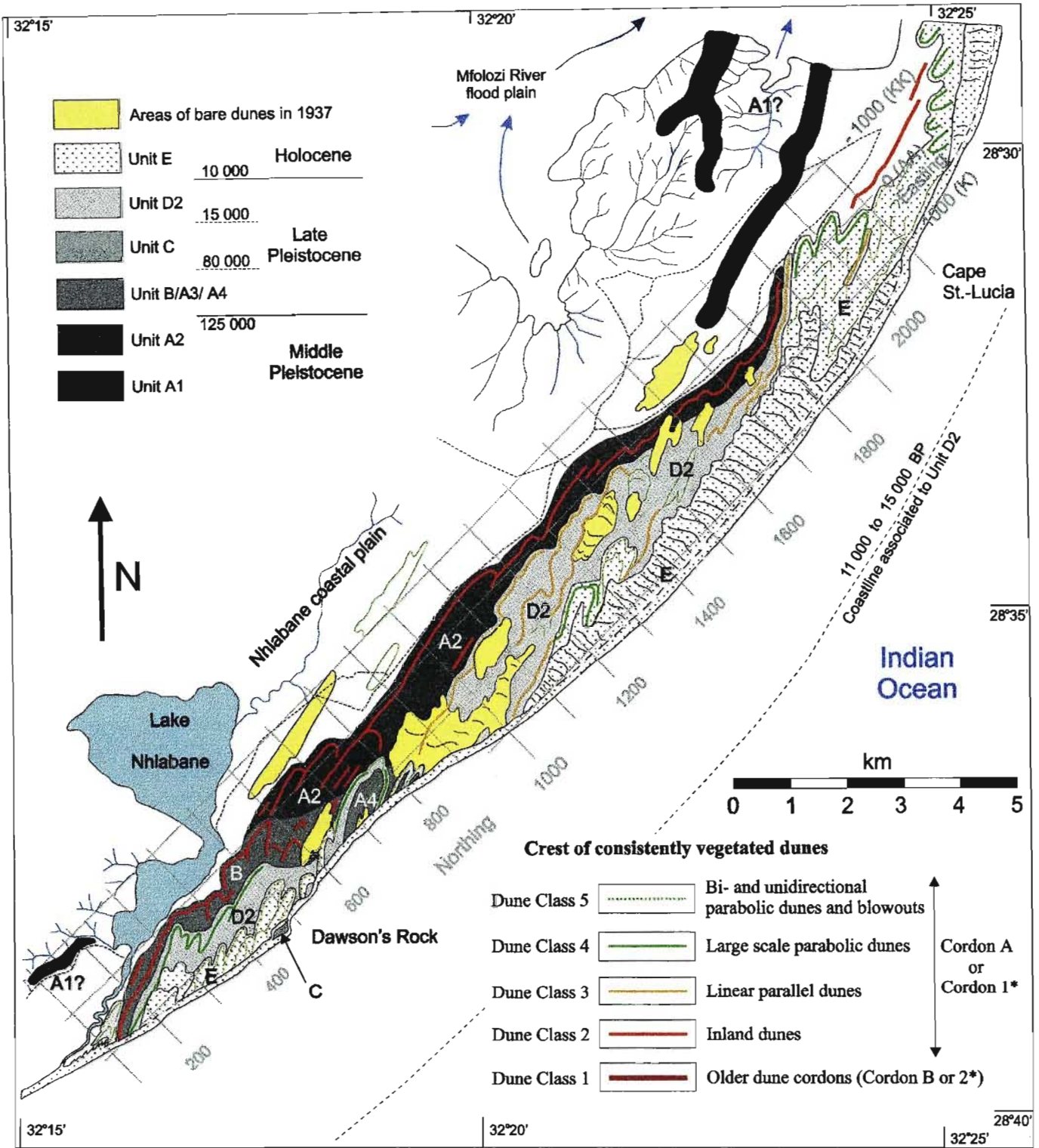


**Figure VII.3.** Geological map of the Zulti North ore body, showing the superficial extension of sedimentological units and the relationship with the surface morphology. \*Cordons A and B of Davies (1975); Cordon 1 and 2 of Wright (1999).

Units A1 and A2 represent the oldest dunes constituting the present coastal dune cordon (Figures VII.4 and VII.5). In the southern portion of the present dune cordon, this penultimate interglacial (oxygen isotope Stage 7) dune cordon(s) is located inland. To the north it is located in the central (at the base of the present cordon, Figure VII.4) and inland (Figure VII.4) portions of the present dune cordon. The coastal side of this old dune cordon(s) was eroded by the last interglacial high sea level (oxygen isotope Stage 5) (Figure VII.4).

The last interglacial (oxygen isotope Stage 5) dune cordon (Units B, A3 and A4) is accreted onto the A1/A2 dune cordon(s) (Figures VII.3, VII.4 and VII.5). The beach - foredune system at its base was characterised in the southern portion of the study area by more extensive progradation compared to the beach - foredune system of the A1/A2 dune cordon(s), as illustrated by the areas covered by respective beach placers (Figure VII.4). This could suggest that the nearshore morphology was steeper in the northern part of the study area.

The last interglacial dune cordon is presently being eroded in the central and southern portions of the study area (Figures VII.4 and VII.5). In other areas younger accreted dunes (Units C, D and E) protect the older dune cordon from erosion (Figures VII.4 to VII.5).

Unit C is the only unit whose sediment was not derived from a beach - foredune system. This unit's unique mineralogy, geochemistry, grain size and grain surfaces suggest that Unit C is composed of sand from a nearby river (Nhlabane River?), which was reworked into proximal aeolian dunes (Section V.6). During the last glaciation (oxygen isotope Stages 5 to 2), sea level gradually lowered to expose the continental shelf. Dune cordons associated to periods of sea level still stand could have deflected the path of the Nhlabane River, forcing the latter to migrate northward (Figure VII.5). Thus the sediment of the Nhlabane River flood plain would have been reworked by onshore winds, to form Unit C (Figure VII.5). During the last glacial maximum (18 000 B.P.), sea level was -130 m below msl and many rivers incised the continental shelf. This may have ceased deposition of Unit C as fluvial sediment was brought directly to the continental slope (Flemming & Hay, 1988).

A topographic palaeo-depression between Units A and C was later filled by younger sediments of Unit D (Figures VII.3 to VII.5). This palaeo-depression is envisaged to have been below sea level in the south and rise to 20 m above msl by N400.

The formation of this palaeo-depression can be explained by a combination of two factors. Firstly, rapid accretion of Unit C built a new dune cordon separated from the previous dune cordon by a small topographic depression (Figure VII.5). Secondly, the coastline configuration between N0 and N400 would have channelled the prevailing winds along this depression. Reworking of the last interglacial (Units A3/A4) dune cordon resulted in the formation of Unit B (Section V.6 and Figure VII.3). The age of this erosional event is thought to be of similar age to the deposition of Unit D1 (being the first unit filling the valley), whose age is not precisely known (late last glaciation?, Table VII.2).

Unit D2 accreted to the coastal dune cordon during the marine transgression following the last glacial maximum, between ca. 15 000 and 11 000 B.P. (Section VI.6). The palaeocoastline at this time was more than 3 km offshore, vegetation was sparse and wind velocity high (Sections II.4, VI.6 and Figure VII.3). This suggests that the sediment composing Unit D2 migrated as giant dune fields across the shelf. Unit D2 was later reworked to form the parabolic and linear dunes of Dune Classes 3 and 4 (Figure VII.3). This reworking event of Unit D2 has been dated at  $6500 \pm 450$  B.P. (Table VII.2).

During the last ten thousand years (Holocene), several transgressive dunes migrated onshore from the nearby shoreline, constituting the heavy mineral rich Unit E (Figure VII.3). Periods of relative stability are recorded as palaeosols within Unit E. One of these palaeosols 5 m beneath the current soil near Dawson's Rock must be younger than 2100 B.P. as indicated by a period of

reworking, identified from luminescence dating, of the sediment immediately beneath it (Figures VII.4 or VII.5).

North of N1000, a net shoreline progradation (deposition of Unit E) has occurred since the Holocene Climatic Optimum (?) (4480 B.P., Section II.4), when sea level began receding to its present level, after eroding Unit D1 (Figure VII.4). South of N1000 coastal retreat, still effective at the present time, eroded any deposits younger than Units A and C (Figure VII.4).

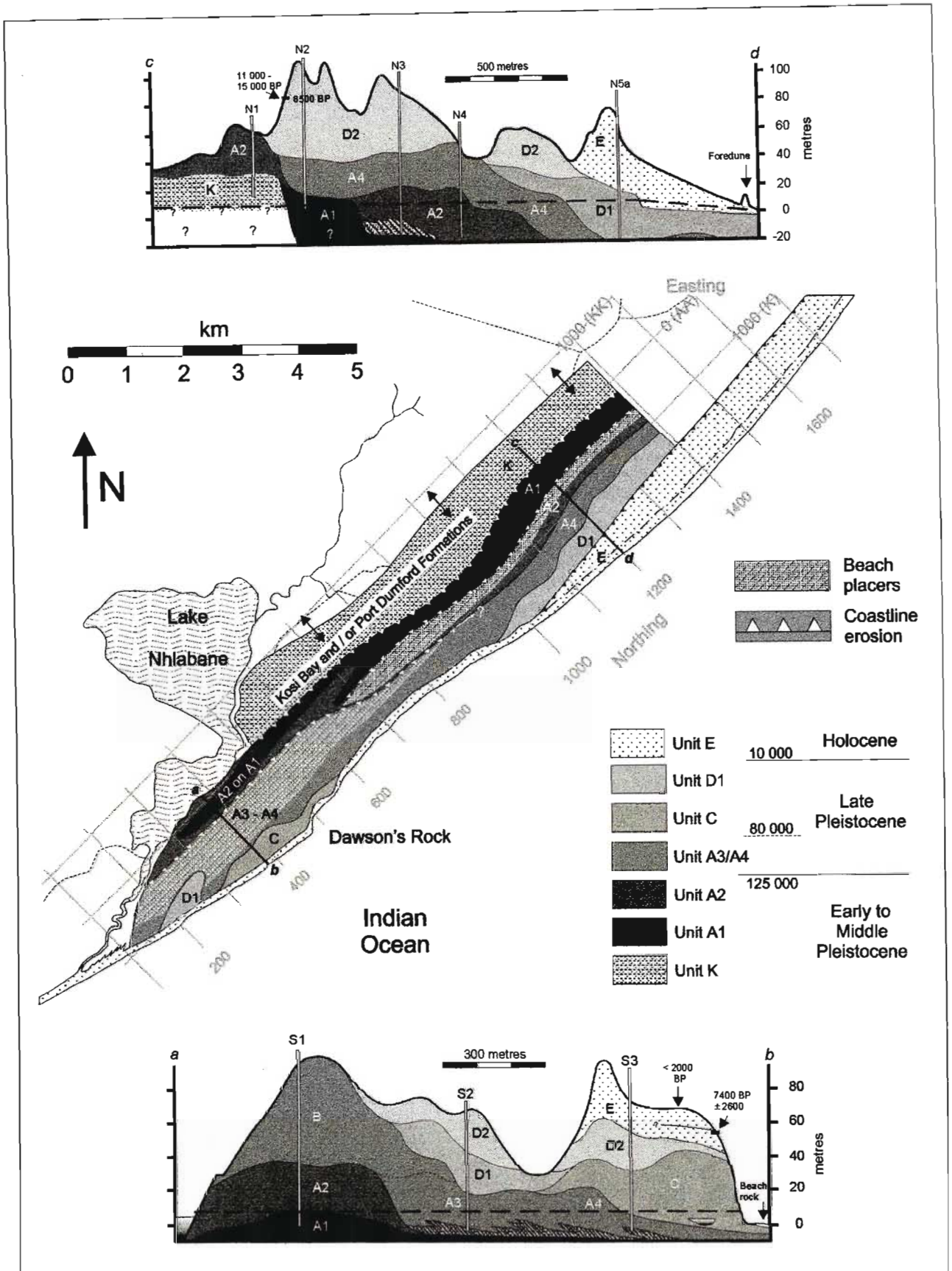


**Figure VII.4.** Geological map of the base of the Zulti North ore body along a horizontal plane at ca. 5 - 10 m above msl. Underlying beach placers have been projected onto this plane.

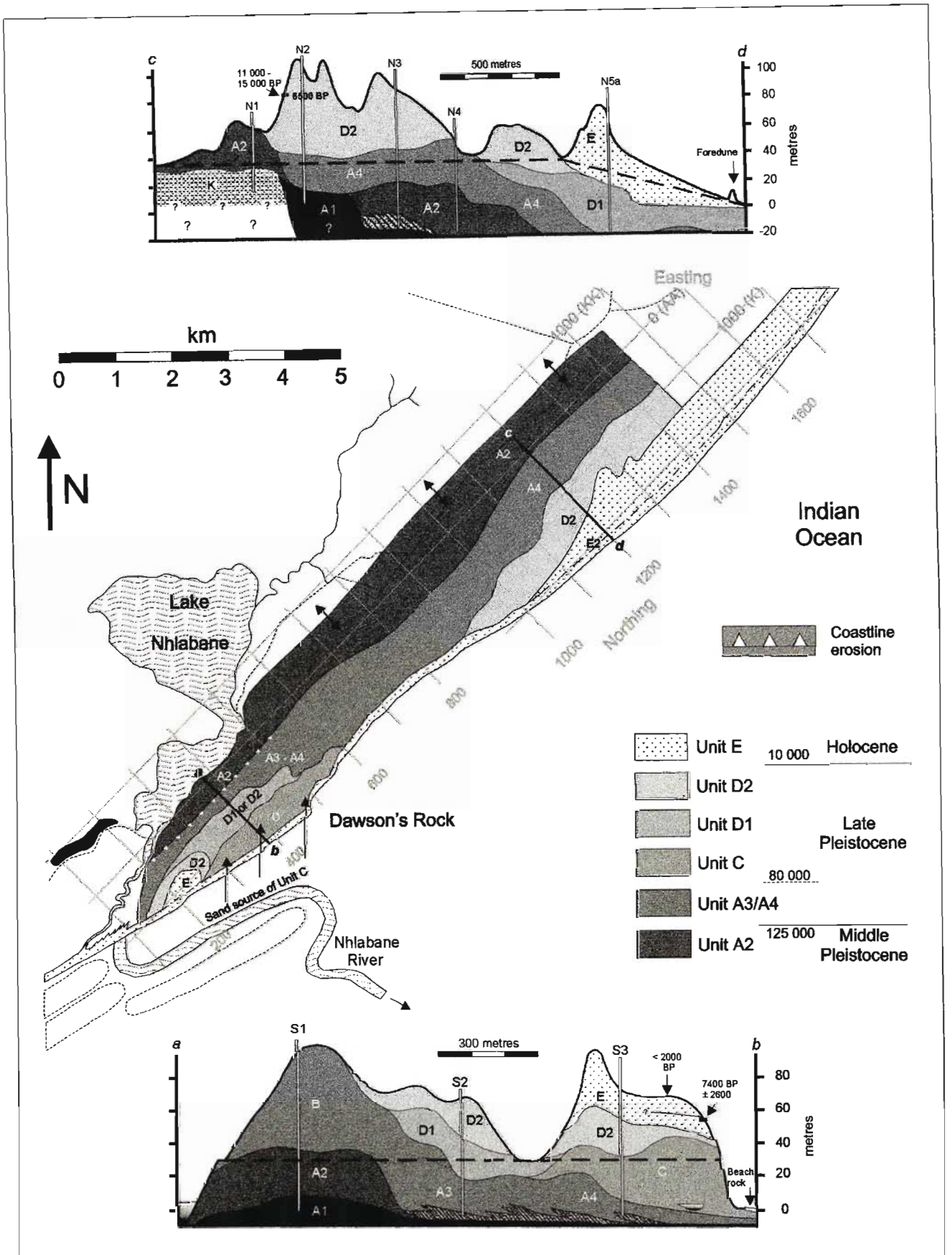


**Figure VII.5.** Geological map of the Zulti North ore body along a horizontal plane at ca. 30 - 35 m above msl.

## VII.4 Conclusion

The present study shows that the northern KwaZulu-Natal coastal dune cordon is a complex system of stacked dunes of various types and ages, overlying beach and marine sediments.

The author believes that the most probable periods of dune accretion onto the present coastal dune cordon are closely associated with high sea levels of interglacial periods or with the interglacial – glacial transition periods. Recognition of basal beach placers and their alteration state help to attribute a relative age to the nine sedimentological units defined in the study. These nine units were regrouped into four sediment packages thought to represent four interglacial periods. The three younger packages were attributed to the penultimate (oxygen isotope Stage 7 or even older?) (Units A1 and A2), last (oxygen isotope Stage 5) (Units A3/A4, B and C?) and “Holocene” (Units D1, D2 and E) interglacials. Therefore, the oldest sediment package (inland Unit K), interpreted as the “Late Pleistocene” Kosi Bay Formation, must be of Middle Pleistocene (or older), which is older than considered by previous studies.

The present coastal dune cordon comprises the three younger sediment packages. Hence the northern KwaZulu-Natal coastal dune cordon studied represents a complex stacking of three generations of coastal dune cordons, and is therefore constituted of sediments ranging in age from at least 200 000 years B.P. to present.

Recognition of dune types on the surface of the coastal cordon is not sufficient to define the occurrence of the three generations of dune cordons. All dunes must be regrouped into dune classes that reflect their relative age, independently of their types and nature. This classification methodology led to the subdivision of three dune classes (Dune Classes 3, 4 and 5) for the “Holocene” dune cordon itself, suggesting at least three recent dune formation events. These depositional and reworking events, dated by luminescence, occurred during the last 15 000 years. Two subtypes of a fourth dune class (Dune Class 2) describe the surface morphology of the two oldest dune cordons.

The present study suggests that sediment source, wind, sea level and hydraulic regime are major factors influencing the heavy mineral ratios and content of an aeolian dune. Unfortunately some hypotheses proposed in this study can only be speculative, due to widely spread samples and to the 6 m vertical thickness of sand intercepted by borehole samples. The characteristics of the borehole samples were also considerably altered during the manipulation and storage processes at RBM.

However, these hypotheses open interesting opportunities for further studies. Detailed sampling and analysis of a beach – foredune – dune system would provide useful information in understanding mineral segregation processes.

## REFERENCES

- Anderson, W. (1907). Third report of the Geological Survey of Natal and Zululand. *Surveyor-General's Department, West, Newman & Co., London.*
- Augustithis, S.S. (1983). Leaching and diffusion in rocks and their weathering products. *Theophrastus Publishing & Proprietary Co, S.A., Athens, Greece.* 562 pp.
- Avery, D.M. (1982). The micromammalian fauna from Border Cave, KwaZulu, South Africa. *J. of Archaeological Science*, **9**, 187-204.
- Bagnold, R.A. (1941). The physics of blown sand and desert dune. *Methuen, London.* 265 pp.
- Basson, I.J. (1997). Contributions to the structural context of sub-economic Veining in the Natal Thrust Front and Natal Nappe Zone, Northern KwazuluNatal. *MSc thesis, University of Natal (Durban)*, 279 pp.
- Begg, G.W. (1978). The estuaries of Natal. *Natal Town and Regional Planning Report*, **41**. 657 pp.
- Berner, R.A. & Schott, J. (1982). Mechanism of pyroxene and amphibole weathering II. Observations of soil grains. *Am. J. Sci.*, **282**, 1214-1231.
- Beukes, N.J. & Cairncross, B. (1991). A lithostratigraphic-sedimentological reference profile for the Late Archean Mozaan Group, Pongola Sequence: application to sequence stratigraphy and correlation with the Witwatersrand Supergroup. *S. Afr. J. Geol.*, **94** (1), 44-69.
- Botha, G.A. Council for Geoscience, Pietermaritzburg.
- Botha, G.A. (1997a). The Maputaland Group: a provisional lithostratigraphy for coastal KwaZulu-Natal. In: *Botha, G.A. (Ed.). Maputaland focus on the Quaternary evolution of the south-east African coastal plain. International Union for Quaternary Research Workshop Abstracts, Council for Geoscience, Private Bag X112, Pretoria, South Africa*; 41.
- Botha, G.A. (1997b). Port Durnford Formation. In: *Botha, G.A. (Ed.). Maputaland focus on the Quaternary evolution of the south-east African coastal plain. International Union for Quaternary Research Workshop Abstracts, Council for Geoscience, Private Bag X112, Pretoria, South Africa*; 41.
- Botha, G.A. (1997c). Port Durnford Formation sea-level and landscape relationships. In: *Botha, G.A. (Ed.). Maputaland focus on the Quaternary evolution of the south-east African coastal plain. International Union for Quaternary Research Workshop Abstracts, Council for Geoscience, Private Bag X112, Pretoria, South Africa*; 41.
- Brown, Hawkesworth and Wilson (1992). Understanding the Earth. *Cambridge University Press.*
- Butzer, K.W., Beaumont, P.B. and Vogel, J.C. (1978). Lithostratigraphy of Border Cave, KwaZulu, South Africa, a Middle Stone Age sequence beginning c. 195'000 B.P. *J. of Archaeological Science*, **5**, 317-341.
- Chappell, J. & Shackleton, N.J. (1986). Oxygen isotopes and sea level. *Nature* **324**, 137-140.
- Clark, R.J. (1998). The geological structure of the Zulti North ore body from heavy mineral ratios. *Hon. thesis, University of Natal, Durban, unpublished.* 141pp.
- Climap Project Members (1984). The Last Interglacial ocean. *Quaternary Research*, **21**, 123-224.
- Collins, L.B. & Hamilton, N.T.M. (1989). Holocene sedimentation and heavy mineral accumulation, Minnipup Shoreline, W.A. *Minerals and Energy Research Institute of Western Australia Report* **42**.
- Cooper, J.A.G. (1991a). Sedimentary models and geomorphological classification of river-mouth on a subtropical, wave-dominated coast, Natal, South Africa. *PhD thesis (unpubl.), University of Natal, Durban.* 401pp.

- Cooper, J.A.G. (1991b). Beachrock formation in low latitudes: implications for coastal evolutionary models. *Marine Geology*, **98**, 145-154.
- Davies, J.L. (1964). A morphogenic approach to world shorelines. *Zeitschr. für Geomorphol.*, **8**, 27-42.
- Davies, J.L. (1980). Geographical variation in coastal development. *Longmans, London*, 2<sup>nd</sup> ed., 212pp.
- Davies, O. (1975). The older coastal dunes in Natal and Zululand and their relation to former shorelines. *Proc. Sth. Afr. Soc. Quat. Res.* (or: *Ann. S. Afr. Mus.* **71** (1976), 19-32).
- Dawson, N.P. (1997). Heavy mineral mineralogy and its relevance to mineral separation plant circuits. In: *Robinson, R.E. (Ed.), Heavy Minerals 1997, The South African Institute of Mining and Metallurgy, Johannesburg.*
- Deacon, J. & Lancaster, N. (1988). Late Quaternary palaeoenvironments of Southern Africa. *Oxford University Press, New York*, 225 pp.
- Dill, H.G. (1998). A review of heavy minerals in clastic sediments with case studies from the alluvial-fan through the nearshore-marine environments. *Earth-Science reviews* **45**, 103-132.
- Dimanche, F. & Bartholomé, P. (1976). The alteration of ilmenite in sediments. *Minerals Sci. Engng.*, **8**, 187-210.
- Dingle R.V., Siesser, W.G. and Newton, A.R (1983). Mesozoic and Cenozoic geology of South Africa. *Balkema, Rotterdam*. 375 pp.
- Dingle, R.V. (1981). The Campanian and Maastrichtian ostracods of South East Africa. *Ann. S. Afr. Mus.*, **85**, 1-181.
- Dryden, L. & Dryden, C. (1946). Comparative rates of some common heavy minerals. *J. Sed. Petrol.*, **16**, 91-96.
- Du Toit, A.L. (1954). The Geology of South Africa. *Oliver and Boyd, Edinburgh*, 3<sup>rd</sup> Edition, 611pp.
- Dunlevey, J.N. (1997). The Berea Red Sand. In: *Robinson, R.E. (Ed.), Heavy Minerals 1997, The South African Institute of Mining and Metallurgy, Johannesburg.*
- Eales, H.V., Marsh, J.S. and Cox, K.G. (1984). The Karoo igneous province: an introduction. *Spec. Publ. Geol. Soc. S. Afr.*, **13**, 1-26.
- Fairbridge, R.W. (1983). The Pleistocene – Holocene boundary. *Quaternary Science Review*, **1**, 215-244.
- Felhaber, T.A. (1984). The geochemistry and sedimentology of Quaternary shelf sediments off the Tugela river, Natal, South Africa. *MSc thesis, University of Cape Town*, 237 pages.
- Flemming, B.W. (1981). Factors controlling shelf sediment dispersal along the southeast African continental margin. *Marine Geology*, **42**, 259-277.
- Flemming, B.W. & Hay, (1988). Sediment distribution and dynamics on the Natal continental shelf. In: *Schumann, E.H. (Ed.), Coastal ocean Studies off Natal, South Africa. Lectures notes on coastal and estuarine studies*, **26**, 101-130, *Springer-Verlag, New York.*
- Fockema, P.D. (1986). The heavy mineral deposits north of Richards Bay. In: *Anhaeusser, C.R. & Maske, S. (Eds), Mineral Deposits of South Africa. Geol. Soc. S. Afr., Johannesburg*, 2301-2307.
- Folk, L. (1971). Longitudinal dunes of the northwestern edge of the Simpson desert, Northern Territory, Australia, 1. Geomorphology and grain size relationships. *Sedimentology*, **16**, 5-54.
- Force, E.R. & Stone, B.D. (1990). Heavy mineral dispersal and deposition in sandy deltas of glacial Lake Quinebaug, Connecticut. *U.S. Geol. Surv. Bull.* **1874**. 21 pp.
- Force, E.R. (1991). Geology of titanium deposits. *Geol. Soc. America, Special Paper* **259**. 112 pp.
- Foucault, A. & Raoult, J.-F. (1995). Dictionnaire de géologie. 4<sup>th</sup> edition, *Masson, Paris*. 324 pp.
- Friedman, G.M. & Sanders, J.E. (1978). Principles of sedimentology. *John Wiley & Sons, New York*.

- Friedman, G.M. (1961). Distinction between dune, beach and river sands from their textural characteristics. *J. Sed. Petrol.*, **31**, 514-529.
- Friedman, G.M. (1979). Address of the retiring president of the International Association of Sedimentologists: differences in size distributions of populations of particles among sands of various origins. *Sedimentology*, **26**, 3-32.
- Fryberger, S.G. & Ahlbrandt, T.S. (1979). Mechanism for the formation of eolian sand seas. *Z. Geomorph. N.J.*, **23**, 440-460.
- Geophysics Study Committee (GSC) (1990). Sea level changes. *Commission on Physical Sciences and Resources, National Research Council. National Academy Press, Washington*. 234 pp.
- Goldich, S.S. (1938). A study of rock weathering. *J. Geol.*, **46**, 17-58.
- Hamilton, N.T.M. & Collins, L.B. (1998). Placer formation in a Holocene barrier system, southwestern Australia. *J. Coastal Research*, **14/1**, 240-255.
- Hammerbeck, E.C.I. (1976). Titanium. In: Coetze, C.B. (Ed.). Mineral resources of the Republic of South Africa. *Geol. Surv. S. Afr. Handbook*, **7**, 5<sup>th</sup> ed. 221-226.
- Haq, B.L. & Van Eysinga, (1987). Geological Time Scale. *Fourth edition, Elsevier*.
- Hayes, M.O. (1979). Barrier island morphology as a function of tidal and wave regime. In: Leatherman, S.P. (Ed.), Barrier islands from the Gulf of Mexico. *Academic Press, New York*, 3-22.
- Henderson, P. (1982). Inorganic geochemistry. *Pergamon Press, Oxford*. 353 pp.
- Hendey, Q.B. & Volman, T.P. (1986). Last Interglacial sea levels and coastal caves in the Cape Province, South Africa. *Quaternary Research* **25**, 189-98.
- Hesp, P. (1988). Morphology, dynamics and internal stratification of some established foredunes in southeast Australia. *Sedim. Geol.*, **55**, 17-41.
- Hobday, D.K. & Orme, A.R. (1974). The Port Durnford Formation: a major Pleistocene barrier-lagoon complex along the Zululand coast. *Trans. Geol. Soc. S. Afr.*, **77**, 141-149.
- Hobday, D.K. (1979). Geological evolution and geomorphology of the Zululand coastal plain. In: Allanson, B.R. (ed.). Lake Sibaya. *Mongraphiae Biologicae*, **36**, 1-20.
- Howard, W.R. (1985). Late Quaternary Southern Indian Ocean circulation. *South African Journal of Science*, **81**, 253-254.
- Hsu S.A. (1988). Coastal meteorology. *Academic Press, Inc., London*, 260 pp.
- Hugo, V.E. & Cornell, D.H. (1991). Altered ilmenites in Holocene dunes from Zululand, South Africa: petrographic evidence for multistage alteration. *S. Afr. J. Geol.*, **94**, 365-378.
- Hugo, V.E. (1988). A mineralogical and chemical study of titanium losses at Richards Bay Minerals. *MSc. thesis (unpubl.)*, University of Natal, Durban. 201 pp.
- Hugo, V.H. (1993). A study of titanium-bearing oxides in heavy mineral deposits along the east coast of South Africa. *PhD thesis (unpubl.)*, University of Natal, Durban. 357 pp.
- Hunter, I.T. (1988). Climate and weather off Natal. In: Schumann, E.H. (Ed.), Coastal Ocean Studies off Natal, South Africa. *Lectures notes on coastal and estuarine studies*, **26**, 81-100.
- Jackson, S.P. & Tyson, P.D. (1971). Aspects of the climate and weather over Southern Africa. *Environmental Studies Occasional Paper*, **6**. Dept. Geog. and Environ. Studies, University of Witwatersrand, Jhb. 13pp.
- Johnson, C.H. (1986). The geology of the Zululand titanium deposits. *Abstracts Geocongress '86. Geol. Soc. S. Afr., Johannesburg*, 417-420.
- Jordaan, L.J. (1996). Durban heavy minerals. Council for Geoscience Geol. Surv., Private Bag X112, Report **96/182**. 16 pp.
- Kaldi, J., Krinsley, D.H. and Lawson D. (1978). Experimentally produced aeolian surface textures on quartz sand grains from various environments. In: Whalley, W.B. (Ed.). Scanning electron microscopy in the study of sediments. *Geo Abstracts, Norwich, England*.
- Kennedy, W.J. & Klinger, H.C. (1975). Cretaceous fauna from Zululand and Natal, South Africa. Introduction, Stratigraphy. *Bull. Brit. Mus. Nat. Hist. Geology*, **25**, 265-315.
- Komar, P.D. & Wang, C. (1984). Processes of selective grain transport and the formation of placers on beaches. *J. Geol.*, **92**, 637-655.

- Komar, P.D. (1976). Beach processes and sedimentation. *Prentice-Hall, INC, Englewood Cliffs, New Jersey*.
- Krinsley, D.H. & Donahue, J. (1968). Environmental interpretation of sand grain surface textures by electron microscopy. *Bulletin of the Geological Society of America*, **79**, 743-748.
- Krinsley, D.H. & Doornkamp, J.C. (1973). Atlas of quartz sand surface textures. *Cambridge University Press, Cambridge*. 91pp.
- Krinsley, D.H. & McCoy, F. (1978). Aeolian quartz and silt. In: *Whalley, W.B. (Ed.)*. Scanning electron microscopy in the study of sediments. *Geo Abstracts, Norwich, England*.
- Lätti, A.D. (1997). The application of QEM\*SEM to the Quelimane heavy minerals deposits, Mozambique. In: *Robinson, R.E. (Ed.)*, Heavy Minerals 1997, *The South African Institute of Mining and Metallurgy, Johannesburg*.
- Le Ribault, L. (1978). Exoscopy of quartz sand grains. In: *Whalley, W.B. (Ed.)*. Scanning electron microscopy in the study of sediments. *Geo Abstracts, Norwich, England*.
- Lin, I.S, Rohrllich, V. and Slatkine, A. (1974). Surface microtextures of heavy minerals from the Mediterranean coast of Israel. *Society of Economic Paleontologists and Mineralogists, December*, 1282-1295.
- Linström, J.C. (1987). The geology of the Dundee area. *Expl. Sheet 3030 Geol. Surv. S. Afr.*, 52 pp.
- Liu, K.W. (1995). Diagenesis of the Neogene Uloa Formation of Zululand, South Africa. *S. Afr. J. Geol.*, **98**, 25-34.
- Luepke, G. (1980). Opaque minerals as aids in distinguishing between source and sorting effects on beach-sand mineralogy in southwestern Oregon. *J. Sed. Petrol.*, **50/2**, 489-496.
- Mabbutt, J.A. (1977). Desert landforms. *The MIT Press, Cambridge, Massachusetts*. 340 pp.
- Malan, O.G. & Schumann, E.H. (1979). Natal shelf circulation revealed by landsat imagery. *South African Journal of Science*, **75**, 136-137.
- Martin, A.K. & Flemming, B.W. (1988). Physiography, structure and geological evolution of the Natal continental shelf. In: *Schumann, E.H. (ed.)*. Coastal Ocean studies off Natal, South Africa. *Lecture notes on coastal and estuarine studies*, **26**. Springer-Verlag, New York.
- Mason, C.C. & Folk, R.L. (1958). Differentiation of beach, dune, and aeolian flat environments by size analysis, Mustang Island, Texas. *J. Sed. Petrol.*, **28/2**, 211-226.
- Matthews, P.E. (1981). Eastern or Natal sector of the Namaqua-Natal Mobile Belt in Southern Africa. In: *Hunter, D.R. (Ed.)*. Precambrian of the Southern Hemisphere. *Developments in Precambrian Geology*, **2**, 705-795, Elsevier Publishers.
- Maud, R.R. & Orr, W.N. (1975). Aspects of post-Karoo geology in the Richards Bay area. *Trans. Geol. Soc. S. Afr.*, **78**, 101-109.
- Maud, R.R. (1968). Quaternary geology and soil formation in coastal Natal. *Z. Geomorph., Supplementband 7*, 155-199.
- Maud, R.R. (1980). The climate and geology of Maputaland. In: *Bruton, M.N. & Cooper, K.H. (Eds.)*, Studies on the ecology of Maputaland. *Rhodes University and the Natal branch of the Wildlife Society of Southern Africa*, 1-7.
- McCarthy, M.J. (1988). Late-Gondwana to recent geology of the Natal north coast. Excursion C guidebook. *Geocongress, Geol. Soc. S. Afr., Durban*.
- McKee, D. (1966). Structures of dunes at White Sands National Monument, New Mexico (and a comparison with structures of dunes from other selected areas). *Sedimentology*, **7**, 3-69.
- McKee, D., Gordon, C. and Tibbitts, J.R. (1964). Primary structures of a seif dune and associated deposits in Lybia. *J. Sedim. Petrol.*, **34 (1)**, 5-17.
- Meyer, R. (1997). Geological information from geohydrological investigations on the Zululand coastal plain. In: *Botha, G.A. (Ed.)*. Maputaland focus on the Quaternary evolution of the south-east African coastal plain. *International Union for Quaternary Research Workshop Abstracts, Council for Geoscience, Private Bag X112, Pretoria, South Africa*; 41.
- Milankovitch, M. (1938). Astronomische Mittel zur Erforschung der erdgeschichtlichen Klimate. In: *Gutenberg, B. (Ed.)*, Handbuch der Geophysik **9**, 593-698, Berlin.

- Minarik, L., Absolon, D., Kollnerova and Klecka (1983). Chemical changes of granite during its weathering. In: *Augustithis, S.S. (Ed.), Leaching and diffusion in rocks and their weathering products. Theophrastus Publishing & Proprietary Co, S.A., Athens, Greece.* 562 pp.
- Moiola, R.J. & Weiser, D. (1968). Textural parameters: an evaluation. *J. Sed. Petrol.*, **38**, 45-53.
- Nesbitt, H.W. & Young, G.M. (1982). Early proterozoic climates and plate motions inferred from major element chemistry of lutites. *Nature*, **299**, 715-717.
- Nordstrom, C.E. & Margolis, S.V. (1972). Sedimentary history of central California shelf sands as revealed by scanning electron microscopy. *J. Sed. Petrol.*, **42/3**, 527-536.
- Oschadleus, H.D., Vogel, J.C. and Scott, L. (1996). Radiometric date for the Port Durnford peat and development of yellow-wood forest along the South African east coast. *S.A. J. Sci.*, **92**, 43-45.
- Partridge, T.C. & Maud, R.R. (1987). Geomorphic evolution of southern Africa since the Mesozoic. *S. Afr. J. Geol.*, **90**, 179-208.
- Pettijohn, F.J. (1957). *Sedimentary rocks. 2<sup>nd</sup> Ed., Harper and Row, New York.* 718 pp.
- Pietersen, K.J. Richards Bay Minerals, P.O. Box 401, Richards Bay, 3900, RSA.
- Pitman, W.V. & Hutchinson, I.P.G. (1975). A preliminary hydrological study of Lake Sibaya. *Hydrological Research Unit Report, 5/75.* 35 pp.
- Pye, K. (1981). Rate of dune reddening in humid tropical climate. *Nature*, vol. **290**, 582-584.
- Pye, K. (1982). Morphological development of coastal dunes in a humid tropical environment, Cape Bedford and Cape Flattery, North Queensland. *Geog. Ann.* **64a**, 213-227.
- Pye, K. (1993). Late Quaternary development of coastal parabolic megadune complexes in northeastern Australia. *Spec. Publ. Int. Ass. Sediment.*, **16**, 23-44.
- Ramsay, P.J. Council for Geoscience, Marine Geoscience Unit, P.O. Box 18091, Dalbridge, 4014, Durban, RSA.
- Ramsay, P.J. (1994). Marine geology of the northern Zululand shelf, southeast Africa. *Marine Geology*, **120 (3/4)**, 225-247.
- Ramsay, P.J. (1995). 9 000 years of sea-level change along the southern African coastline. *Quaternary International*, **27**, 1-5.
- Ramsay, P.J. (1997). Holocene sea level changes. In: *Botha, G.A. (Ed.). Maputaland focus on the Quaternary evolution of the south-east African coastal plain. International Union for Quaternary Research Workshop Abstracts, Council for Geoscience, Private Bag X112, Pretoria, South Africa;* 41.
- Ramsay, P.J., Cooper, J.A.G., Wright, C.I. and Mason, T.R. (1989). The occurrence and formation of ladderback ripples in subtidal, shallow marine sands, Zululand, South Africa. *Marine Geology*, **86 (2/3)**, 229-235.
- Rock-color chart committee (1991). Rock-color chart with genuine Munsell color chips. *7<sup>th</sup> Ed., Geological Society of America, P.O. Box 9140, Boulder, Colorado 80301.*
- Rossouw, J. (1984). Review of existing wave data, wave climate and design waves for South African and South West African (Namibian) coastal waters. *CSIR Report T/SEA 8401, Stellenbosch.* 66pp.
- Ryan, P.J. & Whitfield, G.G. (1979). Basinal analysis of the Ecca and lowermost beaufort beds and associated coal, uranium and heavy mineral beach sand occurrences. *Geocongress 77. Spec. Publ. Geol. Soc. S. Afr.*, **6**, 17-21.
- Sallenger, A.H. (1979). Inverse grading and hydraulic equivalence in grain flow deposits. *J. Sed. Petrol.*, **49**, 553-562.
- Schulze, B.R. (1965). Climate of South Africa. Part 8. General Survey. *Climate Bureau of S. Afr. Publ.*, **28**, Pretoria. 330 pp.
- Schumann, E.H. (1988). Physical oceanography off Natal. In: *Schumann, E.H. (Ed.), Coastal ocean Studies off Natal, South Africa. Lectures notes on coastal and estuarine studies*, **26**, 101-130.
- Short, A.D. (1988). Holocene coastal dune formation in southern Australia: a case study. *Sedim. Geol.*, **55**, 121-142.

- Simpson, E.S.W. & Dingle, R.V. (1973). Offshore sedimentation basins on the southeastern continental margin of South Africa. In: G. Blant (Ed.). Sedimentary basins of the African coasts, Part 2 south and east coast. Paris, Association of African geological Surveys, 63-67.
- Singh, V. & Dunlevey, J.N. (1997). Mineral Stratigraphy of the Kosi Bay Formation, northern, KwaZulu-Natal. In: Robinson, R.E. (Ed.), Heavy Minerals 1997, The South African Institute of Mining and Metallurgy, Johannesburg.
- Singh, V. (1995). Mineral stratigraphy of the Kosi Bay Formation. M.Sc. thesis (unpubl.), University of Westville, Durban, 171pp.
- South African Committee for Stratigraphy (SACS) (1980). Stratigraphy of South Africa, Part 1 (comp. L.E. Kent). Lithostratigraphy of the Republic of South Africa, South West Africa / Namibia, and the Republics of Bophuthatswana, Transkei and Venda. *Geol. Surv. S. Afr.*, **8**, 690 pp.
- Stewart, J. (1998). The geology of the Uloa Formation, Richards Bay. B.Sc. Hon. thesis, University of Natal, Durban, unpublished.
- Strahler, A.H. & Strahler, A.N. (1992). Modern physical geography. John Wiley et Sons Inc., New York, fourth edition.
- Sudan, P., Whitmore, G.P. and Uken, R. (1999). Geomorphological, mineralogical and geochemical characterization of the northern KwaZulu-Natal coastal dune cordon. *Heavy Minerals 1999. Johannesburg, South African Institute of Mining and Metallurgy, 1999.*
- Swart, D.H. (1980). Effect of the Richards Bay harbor development on the adjacent coastline. *CSIR Rep. T/SEA 8015, Stellenbosch.* 40pp.
- Tankard, A.J., Jackson, M.R.A., Eriksson, K.A., Hobday, D.K., Hunter, D.R. and Minter, W.E.L. (1982). Crustal evolution of Southern Africa. *Springer-Verlag, New York*, 523 pp.
- Tavener-Smith, R., Cooper, J.A.G. and Rayner, R.J. (1988). Depositional environments in the Volkrust Formation (Permian) in the Mhlatuze River, Zululand. *S. Afr. J. Geol.*, **91**, 198-206.
- The Air Survey company of Africa limited. Air Survey house, 225 Umbilo Rd, Durban, 4001.
- Thomas, R.J. (1988). Geology of the Port Shepstone area. *Expl. Sheet 3030 (Port Shepstone), Geol. Surv. S. Afr.*, 136 pp.
- Thomas, R.J. (1989). A tale of two tectonic terranes. *S. Afr. J. Geol*, **92**, 306-321.
- Thompson, C.H. (1983). Development and weathering of large parabolic dunes systems along the subtropical coast of eastern Australia. *Z. Geomorph. Supp. Bd.* **45**, 205-225.
- Tinley, K.L. & Van Riet, W.F. (1981). Tongaland: Zonal ecology and rural land use proposals. *Dept. of Cooperation and Development contracted study for the KwaZulu Govt.* 186 pp.
- Tinley, K.L. (1985). Coastal dunes of South Africa. *South African National Scientific Programmes*, **9**. 300 pp.
- Tyson P.D. (1986). Climatic change and variability in Southern Africa. *Oxford University Press, Cap Town*, 220 pp.
- Van Heerden, I.L. & Swart, D.H. (1986). An assessment of past and present geomorphological and sedimentary processes operative in the St.-Lucia estuary and environs. *Marine Geoscience and sediment Dynamics Division, National Research Institute for Oceanology, CSIR Research Report*, **569**.
- Visher, G.S. (1969). Grain size distributions and depositional processes. *J. Sed. Petrol.*, **39**, 1074-1106.
- Walker, T.R. (1967). Formation of red beds in modern and ancient deserts. *Geol. Soc. Am. Bull.*, **78**, 353-368.
- Ware, C. Mineralogy and composition of the fine fraction of the Zulti North mineral lease, northern KwaZulu-Natal, South Africa. *MSc thesis, University of Natal, Durban, in prep.*
- Watkeys, M.K., Mason, T.R. and Goodman, P.S. (1993). The role of geology in the development of Maputaland, South Africa. *J. Afr. Earth. Sci.*, **16** (1/2), 205-221.
- Weisser, P.J. & Marques, F. (1979). Gross vegetation changes in the dune area between Richards Bay and the Mfolozi River, 1937 – 1974. *Bothalia* **12**, **4**, 711-721.

- Whitmore, G.P., Uken, R. and Meth, D.L. (1999). KwaZulu-Natal: 3500 million years of geological history. *Geology Education Museum, University of Natal, Durban*. 8 pages with colour figures.
- Whitmore, G.P., Clarke, R.J., Uken, R. and Sudan, P. (1999). Internal structure of part of the Zululand coastal dune cordon from heavy mineral abundance ratios. *Heavy Minerals 1999. Johannesburg, South African Institute of Mining and Metallurgy, 1999*.
- Wolmarans, L.G. & Du Preez, J.W. (1986). The geology of the St Lucia area. *Geological Survey, Expl. Sheet 27 ½ 32, Government Printer, Pretoria*, 42 pp.
- Woodborne, S. & Collett, G.M. (1999). Luminescence dates for the Zululand dune cordon, Richards Bay, KwaZulu-Natal, South Africa. *In: Sudan, P. Sedimentology, stratigraphy and geological evolution of part of the northern KwaZulu-Natal dune cordon, South Africa. MSc thesis (unpublished), University of Natal, Durban*.
- Woodborne S. Quaternary Dating Research Unit, Environmentek, CSIR. P.O. Box 395, 0001 Pretoria.
- Wright, C.I. (1999). The Cenozoic evolution of the northern KwaZulu-Natal coastal plain, South Africa. *PhD thesis (unpubl.), University of Natal, Durban*. 255 pp.

## **APPENDIX A**

Luminescence dating: RBM 1 and RBM 2 samples

**LUMINESCENCE DATES FOR THE  
ZULULAND DUNE CORDON,  
RICHARDS BAY, KWAZULU-  
NATAL, SOUTH AFRICA.**

STEPHAN WOODBORNE & GILL COLLETT

QUATERNARY DATING RESEARCH UNIT,  
ENVIRONMENTEK  
CSIR

July 1999

**Terms of reference**

The coastal foreland between Richards Bay and St. Lucia on the Zululand coast of Kwazulu-Natal is part of a mining concession held by TISAND (PTY) LIMITED and RICHARDS BAY IRON & TITANIUM (PTY) LIMITED. Geological research on these dunes is being conducted by Mr. Pascal Sudan on behalf of TISAND (PTY) LIMITED and RICHARDS BAY IRON & TITANIUM (PTY) LIMITED. The dating results that are presented in this report were commissioned by Dr. Greg Whitmore of the University of Natal on behalf of Mr. Sudan. The results are subject to a confidentiality agreement between the CSIR and Tisand, and will not be made available by the CSIR to any parties other than Mr. Sudan and Dr. Whitmore at the University of Natal. The CSIR is not obliged to share the results with TISAND (PTY) LIMITED and RICHARDS BAY IRON & TITANIUM (PTY) LIMITED, and any disclosure will be made by Mr. Sudan and Dr. Whitmore in terms of the contractual relationship between TISAND (PTY) LIMITED and RICHARDS BAY IRON & TITANIUM (PTY) LIMITED and the University of Natal and its representatives.

## Introduction

The luminescence dating method is well suited to dating coastal dune formation. The method is based on the accumulation of crystalline damage caused by radiation from trace levels of radio active uranium, thorium and potassium that naturally occur in the minerals that make up the sediment, as well as a constant bombardment by cosmic radiation. The damage is annealed when the sediment is exposed to sufficient heat or light. When the damage is annealed the sand grains release energy in the form of light that is known as *luminescence*. It is normally assumed that coastal dunes are of aeolian origin and the process of wind transport exposes the sand grains to sufficient sunlight to zero the luminescence signal. Once the dune has formed the buried sand grains gradually begin to accumulate the radiation damage. The radiation dose that is absorbed by the sand grains is known as the *Equivalent Dose* ( $D_E$ ). The date of the last exposure to light can be determined by measuring the radiation dose rate in the dune, and comparing the radiation sensitivity of the minerals with the equivalent dose.

There are several prerequisites that underlie the luminescence dating technique. First it is necessary that the radiation dose rate remains constant throughout the entire time that the sediment is buried in the dune. Under certain conditions the radioactive elements that contribute to the radiation dose rate can be mobilised and moved into, or out of the dune. Changes in dose rate can be accommodated by the luminescence dating method if two different minerals can be analysed. This has been demonstrated using potassium feldspars and quartz grains of the same size (Vogel *et al.* In press). Pure quartz contains no internal radioactive elements and is irradiated by sources outside of the grains, while feldspars are irradiated by the same external sources, in addition to internal radiation from radioactive potassium-40. By subtracting the  $D_E$  value of the quartz from the  $D_E$  value of the feldspars the luminescence signal derived from the potassium-40 is isolated. The date is then based on the dose rate from the potassium-40 in the feldspar which remains constant through time.

The second prerequisite for successful luminescence dating, and the subtraction dating method in particular, is adequate zeroing of the luminescence signal at the time of deposition. The luminescence signal in quartz grains is stimulated by heat and is called thermoluminescence (TL). The luminescence signal in feldspars can also be stimulated by heat, but it can also be stimulated by exposure to infrared light. The latter technique is called infrared stimulated luminescence (IRSL). The thermodynamic qualities of the IRSL and TL signals differ, in particular the IRSL signal is rapidly zeroed after minutes of exposure to sunlight while the TL signal requires several days of exposure. In the case of insufficient zeroing any residual luminescence in the minerals invalidates the subtraction dating method, while making the TL and IRSL dates overestimations of the true age of the sediment.

The third prerequisite for accurate luminescence dating is that the sensitivity of the minerals to radiation remains consistent through the course of the analysis.

**Table 1:** Coastal dune sand from the Zululand coast submitted for luminescence dating.

Lab no.	Sample Name	Description
C 6569	RBM 1	Inland dune
C 6570	RBM 2	Coastal dune - Dawsons Rock

Two dunes between Richards Bay and St. Lucia on the Zululand coast were sampled for luminescence dating under the direction of Mr. Pascal Sudan. The context of these dunes is presented in table 1. The samples were subjected to standard IRSL and TL analyses with the objective of calculating a subtraction date for each of the samples.

## Method

The samples were pre-treated using routine procedures for IRSL and TL analyses:

- Carbonates were removed from the bulk material by boiling in concentrated acid (HCl), and organic contaminants were extracted with alkali (3% NaOH).
- The remaining material was sieved to isolate the 250-300 $\mu$ m size fraction and then subjected to a

magnetic separation to reject the magnetic and metallic grains.

- The IRSL analysis was conducted on feldspar grains that were isolated on the basis of their density. A 2.58 SG solution was used to float off the high potassium feldspars.
- A single aliquot regeneration method was used to determine the IRSL  $D_E$  value. Compensation for accumulative effects of radiation and the associated measurement protocol were made according to the approach presented by Duller (1991).
- The TL analysis was conducted on quartz grains that were isolated using a 2.62 SG solution to float off the non-quartz minerals.
- A multiple aliquot regeneration method was used to determine the TL  $D_E$  value.
- The ambient radiation dose rate in the sediments were established by thick source alpha detection on untreated sediment to determine the uranium and thorium concentrations. This approach assumes that the daughter products of these radioactive elements are in secular equilibrium.
- An estimated value for the cosmic radiation contribution was used. The value of  $180 \pm 10 \mu\text{Gy/a}$  corresponds to an average of 2m of overlying sediment since the sample was deposited.
- The potassium content of the sample was measured by X-ray fluorescence analysis.
- The average water content in the sediment since deposition is likely to have varied considerably, and an estimated value of  $8 \pm 4 \%$  is assumed to have an appropriate level of precision.

## Results

The results of the IRSL analyses are presented in figure 1 a-c and in table 2. Figure 1a presents the growth curve for RBM1 and figure 1b presents the growth curve for RBM2. In these illustrations the growth curves represents 5 aliquots and 6 aliquots respectively. The regeneration points for each aliquot have been standardised by a factor that normalises the natural luminescence of all of the aliquots. In both RBM1 and RBM2 the relationship between dose and IRSL approximates linearity as might be expected for such low radiation doses. When the  $D_E$  value for each aliquot is plotted against the natural IRSL (figure 1c) the subtle deviations from linearity become apparent. In the case of RBM1 the plot shows a linear trend while the RBM2 aliquots cluster tightly. A linear trend in a  $D_E$  vs. natural IRSL plot suggests that the sample was not adequately zeroed. Each aliquot reflects a different average degree of zeroing; the greater the zeroing the smaller the IRSL signal and the smaller the  $D_E$  value. This may partly explain the trend in the RBM2 data, but the fact that the trend does not match the apparent sensitivity of the samples (stippled line figure 1c) indicates that the different aliquots may also present slightly different levels of sensitivity to radiation.

The results of the TL analyses are presented in figures 2a-c, 3a-d, and in table 2. The TL glow curves for RBM1 (figure 2a) show peaks at 325 °C and 375 °C that are typical of quartz. Each of the regeneration curves and the natural curve presented in figure 2a is the average of 5 measurements. The ratio between the regeneration curves and the natural curve provides an acceptable plateau in the region 300 - 400 °C (figure 2b). The curves were integrated in this range to produce the regeneration curve in figure 2c. Each point in the regeneration curve represents the integrated values for the 5 measurements that were made for each laboratory dose. The resulting growth curve for RBM1 is slightly sub-linear with good inter aliquot reproducibility.

The average TL glow curves for RBM2 are presented in figure 3a. As was the case for RBM1 each of the regeneration curves is the average of 5 measurements. However the natural glow curve (in bold) has a different shape from that of the regeneration curves resulting in a stepped plateau (figure 3b). The dose required to regenerate the 325 °C peak was less than that required to regenerate the 375 °C peak. The two peaks are thermodynamically different, and the 325 °C peak is more rapidly bleached than the 375 °C peak. Consequently it is possible that a residual luminescence signal remains in the corresponding luminescence trap if insufficient zeroing occurred at the time of deposition. The glow curves and plateaux demonstrate that this has occurred and the different regions of the glow curves have been integrated separately (320-340 °C and 360-390 °C) to produce two different growth curves (figures 3c and 3d). The two growth curves yield slightly different  $D_E$  values of 5.11 Gy and 6.06 Gy indicating a small residual signal in the 375 °C peak.

**Table 2: Results of the IRSL and TL dating analysis of the Zululand dune samples.**

	<b>RBM 1 IRSL</b>	<b>RBM 1 TL</b>	<b>RBM 2 IRSL</b>	<b>RBM 2 (325° TL)</b>	<b>RBM 2 (375° TL)</b>
<b>BULK SAND</b>					
%K	0.23 ± 0.01	0.23 ± 0.01	0.20 ± 0.01	0.20 ± 0.01	0.20 ± 0.01
ppm Th	4.24 ± 0.66	4.24 ± 0.66	2.47 ± 0.05	2.47 ± 0.05	2.47 ± 0.05
ppm U	1.09 ± 0.17	1.09 ± 0.17	1.25 ± 0.03	1.25 ± 0.03	1.25 ± 0.03
% Water	8 ± 4	8 ± 4	8 ± 4	8 ± 4	8 ± 4
<b>GRAINS</b>					
Grain size (µm)	274 ± 25	274 ± 25	274 ± 25	274 ± 25	274 ± 25
Density	<2.58	<2.58	<2.58	<2.58	<2.58
Magnetic separation	Yes	Yes	Yes	Yes	Yes
Etch	0µm	0µm	0µm	0µm	0µm
<b>DOSE RATE (µGy/a)</b>					
Gamma+Cosmic	534 ± 43	534 ± 41	460 ± 21	460 ± 18	460 ± 18
Alpha	49 ± 12	47 ± 12	41 ± 9	39 ± 9	39 ± 9
Beta	1 186 ± 81	356 ± 30	1 146 ± 109	317 ± 19	317 ± 19
Total	1 769 ± 108	937 ± 76	1 648 ± 109	816 ± 38	816 ± 38
<b>EQUIVALENT DOSE (Gy)</b>					
Regeneration	11.5 ± 0.3	12.0 ± 1.7	3.5 ± 0.1	5.1 ± 1.0	6.1 ± 2.1
<b>AGE (a)</b>	<b>6 500 ± 450</b>	<b>12 800 ± 2 100</b>	<b>2 100 ± 142</b>	<b>6 300 ± 1 300</b>	<b>7 400 ± 2 600</b>

In the case of RBM1 the IRSL data suggest inadequate zeroing of the luminescence signal, while the TL plateaux do not, and in RBM2 the TL plateaux suggest inadequate zeroing while the IRSL data does not. The apparent confusion can be understood in terms of the extent of sunlight exposure that each sample received. The RBM1 sample was briefly exposed to sufficient sunlight to affect the IRSL signal, but not enough to affect the TL signal. This would occur if the sediment were rapidly remodelled and in the process the sunlight exposure was in the order of minutes. This might occur if the remodelling were in the form of a landslide or some other similar mechanism. In this scenario the TL date would be older than the IRSL date and it would reflect the original date of dune formation. The IRSL date would reflect the date at which the dune was remodelled. The difference between resulting IRSL and TL dates for RBM1 confirm that inadequate zeroing occurred in this sample.

In the case of RBM2 the sediment must have been exposed to more sunlight than RBM1; enough to zero the IRSL signal but still not sufficient to zero the TL signal. This would happen if the remodelling of the dune resulted in approximately 1 day of sunlight exposure. In this scenario the TL date will underestimate the original deposition of the dune, while the IRSL date will accurately reflect the age of the remodelling.

In both RBM1 and RBM2 the evidence for inadequate zeroing implies that the subtraction dating method could not be applied.

## Conclusions

Since it was not possible to calculate a subtraction date for either of the samples the stability of the dose rate in the Zululand dunes could not be tested. In instances such as this where the samples are relatively young, it is reasonable to assume that the impact of dose rate changes on the final dates would be negligible. The IRSL results from RBM1 suggest that the sample comprises minerals with slightly different sensitivities. There is no way to establish with the available data whether the sensitivity changed in the course of the analysis. To demonstrate this would require a repeat of the analyses using the additive technique. The expense of this exercise is unwarranted because the impact on the final results is unlikely to be significant.

The IRSL date for RBM1 is  $6\,500 \pm 450$  and the TL date is  $12\,800 \pm 2\,100$ . Besides the evidence presented earlier this discrepancy in itself is clearly indicative of inadequate zeroing. The evidence suggests that a very rapid partial bleaching event that removed the equivalent of 50% of the present IRSL signal took place in the last 6 500 years. The original date of deposition of this dune is probably close to 12 800 years ago.

The IRSL date for RBM2 is  $2\,100 \pm 150$  and the TL dates are  $6\,300 \pm 1\,300$  (325 °C peak) and  $7\,400 \pm 2\,600$  (375 °C peak). As is the case for RBM1 this discrepancy supports the earlier evidence that the luminescence signal was not completely zeroed. In this instance a slightly longer period of sunlight exposure is implied, and it can be assumed that the dune was remodelled approximately 2 100 years ago. The original deposition of the dune took place shortly before 7 400 years ago.

The reasons for the partial bleaching of the sediments are not clear. A likely scenario relates to vegetation changes that may have taken place following the mid-Holocene high sea level. It is possible that a brief period of climatic upheaval may have affected the vegetation that currently stabilises the dunes. A single event approximately 2 100 years ago might account for the remobilisation of both of the dunes under consideration, although the possibility of multiple mobilisation events cannot be discounted.

## References

- Duller, G.A.T. (1991). Equivalent dose determination using single aliquots. *Nuclear Tracks and Radiation Measurements* **18**, 371-378.
- Vogel, J.C., Wintle, A. & Woodborne, S. (In press). Luminescence dating of coastal sands: overcoming changes in environmental dose rate. *Journal of Archaeological Science*.

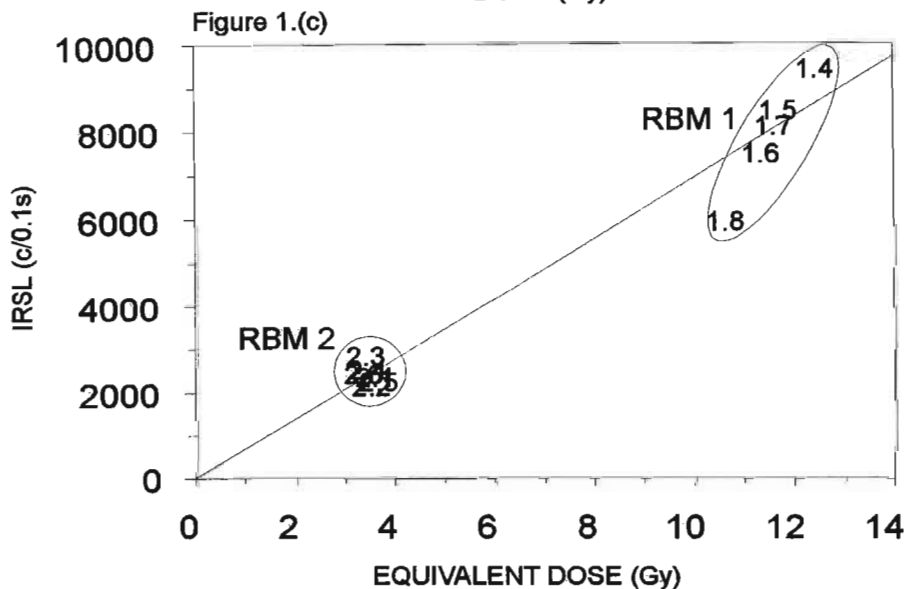
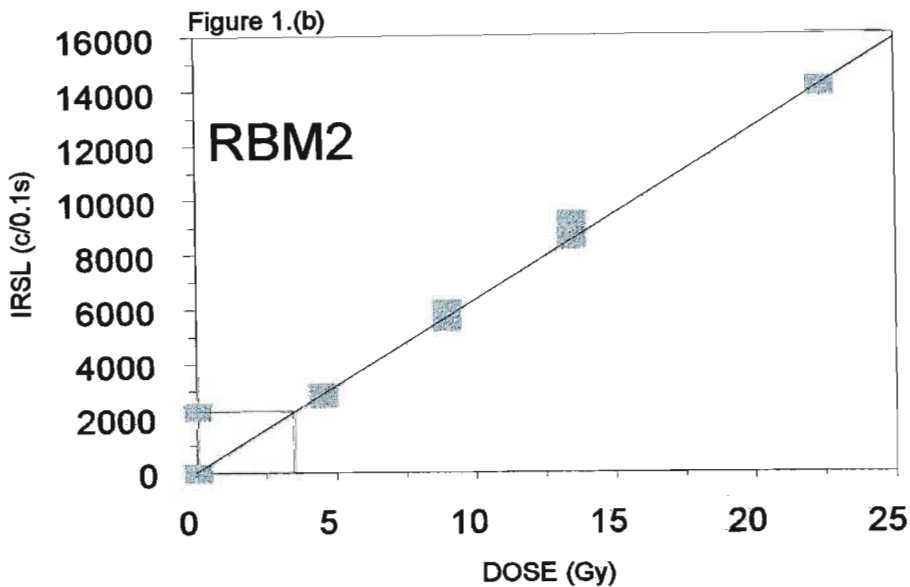
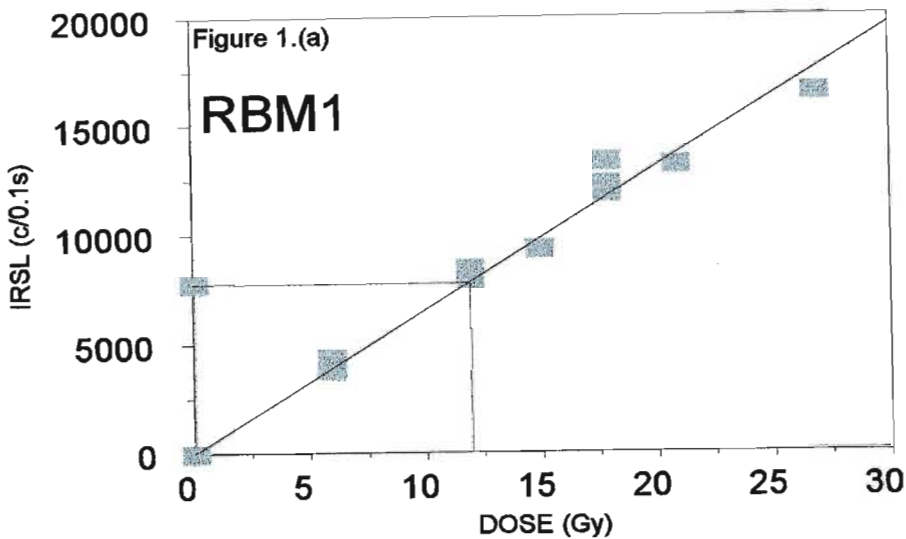


Figure 1. Single disk regeneration infrared stimulated luminescence (IRSL) analysis of samples RBM 1(a) and RBM 2 (b) from Zululand. The values for 5 (RBM1) and 6 (RBM2) aliquots are natural normalised demonstrating a high degree of reproducibility. The inter-aliquot variability is minimal for RBM2, but is linearly related to DE in RBM1 (c). The deviation from the natural sensitivity of the samples (stippled line) indicates a degree of inadequate bleaching and a variability in inter-aliquot sensitivity for RBM1.

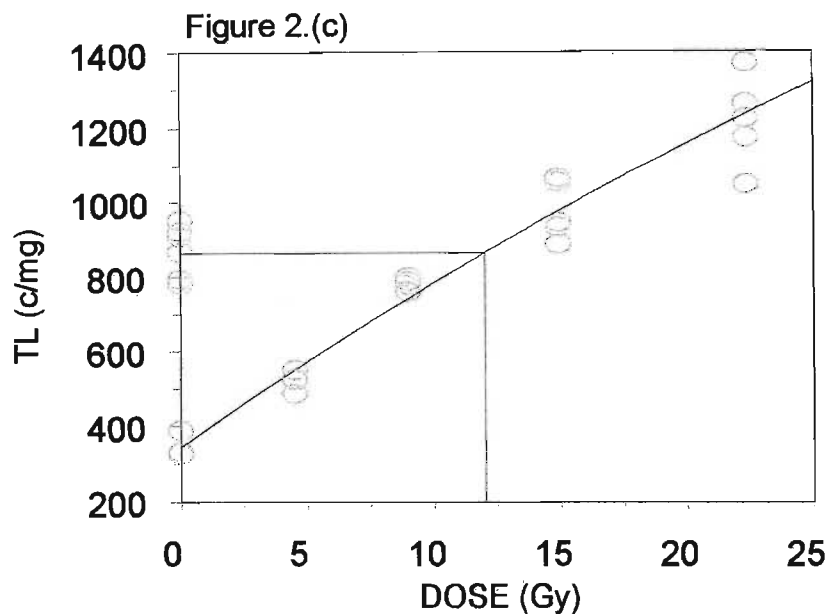
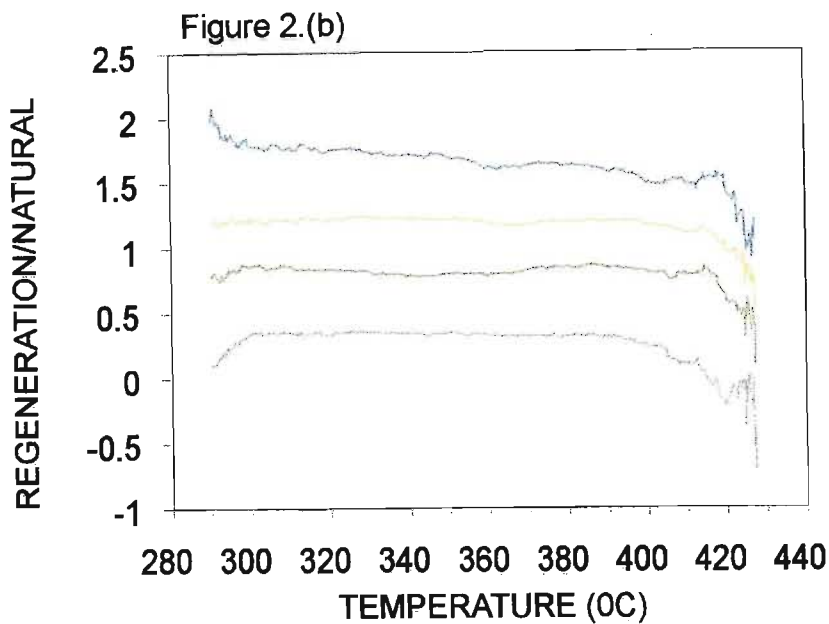
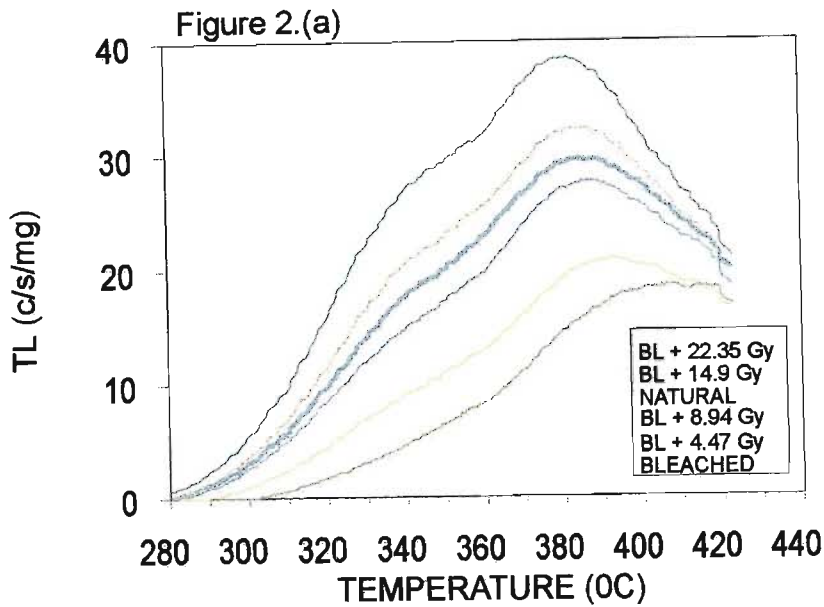


Figure 2. Thermoluminescence (TL ) analysis of sample RBM1 from the Zululand coast. The regeneration glow curves (a) produce adequate plateaux in the region 300-400 oC (b). Integration in this range produced a slightly sub-linear growth curve (c).

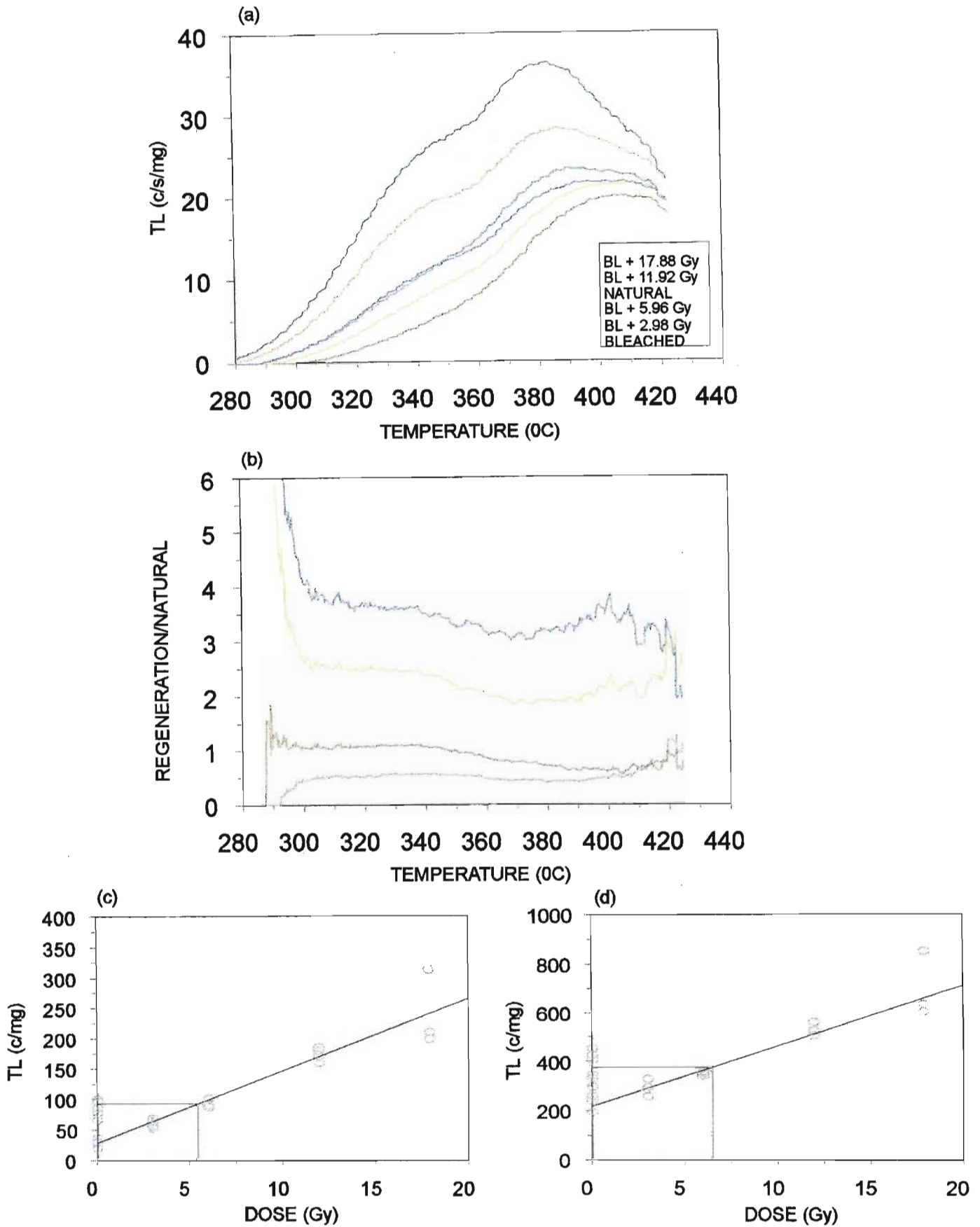


Figure 3. Thermoluminescence (TL ) analysis of sample RBM2 from the Zululand coast. The regeneration glow curves (a) produced a stepped plateaux (b). Integration in the range 320-340 oC corresponding to the 325 oC peak, and 360-390 oC, corresponding to the 375 oC peak, to produce growth curves (c, d) yielded slightly different DE values.

## **APPENDIX B**

Geochemical data: Lines 380 and 1200, and foredune samples

**Borehole S3 (380/M/1)**

**MAJOR ELEMENT COMPOSITIONS - WEIGHT PERCENT**

**+ Foredunes**

sample	SiO <sub>2</sub>	Al <sub>2</sub> O <sub>3</sub>	Fe <sub>2</sub> O <sub>3</sub>	MnO	MgO	CaO	Na <sub>2</sub> O	K <sub>2</sub> O	TiO <sub>2</sub>	P <sub>2</sub> O <sub>5</sub>	TOTAL	L.O.I.
69	82.7	2.82	4.3	0.0785	1.84	5.11	0.52	0.43	1.7144	0.1	99.6	2.93
63	83.63	2.63	3.35	0.0552	1.64	6.52	0.4	0.42	1.0517	0.1	99.81	4.2
57	81.06	2.79	4.64	0.0892	1.92	6.35	0.41	0.42	1.923	0.1	99.69	3.83
51	86.34	2.48	2.31	0.0432	1.26	5.45	0.46	0.47	0.6163	0.08	99.51	3.71
45	87.8	2.46	2.28	0.0393	1	4.19	0.56	0.49	0.7369	0.07	99.61	2.92
39	88.95	2.42	1.49	0.025	0.71	4.41	0.57	0.59	0.4063	0.06	99.64	3.35
33	87.91	2.82	2.45	0.0483	0.78	3.6	0.55	0.62	0.8912	0.07	99.73	2.93
27	90.25	3.18	2.14	0.0351	0.53	1.25	0.62	0.78	0.6653	0.13	99.58	1.26
21	92.36	2.97	1.35	0.0193	0.31	0.5	0.53	0.81	0.327	0.1	99.28	0.91
15	91.41	3.57	1.2	0.0178	0.37	0.91	0.69	1.06	0.2076	0.09	99.54	1.2
3	94.6	1.9	1.25	0.0208	0.16	0.12	0.27	0.59	0.6068	0.02	99.54	0.48
-3	82.43	2.39	7.47	0.1509	0.38	0.76	0.23	0.44	4.6464	0.01	98.9	0.58
F-dune 2	81.91	3.16	4.59	0.1019	1.37	4.99	0.59	0.58	2.0979	0.04	99.44	3.1
F-dune 4	83.56	2.75	5.14	0.1173	0.97	2.76	0.48	0.55	2.8973	0	99.23	1.67

**TRACE ELEMENT COMPOSITIONS - PPM**

sample	Nb	Y	Rb	Zr	Sr	U	Th	Cr	V	La	Zn
69	19.2	24.4	12.4	1204	175.3	2	9.5	221	117.7	8.3	24.2
63	12.3	17.1	13	806.3	236.2	4	7.7	156.8	84.1	7.1	19.6
57	22.8	27.3	12	1630.7	222.6	3.8	9.4	241.9	122.1	9.2	25.2
51	7.6	14.5	12.8	472.9	207.1	1.6	4	134.9	60.1	0.9	14.8
45	9.1	14.7	14.1	706.2	168.4	2.9	6.3	120.4	57.2	8.8	15.4
39	5.1	10.2	16.5	344.4	186.8	2.8	3.9	58.4	37.5	1.4	9.2
33	10.7	15.4	17.4	817.6	161.9	3.2	4.9	111.7	58.4	2.5	16.2
27	4.9	8.9	23.8	313.1	68.7	2.5	3.3	48.5	32.9	3.6	12.1
21	3.1	7.9	29	173.6	87	1.6	2.9	47.1	25.7	0	9.4
15	3.3	8.3	29.4	169.3	89	1.8	2.9	56.7	27.1	0	10.7
3	8.9	10.5	16.8	603.8	37.9	1.7	4.8	51.5	35.4	1.2	10
-3	59.6	55	13.1	5314.5	59.3	5.6	31.6	511.7	195.4	39	40.1
F-dune 2	26.1	25.2	16.4	1612.5	185.4	3.3	16.0	237.8	104.7	16.7	26.8
F-dune 4	37.1	35.8	15.0	3165.4	126.6	0.6	19.1	377.3	126.5	30.6	27.9

**TRACE ELEMENT COMPOSITIONS - PPM**

sample	Cu	Ni	Ba	Sc	S	Pb	Ga	Co	Ce	Nd	As
69	0	17.1	106.1	15.6	211	0.9	1.7	130	20.8	9.7	4.2
63	0	12.5	81.2	12	310	10.4	1.4	139.5	15	3.4	3
57	0	17.7	89.3	17.1	310	2.4	2.4	126.5	37.2	12.7	5.1
51	0	10.4	122.7	9.6	282	7.4	2.5	142.4	15.2	5.9	3.4
45	0	8.8	114.9	6.3	228	4.6	0	209	13.8	4.8	4.9
39	0	4.9	139	6.8	209	1.3	1.7	167.5	16.7	2.8	2
33	0	10.1	172	8.3	213	4.8	0.3	139.5	29	12	3.4
27	0	7.6	214.8	5.8	65	6.3	0.9	302	14.7	0	3
21	0	4.5	304.5	4	52	8.8	2.4	224.3	8.7	0.3	2.2
15	0	5.1	292.6	5.2	62	6.3	3.1	226.8	3.4	0	3.5
3	0	3.5	153.1	4	45	0	0	233.7	18.3	0.1	0.7
-3	0	12.2	113.6	18.9	56	0.9	0.8	155.5	96.3	42.1	8.5
F-dune 2	2.4	21.3	148.5	11.8	243.0	4.6	2.5	119.1	55.9	24.6	6.1
F-dune 4	0.7	14.9	154.5	12.6	178.0	12.1	1.6	114.1	68.8	28.2	7.5

sample	*10E4	*10E3	*10E2	Nb/Ti	Cr/Ti	Th/Zr	*10E6	*10E3	Ni/Ti	Y/Nb	(Ce+La)	
	Ti/Zr	Nb/Zr	Ti/Nb				P/Zr	P/Ti				V/Ti
69	14.239	15.947	8.9292	11.1993	128.91	0.01	83.06	58.329	68.654	9.974	1.2708	0.024
63	13.044	15.255	8.5504	11.6954	149.09	0.01	124	95.084	79.966	11.89	1.3902	0.027
57	11.792	13.982	8.4342	11.8565	125.79	0.01	61.32	52.002	63.495	9.204	1.1974	0.028
51	13.032	16.071	8.1092	12.3317	218.89	0.01	169.2	129.81	97.517	16.87	1.9079	0.034
45	10.435	12.886	8.0978	12.349	163.39	0.01	99.12	94.993	77.622	11.94	1.6154	0.032
39	11.797	14.808	7.9667	12.5523	143.74	0.01	174.2	147.67	92.296	12.06	2	0.053
33	10.9	13.087	8.329	12.0063	125.34	0.01	85.62	78.546	65.53	11.33	1.4393	0.039
27	21.249	15.65	13.578	7.3651	72.899	0.01	415.2	195.4	49.451	11.42	1.8163	0.058
21	18.836	17.857	10.548	9.48012	144.04	0.02	576	305.81	78.593	13.76	2.5484	0.05
15	12.262	19.492	6.2909	15.896	273.12	0.02	531.6	433.53	130.54	24.57	2.5152	0.02
3	10.05	14.74	6.818	14.6671	84.871	0.01	33.12	32.96	58.339	5.768	1.1798	0.032
-3	8.7429	11.215	7.796	12.8271	110.13	0.01	1.882	2.1522	42.054	2.626	0.9228	0.025
F-dune 2	13.01	16.186	8.0379	12.441	113.35	0.01	24.81	19.067	49.907	10.15	0.9655	0.045
F-dune 4	9.153	11.72	7.8094	12.805	130.22	0.01	0	0	43.661	5.143	0.965	0.031

P = P<sub>2</sub>O<sub>5</sub>      Ti = TiO<sub>2</sub>

ratios are calculated using abundances in weight percent for major elements, in ppm for minor elements. This ratio is then multiplied by a factor given on top of each ratio column (see above)

**Borehole S2 (380/G/1)**

**MAJOR ELEMENT COMPOSITIONS - WEIGHT PERCENT**

bottle number	sample	SiO2	Al2O3	Fe2O3	MnO	MgO	CaO	Na2O	K2O	TiO2	P2O5	TOTAL	L.O.I.
1G	63	90.17	2.44	2.87	0.061	0.59	1.2	0.41	0.57	1.0066	0.06	99.37	1.07
2G	57	86.86	2.45	2.95	0.06	0.89	4.39	0.35	0.52	0.8607	0.08	99.42	2.84
3G	51	88.72	2.26	2.46	0.048	0.61	3.9	0.32	0.53	0.6747	0.06	99.59	2.73
4G	45	89.76	2.18	2.64	0.052	0.34	2.89	0.41	0.6	0.7803	0.04	99.7	2.2
5G	39	90.65	2.07	2.35	0.049	0.31	2.64	0.39	0.58	0.552	0.04	99.63	2.09
6G	33	89.3	2.13	3.01	0.058	0.41	2.44	0.26	0.52	1.1605	0.04	99.32	1.85
7G	27	90.4	2.1	2.42	0.043	0.27	2.83	0.36	0.62	0.6997	0.04	99.78	2.35
8G	21	92.39	1.86	1.83	0.034	0.16	1.73	0.18	0.63	0.3723	0.02	99.19	1.41
9G	15	92.77	1.76	2.41	0.05	0.09	0.91	0.3	0.57	0.8372	0.02	99.73	0.82
10G	9	87.24	2.11	5.13	0.115	0.26	1.32	0.24	0.47	2.4367	0.02	99.34	1.49
11G	3	86.74	2.27	5.59	0.121	0.24	0.94	0.16	0.42	2.5876	0.02	99.08	1.26
12G	-3	77.84	2.42	9.59	0.203	0.38	1.01	0.19	0.37	5.9345	0	97.94	1.27

**TRACE ELEMENT COMPOSITIONS - PPM**

bottle number	sample	Nb	Y	Rb	Zr	Sr	U	Th	Zn	Cu	Ni	S
1G	63	11.6	16.8	16.7	840.3	62	0.3	6.3	18.5	15.8	11.6	57
2G	57	9.7	16.6	15.1	682	159.9	2	5.4	17.5	38.5	13.6	192
3G	51	7.8	13.9	15	551.8	150	2.1	3.4	13.7	19.1	11.4	154
4G	45	10	14.6	17.1	868.6	124	1.4	4.5	13.6	16.6	9.9	94
5G	39	7.4	12	15.8	615.7	111.5	0	3	12.8	26.5	10.5	87
6G	33	14.8	17.2	15.7	1250	105.2	1	5.9	16.9	16.7	12.4	78
7G	27	10.3	13.1	18.6	822.3	119	1.3	7.3	13	17.3	9.7	105
8G	21	6	8.8	16.7	426	84.1	0.7	1.3	12.1	30.8	8.2	25
9G	15	11	12.9	15.4	1014	56.5	0	4.4	15.3	23.2	8.5	10
10G	9	34	32.5	12.9	3036	70.8	3.7	11.1	27.8	16.7	15	55
11G	3	35.9	37.3	12.4	3055	60.8	3.1	15.5	34.1	26.5	17.6	76
12G	-3	74.1	61.9	12.1	6195	63.5	4.8	33.7	52.1	14.3	22.4	5259

**TRACE ELEMENT COMPOSITIONS - PPM**

bottle number	sample	Pb	Ga	Co	Ce	Nd	As	Cr	V	La	Ba	Sc
1G	63	5.9	2.1	6.9	20.6	9	7.6	161.9	64.7	0	162.7	8.2
2G	57	5.1	3.2	7.8	13.6	3	9.6	175.5	61	0	118.8	8.9
3G	51	5.7	3	4.5	0	0	4.5	131.2	45.9	0	130	6.5
4G	45	4.4	2.5	5.6	7.9	0.7	6	146.1	51.5	0	147.6	5
5G	39	5	2.3	5.8	0	0	8.1	126.5	38.7	0	140.4	4.3
6G	33	4.6	0.9	4.8	28.7	9.2	7.5	153.9	65.5	0	125.5	7.6
7G	27	6.9	3.1	5.3	16	4.7	6	126.2	45.5	0	157.9	5.2
8G	21	3	3.3	5.3	7.2	0.4	8.7	81.8	30.9	0	147.1	3.1
9G	15	6.9	0.8	4.2	21.3	6.4	2.6	155.8	44.3	0	141.8	3.9
10G	9	6.7	2.4	5.9	44.9	17.5	11.2	339.9	120.2	2.3	120.5	11.1
11G	3	3.6	2.4	8.2	46.4	18.9	14	417.2	133.9	17.3	115.3	15
12G	-3	5.3	0	9.3	104	47.4	17.1	516.7	249	42.5	105.3	20.9

bottle number	sample	*10E4	*10E3	*10E2	Y/Nb	Nb/Ti	Cr/Ti	Th/Zr	*10E6	(Ce+La)/Zr	*10E3	V/Ti	Ni/Ti
		Ti/Zr	Nb/Zr	Ti/Nb					P/Zr		P/Ti		
1G	63	11.979	13.805	8.6776	1.448	11.524	160.84	0.0075	71.403	0.024515	59.607	64.276	11.524
2G	57	12.62	14.223	8.8732	1.711	11.27	203.9	0.0079	117.3	0.019941	92.948	70.873	15.801
3G	51	12.227	14.136	8.65	1.782	11.561	194.46	0.0062	108.74	0	88.928	68.03	16.896
4G	45	8.9834	11.513	7.803	1.46	12.816	187.24	0.0052	46.051	0.009095	51.262	66	12.687
5G	39	8.9654	12.019	7.4595	1.622	13.406	229.17	0.0049	64.967	0	72.464	70.109	19.022
6G	33	9.2833	11.839	7.8412	1.162	12.753	132.62	0.0047	31.997	0.022958	34.468	56.441	10.685
7G	27	8.5091	12.526	6.7932	1.272	14.721	180.36	0.0089	48.644	0.019458	57.167	65.028	13.863
8G	21	8.7394	14.085	6.205	1.467	16.116	219.72	0.0031	46.948	0.016901	53.72	82.998	22.025
9G	15	8.2605	10.853	7.6109	1.173	13.139	186.1	0.0043	19.734	0.021016	23.889	52.914	10.153
10G	9	8.0271	11.2	7.1688	0.956	13.953	139.49	0.0037	6.5885	0.015549	8.2078	49.329	6.1559
11G	3	8.4692	11.75	7.2078	1.039	13.874	161.23	0.0051	6.546	0.020849	7.7292	51.747	6.8017
12G	-3	9.5789	11.96	8.0088	0.835	12.486	87.067	0.0054	0	0.023647	0	41.958	3.7745

P = P2O5      Ti = TiO2

ratios are calculated using abundances in weight percent for major elements, in ppm for minor elements. This ratio is then multiplied by a factor given on top of each ratio column (see above)

**Borehole S1 (380/B/1)**

**MAJOR ELEMENT COMPOSITIONS - WEIGHT PERCENT**

bottle sample	sample	SiO2	Al2O3	Fe2O3	MnO	MgO	CaO	Na2O	K2O	TiO2	P2O5	TOTAL	L.O.I.
1B	89	87.87	2.18	4.48	0.087	0.26	0.88	0.21	0.62	2.4123	0.01	98.8	0.57
2B	83	91.75	2.01	2.85	0.052	0.18	0.79	0.29	0.81	1.1274	0.02	99.47	0.61
3B	77	93.14	1.77	1.89	0.039	0.09	0.86	0.18	0.55	0.5798	0.02	99.11	0.86
4B	71	92.82	1.81	1.68	0.03	0.14	1.39	0.31	0.57	0.5884	0.02	99.36	1.19
5B	65	90.92	1.75	2.88	0.056	0.11	1.24	0.32	0.52	1.2194	0.01	99.03	0.91
6B	59	92.39	1.81	2.01	0.038	0.15	1.29	0.23	0.54	0.7076	0.02	99.19	1.05
7B	53	93.22	1.84	1.84	0.031	0.07	1.11	0.32	0.62	0.5027	0.02	99.58	1.2
8B	47	92.84	1.85	2.35	0.044	0.12	1.12	0.23	0.54	0.9822	0.02	99.89	1.04
9B	41	93.18	1.84	1.84	0.037	0.1	0.83	0.26	0.62	0.61	0.02	99.34	0.85
10B	35	93.12	1.94	2.19	0.045	0.12	0.71	0.22	0.66	0.9249	0.02	99.95	0.92
11B	29	91.2	1.93	2.92	0.066	0.16	0.61	0.22	0.53	1.6899	0.01	99.33	0.65
12B	23	87.82	1.82	4.61	0.094	0.16	0.52	0.22	0.48	3.0505	0	98.77	0.5
13B	17	90.66	1.87	3.16	0.064	0.12	0.49	0.2	0.5	1.8115	0	98.87	0.35
14B	11	91.76	1.86	2.73	0.06	0.12	0.52	0.26	0.48	1.4273	0.01	99.22	0.47
15B	5	92.09	1.85	2.69	0.047	0.03	0.29	0.19	0.5	1.5294	0	99.22	0.68
16B	-1	92.48	2.38	2.17	0.032	0.02	0.31	0.28	0.66	0.9186	0.01	99.25	0.74

**TRACE ELEMENT COMPOSITIONS - PPM**

bottle sample	sample	Nb	Y	Rb	Zr	Sr	U	Th	Zn	Cu	Ni
1B	89	29.4	27.2	17.6	2774	58.5	2.3	13.4	20.2	44	12.1
2B	83	14.5	17.3	17.5	1169	53	0.3	5.1	13.2	26.4	9
3B	77	8	10.6	16.1	609.7	51.6	1.5	6.3	20.3	31.4	7.6
4B	71	6.6	10.4	15.9	510.8	68.7	0	3.6	16.5	49.3	6.6
5B	65	17	18.4	14.7	1667	67.6	2.7	7.6	14.1	24	9.8
6B	59	8.4	11	15.1	721.1	67.4	0.7	2.2	10.1	18.9	7.7
7B	53	7	10	16.8	587.9	63.7	1.8	3.1	8.7	17.7	6.9
8B	47	12.1	13.3	15.5	1023	62.1	0.2	6.1	11	20.3	8.3
9B	41	8.5	10.4	17	664	53.4	1.6	4.3	8.6	17	6.7
10B	35	11.8	14.5	17.7	977.9	62	0.8	4	10.3	22.9	7.4
11B	29	19.9	18.3	15.3	1607	46.7	1	6.7	13.1	16.1	6.7
12B	23	36.3	33.2	13.6	3443	44.4	2.6	17.3	19.8	13.1	10
13B	17	24	21	15.3	2046	43.8	2	8.7	14.8	23.2	8.3
14B	11	18.1	17.5	14.3	1544	44	1.2	5.4	13.4	16.1	8.1
15B	5	18.6	18	14.8	1507	34.5	0.7	8	11.2	21.4	7
16B	-1	11.8	14.7	19	947.6	45.2	0	3.9	13.1	36.8	9.9

**TRACE ELEMENT COMPOSITIONS - PPM**

bottle sample	sample	Pb	Ga	Co	Ce	Nd	As	Cr	V	La	Ba	Sc	S
1B	89	12.7	1.3	5.6	58.3	20.2	10.6	266	103.6	8.6	154.2	8.3	37
2B	83	6.3	3	3.8	13.4	0.4	6	157.6	55.2	0.4	157.8	4.8	30
3B	77	6.1	1.2	3.4	6	0	8.7	104.9	34.2	0	158.9	3.9	16
4B	71	8.8	3	2.8	5.5	0.3	1.2	89.1	33.3	0	149.4	3.5	34
5B	65	9.4	0.8	4.2	24.1	4.2	6.7	158.5	59	0	137.4	3.6	21
6B	59	6.3	0.9	5.9	5	0	5.5	99.1	42.7	0	144.5	4.1	23
7B	53	6.7	3	3.3	10.3	0	6	92.3	34.6	0	151.5	3	10
8B	47	0.2	0.6	5.9	21	8.1	6	116.6	49.2	0	143.1	4.7	10
9B	41	5.3	1.6	5.1	17.4	0.3	2.3	90.6	36.1	0	159.8	3.3	0
10B	35	2.1	2.5	4.5	15.3	4.5	1.2	146.3	43.5	0	171.6	4.9	0
11B	29	1.8	0.9	7.3	24.1	5.5	3.1	208.8	68.2	0	134.7	6.3	0
12B	23	9	1.5	5.8	48	12.4	10.5	325.5	119.7	0.7	115.9	8.3	0
13B	17	6.9	2.5	4	9.8	2.7	5.4	208.7	79.7	0	147.2	6.9	0
14B	11	9	1.4	7.5	15.3	3.3	2.8	175.9	59.8	0	128.3	5.6	0
15B	5	7.3	3.9	5.1	21	4.2	7.9	144.6	69.7	0	123.3	6.6	1
16B	-1	5.1	2.4	5.8	16.3	4.2	1.7	138.2	59.2	3.8	173.9	6.4	46

bottle sample	sample	*10E4 Ti/Zr	*10E3 Nb/Zr	*10E2 Ti/Nb	Y/Nb	Nb/Ti	Cr/Ti	Th/Zr	*10E6 P/Zr	*10E3 (Ce+La)/Zr	P/Ti	V/Ti	Ni/Ti
1B	89	8.696	10.599	8.205	0.925	12.188	110.3	0.0048	3.605	0.024118	4.145	42.947	5.016
2B	83	9.647	12.407	7.775	1.193	12.861	139.8	0.0044	17.11	0.011808	17.74	48.962	7.983
3B	77	9.51	13.121	7.248	1.325	13.798	180.9	0.0103	32.8	0.009841	34.49	58.986	13.108
4B	71	11.48	12.921	8.885	1.576	11.255	151.9	0.007	39.15	0.010767	34.11	56.787	11.255
5B	65	7.317	10.201	7.173	1.082	13.941	130	0.0046	6.001	0.014461	8.201	48.384	8.0367
6B	59	9.813	11.649	8.424	1.31	11.871	140.1	0.0031	27.74	0.006934	28.26	60.345	10.882
7B	53	8.551	11.907	7.181	1.429	13.925	183.6	0.0053	34.02	0.01752	39.79	68.828	13.726
8B	47	9.601	11.828	8.117	1.099	12.319	118.7	0.006	19.55	0.020528	20.36	50.092	8.4504
9B	41	9.187	12.801	7.176	1.224	13.934	148.5	0.0065	30.12	0.026205	32.79	59.18	10.984
10B	35	9.458	12.067	7.838	1.229	12.758	158.2	0.0041	20.45	0.015646	21.62	47.032	8.0009
11B	29	10.52	12.385	8.492	0.92	11.776	123.6	0.0042	6.224	0.014999	5.918	40.357	3.9647
12B	23	8.861	10.545	8.404	0.915	11.9	106.7	0.005	0	0.014147	0	39.239	3.2782
13B	17	8.852	11.728	7.548	0.875	13.249	115.2	0.0043	0	0.004789	0	43.997	4.5818
14B	11	9.244	11.722	7.886	0.967	12.681	123.2	0.0035	6.476	0.009909	7.006	41.897	5.6751
15B	5	10.15	12.34	8.223	0.968	12.162	94.55	0.0053	0	0.013932	0	45.573	4.577
16B	-1	9.694	12.453	7.785	1.246	12.846	150.4	0.0041	10.55	0.021211	10.89	64.446	10.777

P = P2O5      Ti = TiO2

ratios are calculated using abundances in weight percent for major elements, in ppm for minor elements. This ratio is then multiplied by a factor given on top of each ratio column (see above)

Line 1200		MAJOR ELEMENT COMPOSITIONS - WEIGHT PERCENT													bottle
Boreholes	Sample	SiO2	Al2O3	Fe2O3	MnO	MgO	CaO	Na2O	K2O	TiO2	P2O5	TOTAL	L.O.I.	Number	
GER 1200/ B	94	88.27	2.17	2.49	0.0417	0.81	3.88	0.28	0.42	0.982	0.04	99.3	2.71	15	
GER 1200/ B	82	89.79	1.94	1.32	0.0147	0.59	4.54	0.4	0.46	0.2899	0.05	98.38	3.57	28	
GER 1200/ B	52	90.17	1.95	1.34	0.0174	0.56	4.08	0.39	0.48	0.2801	0.05	99.32	3.21	57	
GER 1200/ B	34	90.92	2.09	2.88	0.0524	0.18	0.45	0.32	0.49	0.19121	0	99.1	0.66	75	
GER 1200/ B	16	93.59	1.73	2.14	0.0251	0.07	0.18	0.19	0.41	0.9654	0.01	99.33	1.08	94	
GER 1200/ B	10	93.7	2.44	2.37	0.0073	0	0.11	0.07	0.39	0.4508	0.03	99.56	1.84	100	
GEN 1200/ E/1	73	88.6	2.07	1.99	0.0299	0.7	4.66	0.29	0.48	0.7453	0.06	99.59	3.5	15	
GEN 1200/ E/1	61	89.48	1.99	1.32	0.0122	0.56	4.9	0.44	0.5	0.2805	0.05	99.54	3.86	26	
GEN 1200/ E/1	37	95.3	1.51	1.15	0.0149	0.06	0.23	0.24	0.48	0.5897	0	99.58	0.51	50	
GEN 1200/ E/1	19	91.52	1.94	2.98	0.0491	0.09	0.26	0.24	0.47	1.7441	0.01	99.3	1.12	70	
GEN 1200/ E/1	1	91.18	2.49	3.49	0.0399	0.04	0.1	0.12	0.7	1.2184	0.03	99.41	1.18	86	
GEN 1200/ E/1	-5	63.22	3.39	20.23	0.2283	0.16	0.1	0.03	0.29	9.9658	0.12	97.76	2.21	94	
GEN 1200/ E/1	-10	63.05	2.42	20.77	0.2544	0.14	0.3	0.09	0.59	9.7859	0.13	97.52	1.03	98	
GEN 1200/ H/1	40	93.74	1.82	1.8	0.0318	0.17	0.37	0.23	0.48	0.8908	0.01	99.34	0.69	8	
GEN 1200/ H/1	28	94.36	1.75	1.39	0.0242	0.14	0.34	0.23	0.52	0.7435	0.01	99.49	0.88	20	
GEN 1200/ H/1	10	92.15	2.31	2.79	0.0472	0.06	0.22	0.2	0.6	1.4311	0.03	98.83	1.39	40	
GEN 1200/ H/1	4	94.51	2.2	1.23	0.0085	0.01	0.12	0.35	0.76	0.4989	0.01	99.69	1.03	45	
GEN 1200/ H/1	-8	94.07	1.94	1.74	0.0208	0.01	0.03	0.1	0.64	0.7429	0.01	99.31	1.08	56	
GER 1280/ M	98	82.64	3.05	3.81	0.0884	1.59	6.4	0.43	0.54	1.1638	0.05	99.53	4.05	8	
GER 1280/ M	78	78.81	3.02	5.49	0.1214	1.82	6.32	0.31	0.47	2.7184	0.06	99.12	3.73	26	
GER 1280/ M	60	89.89	2.21	1.77	0.0258	0.5	3.32	0.31	0.6	0.6096	0.05	99.28	2.86	45	
GER 1280/ M	48	92.62	1.9	1.64	0.0258	0.28	1.79	0.36	0.46	0.4242	0.05	99.55	1.84	55	
GEN 1200/ BB/1	53	90.68	1.67	3.11	0.0579	0.12	0.34	0.33	0.43	2.3908	0	99.12	0.63	10	
GEN 1200/ BB/1	78	92.71	1.71	2.18	0.0407	0.12	0.4	0.2	0.42	1.4188	0	99.18	0.82	20	
GEN 1200/ BB/1	60	94.31	1.3	1.57	0.0256	0.03	0.02	0.11	0.29	1.6637	0	99.33	0.63	40	
GEN 1200/ BB/1	48	94.92	2.8	0.59	0.001	0	0	0.09	0.41	0.5888	0	99.4	1.61	43	

Boreholes		TRACE ELEMENT COMPOSITIONS - PPM												
SAMPLE	Nb	Y	Rb	Zr	Sr	U	Th	Cr	V	La	Zn	Cu	Ni	
GER 1200/ B	94	12.4	17.2	10.4	1016.9	147.3	0.0	3.0	189.2	57.9	10.1	18.1	12.6	
GER 1200/ B	82	4.0	9.5	11.9	224.5	173.1	0.2	1.0	56.2	29.2	1.4	10.5	1.5	9.0
GER 1200/ B	52	5.3	8.8	12.9	218.7	159.8	1.9	4.0	66.0	28.2	0.4	11	3.4	9.1
GER 1200/ B	34	23.5	20.3	14.3	2171.4	50.7	2.1	10.9	150.1	73.3	7.8	16.5	2.4	8.4
GER 1200/ B	16	12.4	15.0	12.7	1035.6	25.7	0.1	5.6	91.2	51.8	11.3	13.9	7.5	10.1
GER 1200/ B	10	6.5	13.1	10.9	430.6	17.0	0.5	3.5	140.2	52.8	5.1	12.1	9.4	9.6
GEN 1200/ E/1	73	10.3	13.5	13.6	679.8	179.2	0.2	5.0	92.7	46.3	8.4	12.7	2.8	10.0
GEN 1200/ E/1	61	4.1	8.2	13.6	211.0	187.5	0.2	3.8	56.6	27.7	0.0	9.8	2.6	8.0
GEN 1200/ E/1	37	8.8	10.5	12.4	801.3	34.7	0.0	4.2	81.8	29.9	0.0	9.6	3.6	5.5
GEN 1200/ E/1	19	21.3	21.7	13.9	1672.0	31.6	0.4	8.4	136.5	82.6	18.6	17.5	4.3	11.5
GEN 1200/ E/1	1	15.0	22.2	19.2	1107.8	31.5	0.1	5.4	131.4	72.3	5.4	17.5	4.9	10.0
GEN 1200/ E/1	-5	113.6	95.1	11.5	10335.0	23.2	14.5	70.6	882.8	483.7	96.6	72.7	0.4	26.5
GEN 1200/ E/1	-10	116.8	115.1	19.0	11850.3	40.0	16.9	139.8	963.2	419.0	222.3	90.2	0	23.7
GEN 1200/ H/1	40	12.4	13.7	12.3	1196.0	42.9	0.0	3.1	103.7	42.6	0.4	11.2	2.6	6.4
GEN 1200/ H/1	28	10.6	11.7	15.4	978.3	38.8	0.0	5.7	78.4	36.4	5.3	11.7	3.4	5.5
GEN 1200/ H/1	10	17.3	20.0	16.2	1341.6	37.0	0.5	5.8	117.7	79.0	12.2	17.2	4.4	11.2
GEN 1200/ H/1	4	6.8	10.4	21.1	498.7	39.4	0.8	5.3	43.8	29.8	7.2	10.5	3.5	6.3
GEN 1200/ H/1	-8	10.7	14.2	18.2	684.1	28.0	1.5	6.2	79.8	37.7	2.4	12.4	5.1	7.5
GER 1280/ M	96	13.5	22.1	14.8	988.2	232.2	0.0	4.9	215.8	74.9	2.0	22.6	2.3	18.5
GER 1280/ M	78	32.8	36.6	12.2	2502.3	224.8	3.2	13.9	293.8	131.5	30.2	31.1	0.3	23.4
GER 1280/ M	60	7.9	12.6	15.6	806.7	140.3	0.0	5.3	87.1	36.8	2.1	12	3.1	8.0
GER 1280/ M	48	6.8	10.8	12.2	430.4	67.2	0.6	1.2	67.2	31.0	0.9	14.9	7.2	10.7
GEN 1200/ BB/1	53	31.0	29.4	13.1	3322.1	41.6	2.1	15.0	221.8	80.6	17.9	18.5	1.8	8.3
GEN 1200/ BB/1	78	21.7	21.0	11.9	2250.3	41.2	2.4	6.4	188.7	58.4	12.1	16	3.2	7.0
GEN 1200/ BB/1	60	20.6	18.5	7.4	1896.7	14.6	0.0	10.5	149.6	61.6	19.3	13.8	4.3	6.6
GEN 1200/ BB/1	48	8.4	10.3	13.0	564.1	13.1	0.0	5.6	75.4	25.2	9.6	8.8	4.7	7.7

Boreholes		TRACE ELEMENT COMPOSITIONS - PPM												
SAMPLE	Ba	Sc	S	Pb	Ga	Co	Cs	Nd	As					
GER 1200/ B	94	102.6	7.2	161.0	4.4	3.6	169.9	21.1	3.2	3.2				
GER 1200/ B	82	114.1	4.8	224.0	5.0	2.9	165.5	4.9	0.0	2.7				
GER 1200/ B	52	107.3	4.5	189.0	1.0	2.1	209.1	0.0	0.0	3.1				
GER 1200/ B	34	131.2	7.4	22.0	5.4	0.3	201.4	41.5	7.6	3.4				
GER 1200/ B	16	91.2	5.8	45.0	10.4	1.7	198.8	17.0	5.3	2.8				
GER 1200/ B	10	101.5	9.6	34.0	8.5	3.9	211.4	8.2	12.1	4.9				
GEN 1200/ E/1	73	117.8	5.7	250.0	10.8	1.7	129.3	21.4	6.1	2.8				
GEN 1200/ E/1	61	122.5	3.0	277.0	7.0	1.7	153.7	16.5	4.4	2.0				
GEN 1200/ E/1	37	125.0	2.9	19.0	5.0	0.2	278.8	12.9	1.8	0.4				
GEN 1200/ E/1	19	112.6	9.7	33.0	12.4	2.5	208.2	50.8	16.0	3.3				
GEN 1200/ E/1	1	194.4	12.5	34.0	6.4	3.2	198.1	23.2	9.8	7.4				
GEN 1200/ E/1	-5	106.0	53.2	71.0	12.8	1.2	67.1	230.6	106.7	20.9				
GEN 1200/ E/1	-10	184.8	28.9	54.0	16.9	0.0	113.1	488.3	229.3	20.4				
GEN 1200/ H/1	40	122.4	6.4	16.0	0.0	3.1	195.5	15.5	4.9	3.2				
GEN 1200/ H/1	28	147.1	4.2	13.0	6.5	3.3	219.9	5.9	0.6	0.0				
GEN 1200/ H/1	10	155.9	10.3	29.0	8.9	2.3	177.4	36.6	13.9	4.7				
GEN 1200/ H/1	4	195.5	5.5	23.0	2.8	2.9	225.6	0.0	0.0	3.6				
GEN 1200/ H/1	-8	189.6	6.5	21.0	8.8	0.9	212.2	15.2	5.5	1.8				
GER 1280/ M	96	106.6	11.0	271.0	6.1	3.5	143.4	14.9	7.0	3.1				
GER 1280/ M	78	92.9	15.1	260.0	10.2	1.7	113.0	52.0	24.0	6.6				
GER 1280/ M	60	133.8	5.4	159.0	1.4	2.6	153.2	11.3	2.9	3.3				
GER 1280/ M	48	126.1	6.3	58.0	12.2	1.7	304.1	5.2	0.0	1.3				
GEN 1200/ BB/1	53	118.2	7.1	23.0	1.1	0.4	218.4	46.9	20.8	3.9				
GEN 1200/ BB/1	78	105.6	6.7	17.0	5.2	0.0	241.0	28.1	11.8	2.1				
GEN 1200/ BB/1	60	64.0	6.8	33.0	0.5	0.0	262.0	40.5	13.4	0.1				
GEN 1200/ BB/1	48	89.9	7.3	24.0	2.6	1.5	244.1	34.5	14.7	0.0				

Boreholes		TRACE ELEMENT COMPOSITIONS - PPM												
SAMPLE	Ti/Zr	Nb/Zr	Ti/Nb	Y/Nb	P/Zr	(La+Co)/Zr	Ti/Yr	Nb/Ti	P/Ti	Co/Ti	V/Ti	Ni/Ti		
GER 1200/ B	94	9.46	12.194	7.7581	1.3871	39.335	0.030681	0.00295	0.129	41.58	174.8	60.19	13.1	
GER 1200/ B	82	12.78	17.817	7.1725	2.375	222.72	0.028062	0.00445	0.139	174.28	195.9	101.8	31.37	
GER 1200/ B	52	12.81	24.234	5.2849	1.84906	228.62	0.001829	0.01829	0.189	178.51	235.6	100.7	32.49	
GER 1200/ B	34	8.905	10.823	8.1366	0.86383	0	0.022704	0.00502	0.123	0	78.5	38.33	4.393	
GER 1200/ B	16	9.322	11.974	7.7855	1.20968	9.6562	0.027327	0.00541	0.128	10.358	94.47	53.45	10.46	
GER 1200/ B	10	10.47	15.095	6.9354	2.01538	69.67	0.030687	0.00813	0.144	66.548	311	117.1	21.3	
GEN 1200/ E/1	73	10.96	15.152	7.2359	1.31088	88.261	0.043636	0.00736	0.138	80.504	124.4	62.12	13.42	
GEN 1200/ E/1	61	13.29	19.431	6.8415	2	236.97	0.078199	0.01801	0.146	178.25	201.8	98.75	28.52	
GEN 1200/ E/1	37	7.359	10.982	6.7011	1.19318	0	0.016099	0.00524	0.149	0	138.7	50.7	9.327	
GEN 1200/ E/1	19	10.43	12.739	8.										

## **APPENDIX C**

Grain size data: Lines 380 and 1200, and field samples

Definition of the textural parameters (Friedman, 1961; 1979).

Standard deviation ( $\sigma$ ) =  $(\sum f (m_{\phi} - \bar{x}_{\phi})^2 / 100)^{1/2}$

Cubed deviation ( $\sigma^3$ ) =  $(\sum f (m_{\phi} - \bar{x}_{\phi})^2 / 100)^{3/2}$

Skewness or Third moment ( $\alpha_3$ ) =  $1/100 \sigma^{-3} \sum f (m_{\phi} - \bar{x}_{\phi})^3$

Mean-cubed deviation ( $\alpha_3 \sigma^3$ ) =  $1/100 \sum f (m_{\phi} - \bar{x}_{\phi})^3$

Kurtosis ( $\alpha_4$ ) =  $1/100 \sigma^{-4} \sum f (m_{\phi} - \bar{x}_{\phi})^4$

Simple sorting measure ( $So_s$ ) =  $1/2 (\phi_{95} - \phi_5)$

Simple skewness measure ( $\alpha_s$ ) =  $(\phi_{95} + \phi_5) - 2 (\phi_{50})$

Where "f" is the frequency or abundance of the different grain-size grades present in the sediment and "m<sub>φ</sub>" is the mid point of each grain-size grade in phi values.

Results

Textural parameters	Value range for borehole samples from Lines 380 and 1200 and for field samples	Values for Line 380 borehole samples that differ from the given value range	Values for field samples that differ from the given value range
Standard deviation ( $\sigma$ )	0.47 to 0.68	Bottom sample of Unit A3 = 0.75	F-dune 1, 2, 4 = 0.43, 0.53, 0.44 respectively
Cubed deviation ( $\sigma^3$ )	0.1 to 0.28	Bottom sample of Unit A3 and top sample of Unit B = 0.42 and 0.33 respectively	F-dune 1, 2, 4 = 0.08, 0.15, 0.09 respectively
Skewness or third moment ( $\alpha_3$ )	- 0.1 to 1.05	Unit A3 (three bottom samples), Unit A4 (bottom sample), Unit E2 and bottom sample of Unit A1 = 1.1 to 1.5	
Mean-cubed deviation ( $\alpha_3 \sigma^3$ )	- 0.02 to 0.2	Unit A3 (three bottom samples), Unit A4 (bottom sample) and bottom sample of Unit A1 = 0.25 to 0.5	
Kurtosis ( $\alpha_4$ )	4 to 12	Unit E2 presents the highest values within the given range	
Simple sorting measure ( $So_s$ )	0.67 to 0.95	Unit A3, Unit A4 (bottom sample), sample 15 of Unit C and top sample of Unit B = 0.95 to 1.27	F-dune 1, 2, 4 = 0.69, 0.86, 0.72 respectively
Simple skewness measure ( $\alpha_s$ )	- 0.3 to 0.15	Unit A3 (two bottom samples), Unit A4 (bottom sample), top sample of Unit E2 and bottom sample of Unit A1 = 0.2 to 0.4	F-dune 2 = 0.17 D'Rock 1 = 0.44

**Borehole S1 (380/B/1)**

Midclass		Sample	89	83	77	71	65	59	53	47	35	29	23	17	11	5	-1	-1
micrometres	Phi values																	
1504	-0.5888	0	0	0	0	0	0	0	0	0.4	0	0	0	0	0	0	0	0
1451.5	-0.53754	0.4	0.3	0	0	0.2	0	0.1	0	0.4	0	0	0	0	0	0	0	0
1350	-0.43298	0.4	0.3	0.1	0	0.2	0	0.1	0	0.5	0	0	0	0	0	0	0	0
1255	-0.32769	0.4	0.3	0	0	0.3	0.1	0.1	0	0.5	0	0	0	0	0	0.1	0.1	
1167	-0.2228	0.4	0.4	0.1	0.1	0.2	0	0.1	0	0.5	0	0	0	0	0	0	0	0
1085.5	-0.11836	0.5	0.4	0.1	0.1	0.3	0.1	0.2	0	0.6	0	0	0	0	0	0.1	0.1	
1009.5	-0.01364	0.6	0.5	0.2	0.1	0.4	0.1	0.2	0	0.7	0	0	0	0	0	0.1	0.1	
938.5	0.091571	0.6	0.6	0.2	0.3	0.4	0.2	0.4	0	0.7	0	0	0	0	0	0.1	0.1	
872.5	0.196773	0.6	0.6	0.2	0.3	0.5	0.2	0.3	0.2	0.7	0.2	0	0.1	0.1	0.3	0.2	0.2	
811.5	0.301337	0.6	0.6	0.4	0.3	0.6	0.3	0.4	0.8	1	0.6	0.3	0.2	0.1	0.8	0.2	0.2	
754.5	0.406407	0.9	0.9	0.4	0.5	0.7	0.4	0.6	1.2	1.6	1.1	0.6	0.5	0.4	1	0.2	0.2	
701.5	0.511485	1.5	1.7	0.4	0.8	1	0.4	0.9	1.7	2.2	1.5	1.1	0.8	0.6	1.1	0.4	0.4	
652.5	0.61595	2	2.4	0.8	1.3	1.6	0.7	1.5	1.9	3.2	1.7	1.2	1	0.7	1.5	0.6	0.6	
607	0.720232	2.9	3.5	1.5	2.2	2.7	1.1	2.4	2.2	4.8	2	1.4	1.1	0.7	1.6	1.2	1.2	
564.5	0.824955	4.2	5.3	2	3.1	3.5	1.9	3.6	2.3	5.5	2	1.5	1.2	0.9	1.7	2.3	2.3	
525	0.929611	4.9	6.1	2.9	4.2	4.4	3	4.6	2.6	8	2.4	1.8	1.5	1	1.9	2.9	2.9	
488	1.035047	5.2	6.5	4.5	5.2	5.7	3.9	5.8	3.3	6.5	2.7	2.5	2.1	1.4	2.3	4.1	4.1	
453.5	1.140826	5.6	6.9	6	6.3	6.9	5	6.7	4.1	7	3.4	3.3	2.6	1.9	2.7	5.8	5.8	
422	1.244685	5.8	7.2	7.6	7.7	7.9	6.9	7.9	6.2	7.1	4.7	5.3	4.4	3	3.9	7.2	7.2	
392.5	1.349235	6	7.2	9	8.7	8.7	8.2	8.8	9.2	7.2	7	8.8	7.2	5.3	5.9	8.1	8.1	
365	1.454032	6	7.1	9.8	9.1	9.2	8.9	9.1	10.4	7.1	8.4	10	8.9	6.9	7.3	8.8	8.8	
339.5	1.558517	6.2	6.8	9.9	9.3	8.9	9.3	9	10.4	6.9	9.3	10.4	10.3	8.5	8.7	9.2	9.2	
315.5	1.664288	6.4	6.8	9.3	8.9	8.2	9.3	8.2	10.1	6.5	10	10.6	11.5	10.2	9.9	9.4	9.4	
293.5	1.768568	6.4	6.1	8.2	8.1	7	8.6	7.4	9	5.9	10	11.6	11.1	10.3	8.7	8.7	8.7	
273	1.873027	6.2	6.5	8.9	7	5.8	7.8	6	7.1	5.2	8.5	8.2	9.9	11.1	9.2	7.2	7.2	
254	1.9771	5.9	4.8	5.6	5.9	4.5	6.9	4.3	5.1	3.9	6.5	6.1	7.3	10.2	7.4	5.4	5.4	
236	2.083141	4.9	3.7	4.3	4.2	3.3	5.5	3.8	3.2	2.3	4.5	4.3	4.8	8.9	5.9	3.9	3.9	
219.5	2.187707	3.6	2.2	2.7	2.1	1.9	3.5	2.5	2.4	1.5	3.7	6.5	4.9	3.2	3.2	3.2	3.2	
190	2.395929	2.1	1	1.3	0.7	0.9	1.7	0.7	2	1	2.9	2.7	2.9	3.3	4.3	2.6	2.6	
176.5	2.502226	1.3	0.5	0.8	0	0.4	0.9	0.6	1.4	0.4	2.1	1.9	2.1	2.2	3.2	2	2	
164	2.608232	0.9	0.4	0.5	0.1	0.4	0.5	0.6	0.7	0.3	1.2	0.9	0.9	1.4	1.1	1.2	1.2	
152.5	2.713119	0.6	0.4	0.4	0.3	0.4	0.4	0.5	0.3	0.3	0.4	0.2	0	0.4	0.5	0.6	0.6	
142	2.816037	0.5	0.4	0.4	0.4	0.5	0.2	0.4	0.1	0.4	0.2	0.2	0	0.2	0.1	0.4	0.4	
132	2.92139	0.4	0.2	0.2	0.3	0.3	0.2	0.4	0.3	0.2	0.4	0.5	0.4	0.2	0	0.4	0.4	
122.5	3.028146	0.4	0.3	0.2	0.3	0.2	0.1	0.2	0.5	0.2	0.6	0.8	0.7	0.2	0.1	0.6	0.8	
114	3.132894	0.4	0.2	0.2	0.3	0.1	0.2	0.1	0.5	0.2	0.7	1	0.9	0.2	0.3	0.6	0.6	
106	3.237864	0.4	0.1	0.1	0.2	0.1	0.2	0.1	0.4	0.2	0.6	0.7	0.7	0.4	0.4	0.6	0.6	
98.55	3.343	0.3	0.2	0.2	0.1	0.1	0.2	0.1	0.1	0.1	0.3	0.2	0.4	0.5	0.6	0.4	0.4	
91.75	3.446148	0.3	0.1	0.2	0	0.1	0.1	0	0.1	0.1	0.2	0.1	0.1	0.6	0.4	0.4	0.4	
85.3	3.55131	0.3	0	0.1	0	0	0.1	0.1	0	0	0	0	0	0.4	0.3	0.2	0.2	
79.35	3.655626	0.1	0.1	0.1	0	0	0.1	0	0	0.1	0	0	0	0.3	0.2	0	0	
73.8	3.760235	0	0	0	0	0.1	0	0.1	0	0	0	0	0	0.1	0.1	0.1	0.1	
68.6	3.865648	0	0	0	0	0	0	0	0	0	0	0	0	0	0	0	0	
63.8	3.9703	0.1	0	0	0	0	0	0	0	0	0	0	0	0	0	0	0	
59.35	4.074608	0	0	0.1	0	0	0	0	0	0	0	0	0	0	0.1	0	0	
55.2	4.179188	0	0	0	0.1	0	0	0	0	0	0	0	0	0	0	0	0	
51.35	4.283492	0	0	0	0	0	0	0	0	0	0	0	0	0	0	0	0	
47.75	4.388355	0	0	0	0	0	0	0	0	0	0.1	0.1	0	0	0	0	0.1	0.1
44.4	4.493297	0	0	0	0	0	0	0	0	0.1	0	0	0.1	0.1	0	0	0	0
41.3	4.597714	0	0	0	0	0	0	0.1	0	0	0	0	0	0	0	0.1	0.1	0.1
38.4	4.70275	0	0.1	0	0	0	0	0	0	0	0	0	0	0	0	0.1	0.1	0.1
35.7	4.807932	0	0	0	0	0.1	0	0	0	0	0	0	0	0	0	0	0	0
33.2	4.912673	0	0	0	0	0	0.1	0	0	0	0	0	0	0	0	0	0	0
30.85	5.018586	0	0	0	0	0	0	0	0	0	0	0	0	0	0	0	0	0
28.7	5.122805	0	0	0	0	0	0	0	0	0	0	0	0	0	0	0	0	0
26.7	5.227016	0	0	0	0	0	0	0	0	0	0	0	0	0	0	0	0	0
24.8	5.333516	0	0	0	0	0	0	0	0	0	0	0	0	0	0	0	0	0
23.05	5.439089	0	0	0	0	0	0	0	0	0	0	0	0	0	0	0	0	0
21.45	5.542879	0	0	0	0	0	0	0	0	0	0	0	0	0	0	0	0	0
19.95	5.647467	0	0	0	0	0	0	0	0	0	0	0	0	0	0	0	0	0
18.55	5.752437	0	0	0	0	0	0	0	0	0	0	0	0	0.1	0	0	0	0
17.25	5.85726	0	0	0	0.1	0	0	0	0	0	0	0	0	0	0	0	0	0
15.5	6.011588	0.1	0	0.1	0	0	0	0	0.1	0	0.1	0.1	0.1	0	0	0.2	0.2	0.2

**Borehole S2 (380/G/1)**

Midclass		Sample	63	57	51	45	39	33	27	21	15	3	-3
micrometres	Phi values												
1504	-0.5888	0	0	0	0	0	0	0	0	0	0	0	0
1451.5	-0.53754	0.1	0	0.1	0.3	0.1	0	0.1	0.3	0.3	0	0	0
1350	-0.43298	0	0	0	0.4	0.1	0	0.1	0.2	0.4	0	0	0
1255	-0.32769	0.1	0	0.1	0.4	0.1	0	0.1	0.3	0.4	0	0	0
1167	-0.2228	0.1	0	0.1	0.4	0.1	0	0.2	0.3	0.4	0	0	0
1085.5	-0.11836	0.1	0	0.2	0.4	0.2	0	0.2	0.4	0.4	0	0	0
1009.5	-0.01364	0.2	0	0.2	0.5	0.2	0	0.3	0.4	0.5	0	0	0
938.5	0.091571	0.2	0	0.2	0.6	0.3	0	0.3	0.4	0.5	0	0	0
872.5	0.196773	0.3	0	0.3	0.7	0.4	0	0.4	0.5	0.6	0	0	0
754.5	0.406407	0.4	0.7	0.5	0.9	0.5	0.5	0.7	0.6	0.8	0.5	0.6	0.6
701.5	0.511485	0.5	1.1	0.6	1.6	0.8	1	1	0.9	0.9	0.9	0.8	0.8
652.5	0.61595	0.8	1.6	0.9	2.1	1.1	1.4	1.7	1.4	1.5	1.2	1	1
607	0.720232	1.5	1.8	1.6	3.2	1.9	1.6	2.7	2.1	2.1	1.4	1.1	1.1
564.5	0.824955	2	2.1	2.4	4.6	2.8	1.8	3.7	2.8	2.8	2.1	1.5	1.5
525	0.929611	2.8	2.1	3.4	5.5	3.9	1.9	4.7	3.7	3.7	2.2	1.6	1.6
488	1.035047	4.4	2.5	4.3	6.2	4.7	2.2	5.6	4.5	4.4	2.5	1.9	1.9
453.5	1.140826	5.8	3.2	5.4	6.7	5.9	2.8	6.6	5.5	5.4	2.9	2.3	2.3
422	1.244685	7.2	4	6.9	7.3	7.4	3.4	7.6	6.4	6.2	3.5	2.8	2.8
392.5	1.349235	8.6	6	7.9	7.6	8.4	5.2	8.2	7.3	7	5.2	4.6	4.6
365	1.454032	9.4	9.1	8.5	7.6	8.9	7.9	8.5	8	7.7	7.7	7.2	7.2
339.5	1.558517	9.5	10.2	8.8	7.5	9	9	8.5	8.5	7.9	8.9	8.5	8.5
315.5	1.664288	9.1	9.9	8.6	7.2	8.6	9.3	7					

Borehole S3 (380M/1)

Midclass		69	63	57	51	45	39	33	27	21	15	3	-3	
micrometres	Phi values	Sample												
1504	-0.5888	0	0	0	0	0	0	0	0	0	0	0	0	
1451.5	-0.53754	0	0	0	0	0	0.1	0	0.1	0	1.3	0.2	0	
1350	-0.43296	0	0	0	0	0	0.1	0.1	0.1	0.1	1.4	0.2	0	
1255	-0.32769	0	0	0	0	0	0.1	0.1	0.1	0	1.4	0.2	0	
1167	-0.22228	0	0	0	0	0	0.1	0	0.2	0.2	1.4	0.3	0	
1085.5	-0.11836	0	0	0	0	0	0.2	0.2	0.2	0.1	1.6	0.3	0	
1009.5	-0.01364	0	0	0	0	0	0.2	0.1	0.2	0.3	1.6	0.3	0	
938.5	0.091571	0	0	0	0	0	0.4	0.3	0.3	0.3	1.8	0.5	0	
872.5	0.196773	0	0	0	0	0	0.4	0.2	0.3	0.5	1.9	0.5	0	
811.5	0.301337	0	0	0.1	0	0.1	0	0.4	0.4	0.4	0.5	2	0.5	0
754.5	0.406407	0.2	0.1	0.1	0.1	0.3	0.4	0.6	0.4	0.6	0.7	2.3	0.8	0.2
701.5	0.511485	0.4	0.8	0.2	0.3	0.6	1	0.9	0.7	0.6	1	3.7	1.3	0.8
652.5	0.61595	0.6	0.8	0.4	0.5	1	1.6	1.5	1	1.2	1.8	5.9	1.7	1.3
607	0.720232	0.8	0.8	0.5	0.5	1.1	1.9	2.7	1.6	2	3.1	8.4	2.7	1.4
564.5	0.824955	0.9	0.9	0.6	0.7	1.3	2	3.6	2.6	2.7	4.1	10.2	4.2	1.6
525	0.929611	1	1.2	0.7	0.7	1.4	2.2	4.5	3.7	3.5	5.2	10.7	5.3	1.7
488	1.035047	1.3	2.1	1	1	1.7	2.5	6.4	4.7	5	7.1	9.1	6.4	2
453.5	1.140826	1.7	2.9	1.5	1.3	2.2	3.3	7.8	5.8	6.4	8.7	6.3	7.7	2.6
422	1.244685	2.3	5.1	2	1.8	3	4.2	9.2	7.6	7.6	10.2	5.1	8.9	3.3
392.5	1.349235	3.7	9	3.8	3	4.8	6.6	10.2	8.6	8.7	11.2	4.1	9.7	5.3
365	1.454032	6.3	10.7	6.5	5.3	7.8	10	10.2	9.2	9.4	11	3.4	9.6	8.3
339.5	1.558517	8.1	11.1	8.7	7	9.5	11	9	9.1	9.3	9.3	3.1	8.3	9.5
315.5	1.664288	9.6	11.5	10.6	8.7	10.4	10.4	7.3	8.7	8.6	6.9	2.8	6.8	9.7
293.5	1.768568	11.2	10.7	12.7	10.4	11.4	9.3	5.5	7.7	7.5	4.4	2.6	5.2	9.6
273	1.873027	11.8	8.8	13.3	11.5	11.2	7.8	4.8	6.5	6.2	3.4	2.1	4.4	8.8
254	1.9771	10	6.4	11.4	11.3	9.4	6.6	4	5	5.1	2.9	1.8	3.8	7.2
236	2.083141	7.6	4.2	8.2	10.3	6.9	5.1	3.3	4.3	3.7	2.1	1.3	3.1	5.5
219.5	2.187707	5.2	3.2	4.9	8.5	4.6	3.6	2.2	3.2	2.4	1.2	0.9	2.1	4.2
204.5	2.289927	4	2.5	3.7	6.1	3.5	2.7	1.2	2.2	1.7	0.5	0.5	1	3.3
190	2.395929	3.3	1.8	2.8	3.5	2.8	2	0.6	1.5	1.3	0.2	0.2	0.6	2.8
176.5	2.50226	2.4	0.9	1.9	2.7	1.9	1.3	0.4	1.1	0.8	0.2	0.2	0.4	2.1
164	2.608232	1.2	0.2	0.6	1.5	0.6	0.9	0.5	0.8	0.7	0.4	0.1	0.5	1.4
152.5	2.713119	0.3	0.3	0	0.3	0	0.7	0.4	0.6	0.7	0.6	0.1	0.6	0.8
142	2.816037	0.4	0.6	0.1	0	0	0.5	0.5	0.5	0.6	0.6	0.1	0.5	0.8
132	2.92139	0.7	1.1	0.3	0	0.1	0.5	0.2	0.3	0.5	0.5	0.1	0.4	1.1
122.5	3.029146	1.2	1.2	0.7	0.1	0.5	0.4	0.2	0.3	0.4	0.3	0.1	0.3	1.3
114	3.132894	1.3	0.7	1	0.4	0.5	0.3	0	0.1	0.2	0.1	0.1	0.1	1.4
106	3.237864	1.1	0	0.8	0.5	0.6	0.3	0.1	0.2	0.2	0	0.1	0.1	0.9
98.55	3.343	0.7	0	0.5	0.6	0.3	0.3	0.1	0.1	0.1	0.1	0	0.1	0.4
91.75	3.446148	0.3	0	0.3	0.8	0.2	0.1	0	0.1	0.1	0	0.1	0.1	0
85.3	3.55131	0.2	0	0.1	0.5	0.1	0.2	0.1	0.1	0	0	0	0	0
79.35	3.655626	0	0	0	0.2	0	0	0	0.1	0.1	0	0	0.1	0
73.8	3.760235	0	0	0	0	0	0.1	0.1	0	0	0	0	0	0
68.6	3.865648	0	0	0	0	0	0	0	0.1	0	0.1	0	0	0
63.8	3.9703	0	0.1	0	0	0	0	0	0	0.1	0	0	0.1	0
59.35	4.074608	0	0	0	0	0	0	0	0	0	0	0.1	0	0
55.2	4.179188	0	0	0	0	0	0	0	0	0	0	0	0	0
51.35	4.283492	0	0.1	0	0	0	0	0	0	0	0	0	0	0.1
47.75	4.388355	0.1	0	0	0	0	0	0	0	0	0	0	0	0.1
44.4	4.493297	0.1	0.1	0.1	0	0.1	0.1	0	0	0.1	0	0	0	0.3
41.3	4.597714	0	0	0	0	0	0	0	0	0	0	0	0	0
38.4	4.70275	0	0	0	0	0	0	0	0	0	0	0	0	0
35.7	4.807932	0.1	0	0	0	0	0	0.1	0.1	0	0	0	0	0
33.2	4.912673	0	0	0	0	0	0	0	0	0	0	0	0	0
30.85	5.018586	0	0	0	0	0	0	0	0	0	0	0	0	0
28.7	5.122805	0	0	0	0	0	0	0	0	0	0	0	0	0
26.7	5.227016	0	0	0	0	0	0	0	0	0	0	0	0.1	0
24.8	5.333516	0	0	0	0	0	0	0	0	0	0	0	0	0
23.05	5.439089	0	0	0	0	0	0	0	0	0	0	0	0	0
21.45	5.542879	0	0	0	0	0	0	0	0	0	0	0	0	0
19.95	5.647467	0	0	0	0	0	0	0	0	0	0	0	0	0
18.55	5.752437	0	0	0	0	0	0	0	0	0	0	0	0	0
17.25	5.85726	0	0	0	0	0	0	0	0	0	0	0	0	0
17.25	5.85728	0	0	0	0	0	0	0	0	0	0	0	0	0

Field samples

Midclass		F-dune	1	2	4	D/Rock	1	3	4
micrometres	Phi values								
1504	-0.5888	0	0	0			0	0	0
1451.5	-0.53754	0	0.1	0			0	0.4	0
1350	-0.43296	0	0.2	0			0	0.4	0
1255	-0.32769	0	0.1	0			0	0.4	0
1167	-0.22228	0	0.3	0			0	0.5	0
1085.5	-0.11836	0	0.2	0			0	0.5	0
1009.5	-0.01364	0	0.4	0			0	0.6	0
938.5	0.091571	0	0.5	0			0	0.8	0.1
872.5	0.196773	0	0.6	0			0	0.8	0.2
811.5	0.301337	0	0.6	0			0	0.8	0.2
754.5	0.406407	0.1	0.9	0.1			0.1	1.2	0.4
701.5	0.511485	0.4	1.7	0.5			0.2	2	0.5
652.5	0.61595	0.8	2.3	1.2			0.5	2.8	0.9
607	0.720232	1	3.5	1.3			0.5	4.1	1.5
564.5	0.824955	1.1	5.3	1.4			0.5	5.9	2.3
525	0.929611	1.2	6.6	1.6			0.7	6.9	3.5
488	1.035047	1.7	7.5	1.9			0.9	7.5	4.4
453.5	1.140826	2.8	8.8	2.7			1.3	8.1	5.5
422	1.244685	3.9	9.7	3.5			1.8	8.4	7.4
392.5	1.349235	6.7	10.2	5.9			2.9	8.5	8.6
365	1.454032	11.1	9.7	9.5			5.3	8.1	9.2
339.5	1.558517	12.5	8	11.2			7.2	7.6	9.5
315.5	1.664288	12.2	5.9	11.9			9	6.4	9.2
273	1.873027	9.7	2.8	11.3			11.8	3.9	7.4
254	1.9771	7.4	2.3	8.8			10.6	2.7	6.3
236	2.083141	5.1	1.8	5.7			8.5	1.8	4.7
219.5	2.187707	3.1	1.2	2.8			6.2	1.1	2.7
204.5	2.289827	2.3	0.6	1.7			5	0.7	1.8
190	2.395929	1.7	0.5	1.2			4.2	0.4	1.2
176.5	2.50226	1.2	0.5	0.8			3	0.4	0.6
164	2.608232	0.6	0.8	0.3			1.5	0.3	0.5
152.5	2.713119	0.2	0.9	0.1			0.5	0.4	0.7
142	2.816037	0.1	0.8	0.1			0.4	0.3	0.6
132	2.92139	0.3	0.5	0.3			0.8	0.2	0.5
122.5	3.029146	0.5	0.2	0.6			1.4	0.1	0.4
114	3.132894	0.4	0	0.7			1.5	0	0.3
106	3.237864	0.3	0	0.5			1.2	0.1	0.1
98.55	3.343	0.1	0	0.3			0.7	0	0.1
91.75	3.446148	0	0.1	0.1			0.3	0	0.1
85.3	3.55131	0	0	0			0.1	0	0
79.35	3.655626	0	0.1	0			0	0.1	0
73.8	3.760235	0	0	0			0	0	0
68.6	3.865648	0	0	0			0	0	0
63.8	3.9703	0	0	0			0	0	0
59.35	4.074608	0	0	0			0	0	0
55.2	4.179188	0	0.1	0			0	0.1	0.1
51.35	4.283492	0.1	0	0			0	0	0
47.75	4.388355	0	0	0			0.1	0	0
44.4	4.493297	0	0	0			0	0	0
41.3	4.597714	0	0	0			0.1	0	0.1
38.4	4.70275	0	0	0			0	0	0
35.7	4.807932	0	0	0			0	0	0
33.2	4.912673	0	0	0			0	0	0
30.85	5.018586	0	0	0			0	0	0
28.7	5.122805	0	0	0			0	0	0



Borehole N3 (1200/E/1)

Midclass		85	79	73	67	61	61	49	43	37	31	25	19	13	7	1	-5	-10
micrometres	Phi values	Sample																
1504	-0.5888	0	0	0	0	0	0	0	0	0	0	0	0	0	0	0	0	0
1451.5	-0.53754	0	0	0	0	0	0	0	0.1	0	0	0	0.2	0	0	0.3	0	0.8
1350	-0.43296	0	0	0	0	0	0	0.1	0.1	0	0	0	0.3	0	0	0.3	0	0.8
1255	-0.32769	0	0	0	0	0	0	0	0.2	0	0	0	0.2	0.1	0	0.4	0	0.9
1167	-0.2228	0	0	0	0	0	0	0.1	0.1	0	0	0	0.3	0.1	0	0.3	0	1
1085.5	-0.11836	0	0	0	0	0	0	0.1	0.2	0	0	0	0.3	0.1	0	0.4	0	1.2
1009.5	-0.01364	0	0	0	0	0	0	0.1	0.3	0	0	0	0.3	0.2	0	0.5	0.1	1.3
938.5	0.091571	0	0	0	0	0	0	0.2	0.3	0.1	0	0	0.3	0.3	0.1	0.5	0.1	1.6
872.5	0.196773	0	0	0	0	0	0	0.2	0.3	0.2	0	0	0.4	0.3	0.2	0.5	0.2	1.9
811.5	0.301337	0	0	0	0	0	0	0.3	0.5	0.2	0	0	0.5	0.3	0.4	0.4	0.3	2.2
754.5	0.406407	0	0.1	0	0.1	0	0.1	0.3	0.5	0.4	0	0.2	0.5	0.5	0.5	0.8	0.3	2.6
701.5	0.511485	0.3	0.4	0.4	0.4	0.5	0.5	0.5	0.7	0.5	0.5	0.6	0.7	1.2	0.6	1.7	0.4	2.9
652.5	0.61595	0.6	0.9	0.9	0.8	1.2	1.2	0.9	1.3	0.9	1.5	1	1.1	1.6	1.2	2.5	0.5	3.4
607	0.720232	1.1	1.1	1	1	1.4	1.3	1.3	2.1	1.5	1.7	1.2	1.8	2.5	2.2	3.8	0.5	3.6
564.5	0.824955	1.5	1.2	1.1	1.1	1.5	1.4	2.1	2.8	2.3	1.7	1.3	2.4	4.1	3	5.8	0.6	4
488	1.035047	2.2	1.7	1.6	1.7	2	1.9	3.8	5	4.4	2.3	1.7	3.8	6.1	6.4	7	0.7	4.2
453.5	1.140826	3.2	2.4	2.4	2.8	2.8	2.7	4.7	6.3	5.5	3.1	2.2	4.5	7.2	8.4	7.2	0.7	4.3
422	1.244685	4.4	3.3	3.2	3.9	3.9	3.5	6.2	7.3	7.4	4	2.8	5.2	8.2	10.3	7.3	1.2	4.2
392.5	1.349235	7.2	5.6	5.5	6.7	6.3	5.9	7.2	8.4	8.6	6.3	4.4	5.9	8.9	11.7	7	2.3	4.2
365	1.454032	11.6	9.4	9.3	11.1	10.4	9.5	8.1	9	9.2	10.2	7.1	6.8	9.1	11.8	6.8	3.2	4.1
339.5	1.558517	12.6	11	10.8	12.5	11.9	11.2	8.8	9.1	9.5	11.2	8.6	7.1	8.7	10.2	6.4	4.2	4.2
315.5	1.664288	11.9	12	11.6	12.2	12.1	11.9	9.4	8.7	9.2	11	9.6	7.5	7.8	7.6	6	5.9	4.2
293.5	1.768568	10.4	12	11.8	11.3	11.8	12	9.7	7.8	8.4	10.5	10.4	7.9	6.7	4.9	5.4	7.3	4.3
273	1.873027	8.7	11	11.2	9.7	10.6	11.3	9.1	6.7	7.4	9	10.4	7.8	5.2	3.8	4.8	8.1	4.3
254	1.9771	7	8.8	8.9	7.4	8.1	8.8	7.4	5.6	6.3	6.4	8.9	7.4	3.6	3.2	4	8.6	4.1
236	2.083141	5.1	5.9	6.1	5.1	5.2	5.7	5.1	4.2	4.7	5.2	6.9	6.2	2.9	2.5	3.1	8.8	3.7
219.5	2.187707	3.1	3.2	3.4	3.1	2.6	2.8	2.9	2.3	2.7	3.8	5	4.3	2	1.5	2.1	8.8	3.3
204.5	2.289827	2.3	2.1	2.4	2.3	1.6	1.7	2.1	1.6	1.8	2.6	4.1	3.3	1.1	0.7	1.2	7.5	2.9
190	2.395929	1.4	1.6	1.9	1.7	1.1	1.2	1.5	1	1.2	2.1	3.2	2.4	0.8	0.4	0.8	4.5	2.5
176.5	2.50226	0.7	1	1.2	1.2	0.7	0.8	1.2	0.5	0.6	1.6	2.5	1.3	0.7	0.4	0.5	3.5	2.1
164	2.608232	0.4	0.5	0.6	0.6	0.3	0.3	0.7	0.5	0.5	1	1.3	0.9	0.7	0.7	0.5	2.6	1.8
152.5	2.713119	0.4	0.2	0.1	0.2	0	0.1	0.3	0.6	0.7	0.4	0.5	0.7	0.9	0.8	0.6	1.8	1.6
142	2.816037	0.4	0.2	0.2	0.1	0.1	0.1	0.3	0.6	0.6	0.2	0.3	0.5	0.7	0.7	0.5	1.3	1.3
132	2.92139	0.4	0.6	0.5	0.3	0.3	0.3	0.4	0.5	0.5	0.3	0.6	0.4	0.6	0.6	0.5	1.2	1.2
122.5	3.029146	0.4	0.9	0.7	0.5	0.6	0.6	0.5	0.3	0.4	0.4	0.8	0.5	0.4	0.3	0.4	0.9	1
114	3.132894	0.5	1	0.8	0.4	0.6	0.7	0.6	0.3	0.3	0.4	1	0.4	0.3	0.1	0.4	0.8	0.9
106	3.237864	0.2	0.6	0.6	0.3	0.4	0.5	0.4	0.2	0.1	0.3	0.8	0.6	0.2	0.1	0.4	1.1	0.8
98.55	3.343	0.1	0.3	0.3	0.1	0.3	0.3	0.2	0.1	0.1	0.2	0.5	0.6	0.1	0	0.2	1.4	0.7
91.75	3.446148	0	0	0.1	0	0	0.1	0.1	0.1	0.1	0.1	0.2	0.6	0.1	0.1	0.3	1.4	0.5
85.3	3.55131	0	0	0	0	0	0	0	0	0	0	0	0.2	0.4	0.1	0	1.3	0.4
79.35	3.655626	0	0	0	0	0	0	0	0	0	0	0	0.3	0	0.1	0.1	0.9	0.2
73.8	3.760235	0	0	0	0	0	0	0	0	0	0	0	0.1	0.1	0	0.1	0.5	0.2
68.6	3.865648	0	0	0	0	0	0	0	0	0	0	0	0.1	0	0	0	0.2	0
63.8	3.9703	0	0	0	0	0	0	0	0	0	0	0	0	0.1	-0.1	0.1	0.2	0
59.35	4.074608	0.1	0	0	0	0	0	0	0	0	0	0	0	0	0	0	0	0
55.2	4.179188	0	0	0	0	0	0	0	0.1	0.1	0	0	0	0	0.1	0	0.1	0.1
51.35	4.283492	0	0	0	0.1	0	0	0	0	0	0.1	0	0	0.1	0	0.1	0.1	0
47.75	4.388355	0.1	0	0	0	0	0	0	0	0	0	0	0	0	0	0.1	0.2	0
44.4	4.493297	0	0.1	0	0	0	0	0	0	0	0	0.1	0.1	0	0	0	0.2	0
41.3	4.597714	0	0	0	0	0	0	0.1	0	0.1	0	0.1	0	0.1	0.1	0.1	0.2	0
38.4	4.70275	0.1	0.1	0.1	0.1	0.1	0	0	0	0	0	0	0	0	0	0.1	0.3	0.1
35.7	4.807932	0	0	0	0	0	0	0	0	0	0.1	0	0	0	0	0	0.3	0
33.2	4.912673	0	0	0	0	0	0	0	0	0	0	0	0.1	0	0	0	0.3	0
30.85	5.018586	0	0	0	0	0	0	0	0	0	0	0	0	0	0	0	0.2	0
28.7	5.122805	0	0	0	0	0	0	0	0	0	0	0	0	0	0.1	0	0.1	0
26.7	5.227016	0	0	0	0	0	0	0	0	0	0	0	0	0	0	0	0.1	0
24.8	5.333516	0	0	0	0	0	0	0	0	0	0	0	0	0	0	0	0	0
23.05	5.439089	0	0	0	0	0	0	0	0	0	0	0	0	0	0	0	0	0
21.45	5.542879	0	0	0	0	0	0	0	0	0	0	0	0	0	0	0.1	0.1	0
19.95	5.647467	0	0	0	0	0	0	0	0	0	0	0	0	0	0	0	0.2	0.1
18.55	5.752437	0	0	0	0	0	0	0	0	0	0	0	0	0	0	0	0.2	0
17.25	5.85726	0	0	0	0	0	0	0	0.1	0	0	0	0	0.1	0	0.1	0.4	0
15.5	6.011588	0	0	0	0	0	0	0	0	0	0	0.1	0.1	0.1	0.1	0.7	2.1	0.3



## **APPENDIX D**

Point count data: Line 1200

